Journal of GEOMATICS

Journal of Geomatics

(A publication of the Indian Society of Geomatics)

Journal of Geomatics

(A Publication of the Indian Society of Geomatics)

Futuristic Model of Hydrometeorological Drought Risk Using the Buckley Geometric Mean Model and GIS Techniques – A Case Study

B. Kumi-Boateng* M. S. Peprah and E. K. Larbi
Department of Geomatic Engineering, University of Mines and Technology, Tarkwa, Ghana
Email: kumi@umat.edu.gh

Abstract: The quest for drought studies have become obligatory due to the increasing rate of human population and the suddenly change of global climate. This has resulted in the rise in water demand and has drawn the attention of numerous researchers in the areas of drought studies. As a natural hazard, many countries have faced the challenges of increasing famine, power fluctuations; shortage of potable drinking water caused by low rainfall and reduce ground water levels. Hence, the prediction and assessment of drought risk is a crucial step towards the mitigation and adaptation planning. Drought is best characterized by multiple hydrometeorological parameters. The study area, which lies in the main rainforest of Ghana, is convenient for cultivation of many cash crop agricultural products of Ghana because of its fertile soils and microclimate properties. In this study, drought analysis was carried out for the area using a method combination of multicriteria decision analysis (MCDA), fuzzy logics and GIS techniques, which can capture the potential relationship between factors affecting drought and the capacity of quantifying uncertainty and utilizing both data and knowledge-based sources were proposed to assess drought risk. The precipitation and temperature data used in this study were downloaded from the World climate website, https://www.worldclim.org/data/index.html that happens to be a six year annual data (from 2012 to 2018). The TRMM data had a resolution of 30 seconds and was used for the research investigations and analysis. The other important geo-environmental factors data were obtained from the Survey and Mapping Division Department of the Lands Commission of Ghana and comprises of the slope, water bodies and land cover (forest) data. The Buckley Geometric Mean Model was used to calculate the fuzzy weights of the selected criteria. The achieved result is much better and reliable because of the fuzzification of the conventional AHP. Additionally, a consistency ratio of 0.093 was obtained which implies that the obtained results were valid. The output results revealed that, the very high drought risks areas were about 0.3% to the overall drought occurrences. The High-risk areas recorded 18.9%, the moderately affected and low drought risk areas were 68.5% and 12.3% respectively. Areas, which recorded very high risk of droughts, are Bogoso, Tarkwa Breman and Eshireso. Those with high risk includes Brabone, Abokyi and Huni Valley. Moderately affected areas are Aboso, Tarkwa, Brumase, Juabeng, Atoabo, Teberebe and Akyempim. The least drought risk areas include Pataho, Bonsa, Bramiankor JCT, Benso and Techiman. The paper aims to show the varying levels of susceptibility of the study area to hydrometeorological drought. Also, it can be used in taking mitigation measures to minimize the loss in agriculture production, power fluctuations and water scarcity in drought prone areas.

Keywords: Analytical Hierarchy Process, Drought modelling, Fuzzy Logics, Hazard Risks, Hydrometeorological

1. Introduction

Droughts are seen as one of the environmental hazards, and have drawn the attention of environmentalists, ecologists, hydrologists, meteorologists, geologists, geophysics and agricultural scientists (Mishra and Singh, 2010). Droughts normally occur in all climates, such as high and low rainforest zones, amazons, tropics, sub Saharan areas and are mostly related to the reduction in the amount of the precipitation. Additionally, drought studies have become important as a result of the increased rate of human population, expansion of agriculture, hydraulic power energy and industry sectors. This called for the highly demand of water, which becomes scarce in most part of the world and many rely on unwholesome water which have negative impacts on human lives (Joe-Asare *et al.*, 2018; Kortatsi, 2004). Moreover, other factors such as climate change and contamination of water supplies have further contributed to the scarcity of water (Seidu and Ewusi, 2018; Ewusi and Kuma, 2014). Droughts are of great importance in planning and management of water resources for future purposes. Droughts have negative impacts on both surface and ground water resources. This can lead to reduction in

water supply, deteriorated water quality, crop failure, reduced range productivity, diminished power generation, disturbed riparian habitats, and suspended recreation activities, as well as affect a host of economic and social activities (Mishra and Singh, 2010). Droughts have become the world's expensive natural occurring disasters, causing billions of dollars in global damages annually and collectively affecting more people than any other form of natural disaster (Keyantash and Dracup, 2002). Therefore, it has become obligatory to assess drought severity in order to mitigate its menace. The quantification of drought is a difficult geophysical endeavor. Several researchers have proposed different methodologies in quantifying drought to either reduce or avoid the impacts of drought (Jamro *et al.*, 2020; Hayes *et al.*, 2011).

Time series information about the onset of drought, extent, intensity, duration and impacts can help in mitigating the drought related loses of life, human suffering and damage to economy and environment (Yalti and Aksu, 2019). Thus, drought severity, characters and impacts need to be explained in terms of intensity, magnitude and duration. Several studies have been

conducted on assessing of droughts based on probabilistic and stochastic models. Droughts have been categorized into different types depending on which stage in the hydrometeorological cycle; the effects are felt as detailed in (Jamro *et al*., 2020; Hayes *et al*., 2011; Keyantash and Dracup, 2002). Numerous drought models have been developed to monitor drought severity and intensity. A drought model assimilates data on snow pack, stream flow, precipitation, temperature, and other water supply indicators into an understandable picture (Dodamani *et al*., 2015). Some of the most widely used drought indices in drought model studies over the years include Palmer Drought Severity Index (PDVI), Crop Moisture Index (CMI), Standardized Precipitation Index (SPI),Surface Water Supply Index (SWSI), Normalized Difference Vegetation Index (NDVI), Vegetation Condition Index (VCI), Land Surface Temperature (LST), Reconnaissance Drought Index (RDI), Stream flow Drought Index (SDI) and Temperature Condition Index (TCI) (Jamro *et al*., 2020; Yalti and Aksu, 2019; Bunea, 2019; Dodamani *et al*., 2015; Belal *et al*., 2012; Wang *et al*., 2003). Based on these indices numerous studies have been conducted to monitor drought. The integration of linear regression and soft computing methods have also been applied in drought studies in the recent decades. Notable among the linear regression models are Autoregressive Integrated Moving Average (ARIMA) (Han *et al*., 2010), and Multiple Linear Regression (Dodamani *et al*., 2015). Some of the examples of the soft computing methods that have been used for effective monitoring of drought at real time include Wavelet Transform model (Kim and Valdes, 2003), and Artificial Neural Network (ANN) (Mokhtari and Akhoondzadeh, 2019; Belayneh and Adamowski, 2013; Dawson and Wilby, 2001).

Most data required for drought risk assessment have a spatial component and also change over time. Therefore, the use of Geographic Information System (GIS) and Remote Sensing (RS) has become essential in drought hazard risk mapping. It is evident that GIS has a great role to play in drought risk assessment because natural hazards are multi-dimensional. The main advantage of using GIS for drought risk assessment is that, it does not only generate a visualization of hazard but also creates potential to further analyze this product to estimate probable damage due to drought hazard. Drought risk assessment requires up-to-date and accurate information on the terrain topography and the land use land cover. Some of the applications of GIS and RS techniques in drought assessment are presented in the following literatures (Jimenez-Donaire *et al*., 2020; Heumann, 2011; Belal *et al*., 2012; Han *et al*., 2010; Wang *et al*., 2003). The aim of the present study is to use GIS, the Analytical Hierarchy Process (AHP), and Fuzzy Logics approach in assessing the drought risks of the study area by creating a drought hazard map of the area. Multi-criteria Decision Analysis (MCDA) and GIS are very useful tools for solving problems in spatial context because various decision variables can be evaluated and weighted according to their relative importance to attain the final optimal decision (Broekhuizen *et al*., 2015; Kihoro *et al*., 2013). Also, MCDA has the ability to judge qualitative criteria along with quantitative criteria

(Boroushaki and Malczewski, 2008). Moreover, it is simple to understand, easy to implement, modify, and suitable for problems which have a hierarchical framework (Peprah *et al*., 2018; Aslani and Alesheikh, 2011). Hence, MCDA and GIS techniques were adopted in the present study.

The study area is within the rainfall forest of Ghana that records the highest rainfall in Ghana and few dry seasons (Larbi *et al*., 2018; Peprah and Mensah, 2017). The area is also well known for mining activities, host several private and public companies, farming of numerous cash crops as cocoa, cola, palm fruits, rubber, and many others (Larbi *et al*., 2018; Boye *et al*., 2018) which contributes significantly to the national income of Ghana. The area experience water crises in times of dry seasons and wet seasons and many rely on non-potable water for their daily activities (Joe-Asare *et al*., 2018; Seidu and Ewusi, 2018). This has called for the need to assess the drought risk of the study region. However, upon carefully review of existing literatures, no study has been conducted utilizing the fuzzy AHP method integrated with GIS for drought assessment in the study area. In this study, a fuzzy AHP approach in a multi criteria decision analysis (MCDA) approach, integrating GIS has been applied for drought hazard modeling through a risk map in the Wassa West District, which is situated in the Western part of Ghana. This modeling method uses the expert ideas to express the importance and priority of effective factors in drought studies. These expert ideas are expressed by linguistic variables (just equal, equally important, weakly more important, strongly more important, very strongly more important, and absolutely more important) for comparing of the effective factors in drought occurrence (Eskandari, 2017; Sharma *et al.,* 2012). The fuzzy sets enter to modeling process to express the uncertainty and to get the more accurate results than AHP method (Chang and Wang, 2009, Zadeh, 1965). Therefore, weights and maps of effective factors have fuzzy characteristics in this modeling approach. Finally, the drought model is obtained based on the fuzzy weights. The map obtained from fuzzy AHP model in this study is capable to predict the future droughts in the study area as a function of topographic, biologic, climatic, and anthropogenic factors. In the first step of the research, a hierarchical structure of drought risk criteria and sub-criteria is developed and the criteria and sub-criteria maps are prepared. In the second step, the fuzzy weights of criteria and sub-criteria are determined and the drought risk model is obtained using fuzzy AHP. In the last step, the drought risk map is obtained by weighted overlay of the criteria fuzzy maps considering to drought risk model in GIS platform. In assessing the risks of the drought in the area, we are looking at the probability of the hazard occurrence and its impacts on different natural or anthropic systems, which are more or less vulnerable to external disturbances. The outcome of the present study can be used in taking mitigation measures to minimize the loss in agricultural production, human lives, industrial sectors, and many more of the drought prone areas. The results will also provide information on prevalence, severity level and persistence of drought conditions, which will be instrumented for the planners to optimally

allocate deep boreholes and pipe borne waters to the affected areas.

2. Study Area

Wassa West District (Figure 1) is located in the middle part of Western South Region of Ghana and lies within latitude 5°30'N to 6°15'N and longitude 1°45'W to 2°11'W. It has a total land area of about 2578 km² with Aboso as its capital (Larbi *et al.*, 2018). It is bounded to the west by Sefwi Wiaso and Aowin districts, to the south by Ellembele and Jomoro, to the southeast by Prestea-Huni Valley and to the north by Bibiani. The area is endowed with natural resources such as Gold, Manganese and Bauxite, which contributes significantly to the economic development of Ghana (Boye *et al.*, 2018; Joe-Asare *et al.*, 2018). It has a total of 92, 152 inhabitants (Asiedu and Dankwa, 2014). There is a good network of water bodies such as rivers, streams, notable among them are river Tano, and Ankobra but most of these water bodies are polluted due to mining and farming activities. The main economic crops grown in the district are cocoa, rubber, oil palm, citrus and kola (Avotri *et al.*, 2002). It has a tropical climate associated with significant rainfalls and a short dry season (Peprah and Mensah, 2017). There

are two main rainfall regimes: thus; March to July and September to early December and the dry season starts from October to February. The interplay of heavy rainfall and soil types find expression in the vegetation cover. The semi deciduous forest is found in the northern part while the tropical rainforest is to the south where rainfall is heaviest (Larbi *et al.*, 2018). Geographically, the land is generally undulating with steep slopes parallel to each other and to the strike of the rocks in the North south direction with several hills making farming and other developmental activities a bit stressful (Kortatsi, 2004). It is found within the main gold belt of the Republic of Ghana that stretches from Axim in the Southwest direction, to Konongo in the Northeast direction (Kortatsi, 2004; Asklunel and Eldvall, 2005). The type of coordinate system used in the study area is the Ghana projected grid derived from the Transverse Mercator 1 º NW and the (WGS84) (UTM Zone 30N) (Yakubu *et al.*, 2018; Peprah *et al.*, 2017). The average annual temperature is 26˚ with small daily temperature variations. Relative humidity varies from 61 % in January to a maximum of 80 % in August and September (Peprah and Mensah, 2017). It has an average annual precipitation of 1696 mm. A detailed of the geology of the place can be found in (Asante-Annor *et al.*, 2018).
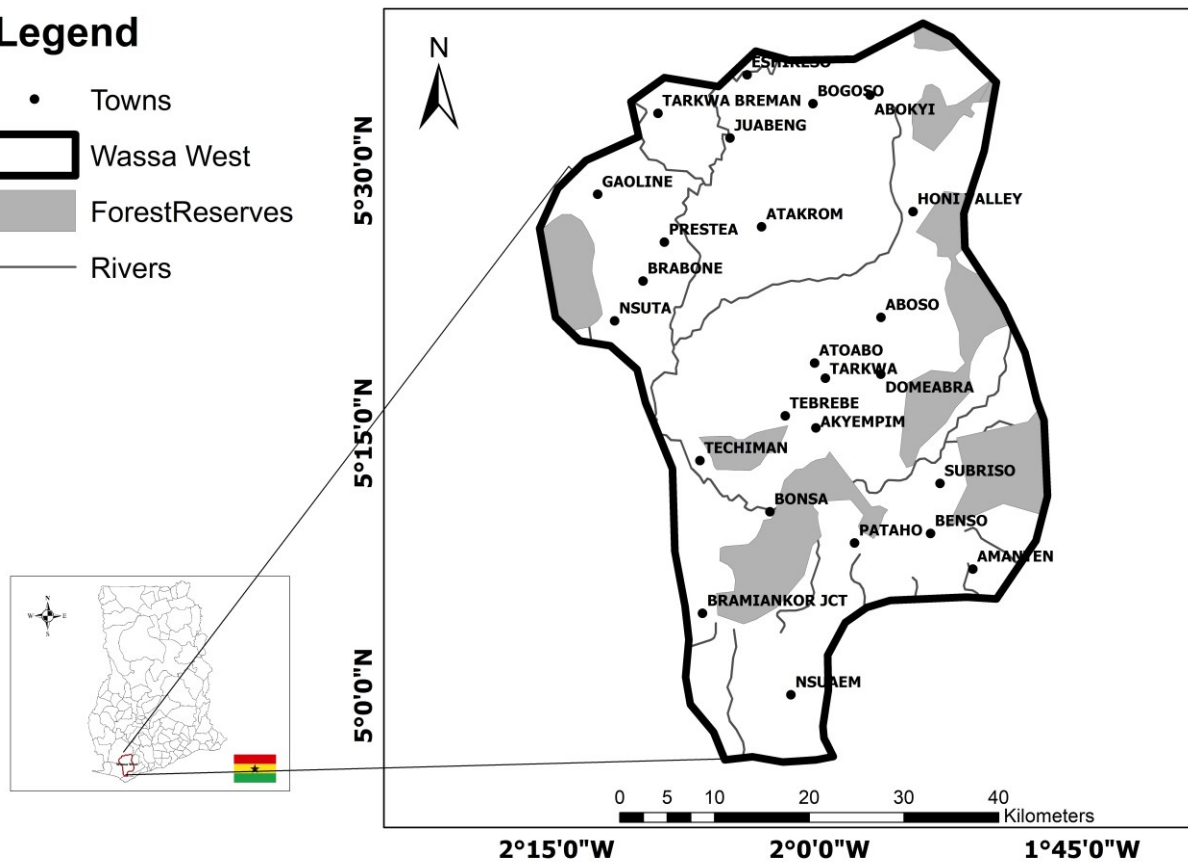
Figure 1. A Map of the Study Area

3. Resources and Methods used

3.1 Resources

The resources used for the investigating of the research findings include: Annual TRMM Precipitation and Temperature data that spans from 2012 to 2018 obtained from World Climate website; Ghana Country Shapefiles (slope, forest and water bodies) obtained from the Survey and Mapping Division of the Land Commission of Ghana; ArcGIS software; and Microsoft office software. The TRMM data had a resolution of 30 arc seconds and was used for the research investigations and analysis. Precipitation data is the downloaded annual TRMM precipitation data shown in Figure 2.

3.2 Methods Used
3.2.1   Model Generation

The Buckley Geometric mean model was used to assign the weights to the various cost criteria. Both Fuzzy AHP and AHP were employed in this study. First, a consistency check was carried out to determine the consistency of the selected criteria. The calculated Consistency ratio, C_r for the cost criteria using AHP was 0.093, this implies the calculated weights were consistent. The consistent set criteria were then fed into the fuzzy AHP using the triangular fuzzy membership function. The obtained Triangular fuzzy weights were used to obtain the crisp weights using the center of area method before it was finally normalized to obtain the required weights for the hydrometeorological factors. The Drought susceptibility model was generated in the ArcGIS

environment given by Equation (1) (Peprah *et al.*, 2018) as:

$$D = \sum_{i=1}^{n} W_i C_i \prod_{j=1}^{n} r_j \qquad (1)$$

where; D = Drought Model; W_i = weight of variables; C_i =Model variables; n = criteria; r_j = Restrictions.

3.2.2 Buckley Geometric Mean Model

In this study, the Buckley Geometric Mean Model (BGM) was used for making the Analytical Hierarchy Process (AHP) Fuzzy. BGM is one of the improved mathematical development using AHP techniques (Firoozi et al., 2017). In this case, triangular fuzzy numbers were used to represent the expert opinions. The fuzzy numbers are shown as; $\tilde{r} = (x_{ij}, y_{ij}, z_{ij})$ and in geometric space as shown in Figure 3. In MCDA method application, firstly, the decision tree is formed to prioritize the various criteria and sub-criteria. The judgement matrix is then formed based on the respondents and experts' advice. Consider the fuzzy judgment matrix in Equation 2:

$$\begin{bmatrix} (1,1,1) & (x_{12}, y_{12}, z_{12}) & \cdots & (x_{1n}, y_{1n}, z_{1n}) \\ (x_{21}, y_{21}, z_{21}) & (1,1,1) & & (x_{2n}, y_{2n}, z_{2n}) \\ & & \vdots & \\ (x_{n1}, y_{n1}, z_{n1}) & (x_{n2}, y_{n2}, z_{n2}) & \cdots & (1,1,1) \end{bmatrix} (2)$$
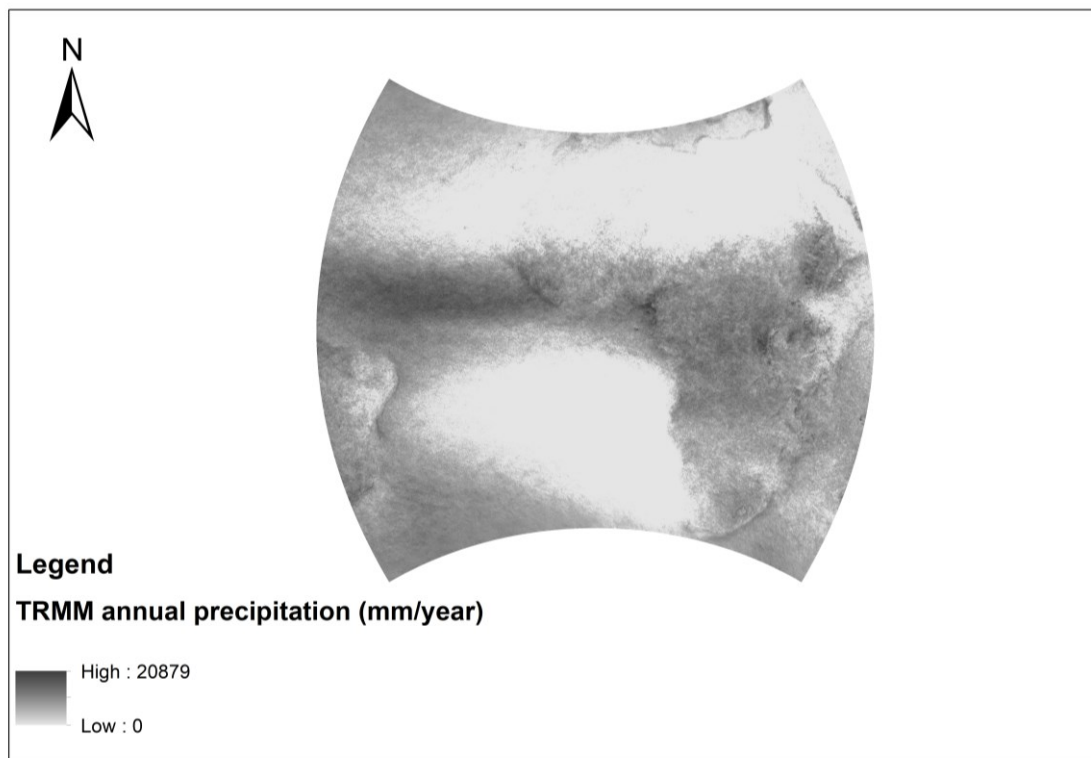
Figure 2. TRMM 2b31 Annual Precipitation map
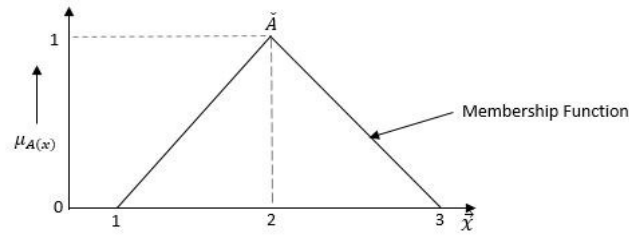
Figure 3. Triangular Fuzzy Membership Distribution

The Geometric Mean is then calculated from each row as shown in Equation (3) given as:

$$\breve{t}_i = \left(\prod_{j-1}^{n} \breve{r}_{ij} \right)^{\frac{1}{n}} \quad (3)$$

where; $\breve{t}_i$ = Geometric Mean Values; $\breve{r}_{ij}$ = Triangular Fuzzy Members; and n = Number of criteria. The Fuzzy Geometric Mean is obtained by the summation of the corresponding columns of the obtained Geometric Mean of each criteria according to Equation 4 given as:

$$\sum_{i-1}^{n} \breve{t}_i = \breve{t}_1 + \breve{t}_2 + \breve{t}_3 + \cdots \breve{t}_n \quad (4)$$

The Weights are then calculated by normalization of the Fuzzy Geometric as shown in Equation (5) denoted by:

$$\widetilde{q_{ij}} = \widetilde{W}_i = \frac{\breve{t}_i}{\sum_{i=1}^{n} \breve{t}_i} \quad (5)$$

where; $\widetilde{q_{ij}}$ = normalized weights of the secondary variables (option i weight than criterion j); and $\widetilde{w}_i$ = weights of the main variable or criteria. The final weights are then obtained from the combination of the option weights and the criteria giving by Equation 6 as:

$$\breve{g}_i = \sum_{j-1}^{n} \widetilde{w}_i \widetilde{q}_{ij} \quad (6)$$

3.2.3 Consistency Check

A test was carried out to verify whether the variables chosen for the pairwise matrix were consistent. The consistency ratio was used to check whether the threshold value proposed by Saaty was not exceeded (Larbi et al., 2018). For consistency, the consistency ratio should not exceed 0.10 $(c_r < 0.10)$. The consistency ratio is obtained by dividing the calculated consistency index by its corresponding criteria Random Index. First, the weighted sum is multiplied by the criteria matrix. The Eigen Vector is calculated by division of the weighted sum vector by the criteria weights given by Equation (7) as:

$$W_s = \begin{bmatrix} w_1 \\ w_2 \\ w_3 \\ w_4 \end{bmatrix} \quad (7)$$

where;
w_s = Weighted Sum Vector.

$$e_i = \frac{1}{\widetilde{w}_i}(w_s) \quad (8)$$

where;

e_i = Eigen Vectors; and $\widetilde{w}_i$ = Weights of the main variable. Equation 8 denotes the average of the eigen vectors given as:

$$\lambda_{max} = \frac{\sum_{i=1}^{n} e_i}{n} \quad (9)$$

where; λ_{max} = Average of the Eigen Vectors; and n = Number of criteria. The Consistency Index, C_i is expressed in Equation (10) as:

$$C_i = \frac{\lambda_{max} - n}{n - 1} \quad (10)$$

Finally, the Consistency Ratio, C_r is obtained by dividing the consistency index by the corresponding criteria Random Inconsistency Index, R_i given by Equation 11 as:

$$C_r = \frac{C_i}{R_i} \quad (11)$$

3.2.4 Cost Criteria

The Cost Surface is a raster dataset represented by grid cells. This is based on a set of defined criteria. Various thematic maps according to the defined cost criteria were generated in the ArcGIS environment to assist in identifying areas susceptible to drought risks in intensifying degrees. In this study, four main cost factors were identified and used for the drought analysis according to the experts' advice;

Precipitation
Drought is a prolonged and abnormal moisture deficiency as defined by the American Meteorological Society (Palmer and White, 1965). Precipitation is the main causative agent to consider in prediction and analysis of drought. Droughts can occur when there is the lack of precipitation (rain and snow) in a particular area or environment within a period of time. In this research, precipitation data (TRMM) over a period of 6 years (2012 to 2018) from the World Climate website, (https://www.worldclim.org/data/index.html) was downloaded in raster format. The downloaded data had a resolution of 1 km². The particular precipitation data covering the entire study area was extracted and used for the studies.

Land Cover (Forest)
Land cover represents the actual or physical presence of vegetation or other materials were vegetation is non-existent on the land surface (Fry et al., 2011). In this study, Forest was considered as one of the contributing criteria in drought analysis. Trees play a major role in the

fight against drought through various ways. Trees covers help in the preservation of moisture content by preventing evaporation from the rivers, reservoirs and soil saving water for drinking and agriculture. It also helps in evapotranspiration, which helps in triggering rainfall. The root system provides hydrological and mechanical effects that stabilizes soil slopes and minimizes water run-off, thereby increasing soil moisture content and effect guards against agricultural drought (Belal et al., 2012). The Forest Cover data was obtained from the Survey and Mapping Division of Ghana. The Forest cover area required for the study was clipped out. A map was then generated at a scale of 1:500 000 in the ArcGIS environment.

Water bodies (Rivers)
Rivers, which were the main water bodies in the study area, were considered in the drought analysis. Whenever there is a deficiency of surface water and ground water supply in a region it results in hydrological drought, it normally results from reduction in expected precipitation in an area over a long period of time and the over reliance on the surface water supply. The river extent data of the study area was also obtained from the Survey and Mapping Division and worked on in the ArcGIS environment.
Elevation

Elevation is the vertical distance from a specified surface to a reference datum. The contour topography was obtained from the Survey and Mapping Division of Ghana, then used in the generation of the Digital Elevation Model (DEM) of the study area. The DEM was then used to generate the slope data for the drought analysis in ArcGIS environment. The DEM data has a 30m by 30m resolution scale.

Slope
Slope plays a major role in agricultural drought. The higher the slope of a land the lesser its water holding capacity, hence more run-off water flows away onto areas with lower slopes or lesser altitudes. More water is retained on flat lands, this result in a more seepage of water into the soil, thereby increasing the soil moisture content for agricultural purposes.
Temperature
Temperature is one of the main dynamic factors contributing to drought. The higher the temperature, the faster the rate of water loss or evaporation and vice versa. Temperature also reduces with increasing elevation and increases with a reduction in elevation. The Annual Temperature data spans from 2012 to 2018. It was downloaded from the World Climate website, https://www.worldclim.org/data/index.html at a resolution of 30 seconds (~1km^2). Table 1 is the classification of Drought Cost Variables.

Table 1. Classification of the hydrometeorological drought variables

Variables	Classes	Values
River length (km)	0.06-0.15	5
	0.15-0.32	7
Temperature	<24°C	2
	(25.3-25.6)°C	4
	(25.6-26)°C	6
	>26°C	8
slope	0°-0.12°	6
	0.13°-0.31°	4
	0.32°-0.87°	3
	0.88°-2.53°	2
Elevation(m)	<60	6
	60-100	4
	100-140	3
	>140	2
Precipitation(mm)	246-272	2
	272-292	3
	292-313	4
	313-338	6
	338-370	8
Forest (km^2)	0.3-55.8	4
	55.8-119.71	6

3.2.4 Weighted Overlay of Cost Maps
Using the Weighted Overlay function under the Spatial Analyst Tool, the cost maps within the criteria used were combined to give a combined cost (friction) surface for such theme. The hybrid cost friction surface was produced by assigning equal weights to them based on the Buckley Geometric Mean Model and combined using the Weighted Overlay function. Figure 4 is the flowchart for the overlay analysis.

4. Results and Discussions

4.1 Results
4.1.1 Relative Weights of Cost Factors
The Buckley Geometric Mean Model was used to assign weights to the various criteria. The triangular fuzzy member function was employed in this study. Equation (11) shows the pairwise fuzzy matrix and the geometric means of the selected criteria. The obtained Triangular fuzzy weights were defuzzied to obtain the crisp weights using the center of area method before it was finally normalized to obtain the percentage weights as shown in Table 2. A consistency check was carried out to verify the

consistency of the obtain weights from the Buckley Geometric Mean Model. Table 3 shows the Eigen Vectors. The calculated Consistency ratio, C_r was 0.093, this implies the calculated weights are consistent as it is less than 0.10 (<0.10).

$$\begin{bmatrix} n & R & T & S & E & P & F & GM \\ R & (1,1,1) & (1,1,1) & (1,1,1) & (1,1,1) & (1,1,1) & (1,2,3) & (1,1.122,1.201) \\ T & (1,1,1) & (1,1,1) & (1,1,1) & (1,2,3) & \left(\frac{1}{3},\frac{1}{2},1\right) & (1,1,1) & (0.833,1,1.201) \\ S & (1,1,1) & (1,1,1) & (1,1,1) & (1,1,1) & \left(\frac{1}{3},\frac{1}{2},1\right) & (1,1,1) & (0.833,0.891,1) \\ E & (1,1,1) & (1,1,1) & (1,1,1) & (1,1,1) & \left(\frac{1}{3},\frac{1}{2},1\right) & (1,1,1) & (0.833,0.891,1) \\ P & (1,1,1) & (1,2,3) & (1,2,3) & (1,2,3) & (1,1,1) & (1,2,3) & (1,1.587,2.080) \\ F & \left(\frac{1}{3},\frac{1}{2},1\right) & (1,1,1) & (1,1,1) & (1,1,1) & \left(\frac{1}{3},\frac{1}{2},1\right) & (1,1,1) & (0.693,0.794,1) \end{bmatrix} \text{(12)}$$

where; n = Number of Criteria; P = Precipitation; S = Slope; F Forest; R = Rivers; E = Elevation; T = Temperature; and GM = Geometric Mean.
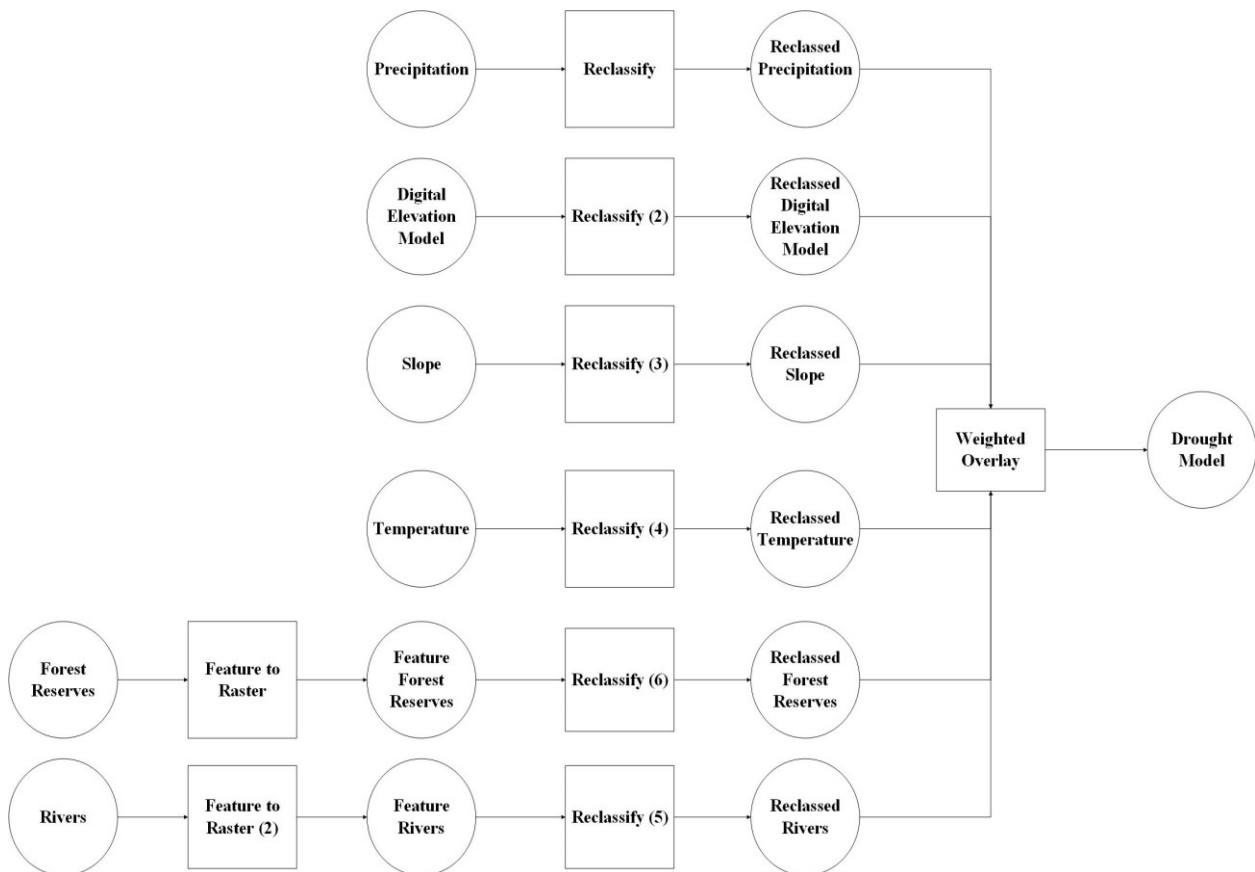
Figure 4. Flow Chart of the Weighted Criteria Overlay

Table 2. Triangular Fuzzy and Normalized Weights

Criteria(n)	Lower Values	Middle Values	Upper Values	Crisp Weights	Normalized Weights (%)
Rivers	1	1.122	1.201	0.181	17
Temperature	0.833	1	1.201	0.167	16
Slope	0.833	0.891	1	0.149	14
Elevation	0.833	0.891	1	0.149	14
Precipitation	1	1.587	2.080	0.262	25
Forest	0.693	0.794	1	0.137	13

Table 3. The Eigen Vectors

Criteria (n)	Precipitation	Temperature	Slope	Elevation	Precipitation	Forest	Eigen Vectors
Rivers	0.18	0.18	0.18	0.18	0.18	0.36	7
Temperature	0.16	0.16	0.16	0.32	0.08	0.16	6.50
Slope	0.14	0.14	0.14	0.14	0.07	0.14	5.50
Elevation	0.14	0.14	0.14	0.14	0.07	0.14	5.50
Precipitation	0.25	0.50	0.50	0.50	0.25	0.50	10
Forest	0.06	0.13	0.13	0.13	0.06	0.13	5

4.1.2 Cost Surface Maps
The cost surface maps were generated in the ArcGIS environment using Arc map 10.4 software. They represent the selected criteria in this study. Figure 5 is the surface map of the accumulated annual precipitation in Wassa West over a period of 6 years (2012 to 2018). The annual rainfall was is found between 246mm to 370mm of rain. The Forest Canopy (Land cover) in the study area is shown in Figure 6. Figure 7 is the map of rivers in the study area which plays a major role in drought analysis. The topographic contours of the study area were used to generate the Digital Elevation Models (DEMs). The DEM was then used to generate the slope map which were reclassified into four (4) classes. Areas with higher slopes experience more water run-off as a result, its

unable to retain more water after rainfall. Areas with higher slopes have a low soil moisture content compared with areas with lower slopes. In situations where there is lack of expected rainfall within an extended period of time, areas with higher slopes tend to be more prone to agricultural drought. The Temperature map of Wassa West is shown in Figure 8. Figure 9 is the slope map. Figure 10 displays the digital elevation model of the study area. Figure 11 obtained from the weighted overlay of the various cost criteria. The drought map was simply reclassified into three (3) main classes; low, moderate and high. The higher-class category shows areas that are highly prone to droughts, the moderate category has an intermediate drought occurrence and the lower-class category shows areas that have the least prone to drought.
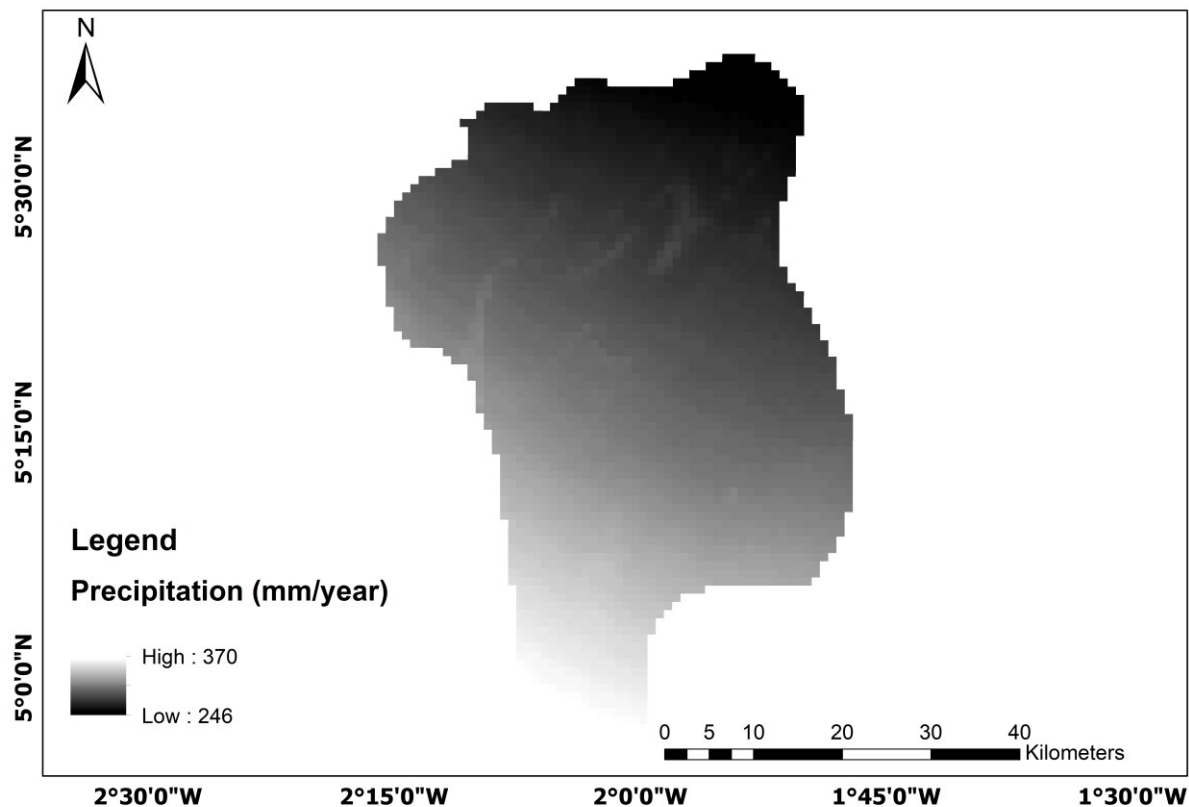
Figure 5. Precipitation Map
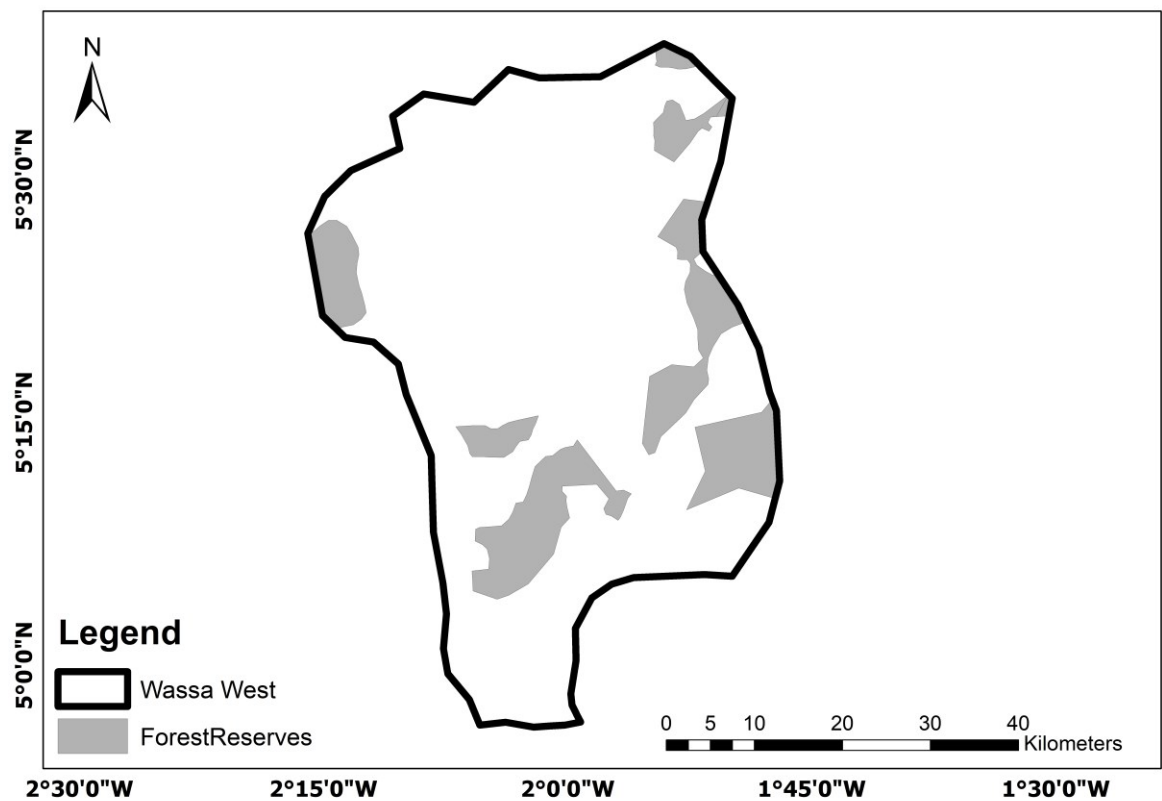
Figure 6. Map of Forest Resources
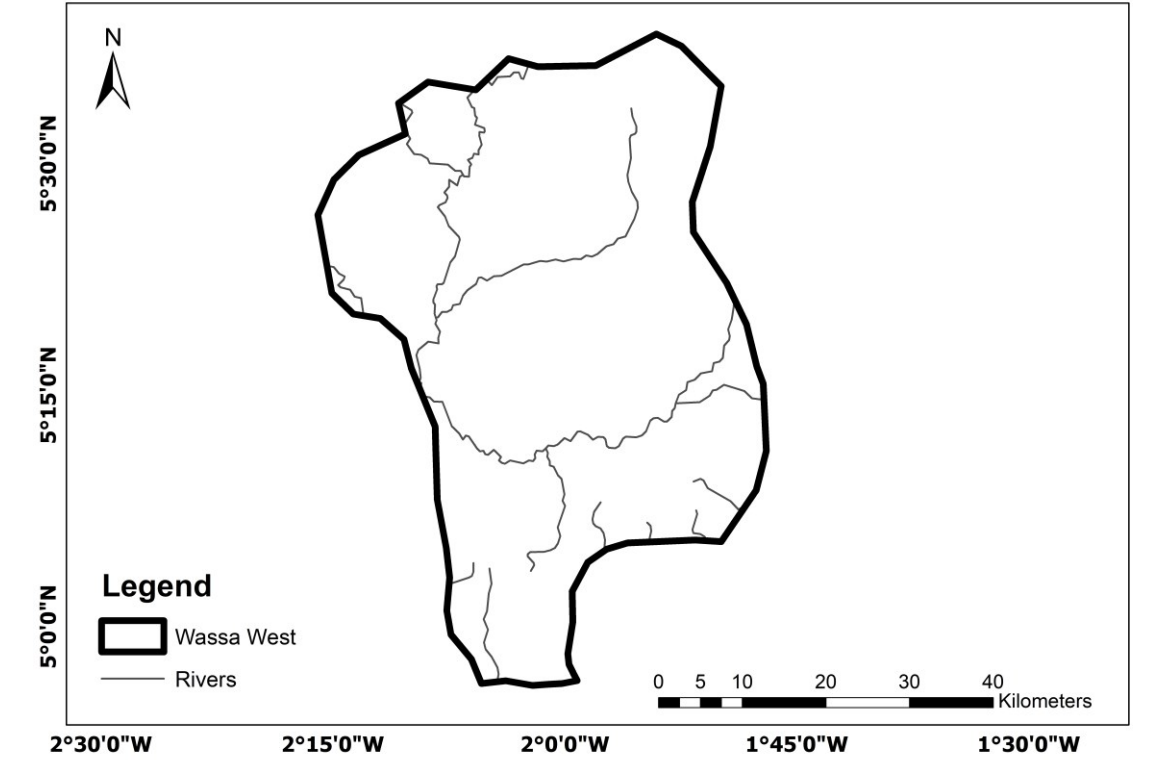
Figure 7. A Map of Rivers
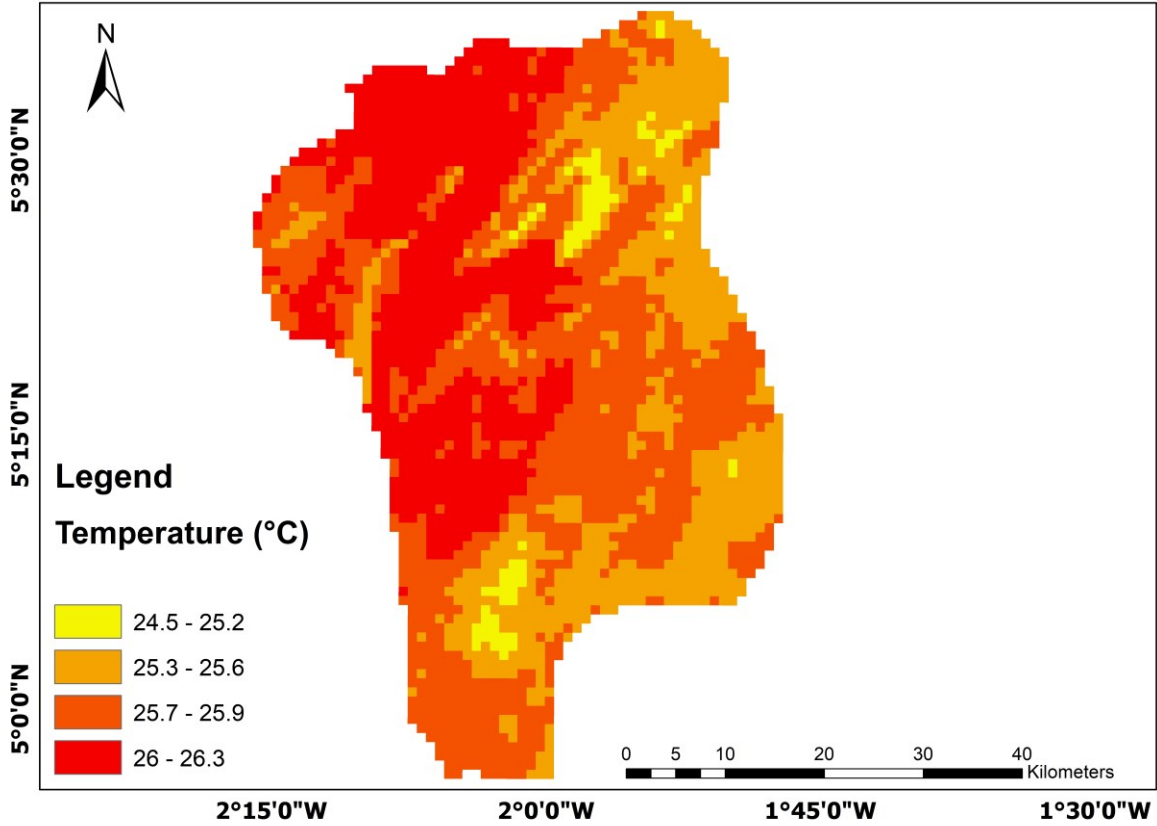
Figure 8. Temperature
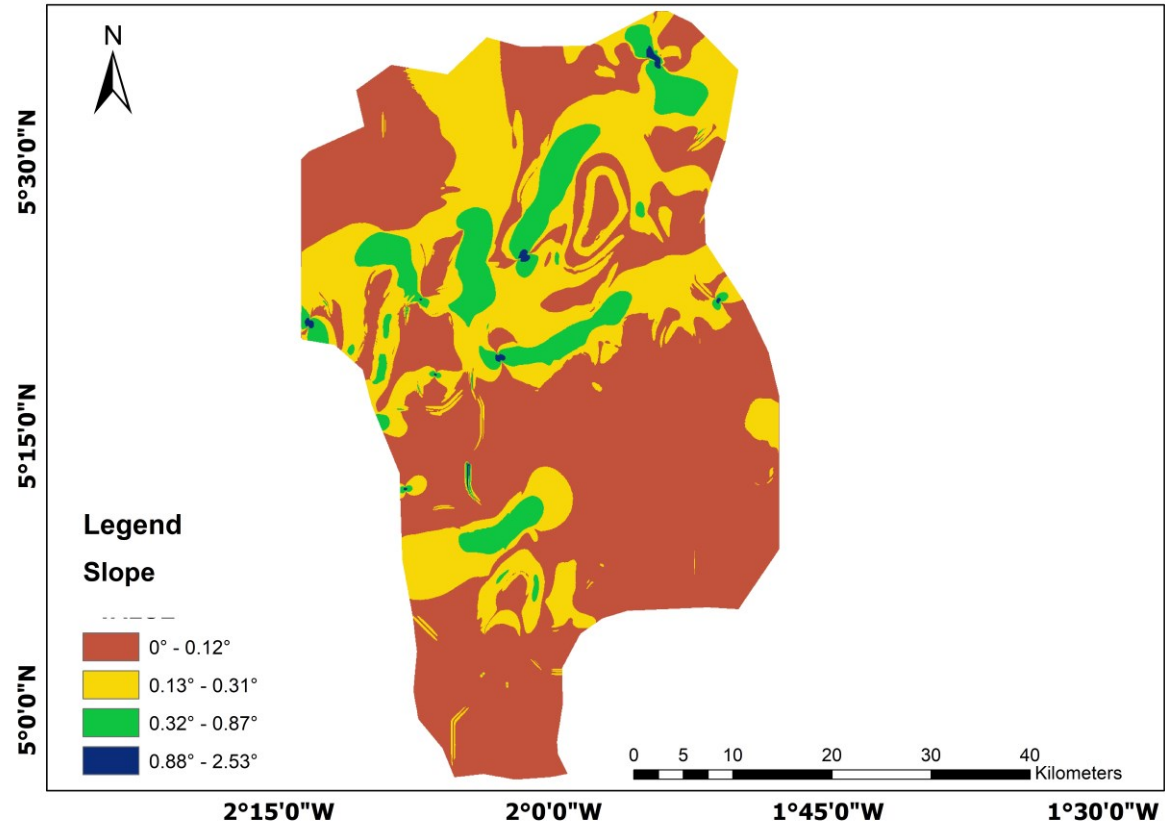
Figure 9. Slope Map
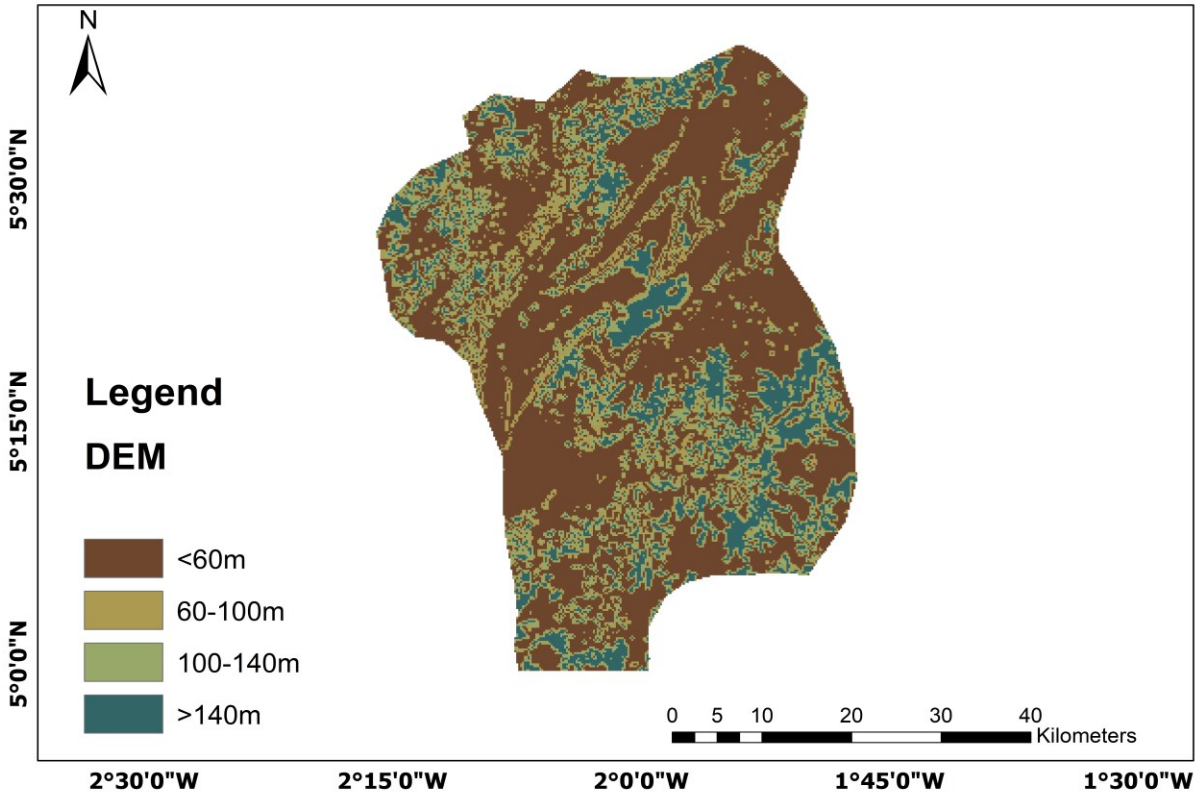
Figure 10. Digital Elevation Map
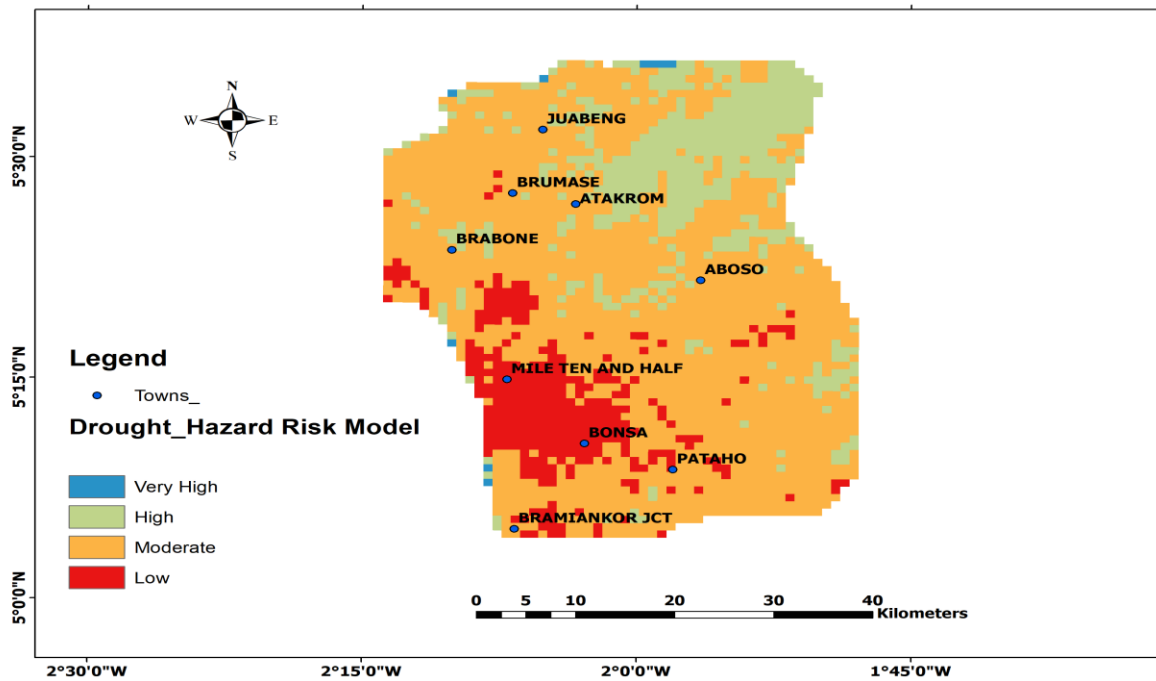
Figure 11. Hydrometeorological drought map

Table 4. Area and Percentage coverage of drought

Description	Area (km²)	Coverage (%)
Very High	8.59	0.33
High	486.78	18.88
Moderate	1764.80	68.46
Low	317.84	12.33
Total	**2578.01**	100

4.2 Discussions

The use of Geographic Information System (GIS) and the Buckley Geometric Mean Model (BGM) have proven to be essential tools in drought analysis. The objective of this study was to generate a map to show the varying levels of susceptibility of the study area to hydrometeorological drought. This was carried out based on a set criterion using the drought model given in Equation 1 in the ArcGIS environment. The BGM was used to calculate the fuzzy weights of the selected criteria. The conventional AHP method could not accurately take care of the uncertainties due to subjective human preferences hence the need for a fuzzy AHP which could accurately reflect the human thinking style (Askin and Guzin, 2007). BGM was obtained by applying fuzziness to the classical Analytical Hierarchy method (AHP) method to deal with the unbalanced scale of judgement. Firstly, a judgement matrix was formed for the pairwise comparison of the cost criteria based on experts' advice given in Equation 2. The Geometric mean was then calculated according to Equation 3. The Fuzzy Geometric Mean is obtained by the summation of the corresponding columns of the obtained Geometric Mean of each criteria using Equation 4. The Weights are then calculated by normalization of the Fuzzy Geometric mean denoted by Equation 5. Figure 3 shows the distribution of

the triangular fuzzy membership method employed for the three-set opinion judgement matrix. A consistency check was carried out to verify the validity of the model. The weighted sum vector is shown in Equation 7. The Eigen vectors obtained by dividing the weighted sum vector by its corresponding weight is denoted by Equation 8. The average of the Eigen vectors is denoted by Equation 9 known as λ_{max}. Equation 10 represents the calculation of the consistency Index for the calculation of the consistency ratio given in Equation 11 using the random inconsistencies. The consistency ratio was 0.093 which implies the weights are consistent. Table 1 represents the classification of the hydrometeorological factors and their corresponding scores. Figure 4 shows the flow chart of the weighted overlay of the cost criteria. The results of the judgement matrix and the Geometric mean set is given in Equation 12. Table 2 and 3 represents the fuzzified weights and Eigen vectors respectively. Figure 5 is a precipitation map of the study area ranging from 246 mm to 370 mm. The map of forest resources and rivers are shown in Figure 6 and Figure 7 respectively. Figure 8 is the map of temperature ranging from 24.5°C to 26.3°C. Figure 9 represents the slope map of the study area grouped into four (4) classes. The highest slope value is 2.53°. The DEM is represented by Figure 10. The highest elevation exceeds 140m. Figure 11 represents the hydrometeorological drought map

generated to show the varying levels of the various areas prone to drought. It was classified into Very High, High, Moderate and Low drought risk areas. Very high drought risk areas contributed 0.3% to the overall drought occurrence, High risk areas recorded 18.9%, areas which can be moderately affected by drought issues were 68.5%, and the least drought risk areas formed 12.3% of the whole area as tabulated in Table 4. Areas which recorded very high risk of droughts are Bogoso, Tarkwa Breman and Eshireso. Those with high risk includes Brabone, Abokyi and Huni Valley. Moderately affected areas are Aboso, Tarkwa, Brumase, Juabeng, Atoabo, Teberebe and Akyempim. The least drought risk areas include Pataho, Bonsa, Bramiankor JCT, Benso and Techiman. The study area has a tropical climate and is one of the areas with a high record of rainfalls in Ghana. Farming is one of the major activities in the study area. Ghana depends on a rain fed agriculture, hence the need to plan ahead so as to safe guard against future famine due to drought. Drought map is very essential in taking various decisions pertaining to climatic conditions. Drought map pre-informs various stakeholders in Meteorological and Climatic studies. This enables them to plan ahead of time, put measures in place to guard against an impending disaster to reduce its effect to the best way possible. Additionally, it will help them to narrow down on areas in high need of drastic measures. This in effect will help to allocate available resources into a very judicious use.

5. Conclusions and Recommendations

Hydrometeorological drought studies are very important and is one of the natural disasters that can have destructive and negative effects such as loss of vegetation, soil erosion, food shortages, power cuts, water shortages in developing countries including Ghana, since the droughts can result into a huge loss of lives and properties. This is due to rapid human inferences, climate changes, and anthropogenic activities influence the occurrence of droughts. Drought modelling helps geospatial professionals, planners, governmental and non-governmental agencies to know about the relative likelihood of future occurrences based solely on the properties of the area which can put forward useful recommendation to minimize its effects. With the advancement of remote sensing, many of the parameters affecting this event can be estimated, calculated and evaluated to their severity level. In this study, modelling of the drought was done based on a combined MCDA, fuzzy logics and GIS approach have been developed and implemented for drought modelling in some parts of the Western south using precipitation data, temperature, water bodies, land cover (forest), and slope of the area under study with soft computing algorithms of AHP and Fuzzy AHP. Fuzzy logics techniques which is one of the best soft computing methods has been able to provide acceptable results in this research. The AHP mathematical decision rule-based concept has been proposed for severity assessment. The combined MCDA, fuzzy logics and GIS approach were based on a probabilistic and objective method for determining the weights and rankings of the causative factors and their

categories for drought occurrences. It was observed from this present study that; the proposed raster optimal map shows some areas of the study area are very high and will suffer future water shortages. The map also depicts different classes of severely of risk from low, moderate and high risk for various categories of droughts. The adopted Fuzzy AHP decision rule is an objective way of assigning weights for drought susceptibility mapping and generating matrices, where a lot of subjectively and bias rules are involved. Also, implementing Fuzzy AHP concept in ArcGIS environment is quite easy as compared to the conventional techniques such as frequency ratio, logistic regression, weights of evidence, the analytical hierarchy process and multiple criteria decision analysis.

The outcome of the present study can be used in taking mitigation measures to minimize the loss in agricultural production, power fluctuations, water scarcity in drought prone areas. The Severity levels It is recommended that; decision makers should use this map in allocating deep boreholes at very high areas. Moreover, the Geological and Survey Department, Survey and Mapping Division Department, and Meteorological Department of the country should produce an up to date rainfall map, aspect map, and geomorphological map of the study area for further studies to review the affected areas and help give relevant solutions to mitigate the menace to prevent loss of lives and properties. However, other machine learning algorithms such as artificial neural networks, generalized regression neural networks, radial basis functions, gaussian approach, decision tree, least square support vector machines, random forest algorithms, genetic algorithms, monte Carlo simulation, multivariate adaptive regression splines, box Jenkins, extreme learning machines, wavelet transform model, ARIMA, Bayesian network model, particle swarm optimization, convolutional neural networks and many others that was not considered in this study can be used in the future research. It is recommended that further research be put in place to add more criteria to enhance the results obtained. Government and other stakeholders in climatic studies and decision making should employ the use of this important tool to their advantage. The Ministry of Climatic and Weather Forecast should engage on mass education of the populace about the various measures to put in place to guard against drought, for instance the over reliance on surface waters could result in hydrological drought. Farmers should be advised and trained on the creation of sand dams and reservoirs to reduce the over reliance on rain fed agriculture. Government should embark on mass irrigation projects on the hard-hit areas so as ensure farming throughout the season.

References

Asante-Annor, A., Konadu, S. A., and Ansah, E. (2018), Determination of Potential Landfill Site in Tarkwa Area Using Multi-Criteria GIS, Geophysical and Geotechnical Evaluation, Journal of Geoscience and Environment Protection, 6, 1-27.

Asiedu, L. and S. Dankwa. (2014), 2010 Population and Housing Census, Unpublished District Analytical Report, Ghana Statistical Service, Ghana, pp.9-10.

Askin, O., and Guzin, O. (2007), Comparison of AHP and Fuzzy AHP for the Multi-Criteria Decision-Making Process with Linguistic Evaluations, Unpublished Technical Report, Istanbul Ticaret Universitesi, Istanbul, Turkey, pp 65-85.

Asklunel, R., and Eldvall, B. (2005), Contamination of Water Resources in Tarkwa Mining Area of Ghana, Unpublished MSc Thesis, Department of Engineering Geology, Royal Institute of Technology, LTh Ekosystemteknk, pp. 1-72.

Aslani, M., and Alesheikh, A. A. (2011), Site selection for small gas stations using GIS, Scientific Research and Essays, 6(15), 3161-3171.

Avotri, T. S. M., Amegbey, N. A., Sandow, M. A., and Forson, S. A. K. (2002), The Health Impact of Cyanide Spillage at Goldfields Ghana Limited, Unpublished Technical Report, Tarkwa, Ghana, pp. 1-15.

Belal, A. A., El-Ramady, H. R., Mohamed, E. S., and Saleh, A. M. (2012), Drought Risk Assessment Using Remote Sensing and GIS Techniques, Arabian Journal of Geosciences, 1-21.

Belayneh, A., and Adamowski, J. (2013), Drought forecasting using new machine learning methods/Prognozowanie suszyz wykorzystaniem automatycznych samouczących się metod, Journal of Water and Land Development, 18(9), 3-12.

Boroushaki, S., and Malczewski, J. (2008), Implementing and extension of the analytical hierarchy process using ordered weighted averaging operators with fuzzy quantifiers in ArcGIS, Computer and. Geoscience, 34, 399-410.

Boye, C. B., Peprah, M. S., and Kodie, N. K. (2018), Geographic Assessment of Telecommunication Signals in a Mining Community: A Case Study of Tarkwa and Its Environs, Ghana Journal of Technology, 2(2), 41-49.

Broekhuizen, H., Groothuis-Oudshoorn, C. G. M., Van Til, J. A., Hummel, J. M. and Ijzerman, M. J. (2015), A review and classification of approaches for dealing with uncertainty in multi-criteria decision analysis for healthcare decisions, Pharmaco Economics, 33, 445-455.

Bunea, A. I. (2019), Drought Risk Assessment by means of Drought Hazard and Vulnerability Indices in Muntenia Region, Riscuri Si Catastrofe, 25, . 73-84.

Chang, T.H. and Wang, T.C. (2009), Using the fuzzy multi-criteria decision-making approach for measuring the possibility of successful knowledge management, Information Sciences, 179(4), 355-70.

Dawson, C., and Wilby, R. (2001), Hydrological modelling using artificial neural networks, Progress in Physical Geography, 25(1), 80-108.

Dodamani, B. M., Anoop, R., and Mahajan, D. R. (2015), Agricultural Drought Modelling Using Remote Sensing, International Journal of Environmental Science and Development, 6(5), 326-331.

Eskandari, S. (2017), A New Approach for Forest Fire Risk Modelling Using Fuzzy AHP and GIS in Hyrcanian Forests of Iran, Arab j. Geosci, 10(190), 1-13.

Ewusi, A., and Kuma, J. S. Y. (2014), Groundwater Assessment for Current and Future Water Demand in the Daka Catchment, Northern Region, Ghana, Natural Resources Research, 1-12.

Firoozi, M.A., Goodarzi, M. and Shirali, R. (2017), Assessment and Potential Survey of Lands in Khuzestan Province using the Buckley Geometric Mean Model and Geographic Information System (GIS). Open Journal of Geology, 7, 234-241.

Fry, J., Xian, G., Jin, S., Dewitz, J., Homer, C., Yang, L., Barnes, C., Herold, N., and Wickham, J. (2011), Completion of the 2006 National Land Cover Database for the Conterminous United States, Photogramm. Eng. And Rem. S., 77(9), 858-864.

Han, P., Wang, P. X., Zhang, S. Y., and Zhu, D. H. (2010), Drought forecasting based on the remote sensing data using ARIMA models, Math Comput Model, 51, 1398–1403.

Hayes, M., Svoboda, M., Wall, N., and Widhalm, M. (2011), The Lincoln Declaration on Drought Indices, Universal Meteorological Drought Index Recommended, American Meteorological Society, 485-488.

Heumann, B. W. (2011), Satellite remote sensing of mangrove forests: Recent advances and future opportunities, Progress in Physical Geography, 35(1), 87-108.

Jamro, S., Channa F. N., Dars, G. H., Ansari, K., and Krakauer, N. Y. (2020), Exploring the Evolution of Drought Characteristics in Balochistan, Pakistan, Applied Sciences, 10(913), 1-15.

Jimenez-Donaire, M. D. P., Tarquis, A., and Giraldez, J. V. (2020), Evaluation of a Combined Drought Indicator and Its Potential for Agricultural Drought Prediction in Southern Spain, Nat. Hazards Earth Syst. Sc., 20, 21-33.

Joe-Asare, T., Peprah, M. S., Opoku, M. M. (2018), Assessment of the Potability of Underground Water from a Small Scale Underground Mine: A Case Study, Ghana Mining Journal, 18(2), 61 - 67.

Keyantash, J., and Dracup, J. A. (2002), The Quantification of Drought: An Evaluation of Drought Indices, American Meteorological Society, 1167-1180.

Kihoro, J., Bosco, N. J. and Murage, H. (2013), Suitability analysis for rice growing sites using a multi-criteria evaluation and GIS approach in Great Mwea Region, Kenya, Springerplus, 2(365), 1-9.

Kim, T.-W., and Valdés, J. B. (2003), Nonlinear model for drought forecasting based on a conjunction of wavelet transforms and neural networks, Journal of Hydrologic Engineering, 8(6), 319-328.

Kortatsi, B. K. (2004), Hydrochemistry of Groundwater in the Mining Area of TarkwaPrestea, Ghana, Unpublished PhD Thesis, University of Ghana, Legon-Accra, Ghana, pp. 1-45.

Larbi, E. K., Boye, C. B., and Peprah, M. S. (2018), A GIS Approach in Optimal Route Selection in the Mining Communities Using the Analytical Hierarchy Process and the Least Cost Path Analysis, 5th UMaT Biennial International Mining and Mineral Conference, pp. GLM 50-62.

Mishra, A. K., and Singh, V. P. (2010), A Review of Drought Concepts, Journal of Hydrology, 1-15.

Mokhtari, R., and Akhoondzadeh, M. (2019), Neural Network Method for Drought Modelling Using Satellite Data, The International Archives of the Photogrammetry, Remote Sensing and Spatial Information Sciences, Volume XLII-4/W18, 2019, Geospatial Conference 2019-Joint Conferences of SMPR and GI Research, 12-14 October, Karaj, Iran, pp. 749-753.

Palmer, W.C. and R.M. White. (1965), Meteorological Drought, Unpublished Technical Report, U.S Weather Bureau, Office of Climatology, Washington, D.C, pp.1-65.

Peprah, M. S., Boye, C. B., Larbi, E. K., and Opoku Appau, P. (2018), Suitability Analysis for Sitting Oil and Gas Filling Stations Using Multi-criteria Decision Analysis and GIS Approach – A Case Study in Tarkwa and Its Environs, Journal of Geomatics, 12(2), 158-166.

Peprah, M. S., Ziggah, Y. Y., and Yakubu, I. (2017), Performance Evaluation of the Earth Gravitational Model (EGM2008) – A Case Study, South African Journal of Geomatics, 6(1), 47-72.

Peprah, M. S., and Mensah, I. O. (2017), Performance Evaluation of the Ordinary Least Square (OLS) and Total Least Square (TLS) in Adjusting Field Data: An Empirical Study on a DGPS Data, South African Journal of Geomatics, 6(1), 73-89.

Seidu, J., and Ewusi, A. (2018), Assessment of Groundwater Quality Using Hydrogeochemical Indices and Statistical Analysis in the Tarkwa Mining Area of Ghana, Journal of Environmental Hydrology, 26, 1-15.

Sharma, L. K., Kanga, S., Nathawat, M. S., Sinha, S., and Pandey, P. C. (2012), Fuzzy AHP for Forest Fire Risk Modelling', Disaster Prevention and Management, 21(2), 160-171.

Wang, P. X., Wan, Z. M., Gong, J. Y., Li, X. W., and Wang, J. D. (2003), Advances in drought monitoring by using remotely sensed normalized difference vegetation index and land surface temperature products, Adv Earth Sci, 18(4), 527–533.

Yakubu, I., Ziggah, Y. Y., and Peprah, M. S. (2018), Adjustment of DGPS Data using artificial intelligence and classical least square techniques, Journal of Geomatics, 12(1), 13-20.

Yalti, S., and Aksu, H. (2019), Drought Analysis of Igdir Turkey, Turkish Journal of Agriculture-Food Science and Technology, 7(12), 2227-2232.

Zadeh, L.A. (1965), Fuzzy sets, Information Control, 8(3), 338-53.

Investigation of flood (waterlog) flow pattern of University Road and Dan Fodio Boulevard in Akoka, Yaba, Lagos, Nigeria

O.G. Omogunloye, O.A. Olunlade, O.E Abiodun, A.I. Moshood and O.A. Babatunde
Department of Surveying and Geoinformatics, University of Lagos, Akoka, Lagos, Nigeria.
Email: gabolushohan@yahoo.com

Abstract: Flooding occurs when a river's discharge exceeds its channel's volume causing the river to overflow onto the area surrounding the channel, known as the floodplain. The increase in discharge can be triggered by several events. The most common cause of flooding (waterlog) is prolonged rainfall. If it rains for a long time, the ground will become saturated and the soil will no longer be able to store water leading to increased surface runoff. Poor drainage system could also make rainwater, not properly channelized, thereby leading to higher discharge levels and floods along the busy road. The study investigated the vulnerability of flood along a route (2.64km) in the study area, alongside its' drainage architecture systems. The route (road) field survey, longitudinal profile and cross sections were carried out. The relative elevation of points along the center line of a road is achieved through longitudinal profile while elevation of points across the center line is achieved through the cross sections. The (X, Y, Z) coordinates, the longitudinal profile of the route and the cross sections across the route, were used to determine the flow direction, flow accumulation, and the flow length using ARCGIS 10.2 and plotting was achieved with the aid of AutoCAD 2012 at a horizontal scale of 1:5000 and vertical scale of 1:100. The study showed that inadequacies in the depth of the two side drainages along the route, blockages by sediments in form of refuse along the drainages, Ngoc and Lalit (2017), played a major role in the ill-free flow of water along the drainages and the resultant over flow of water along the route during heavy downpour of rainfall.

Keyword: Runoff, Flood, Route, Flow, Drainages, Rainfall.

1. Introduction

Before investigation survey can be carried out successfully on flooding, certain factors must be known. A survey begins long before actual data collection starts, Josh et al. (2019) and Firebrace et al, (1915). Some elements which must be considered are: Exact area or location of the survey (University Road, Akoka,Yaba, Lagos.); Type of survey (reconnaissance or standard), scaled to meet standards of map to be produced, (Elissavet et al. 2019 and Kanetkar et al. 1966); Scope of the survey (short or long term); Platforms available (aircraft, satellitesetc.); Support work required (aerial or satellite photography, geodetics etc.); and Limiting factors, (budget, politics, geographic or operational constraints, positioning system limitations, logistics).

Flooding is the unusual presence of water on land to a depth, which affects normal activities (Mohamed et al. 2019). Flooding can arise from Overflowing Rivers (river flooding); Heavy rainfall over a short duration (flash floods); or An unusual inflow of seawater onto land (ocean flooding). Ocean flooding can be caused by storms such as hurricanes (storm surge), high tides (tidal flooding), seismic events (tsunami) or large landslides (sometime also called tsunami), (Addison, 1946).

Rainwater will enter the river much faster than it would if the ground was not saturated leading to higher discharge levels and floods (Sally et al. 2019).

The flood plain investigation along any route (road) demands, the carrying out of proper route survey, in order to determine the cause of flooding, as well as, the creation of a 3D model map (Omogunloye, et al. 2013), that can assist to proffer solution to the flooding (Davis, 1966). Route surveying is one of the aspects of engineering

surveying, and could be pipeline, power-line, underground cable or road survey. Route survey (road) comprises longitudinal profile and cross sections (Clark, 1954). The relative elevation of points along the Centre line of a road is achieved through longitudinal profile while elevation of points across the Centre line is achieved through the cross sections. The two are important to civil engineers and Surveyors to enable him realize the cut area and the fill area depending on the purpose of the road (David, 1973).

The results of the project work are the route, the longitudinal profile of the route and the cross sections across the route. These were plotted with the aid of Auto CAD 2012 at a horizontal scale of 1:5000 and vertical scale of 1:100, (Omogunloye, O. G., et al 2011 and 2012).

At the end of the fieldwork and the plotting of the data, we were able to find out that there were gullies at the Centre of the route which could have been caused as a consequence of erosion that dominates the environment. Also we were able to find out that the route at the beginning is at depression and as we progressed towards the end of the route, the route tended to be elevated.

This study is to acquire information about the nature of the surface of the flood plain along the University Road Akoka, Yaba, Lagos Nigeria and produce a topographical map in 3D depicting the longitudinal profile and cross-sectioning of the various drainage system (canals and gutters) affecting the different part of the study area as well as analyzing changes that may have taken place over the past immediate years, (Jingwei and Yixian, 2020; Kanetkar et al. 1966 and Omogunloye, et al. 2017) and to proffer a model that could be adopted in order to manage and provide a lasting solution to forestall a reoccurrence.

1.1 Study Area

The Study Area (Figure 1) is the route along the University of Lagos road within Akoka, Yaba, Lagos, Nigeria. The length to be covered is about 2.64km along this route line. In this study, a longitudinal profile of the route was obtained by picking heights of points at 25m interval along the Centre line of the route. The coordinates of the points along the route, the heights of the points and the cross sections at 25m intervals were obtained simultaneously (Davis, 1966). The plotting of the route was divided into five segments of 1.115km each for easy plotting and delineation of notice-able features.

This route is one of the longest routes to Yaba axis, between the University of Lagos main gate and the Herbert Macaulay road. Data acquisition was carried out on this route; there are two big drainages on both sides of the road; there is usually heavy traffic at peak period as well as persistent flooding (waterlog), when there is a slight and heavy down pour of rain, resulting most often to pot holes formation along the road due to waterlog occupation and continuous usage of the road by vehicles. Thus, there is a need for this study to ameliorate the condition of the road for perfect flow of traffic.

Scope of Project comprises: Acquiring the base map of the area of study, showing clearly all features of this route; Leveling of both sides of the road at a 25m chainage to determine the relative elevation (height) of the route; Position fixing of the leveled points with GPS; Locating the controls along the route at intervals in other to check the accuracy and consistency of the work done so far; Mapping of the study area using total station instrument; Data processing, analysis and presentation.

2. Research Methodology

The methodology employed for this study is the Conventional Ground Survey method (Figure 2) (Ewing et al. 1970). The surveys were carried out using Leica Total Station for traversing, leveling technique (leveling instrument), while a Differential Global Positioning System (DGPS) was used for the confirmation and establishment of the accuracy of both the starting and the ending survey controls stations. The procedures and processes applied are discussed below.

2.1 Instrument Test

Total Station Instrument: The Leica Total Station Instrument used for this study was tested for collimation and index errors. Also the battery was checked to ensure that the voltage was sufficient (SURCON, 2003). The result showed that the instrument was in good working condition.

Leveling instrument: The Level instrument used for this project was tested for collimation and index errors. The result showed that the instrument was in good working condition.

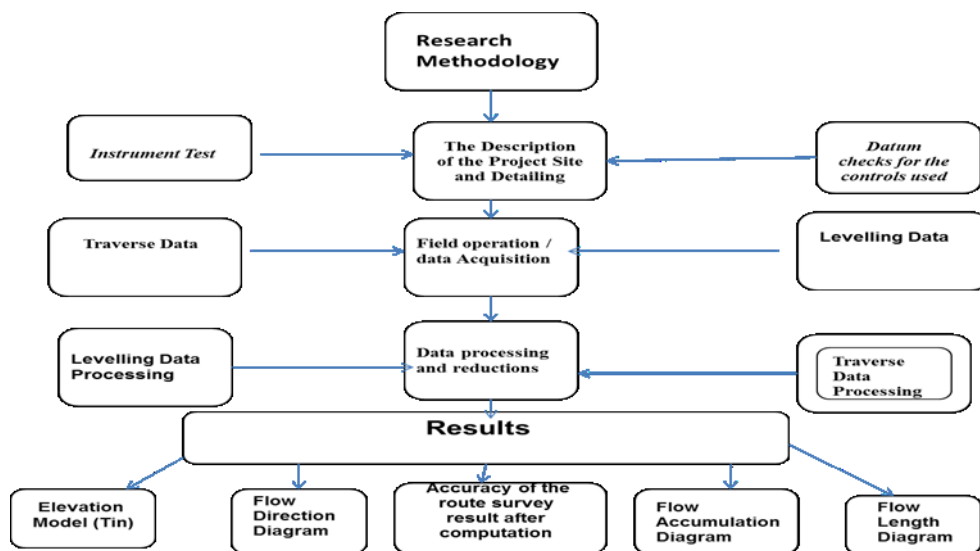**Figure 1. Base Map of the Study Area**

Figure 2. Research Methodology

2.2 Datum checks for the controls used
The control used (GME 04 & 05) were checked to ascertain its stability or displacement from its original position (Torge, 1991 and Omogunloye et al. 2017). At the end of the checks, it was found to be stable and intact in its original position,

2.3 Instrument / Materials used are
The instruments used for the study are made up of both Hardware and software:

Hardware instrument used are: 1 no of Total station (Leica TS 06) with accessories; A differential GPS with accessories; A level instrument with accessories; Leveling staff; Marker (paint); Reflector; 1 No. Plumb bob; 1 No. Linen tape (100m); Field books; Nail and bottle corks; A gallon of gloss paint; Brush; HP Computer System (Laptop); 32GB Flash drive; and Hp Laser Jet Printer.

Software used are: Auto CAD software for plotting; Google Earth Pro; Arc MAP 10.2; Suffer 15; Microsoft office 2012 (Word, Excel, Power-Point); and Notepad

2.4 The Description of the Project Site and Detailing.
The project site is a route along the University road from UNILAG Senate junction through the UNILAG main gate to UNILAG junction Point, as shown in Figure (1).The project started on a control Points, GME 04 and GME 05; the project site forms a "T" junction with Herbert Macaulay Way. The road comprises of two segments and four lanes. The chainage of the centre line of the road starts from the junction adjacent to UNILAG senate building at 25m interval, the cross section chainage was measured 9m across to both left and right of the centre line. The road surface is relatively flat with some certain undulations as seen in all the longitudinal profiles in Figures (3, 4 & 5).

The highest point was recorded at a chainage 2+100m, with a height of 11.946m above the reference datum. The study area terminates at UNILAG junction, the traversing was closed on the known control beacon marked SUG 04,

while the azimuth observation was closed on the established control marked, SUG 05.

2.5 Field operation / data Acquisition
Traversing method was adopted to obtain the horizontal alignment of the route along the Centre line at the specified interval of 25m. Both the traversing and longitudinal data acquisitions were carried out simultaneously. The two field operations were closed on established pillar: SUG 04 and SUG 05. Acquired Data (X, Y, Z) coordinates of points was stored in the Total Station instrument for the traversing observation, while for that of the leveling, the heights were recorded in a field book, and the processing of the data was done in the office. An estimated length of about 2.64Km was covered.

2.6 Data processing and reductions
Data processing is an intermediate stage between fieldwork and Result presentation. At this stage, all the raw data obtained from the field measurements were refined to a more usable form to make them useful for other purposes required by the study, Thomas (2010). Also all the redundant data were filtered at this stage, Udabhor (2014).

2.7 Traverse Data Processing
Using the X, Y and Z data acquired from the Total Station, an AutoCAD Script file was created in this format "_text Easting's, Northing's text height

Height Point ID" as a layer, and the points where connected according to the field book. Layers were also created for other features in the AutoCAD. The X, Y and Z coordinates of points were plotted using the AutoCAD Civil 3D 2017 software and a map of the study area was created in digital format.

2.8 Levelling Data Processing
Using the data acquired from Digital Level Instrument, the heights of the corresponding points were computed using the Height of Plane Collimation method of levelling technique. A digital format level profile of the centre line of the route was created using the AutoCAD Civil 3D 2017 software.

3. Results

3.1 Accuracy of the route survey result after computation

A Linear accuracy of 1:23,000 for a distance of 2.64Km was obtained against the minimum accuracy (1:3000) required of a third-order job in accordance with SURCON specifications on large scale cadastral and engineering survey in Nigeria, Ewing et al, (1970).

At the end of project, SUG 04 was closed on. The coordinates of the established SUG 04 using DGPS and the coordinates of the measured SUG 04 as the closing control are given in the table 1:

The minimum accuracy of third-order job required in accordance with SURCON specifications on large scale

cadastral and engineering survey in Nigeria is 1:3000. The formulae used in calculating the linear accuracy was:

$$\frac{1}{\sqrt{\frac{\Delta N^2 + \Delta E^2}{\sum D}}}$$

Where

ΔN = Misclosure in the Northing, between coordinates of the closing control and Observed.

ΔE = Misclosure in Easting, between coordinates of the closing control and the Observed.

$\sum D$ = Summation of distances within the network

$$\frac{1}{\sqrt{\frac{-0.001^2 + 0.002^2}{2640}}}$$

Table 1. The misclosures of closing controls

	EASTINGS(m)	NORTHINGS(m)
COORDINATES OF ESTABLISHED SUG 04 (DGPS)	540821.222	720233.804
COORDINATES OF MEASURED SUG04(Total station)	540821.223	720233.806
MISCLOSURE	-0.001	+0.002
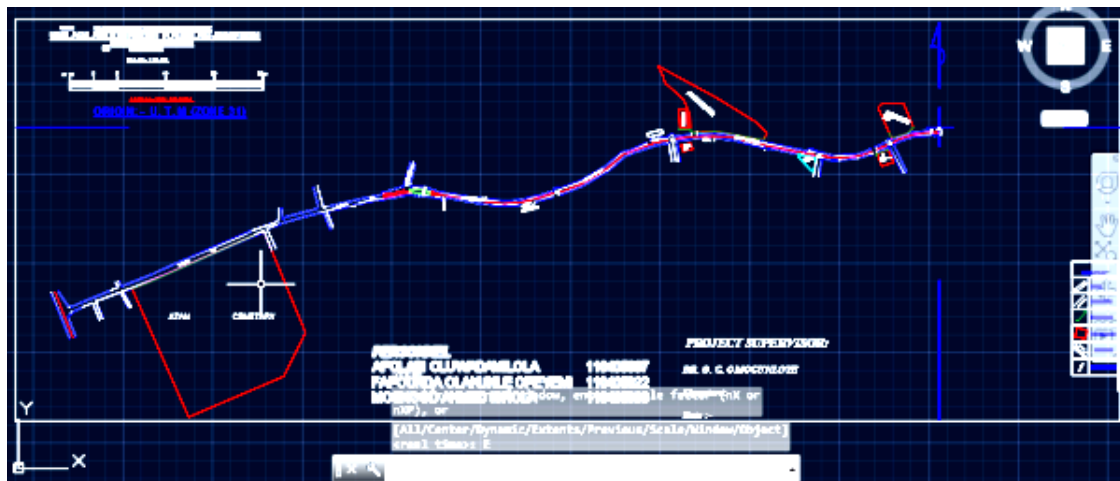
Figure 3. Traverse Network (Autocad 2012)
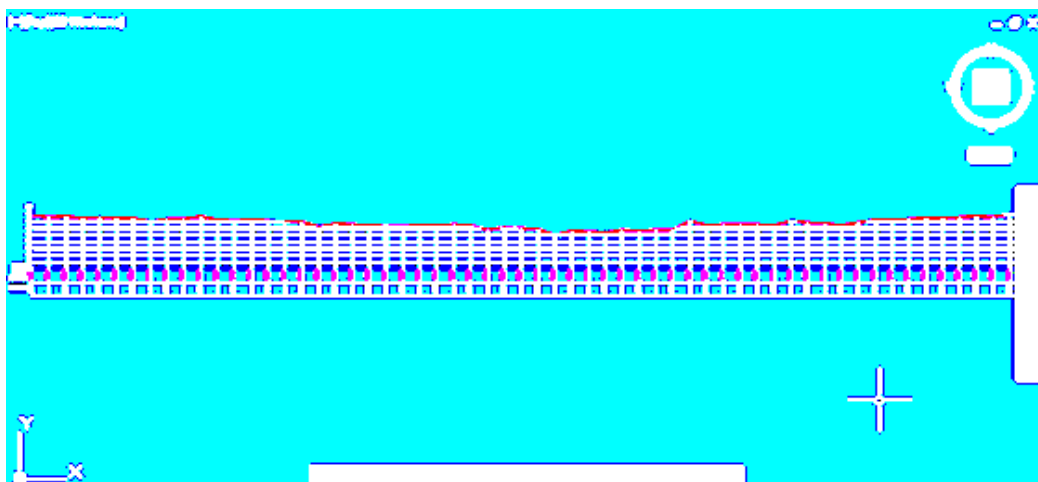
Figure 4. Leveling Profile (Autocad, 2012)

3.2 Elevation Model (Tin)

A Triangulated Irregular Network (TIN) surface was generated from surface source measurements on a point feature, which contain elevations information. Points were used as spot locations of elevations data, each color showing the elevation range of each region. The highest elevation is in red color which is around the Abule-Oja area.

3.3 Flow Direction

This tool takes the kriging surface as input and outputs a raster showing the direction of flow out of each cell (Figure 6). There are eight valid output directions relating to the eight adjacent cells into which flow could travel. This approach is commonly referred to as an eight-direction (D8) flow model (Addison, 1946).

This function is used to identify the water flow direction on a surface, or identify the steepest descending direction of each cell in a DEM (Figure 7) (Omogunloye et al. 2013). The 8 cells surrounding the central cell are coded by the powers of 2. From the right of the central cell, the cells are coded as 2 to the power of 0, 1, 2, 3, 4, 5, 6, 7, that is 1, 2, 4, 8, 16, 32, 64, 128, thus represent the water flow direction of the central cell to be east, southeast, south, southwest, west, northwest, north and northeast, as the image below shows.

Every central cell's water flow direction is determined by one of the eight values. For example, if a central cell's water flow direction is west, it will be given the value 16 (Omogunloye et al. 2012).
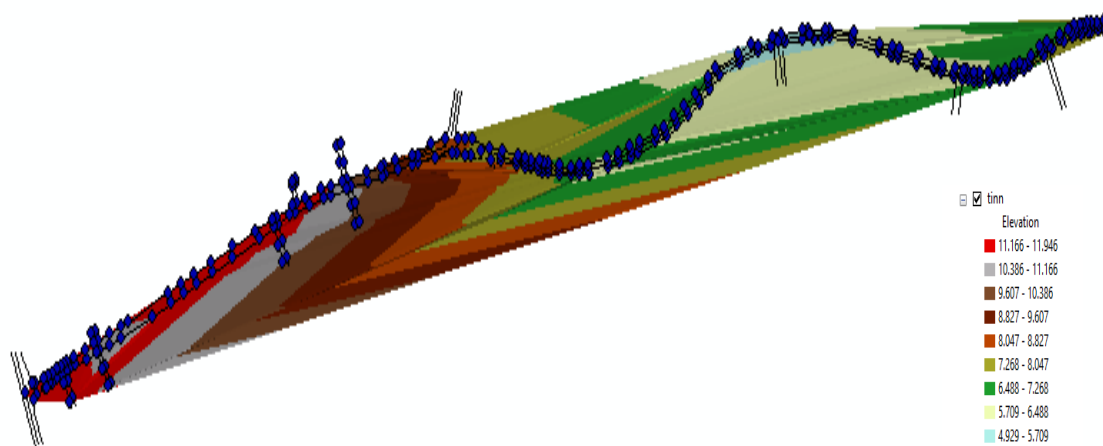
Figure 5. Showing the Triangulated Irregular Network of the Tarrain
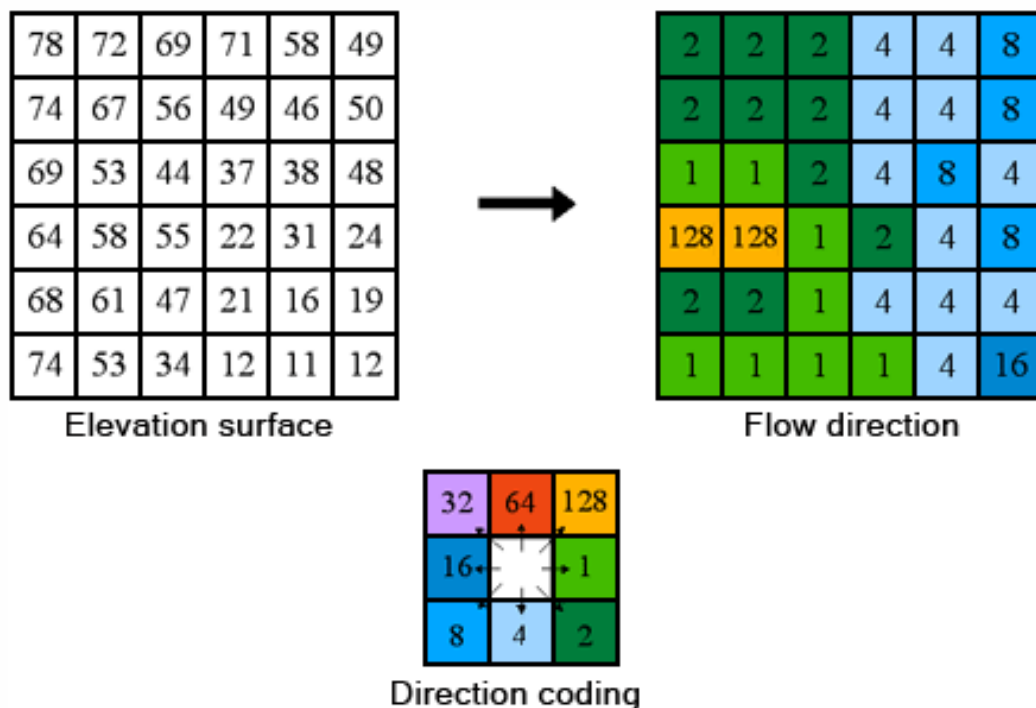
Figure 6. Direction Coding
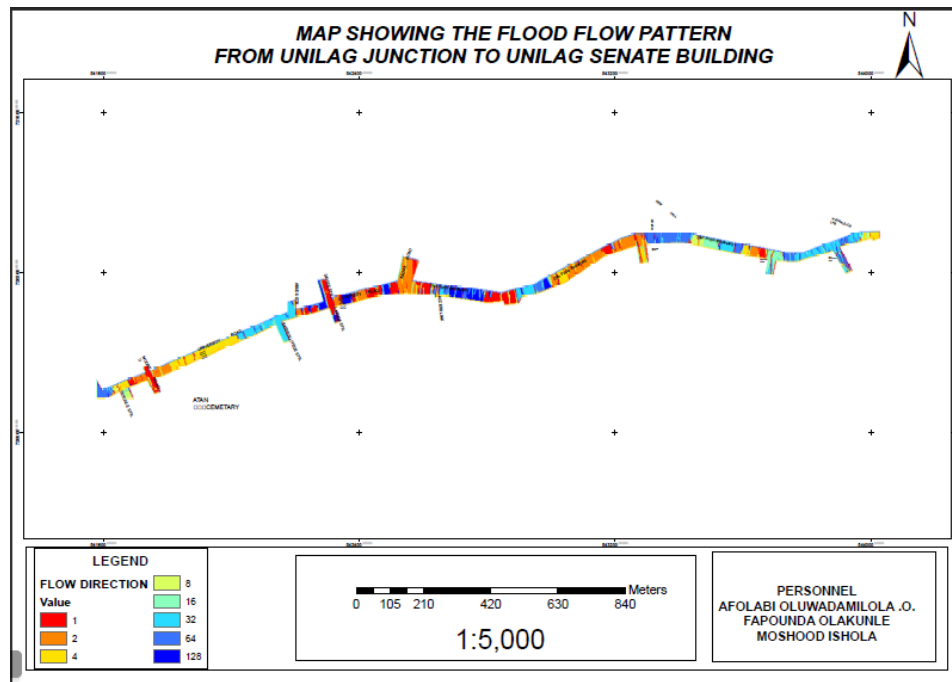
Figure 7. Showing The Flow Direction

3.4 Flow Accumulation
This function is used to create a network to show accumulated flow into each cell, Figures (8, 9, 10, 11 & 12). The basic thoughts of Flow Accumulation is supposing that there is one unit of water in each cell of the raster data, and calculate the accumulated flow of each cell through the Flow Direction Map. Gmn represent the cell at row m, column n. G42 has 0 unit of water since there is no cell which flow into it, G32 has 3 units of water since it receives water from G41, G31 and G21. G22 has 1 unit of water since it receives water from G11. G33 receives water from three cells: G42, G32 and G22, 3+3+G42+G32+G22=7, therefore it has 7 units of water.

- The result of Flow Accumulation is a raster of accumulated flow to each cell, as determined by accumulating the weight for all cells that flow into each down slope cell.
- Cells of undefined flow direction will only receive flow; they will not contribute to any downstream flow. A cell is considered to have an undefined flow direction, if its value in the flow direction raster is anything other than 1, 2, 4, 8, 16, 32, 64, or 128.
- The accumulated flow is based on the number of cells flowing into each cell in the output raster. The current processing cell is not considered in this accumulation.
- Output cells with a high flow accumulation are areas of concentrated flow and can be used to identify stream channels.
- Output cells with a flow accumulation of zero are local topographic highs and can be used to identify ridges.
- If the input flow direction raster is not created with the Flow Direction tool, there is a chance that the defined flow could loop. If the flow direction does loop, Flow Accumulation will go into an infinite loop. Flow Accumulation will go into an infinite loop and never finish.

The Flow accumulation operation performs a cumulative count of the number of pixels that naturally drain into outlets. The operation can be used to find the drainage pattern of a terrain.
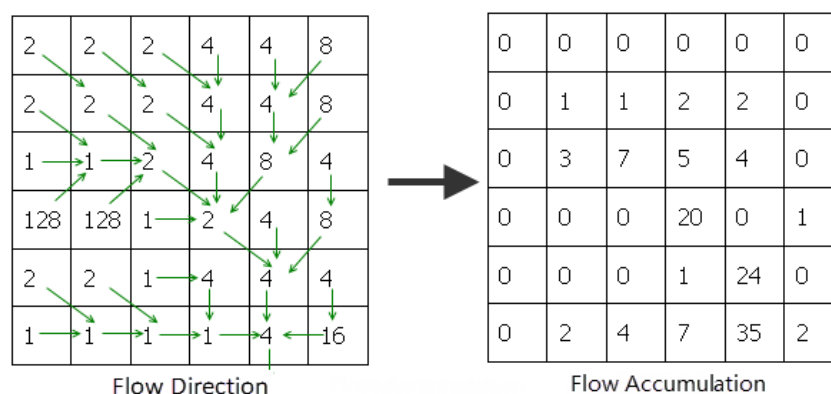
Figure 8. Flow Direction to Flow Accumulation

Calculating flow directions
from a DEM
(steepest slope)

Output flow direction map

58	52	55	53	56	58
55	40	42	45	51	55
48	33	35	33	48	52
33	23	28	27	25	38
17	17	17	22	17	12
12	10	15	18	16	14

?	?	?	?	?	?
?	S	S	S	SW	?
?	S	SW	S	S	?
?	S	S	SE	SE	?
?	S	SW	E	E	?
?	?	?	?	?	?

Figure 9: How to Calculate Flow Direction

Calculating flow
accumulation

Output flow accumulation
map

1	1	1	1	1	1
1	1	1	1	1	1
1	2	2	3	1	1
1	5	1	4	2	1
1	6	2	1	6	9
1	9	1	1	1	1

1	1	1	1	1	1
1	1	1	1	1	1
1	2	2	3	1	1
1	5	1	4	2	1
1	6	2	1	6	9
1	9	1	1	1	1

Figure 10. How to Calculate Flow Accumulation
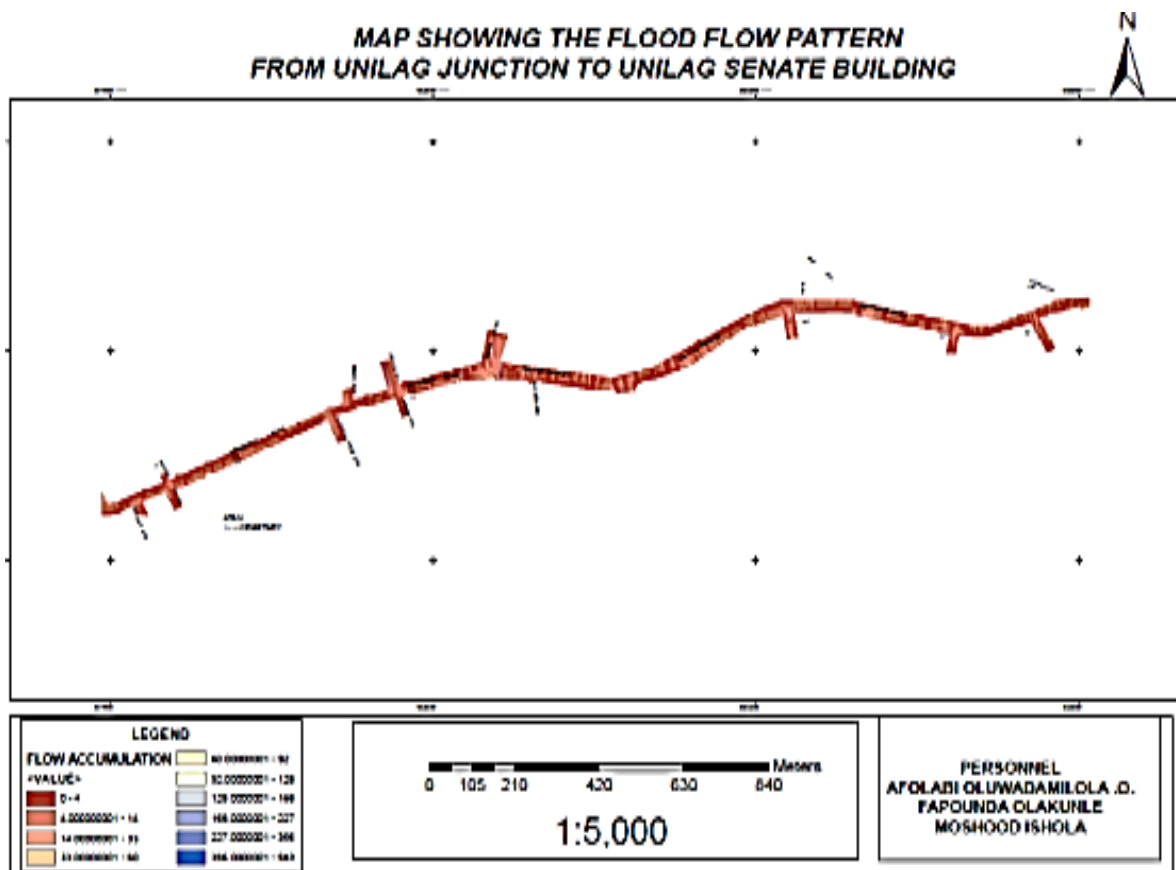
Figure 11. Showing the Flow Accumulation

3.5 Flow Length
Every cell in a raster has a flow path which passes it. Flow Length is used to calculate the length between each cell and the outlet (or source) along the flow path, the result is a Grid dataset. Flow Length is commonly used for flood calculation, Omogunloye et al (2011), water flows can be affected by factors such as slope, soil moisture and vegetation cover, weight dataset is needed to model these factors, Kanetkar et al, (1966). When it rains, a drop of water landing somewhere in the basin must first travel some distance before reaching the outlet. Assuming constant flow velocities (an assumption we will relax later) the pixel with the greatest flow length to the outlet represents the hydrological most remote pixel. Its flow length divided by the flow velocity represents a representative lag time for the basin. The lag time quantifies how long before the entire basin is contributing to flow at the outlet and is a representative scale of the basin.

In Flow Length Analysis, Flow Direction Data provides the flow direction of streams; this dataset can be created through Flow Direction Analysis. Weight dataset defines the impedance of each cell in the raster.

There are two kinds of Flow Length Analysis:
- Upstream: Calculate the length of the longest flow path between each cell and its source cell on the watershed boundary.
- Downstream: Calculate the length of the flow path between each cell and its corresponding outlet on the edge of the raster.

Each colour showing the flood flow pattern of the route. From regions with low flood pattern to regions with high flood flow pattern.

The results obtained were analysed in detail. The following are the inferences drawn from the analysis of the results;
- Studying the flood flow pattern shows that areas with high elevation height tend to have low flood, thus causing water to tend to flow to places with low height elevation.
- The elevation model also shows that the road is at the same height with the drainages coupled with the fact that there is no hole in the drainages to allow the flow of water from the road.
- Also, the regions with low height elevation drainages are no longer functioning in other to channel the flow of water into the neighbourhood canal, this tend to cause stagnant water around the canal region.
- All things being equal, some regions in the map are also liable to more flooding in the future, such as the front of the emerald hall (Akoka Road).

It should be noted that this undulation is not primarily the cause of flooding and water log on this route, rather after proper investigation, it was noticed that flooding on this route is cause due to the blockage of the drainages (canal, gutter) along the route.

3.6 Result and Accuracy of the controls used
Table 2 and 3 shows the accuracy of the controls used
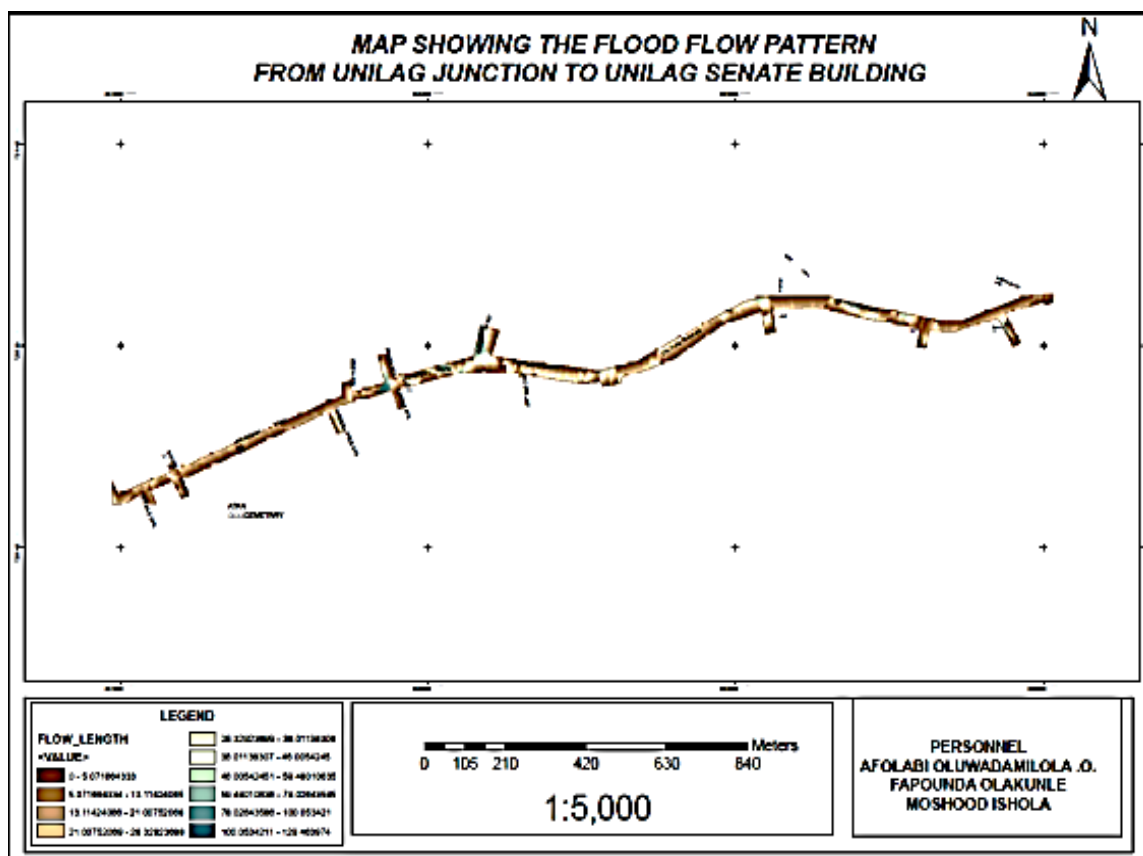
Figure 12. Showing The Flow Lenght

Table 2. Accuracy of the controls

CONTROL POINTS USED				
Name		Eastings (m)	Northings (m)	Orthometric height (m)
GME 04	Components (m)	543891.542	720583.891	8.165
	95 % Error	0.000	0.000	0.000
	Status Control	Fixed	fixed	fixed
	Linear accuracy	1:100,000		
Name		Eastings(m)	Northings(m)	Orthometric height(m)
GME 05	Components (m)	544028.845	720627.622	7.965
	95 % Error	0.000	0.000	0.000
	Status Control	Fixed	fixed	fixed
	Linear accuracy	1:100,000		

Table 3. The coordinates and accuracies of the starting control points used for the project

NAME		EASTING (m)	NORTHING (m)	ORTHOMETRIC HIEGHT(m)
SUG 04	Components(m)	540821.222	720233.804	8.889 processed (static)
	95 % Error	0.000	0.001	0.004
	Status Control	processed (static)	processed (static)	processed (static)
	Linear Accuracy	1:75,000		
SUG 05	Components(m)	540875.703	720234.032	8.540
	95 % Error	0.002	0.001	0.003
	Status Control	processed (static)	processed (static)	processed (static)
	Linear Accuracy	1:33,000		

4. Conclusions

Engineering survey is an essential aspect of Geo-Information and a must for all engineering design and construction. Flood assessment, monitoring and prediction are crucial for environmental sustainability, particularly within areas traversed by water logging. This study has shown the need to compute flood (waterlog) flow analysis and the usefulness of geographic information system (GIS) as a spatial tool for inundation mapping within water logged area. Also, the study has demonstrated the importance of depicting the frequency of occurrence of flood to the production of the aforementioned GIS-based water logged zone mapping.

However, one of the most challenging issues in this study is the choice of suitable flow length analysis. This challenge has been surmounted in this study with

simultaneous examination of two established and widely used methods of upstream and downstream flow length techniques in GIS.

4.1 Recommendations
i.   The government should ensure that some personnel are put in charge of proper cleaning of drainage.
ii. Also the personnel should do a monthly check on the status of the drainage and canal, due to unwanted plants growing around this canal which also facilitate stagnant water and flood along this route.
iii. The drainages should be reconstructed in other to have a deeper drainage for proper channelling of water.
iv. The Government should setup monitoring agency to check indiscriminate deposit of waste into the drainages.
v.   Regular Engineering surveys should be encouraged by both the Government and the Department in charge of the proper management and maintenance of the route and its environment.

References
Addison, H. (1946). Hydraulic Measurements, 2nd edition, Chapman & Hall Ltd., London, pp 152.

Clarke, D. (1954). Plane and Geodetic Surveying, Vol. 1, 4th edition, Constable Publishers, London.

Clarke, D. (1973). Plane and Geodetic Surveying for Engineers, Vol. II Sixth Edition, John Wiley Publishers, USA.

Davis, R., Foote, F. and Kelly, J. (1966). Surveying, 5th edition, McGraw-Hill, New York.

Firebrace, F. and Veale, C. J. (1915). Surveying, Part 1, 11th edition, Government press, Allahabad.

Elissavet, F., Ioannis, M. and Evangelos, B. (2019). Flood vulnerability assessment using a GIS-based multi-criteria approach—The case of Attica region, https://doi.org/10.1111/jfr3.12563.

Jingwei, H. and Yixian, D. (2020). Spatial simulation of rainstorm water logging based on a water accumulation diffusion algorithm, Published online: 06 Jan 2020, pp 71-87.

Josh, W., Jillian, C. L., Amanda, S. and Mofakkarul, I. (2019). Barriers to the uptake and implementation of natural flood management: A social-ecological analysis, Nottingham Trent University; NTSU Green Leaders; Trent Regional Flood and Coastal Committee, https://doi.org/10.1111/jfr3.12561.

Kanetkar, T.P. and Kulkarni, S. V. (1966). Surveying & Levelling, Part 1, 22nd edition, A.V.G. press, India.

Ewing, C. E. and Mitchell, M. M. (1970). Introduction to Geodesy Published by American Elsevier Company, Inc, New York.

Mohamed, A. et al. (2019). Flash flood risk assessment in urban arid environment: case study of Taibah and Islamic universities' campuses, Medina, Kingdom of Saudi Arabia, Geomatics, Natural Hazards and Risk, 10(1), Published online.

Ngoc, D. and Lalit, K. (2017). Application of remote sensing and GIS-based hydrological modeling for flood risk analysis: a case study of District 8, Ho Chi Minh city, Vietnam, 1792-1811

Omogunloye, O. G., Ipadeola, A. O., Shittu, O. G. and Ojegbile, B. M. (2017). Application of Iterative Weighted Similarity Transformation (IWST) Deformation Detection Method Using Coordinate Differences From Different Observational Campaigns, Nigerian Journal of Surveying & Geoinformatics, Peer Review Report-NJSG, 5(1), 61 – 75.

Omogunloye, O. G., Oladiboye, E. O., Quadri, J. A. and Omogunloye, H. B. (2013). Determination of Spot Heights of the University of Lagos Campus, Journal of Environmental Science and Resource Management, 5(1), 97- 110

Omogunloye, O. G. and Ayeni, O. O. (2012). Geospatial Analysis of Hotels in Lagos State with Respect to Other Spatial Features, Research Journal in Engineering and Applied Sciences 1(6), Emerging Academy Resources, (ISSN-2276-8467), RJEA, 1(6), 393 – 403.

Omogunloye, O. G., Olaleye, J. B., Akande, S. H. and Adekoya, O.O. (2011). A GIS Analysis for courier companies in Lagos state (a case study of all Local Government area), Journal of Geomatics, Indian Society of Geomatics (ISG), 5(1), 47 – 51.

Sally, B., Matthew, P. W., Robert, J. N,, Ali, S., Zammath, K., Jochen, H., Daniel, L. and Maurice V. M. (2019). Land raising as a solution to sea-level rise: An analysis of coastal flooding on an artificial island in the Maldives, https://doi.org/10.1111/jfr3.12567.

Surveyors Council of Nigeria (SURCON) (2003). Specifications for large scale cadastral and engineering survey in Nigeria.

Thomas, F. (2010). History of Mathematical Astronomy. University of New Brunswick

Torge, W. (1991). Geodesy (3rd Edition), Published by de Gruyter, New York.

Udabhor, G A. (2014). Potential Theory and Spherical Harmonics Lecture Note, Department of Surveying and Geoinformatics, University of Lagos.

Past and future stream flow simulations in Narmada river basin using conceptual stream flow model

P K Gupta[1*] and R Maity[2]
[1]Space Applications Centre, ISRO Ahmedabad
[2]Department of Civil Engineering, IIT Kharagpur, West Bengal
*E-mail: pkgupta@sac.isro.gov.in

Abstract: In this study, a conceptual stream flow model, which works on the system concept of the watershed, has been applied over Narmada river basin for stream flow simulations. This model represents all important hydrological process of watershed. Satellite data such as ASTER-DEM, Landsat and AWiFS along with other ancillary data like IMD rainfall, RCM rainfall projections and stream flow observations were used. Calibration and validation of the model is carried for five major sub-basins within Narmada basin using montly stream flows. It is found that model performance was satisfactory for monthly river flow simulations. Model parameters for future scenario are projected through the historical changes and attributed to the land use / land cover change. Results of streamflow magnitudes for past (1983-84, 1997-98, 2008-09) and future (2080) scenarios indicates that the streamflow values are increasing for early monsoon period whereas it is decreasing for late monsoon period.

Keywords: Conceptual model, Stream flow, Narmada basin, Climate projection, LULC

1. Introduction

In hydrology stream flow plays an important role in establishing some of the critical interactions that occur between physical and socio-economic processes including population dynamics, land use transformation and agricultural practices closely interact with and greatly affect hydrological processes, such as spatio-temporal variation of rainfall, eco-hydrological modification and stream flow variation and so on. Surface hydrology and hydro-climatology are the field that encompasses all surface waters of the globe (overland flows, rivers, lakes, wetlands, estuaries, oceans, etc.) and establish link to different climatic information. River basin hydrology that deals with the integration of hydrologic processes sub-basin scales to determine influence by combined process of surface hydrology and hydro-climatology as well as climatic influences.

Mathematical models are fundamental to water resources assessment, development, and management. They are, for example, used to analyze the stream flow variation, reservoir system operations, water distribution systems, water use and a range of water resources management activities. Hydrologic phenomenons are complex and difficult to understand fully. However, in the absence of knowledge they may be represented in a simplified way by means of the system concept. A system is a set of connected parts that form the whole. The objective of hydrology system analysis is to study the system operation and predict and/or simulate its output. A hydrologic system model is an approximation of the actual system; its inputs and outputs are measurable hydrologic variables and its structure is a set of equations linking the inputs and outputs. Central to the model structure is the concept of a system transformation (chow, 1988). However, due to the high complexity it is not possible to describe some hydrologic processes with exact physical laws. By using the system concept, effort is directed to the construction of a model relating inputs and outputs rather than to the extremely difficult task of exact representation of the system details, which may not be significant from a practical point of view or may not be known. Nevertheless, knowledge of the physical system helps in developing a conceptually clear model.

Land use change is an important characteristic in the runoff process that affects infiltration, erosion, and evapotranspiration (Fu et al., 2009; Garg et al. 2017). Due to rapid development, land cover is subjected to changes causing decrease in the soil infiltration rate and consequently increase in the amount of runoff disturbing the hydrological balance (Kosmas et al., 1997; Brath et al., 2006). Deforestation, urbanization, and other land-use activities can significantly alter the seasonal and annual distribution of runoff (Dunne 1978; Wagner et al. 2013).

The conventional methods of detecting land use changes are costly and low in accuracy. Remote sensing technique, because of its capability of synoptic viewing and repetitive coverage provides useful information on land use dynamics. The changes in land use due to natural and human activities can be observed using current and archived remotely sensed data. There is a need to investigate the relationship between the landuse change and the runoff water availability (Saddique et al. 2019b). Hydrological modeling is a powerful technique of hydrological system investigation for the management of water resources (Seth et al., 1999; Xia et al., 2012; Li et al. (2018)). With advances in computational power and the growing availability of spatial data, it is possible to accurately describe watershed characteristics when determining runoff response to rainfall input (kite and piteroniro, 1996; Singh and Woolhiser 2002). Using geographic information system (GIS) and remote sensing techniques, we can enumerate various interactive hydrological processes considering spatial heterogeneity (Mohan and Shrestha 2000). In the current research work past and future stream flow modeling carried out by taking into account change in model parameters induced due to changes in different land use categories.

2. Study Area

Narmada is the largest west flowing river of Indian peninsula. The River is an inter-state river draining a large area in Madhya Pradesh, Maharashtra and Gujarat. It originates from Maikala ranges at Amarkantak in Madhya Pradesh at an elevation of 900 m and flows westwards over a length of 1312 km before draining into the Gulf of Cambay. The basin lies between east longitudes 72° 32' and 81° 45', and north latitudes 21° 20' and 23° 45'. River basin is bounded on the north by Vindhyas, on the east by the Maikala range, on the south by the Satpuras and on the west by the Arabian Sea. The basin has an elongated shape almost like a thin ribbon with total catchment area of 98796 km2, about 87% of catchment lies in Madhya Pradesh, 2% in Maharashtra and 11% in Gujarat (Fig. 1). The climate over the basin can be classified as humid tropical. Extreme hot and cold events are experienced over the basin. The temperature ranges from 8° C to 42°C. The range of daily evaporation rates is observed between 1 mm to 9 mm in winter months (October to March), and between 6 mm to 28 mm in summer (April to June) (Gupta and Chakrapani, 2005). Annual rainfall depth over the basin ranges from 80 cm to 160 cm with the basin average of 118 cm. Over 85 % of rainfall takes place in the period of active south west monsoon (July to September). As the major portion of Narmada catchment (Upper and Middle reaches) is situated on leeward side of the Western Ghats, the intensity and rainfall depths are moderate over the catchment leading to smaller flood discharges. Monsoon disturbances originating from Bay of Bengal mostly travel from east to west, parallel to Narmada basin over central India. Very large volumes of floods are then observed in Narmada, when flood wave from the upper reaches and heavy rainfall in the middle or lower reaches of the river travel together resulting in severe floods in lower reach (Dhar and Nandargi, 2003). The monsoon discharge in Narmada ranges from 48 % to 78% of total annual flow at various locations in the basin (Gupta and Chakrapani 2005). But it is also observed that there is significant stream flow in Narmada, at selected locations in non-monsoon periods also and can be attributed to groundwater contribution from raised ground water tables during monsoon months (CGWB, 2004).

3. Data and Method

Landsat 1 MSS (multi spectral scanner) images with spatial resolution of 57 m are used for the LULC map of 1972 whereas AWiFS images with 56 m spatial resolution are used to prepare LULC map of year 2004.

Topography is defined by a DEM that describes the elevation of any point in a given area at a specific spatial resolution. In this study, 30m resolution ASTER DEM data were used. The ASTER GDEM was download from Earth Remote Sensing Data Analysis Center (ERSDAC) at: www.gdem.aster.ersdac.or.jp. The DEM is used to delineate the sub-catchments and to analyze the drainage patterns (Fig.1). For delineation of sub-basin, a pour point of a stream is selected and the cells contributing the flow to that stream are marked as a sub-basin. Sub-basin

parameters such as slope gradient, slope length of the terrain, and the stream network characteristics such as channel slope, length, and width are derived from the DEM. The gridded (1^0 X 1^0 Lat/Long) daily rainfall data from Indian Meteorological Department (IMD) for Narmada river basin is used. The data used for analysis is of the year 1984-1987 and 1995-1998. The gridded (0.1^0 X 0.1^0 Lat/Long) daily rainfall data from Climate Prediction Centre (NOAA, ftp.cpc.ncep.noaa.gov/fews/S.Asia) for Narmada river basin was downloaded. The data used for analysis is of the year 2006-09. The gridded (0.4425^0 X 0.4425^0 Lat/Long) Regional Climate Model (RCM) projected daily rainfall data is collected from Indian Institute of Tropical Meteorology (IITM) for Narmada river basin. The data used for analysis is average of the years 2075-2085. The monthly stream flow data is collected from gauging stations namely Sandia, Hoshangabad, Mandleshwar (1981-1984, 1995-1998 and 2006-09) and Rajghat, Garudeshwar (1981-1984, 1995-1998) from Central Water Commission.

3.1 Conceptual stream flow model (CSFM)

The 'system' concept of the watershed is used in the conceptual rainfall-runoff model. The watershed is treated as a 'system' that receives rainfall as input, processes it and generates stream flow as its 'response'. The 'response' depends on various factors, depending on the time-dependent as well as time-invariant characteristics of the watershed. For instance, topograhy, shape of the catchment, soil properties and even vegetation are treated as time-invariant whereas wetness condition of watershed, rainfall over catchment, continuous loss due to various reasons etc. are treated as time dependent. The time dependent characteristic of 'response' is being updated over time whereas time-invariant properties are captured in model calibration for a particular watershed. However, time-invariant properties of 'response' do vary from one watershed to another. Thus fresh model calibration is needed for each different watershed, keeping basic approach as the same. The model is described below.

The 'system wetness condition' (SWC) is a representation of the amount of water that is stored in the near-surface of the watershed as depression storage, soil water retention etc. SWC is time-dependent and is denoted as V_t, where t is the time subscript. V_t ranges between 0 and maximum capacity of the system, V_{max}. Conceptually, V_t equals V_{max}, indicates that the entire amount of rainfall contributes to the runoff. On the other hand if V_t equals 0, no contribution to runoff from the rainfall is present from the 'system'. In between these two extremes, the amount of rainfall that contributes to runoff, as a system response, depends on V_t/V_{max}. Thus, at any instant of time, V_t/V_{max} is a dynamic condition of the system, that determines the runoff contribution to rainfall R_t^e that contributes to runoff, as a system response. This, R_t^e is time dependent through its dependence on the dynamic condition of the system, i.e., V_t/V_{max}
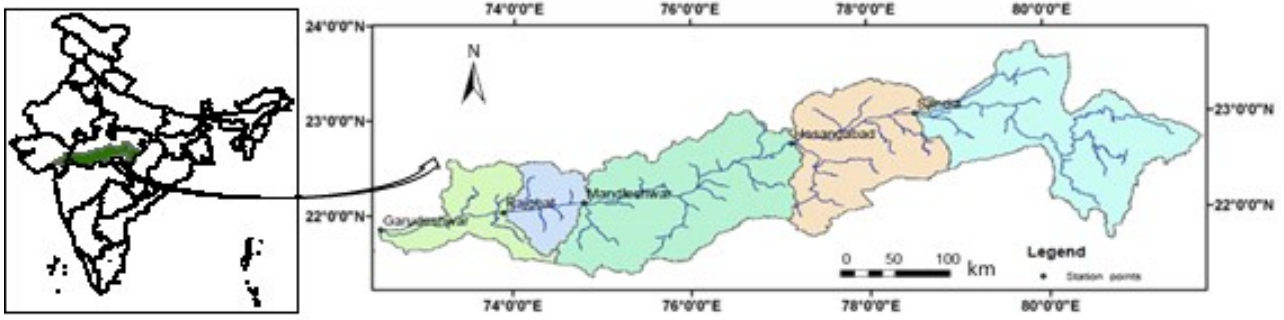
Figure 1. Major sub-basins of Narmada River

If $V_t > 0$, there will be a continuous loss L_t from V_t in the form of evaporation, evapotranspiration, deep percolation etc.,. L_t is reckoned as $k\%$ of V_{max}.

Denoting R_t as rainfall at time t, the above discussion. Both parameters, V_{max} and k depend on the catchment characteristics, which directly or indirectly influence the system response and may also be interrelated. So, V_{max} and k are to be simultaneously estimated during model calibration by minimizing the mean square error (MMSE).

The observed stream flow, at a particular time step, is divided into two parts – a) stream flow as 'usual response' of the system, i.e., without the influence of any external force, and b) stream flow as the 'response' of the system due to 'external forces'. Temperature, large-scale atmospheric circulations, rainfall etc., may be termed as various 'external forces'. However, variation of rainfall is the most influencing component, influencing the stream flow at daily time-scale among the various external forces.

Under steady state condition, the stream flow as a 'usual response' of the system is zero for ephemeral rivers and is the base flow for perennial rivers. However, the stream flow as the 'usual response' during the transition period, i.e., immediately after rainfall stops, will be different in nature. It is assumed that, during the transition period, the stream flow will reduce exponentially towards zero or base flow as the case may be. Thus, stream flow at time step t, S_t, can be expressed as the summation of stream flows as the 'response' of the system due to 'external forces' at time step t (denoted as S_t^e) and the exponentially reducing contributions of stream flows as the 'response' of the system due to 'external forces' at previous time steps, $t-1$, $t-2$, $t-3$ and so on. Thus,

$$S_t = S_t^e + \left(\frac{d}{100}\right)S_{t-1}^e + \left(\frac{d}{100}\right)^2 S_{t-2}^e + \left(\frac{d}{100}\right)^3 S_{t-3}^e + \cdots \quad (1)$$

where d is the exponential decay factor, expressed as a percentage.

$$S_t^e = S_t - \frac{d}{100} S_{t-1} \quad (2)$$

It is obvious that lower bound of S_t is the steady-state usual response, which is zero for ephemeral rivers and base flow for perennial rivers. However, the lower bound S_t^e is zero in both the cases. Thus, parameter d can be estimated ($\hat{d}$) during model calibration period as;

$$\hat{d} = SUP\left[\{d\}\big| S_t^e(t) \geq 0\right] \qquad \forall\, t \quad (3)$$

where 'SUP' stands for 'supremum'. However, to be on the conservative side, value of d is preferred to be slightly less than the estimated one ($\hat{d}$) because it is unlikely, in a statistical sense, to cover the complete flow regime in a sample of stream flow data.

After obtaining S_t^e and R_t^e as described above, S_t^e is regressed on R_{t-1}^e, R_{t-2}^e, ..., R_{t-m}^e where m is the total number of previous time steps considered. m can be determined by correlation analysis during model calibration period as the number of lags upto which the correlation coefficient is statistically significant. Obviously, the larger the size of the upstream catchment the greater the value of m.

Finally, predicted stream flow, $\hat{S}_t$, is obtained as

$$\hat{S}_t = \hat{S}_t^e + \frac{d}{100} S_{t-1} \quad (4)$$

where $\hat{S}_t^e$ is the estimated 'response' of the system due to 'external forces' being the contribution of rainfall to the runoff.

It may be noted that, in the above method, instead of using different catchment properties with spatial attributes as separate parameters, the total response of the watershed as a system, as a comprehensive parameter is used. Thus, the model parameters contain the information of cause-response (rainfall-stream flow) pattern of the watershed, which is considered as a system. This preserves all the characteristics of the catchment, which directly or indirectly influence the response of the watershed, in terms of various model parameters. To get the integrated effect of hydrological processes at the basin outlet, model was used at monthly scales. The methodology, being general, can be applied to any other watershed. However, the

methodology needs a well representative rainfall and stream flow time series, consisting of all possible flow regimes, for estimation of parameters. Model calibration and validation done was done using different year datasets, subsequently model simulations were carried out for past and future climate scenarios.

4. Result

4.1 LULC change during 1972 to 2004

Land use/cover is one of the most important factors that affects stream flow, surface erosion, runoff, and evapotranspiration in a watershed. Land use/cover map of Narmada River basin is generated for the year 1972 and 2004. The major classes of land use-land cover are; Agriculture, Forest, Others (Barren\Fallow\Dry channels etc.), Water bodies/River, Settlements. Land cover analysis: The overall classification accuracy for the LULC map of 2004 was 92% and for 1970's map it was 91.7%. The KAPPA coefficient was used to test the validity of classification results (Cohen 1960).

KAPPA analysis is done by calculating KHAT statistics (an estimate of KAPPA), which is a measure of accuracy. The kappa statistics was 0.9245 for 1972 map and 0.9313 for 2004 map. The area statistics shows that the agriculture area has increased by 2.22% (130176.6 ha) whereas area under forest has declined by -1.67% (39211.3 ha) (Table 1). The other class which includes barren, fallow and dried river channels showed decline of -71.9% (209743.2 ha). Agriculture covers the largest area among all classes followed by forest. Area under settlements greatly increased by 228.7% (18185.4 ha) and as expected water bodies area also show significant increase of 124.9% (100592.5 ha). Classified land cover maps for 1972 and 2004 are presented in Fig.2.

The area statistics shows the overall increasing trend of agricultural and urban development in the river basin. These changes were mainly due to enhanced availability of water for agriculture which was made available from many large reservoirs which have come up in the basin. This increase has been achieved at the cost of loss of some forested area, but on the positive side, it was evident that mostly the area which was not under any kind of utilization has been brought under some development. The multipurpose projects developed in the basins have significantly proven useful to improve agriculture over the area. This increase obviously has also been supported by increase in the water availability.

4.2 Parameter estimation

Every hydrological model has some model control parameters as constants which changes with different basin hence to run any hydrological model first thing is to find the constant parameters of the basin. To find these parameters, observed stream flow and observed rainfall is used. The basin parameter estimation is done to run conceptual model simulation and result of first sub-basin (Sandia) is shown in Fig. 3 as example. For developed

model three parameter constants are maximum capacity of the system (Vmax), continuous loss (k) and d is the exponential decay factor. Other major sub-basins are Hoshangabad, Mandleshwar, Rajghat and Garudeshwar. The estimated parameters are shown in following Table 2
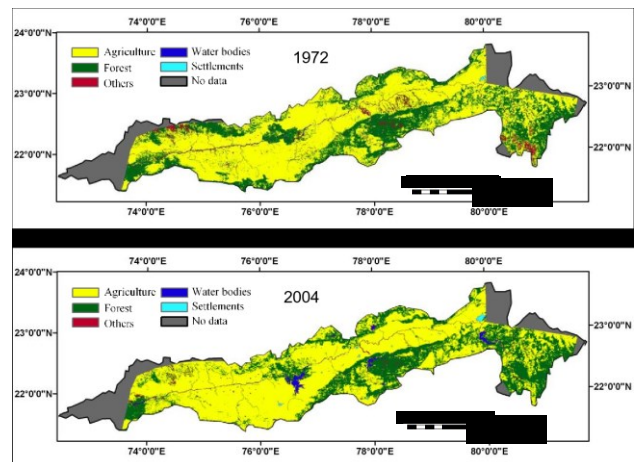
Figure 2. Land use and land cover classification in Narmada river basin during 1972 and 2004.

It is found that the Vmax value which is maximum system wetness capacity is decreasing for almost all sub-basin except Mandleshwar and Rajghat. This might be because of construction of major dams or barrage in that basin which increase storage capacity of basin. However, the effect of Bargi dam in the upstream of Sandia might be overcome by the land use change as V_{max} is decreasing for this basin.

Parameters for the future scenario is projected through the historical changes of the parameter and attributed to the land use / land cover change.
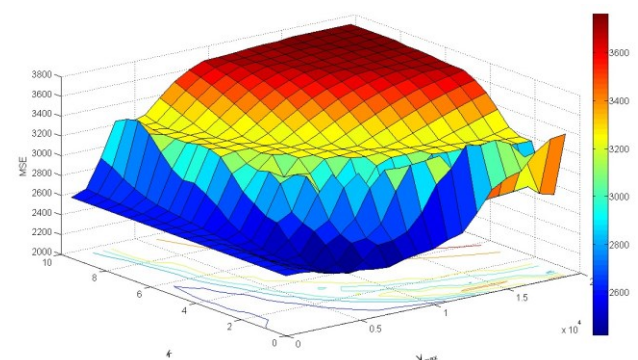
Figure 3. The Parameter estimation results of Sandia sub-basin for year 2006-08.

4.3 Calibration and validation of the model

This is done pre and post construction of Bargi dam. Data for 1981–1983 is used for model calibration during pre-construction period whereas 1995–1997 data is used for model calibration during post construction period. Model is also calibrated for period of 2006-2008. Results are shown in Table 3 and Fig. 4. The model is calibrated during 1981-83 and 2006-08.

Table 1. Land cover classification analysis

Class name	Area gained or lost to classes				
	Agriculture	Forest	Other classes	Water bodies	Settlements
Agriculture	-	18121.7	191583.6	-62598	-16930.6
Forest	-18121.7	-	12493.8	-33316.2	-267.2
Other Class	-191583.6	-12493.8	-	-4684.9	-980.9
Water bodies	62598	33316.2	4684.9	-	-6.6
Settlements	16930.6	267.2	980.9	6.6	-
Net change	130176.6	-39211.3	209743.2	100592.5	18185.4

Table 2. Estimated parameters for five main sub-basins of Narmada

Sl. No	Station names	1981-83			1995-97			2006-08			2080		
		Vmax	k	d	Vmax	k	d	Vmax	k	d	Vmax	k	d
1	Sandia	18100	0.6	0.4	15100	0.6	0.4	5100	0.6	0.4	1785	0.6	0.4
2	Hoshangabad	15100	0.1	0.4	10100	0.6	0.4	3100	1.6	0.4	1085	1.6	0.4
3	Mandleshwar	9100	1.1	0.4	9100	0.6	0.4	10100	1.6	0.4	3534	1.6	0.4
4	Rajghat	5000	0.6	0.4	11100	0.1	0.4	10100	0.1	0.4	3534	0.1	0.4
5	Garudeshwar	9100	0.1	0.4	4100	0.1	0.4	3100	1.6	0.4	1085	1.6	0.4

Table 3. Correlation coefficient during model calibration and validation periods.

Gauging Station Name	Model Calibration		Model Validation	
	Monthly Stream flow 1981-83	Monthly Stream flow 2006-07	Monthly Stream flow 1983-84	Monthly Stream flow 2007-08
Sandia	0.78	0.73	0.78	0.78
Hoshangabad	0.95	0.83	0.78	0.76
Mandaleshwar	0.98	0.79	0.99	0.70
Rajghat	0.98	0.77	0.57	0.69
Garudeshwar	0.93	0.80	0.97	0.67

It is found that it captures Correlation coefficient of 0.73 to 0.98 for monthly streamflow. Also model is validated for two decades one from 1983-84 and from 1997-98. Model validation is done pre and post construction of Bargi dam.

Data for 1983 – 1984 is used for pre-construction period whereas 1997-1998 data is used for post construction period. Correlation coefficients are found to be from 0.57 to 0.99 for monthly scale. The model performance found to be adequate for monthly scale stream flows.

It is observed that stream flow intensity in monsoon months is increasing in every decade. Secondly, the peak of stream flow is being shifted from August to July. It is further observed that stream flow values are increasing for monsoon period whereas it is decreasing for non-monsoon period. The variability throughtout year is high for sub-basin which are at main river strech compared to the sub-basins on tributary. Results of stream flow magnitudes for past (1983-84, 1997-98, 2008-09) and future (2080) scenarios for few sub-basins are presented in Figs. 5-6. Stream flow is increasing in early monsoon months and decreasing in late monsoon months for the major sub-basins in the Narmada river system.
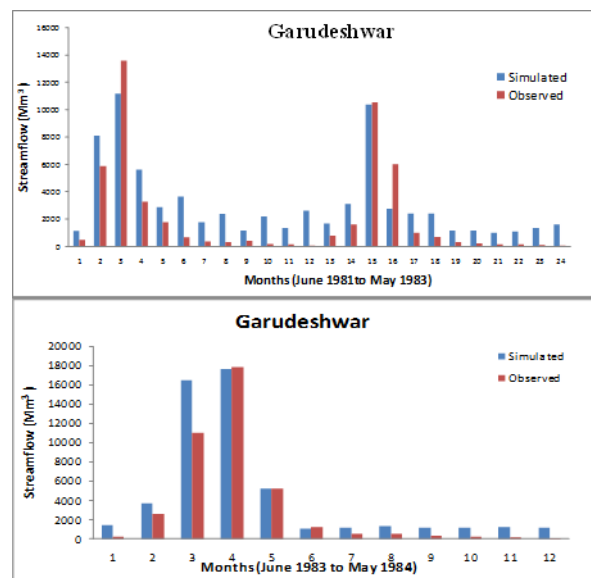

Figure 4. Model performance during calibration (1981-83) and validation period at Garudeshwar (1983-84).
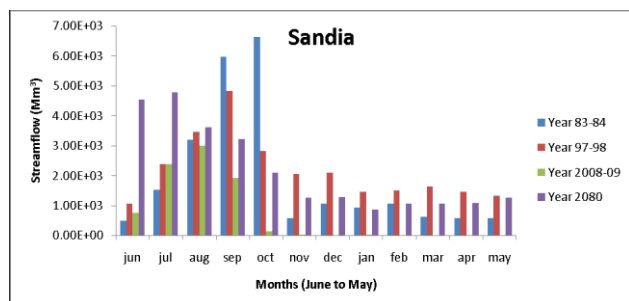
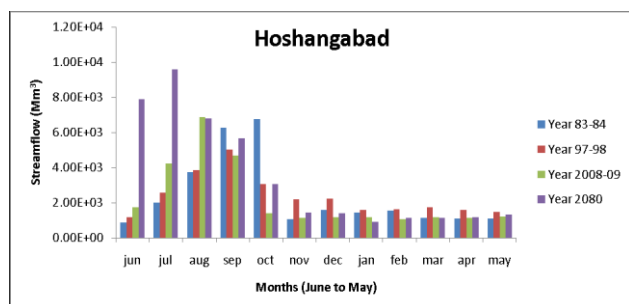**Figure 5. Stream flow analysis for past, present and future scenarios for Sandia.**

Figure 6. Stream flow analysis for past, present and future scenarios for Hoshangabad.

5. Conclusions

A conceptual stream flow model (CSFM) was applied for river basin stream flow modelling. This model is a conceptual and dynamic, which represents all important hydrological process of watershed. The model is applied for Narmada Basin. Calibration and validation of the model is carried for five major sub-basins having their outlets at Sandia, Hoshangabad, Mandleshwar, Rajghat and Gurudeshwar. The model is calibrated for three decades separately - 1981-83 and 2006-08. It is found that the correlation coefficient varies between 0.61 to 0.98 for monthly scale. It is found that performance at monthly scale is satisfactory. Change pattern in the land use/cover during 1972 to 2004 were delineated and attributed for the change in the model parameters. Significant change in the LULC pattern has been observed, because of construction of several new dams in the Narmada river. Increased water availability due to large dam projects has acted as one of the encouraging factor for agricultural and urban development. Results of streamflow magnitudes indicates that the streamflow values are increasing for early monsoon period whereas it is decreasing for late monsoon period. Similar results are obtained for future scenario also. Historical and future monthly stream flow simulations are useful to analyse water availability pattern in a particular river basin.

References

Brath, A., A. Montanari, and G. Moretti (2006). Assessing the effect on flood frequency of land use change via hydrological simulation (with uncertainty), Journal of Hydrology, 324, 141-153.

Chow, V. T. D. R. Maidment and L. W. Mays, (1988). Applied Hydrology; McGraw-Hill, Inc., USA

CGWB (2004). Annual report of Central Ground Water Board 2004.

Cohen, J. (1960). A coefficient of agreement for nominal scales. Educ. Psychol. Meas., 20(1), 37–46.

Dhar, O. N. and S. Nandargi, (2003). Hydrometeorological Aspects of Floods in India, Natural Hazards, 28, 1–33.

Dunne, T. (1978). Hill slope hydrology (Edited by M J Kirkby), John Wiley & Sons, Chichestler, UK (1978).

Fu, B., Y. Wang, Y. Lu, C. He, L. Chen, and C. Song (2009). The effects of land-use combinations on soil erosion: a case study in the Loess Plateau of China, Progress in Physical Geography, 33, 793-804.

Garg V, S. P. A. Prasun, K. G. Bhaskar (2017). Assessment of land use land cover change impact on hydrological regime of a basin. Environ Earth Sci 76(18), 1–17. https ://doi.org/10.1007/s12665-017-6976-z.

Gupta, H. G. J. Chakrapani (2005), Temporal and spatial variations in water flow and sediment load in Narmada River Basin, India: natural and man-made factors, Environ Geology, 48, 579–589.

Kite, G. W. and A. Piteroniro (1996). Remote sensing applications in hydrological modeling. Hydrological Science Journal, 41 (4), 561–591.

Kosmas, C., N. Danalatos, L. H. Cammeraat, M. Chabart, J. Diamantopoulos, R. Farand, L. Gutierrez, A. Jacob, H. Marques, and J. Martinez-Fernandez (1997). The effect of land use on runoff and soil erosion rates under Mediterranean conditions, Catena, 29, 45-59.

Li S, H. Yang, M. Lacayo, J. Liu and G. Lei (2018). Impacts of land-use and land-cover changes on water yield: a case study in Jing-Jin-Ji China. Sustainability 10(4), 1–16. https ://doi.org/10.3390/su100.40960.

Mohan and N. S. Madhav (2000). A GIS based Integrated Model for Assessment of Hydrological change due to Land use modifications, proceeding of symposium on Restoration of Lakes and Wetlands, Indian Institute of Science, November 27-29, 2000, Banglore, India.

Saddique N., M. Usman and C. Bernhofer (2019b). Simulating the impact of climate change on the hydrological regimes of a sparsely Gauged Mountainous Basin Northern Pakistan. Water 11(10), 2141. https://doi.org/10.3390/w1110 2141

Seth, S. M., S. K. Jain, and M. K. Jain (1999). Remote Sensing and GIS Application Studies at National Institute of Hydrology. Map India, 1999.

Singh, V. P., and D. A. Woolhiser (2002). Mathematical modeling of watershed hydrology. Journal of Hydrological Engineering, 7 (4), 270–292.

Wagner P. D., S. Kumar and K. Schneider (2013). An assessment of land use change impacts on the water resources of the Mula and Mutha Rivers catchment upstream of Pune India. Hydrolological Earth System Science, https ://doi.org/10.5194/hess-17-2233-2013

Xia, L. L., R. Z. Liu and Y. W. Zao (2012). Correlation Analysis of Landscape Pattern and Water Quality in Baiyangdian Watershed, Procedia Environmental Sciences, 13, 2188-2196.

Estimation of Surface Soil Wetness over Rainfed Agricultural Landscape of Mongolia

Devansh Desai[1*], Rahul Nigam[2], Sainjargal Baatarchuluun[3] and B.K. Bhattacharya[2]
[1]Department of Physics, Electronics & Space Sciences, Gujarat University, Ahmedabad
[2]Agriculture & Land Ecosystem Division, Space Applications Center (ISRO), Ahmedabad
[3]Department of Meteorology Hydrology and Environment Monitoring in Darkhan province, Mongolia.
[*]Email: ddesai107@hotmail.com

Abstract: Remote sensing provides exceedingly powerful means for estimation of surface soil moisture at spatial scale, especially for rainfall deficit country like Mongolia, for water security and guided irrigation. In the present study surface soil moisture indicator at moderate and high spatial resolution is estimated using Land Surface Temperature (LST) (thermal spectral bands) and Normalized Difference Vegetation Index (NDVI) (optical spectral bands) from MODIS AQUA (1 km) and LANDSAT-8 (30 m). Two-dimensional scatter plots between NDVI and LST is generated using 'triangle' based contexture model to obtain a Soil Wetness Index (SWI) from time series of MODIS AQUA and LANDSAT-8 over *Darkhan-Uul* province of Mongolia. The estimated SWI varied between 0.2 to 0.4 for May to June and gradually increases up to 0.7 for August month followed by gradual decrease in the month of September. The estimated temporal SWI is found well correlated with *in situ* measured surface soil moisture during agricultural season from May to September. The present study demonstrated the new technique to derive a soil wetness index using optical and thermal remote sensing data and act as a surrogate for volumetric surface moisture content in cropped soils at field to landscape scales over selected agricultural region of Mongolia.

Keywords: LST-NDVI triangle, Soil wetness Index (SWI), Mongolia

1. Introduction

Near-surface soil moisture (0–5 cm) is an important hydrological variable influencing the interactions between the land surface and atmospheric processes (Brubaker and Entekhabi, 1996). The soil moisture content in the surface layers of the soil is an important parameter for many hydrology, agricultural and meteorology applications. Soil moisture is one of the directly observable hydrological variables that plays a vital role in the water and energy budgets to study climate change. In agriculture soil, moisture information is essential for many farm managements practices such as irrigation scheduling and detection of moisture stress to improve resource use efficiency and crop yield. Soil moisture also determines partitioning of net radiation into latent and sensible heat components in the field of meteorology. Therefore, accurate and reliable soil moisture estimates are essential to investigate effect of climate change, land surface hydrological variables such as infiltration fluxes, runoff and surface temperature on the energy and mass exchange between soil plant atmosphere continuum. It also helps to examine the impact of assimilation of the derived land surface variables on predictive capabilities of numerical weather prediction (NWP) models. (de Rosnay et al. 2012).

Water deficit has become a leading environmental problem that limits crop photosynthesis, productivity and yield. (Farooq et al. 2009) Soil moisture and its availability to support plant growth is a primary factor in farm productivity. The continuous soil moisture stress can result in yield loss, root disease and decay of plant. Soil moisture especially in wheat and other agricultural crops, is a major factor for yield reduction in country like Mongolia since there is scarcity of rainfall and with no irrigation facilities (Karthe et al. 2015). Therefore, it is important to identify soil moisture early in the spring, with the use of satellite data for planning of selection of crop type, sowing and management practices.

Various satellite based remote sensing techniques have been used in the past to estimate soil moisture at various spatial scale. The different microwave frequencies having higher sensitivity to dielectrics and canopy structure and ideal for surface soil moisture estimation over different land use land cover. But its soil moisture sensitivity decreases significantly with the increase in fractional vegetation cover due to the increase in crop biomass and height during crop growing season (Singh and Alderfer, 1966). Whereas, thermal remote sensing provide better soil moisture estimates both in bare and higher crop fraction conditions. However, on some occasions cloud contamination limits its usage during agricultural growing season.

Large-scale soil wetness information is more preferred than volumetric soil moisture (Mallick et al. 2009) in agro-advisories services to farmers on crop sowing and other farm management practices due to (i) dynamic range of soil wetness is higher (0-1) than volumetric soil moisture (0-0.5), (ii) soil wetness is supposed to have better accuracy than volumetric soil moisture because latter requires precise soil moisture constants such as field capacity, permanent wilting point, air dry moisture content at each pixel and getting all information at pixel level is uphill task.

1.1 Objectives
The main aim of present study is to test the performance of thermal-optical remote sensing to assess spatial and temporal variability of large-scale surface soil wetness over agricultural dominant rainfed regions of Mongolia. The objectives of the present study are as follows:

1. To derive Surface Soil Wetness Index (SWI) from dry-wet edge parameters generated from optical and thermal remote sensing data.
2. Comparison of SWI derived from finer (~30m from LANDSAT-8) and moderate spatial resolution (~ 923 m from MODIS AQUA) over agricultural patches.

2. Study area

Darkhan-Uul Aimag, third largest city in Mongolia and the capital of Darkhan-Uul Province, is selected as the study area. It is located at latitude of 49.3° N to 49.5° N and longitude of 106.15° E to 106.25° E, which covers about 3,275 km². The area has elevation range at 700-1000 meter above mean sea level. (Fig. 1). Uul Province. Darkhan has a humid continental climate with extremely cold and dry winters however the summers are warmer and very humid. DarkhanUul Aimag is situated in the agricultural heartland of Mongolia and it is the major agricultural producer state in Mongolia with rich natural resources for agricultural practices. This area located at a lower altitude as compared to others part of the country and have a hot climate. The mean air temperature and rainfall of the study region is 11-21 °C and 266 mm respectively during May to September months. The surface soil is deep dark brown and medium loam.

3. Data used and methodology

3.1 Satellite data

3.1.1. MODIS data
Satellite data used for study are MODIS AQUA land surface temperature and surface reflectance. The product names are MYD11A2 (LST) and MOD13A2 (NDVI), respectively. LST product has spatial resolution of 923 m and NDVI product as spatial resolution of 500 m. NDVI product is resampled at LST spatial resolution of 923m and is used in this study. The data from May to September months for 2015 and 2016 are used in this study.

3.1.2. LANDSAT-8
LANDSAT 8 is a LANDSAT series of NASA satellite. LANDSAT 8 data is available on Earth Explorer website. In this study, data from band number (1, 2, 3, 4, 5, 7, 10 and 11) are used to fulfill the requirements of present study. Normalized Difference Vegetation Index (NDVI) has been computed using band 4 (red) and band 5 (near infrared) reflectances. LST is derived from LANDSAT-8 data using split-window algorithm as described by Rajeshwari and Mani (2014).

3.1.3. In- situ data
The measured daily rainfall data of Darkhan station of Mongolia as listed in Table 1 for the period May to September 2015 and May to September 2016 months were used in the present study for evaluating of SWI derived from satellite optical-thermal remote sensing observations.

Figure 1. Location map of Study area

Table1. In situ measurements sites

S. No	Place	Latitude (°N)	Longitude (°E)
1	Tsaidam	52.85	106.07
2	Belcheer	53.65	105.98
3	Tomc	53.01	105.96
4	Alt.G	52.18	105.98

3.2 LST-NDVI two-dimensional scatter plots

Surface soil wetness determines moisture availability that governs and control the feedback mechanism between land surface and atmosphere process. Triangular scatter plots from NDVI and LST space is utilized to obtain a soil wetness index (SWI), with the combination of dry and wet edges using data from MODIS AQUA for landscape scale studies over study region in Mongolia.

The conceptual LST–NDVI triangular space, with LST (y-axis) plotted as a function of NDVI (x-axis) is shown in Fig. 2 The hypotenuse of the triangle denotes a warm / dry edge comprising of a group of points represents zero surface soil wetness for various NDVI classes (NDVI<0.25, 0.25<NDVI<0.4; 0.4<NDVI<0.6; NDVI>0.6) in contrast to the cold/wet edge represented by the base of the triangle having maximum surface soil wetness conditions at various NDVI classes. The dry to wet (top-down) on left edge signifies bare soil. The LST for bare soils is primarily determined by soil moisture content, via evaporative control and thermal properties of the surface at constant irradiance. But as the greenness increases along the x-axis (with NDVI), the maximum LST (=T_{smax}) declines as shown in Fig. 2.
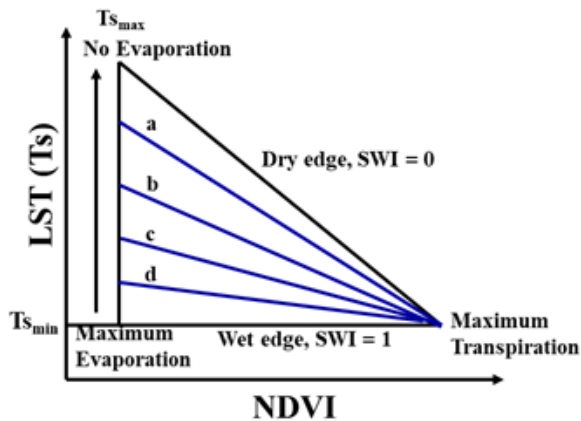

Figure 2. Conceptual diagram of LST–NDVI triangle for estimation of SWI

For typical dry situations, the negative relation is defined by the warm /dry edge, which is the upper limit of LST for a given surface type and climate forcing. The 'wet' edge consists of a group of points forming a horizontal or sloping line (at the level of $T_{s\,min}$) for various surface types or fractional cover.

In Fig. 2, highest LST ($T_{s\,max}$) along the dry edge represents the driest surface soil conditions when surface soil wetness approaching toward zero. The wettest (saturated) soil conditions are represented through the minimum LST (=$T_{s\,min}$) along the 'wet edge' when surface soil wetness is the highest. It is assumed that moisture availability varies linearly from the dry to wet edge. This agrees with previous interpretations of LST–NDVI space as given by Carlson (2007) and Stisen et al. (2008).

A soil wetness index (SWI) on a given day or time (t), representing relative surface soil moisture, is defined as:

$$SWI(t) = \frac{T_{s\,max(i)} - T_{s\,(i)}}{T_{s\,max(i)} - T_{s\,min}} \qquad (1)$$

where, $T_{s(i)}$ is the LST of ith pixel. $T_{s\,min}$ is the minimum LST in the triangle that defines the wet edge. $T_{s\,max(i)}$ is the maximum LST for i^{th} NDVI. Carlson (2007) objectively determined the dry edge as the least square fit to NDVI using a polynomial (of the 3rd or 4th order) using fine resolution thermal data as well assimilated data from Soil Vegetation Atmosphere Transfer (SVAT) model. In the present study, most of the LST–NDVI scatter plots from 927m spatial resolution showed a clear triangle with prominent linear dry edge and horizontal wet edge (Fig. 5a). The LST–NDVI scatter plots at 30m pixel solution showed a non-linear trend along the dry edge at higher NDVI values and a sloping wet edge (Fig. 5b). However, to keep the simplicity and uniformity in approach across different scales, the dry edge was modelled via a linear empirical fit to NDVI:

$$T_{s\,max(i)} = o + pNDVI_i \qquad (2)$$

Here, NDVI is the normalized difference vegetation index of the ith pixel, 'p' is the slope and 'o' is the intercept of the linear dry edge. $T_{s\,max}$ values for different NDVI classes were extracted with a NDVI interval of 0.05. Then 'dry edge' parameters were estimated through regression analysis. The 'wet edge' is the horizontal linear presented by $T_{s\,min}$.

Along the dry edge, SWI = 0, whereas it equals 1 along the wet edge. Isolines (a, b, c and d) of SWI in Fig. 2 represent equal surface moisture availability.

4. Results and discussion

4.1. Temporal variation of NDVI

The NDVI is a surrogate of green vegetation vegour and it's value increses with enhacement in canopy greenes and leaf area index (LAI) (Nigam et al. 2014). The temporal NDVI profile over four known agricultral station of Mongolia is extracted for two consecutive agricultre year viz. 2015 and 2016 and shown in Fig. 3. These four stations mainly grow wheat and potato crops. The station Tsaidam, Toms and Alt.G is dominated with wheat and Toms with potato crop whereas, Belcheer having mixed agriculture cropped area. The NDVI temporal profile showed that NDVI used to increase from second fortnight of June and it is slope remain positive during next 60 days due to active vegetative phase of different agriculural crops and afterward it start decreasing in first fortnight of September. The Fig. 3 showed that duration of vegetaive phase in 2016 is more as compare to 2015.

4.2. Temporal variation of LST

During crop growing season of 2015 the LST varied between 290 to 310 K but in vegtative phase it varied from 290 to 305 K only and this will lead to enhancement of vegetaive growth duration. In 2016 LST vary from 292 to 306 K lead to increase the duration of vegetative / crop duration phase in year 2016. All the four agriclutral stations showed persistent trend in both the year for example the Tomc and Belcheer station showed low and high LST respectively in both the years during crop

growing season. The temporal variation in LST is shown in Fig. 4 for all four study sites.

4.3. Scatter plot between NDVI & LST

The scatter between NDVI and LST are plotted with MODIS (optical and thermal data) for different crop stages and shown in Fig. 5. The scatter plot between NDVI and LST is used to compute dry and wet edge for different pheno-phases of crop. The angle between dry and wet edge is more in start of the crop-growing season and at vegetative growth it was observed low and again in senescence and physiological maturity stage it rises again. This signifies that variation LST is found low during vegetative phase due to greenness of the crops since crop was able to transpire more, which in turn lead to decrease its LST. During early and late stage of the crop, the transpiration is low which in turn lead to rise in LST even though soil moisture is high. Hence, when canopy cover / vegetation fraction is high the LST is dominated by the characteristic of crop growth stage and its ability for transpiration with respect to available soil moisture. The Fig. 5 (a) shows that at 1 km the dry and wet edge vary significantly with the change in crop stage. This is again replicated with scatter plot between NDVI and LST from LANDSAT data as shown in Fig. 5 (b). The behavior of the scatter plot remains same with high-resolution spatial data from LANDSAT data. A clear triangular pattern was visible for all scatter plots. Here, we take in to consideration only zero trend for wet edge and don't consider the negative sloping wet edge values (Mallick et al. 2009).

4.4. Estimated spatial soil wetness index (SWI)

Spatial distributions of surface SWI over agricultural regions of Mongolia are shown in Fig. 6 for different calendar days. Spatial patterns matched quite well during the period of low vegetation activity in contrast to peak growth stages as shown in Fig 6. The spatial pattern of SWI from the two sensors showed close resemblance in initial phase of crop growth stage (up to emergence stage). In initial phase of the crop, the soil exposure is dominant and the SWI matches well for both the years. On the contrary, in advance crop stage poor spatial coherence is observed (Fig. 6). This may due to sub-pixel heterogeneity of MODIS, which is represented well in LANDSAT high-resolution data. As the crop grow, the crop morphological and phenological development in each pixel is a function of crop cultivar, meteorological parameters and soil moisture. Hence, the growth of crop in high-resolution pixel (LANDSAT) having different crop stage and morphological characteristics lead to sub-pixel heterogeneity in the MODIS pixel. The uncertainty of SWI is also due to high fractional vegetation cover where the wetness isolines are closely set (Sandholt et al. 2002). This is due to the fact that most of the soil is obscured at high fractional vegetation cover. Thus, the lower part of the triangle is an area where the errors in the inferred soil moisture content will be the largest. Therefore, Gillies and Carlson (1995) suggested that reliable results may be obtained by limiting evaluation of soil moisture to the range of fractional vegetation cover between 0 and 80%. The high-resolution LANDSAT data is able to capture more heterogeneity in SWI in vegetative phase and latter crop stage as compared to MODIS. At field scale soil information better captured by LANDSAT whereas, MODIS is able to provide landscape scale SWI. But MODIS is having an advantage of high temporal (1- day) resolution and able to provide more cloud free data.
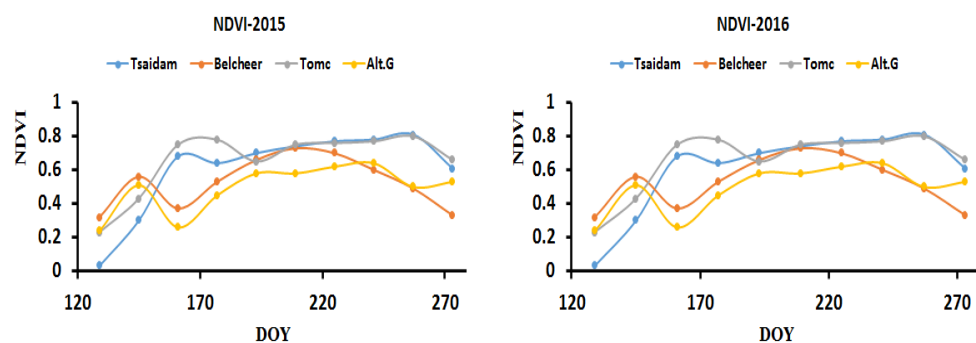
Figure 3. Temporal behavior of NDVI over different agricultural stations of Darkhan-Uul Province of Mongolia during crop growing season
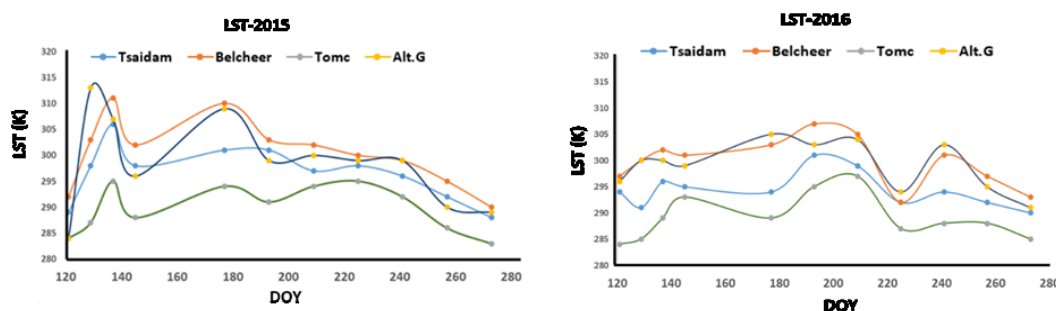
Figure 4. Temporal behavior of LST over different agricultural stations of Darkhan-Uul Province of Mongolia during crop growing season
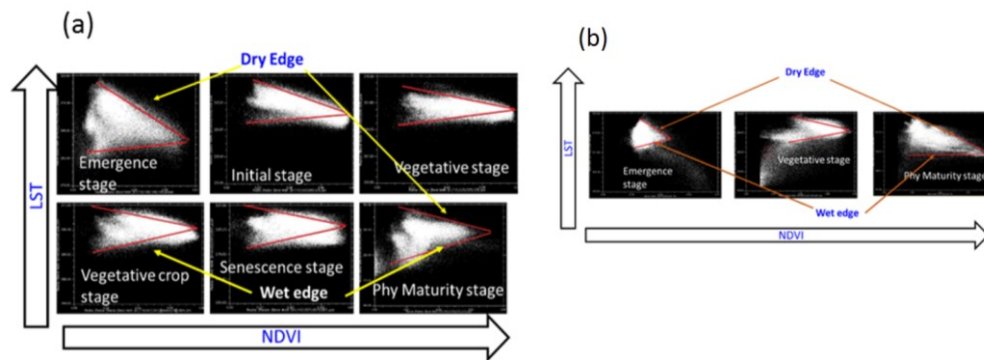
Figure 5. 2-D Scatter between (a) MODIS & (b) LANDSAT between NDVI and LST over different phenological stage of crop growth
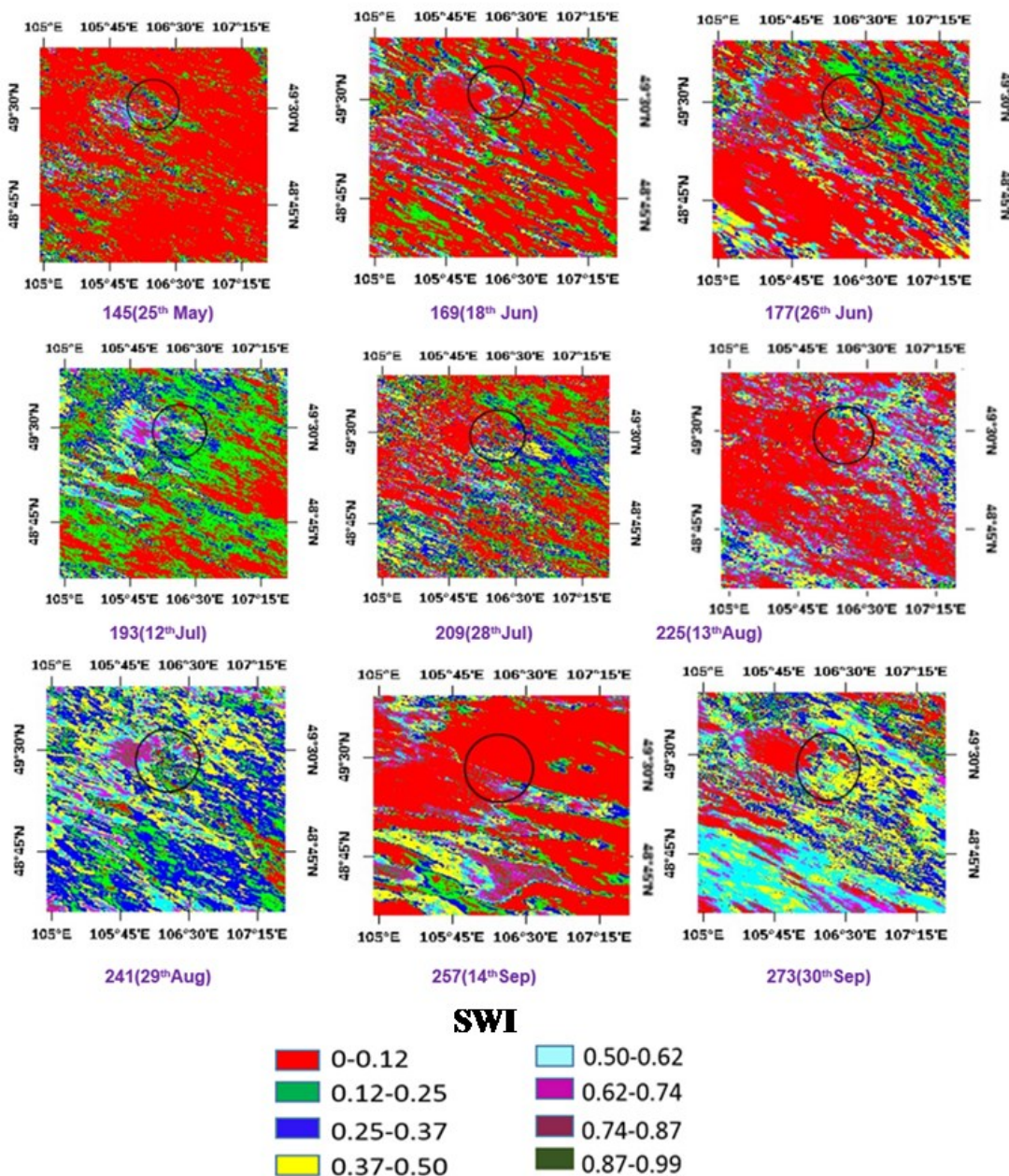
Figure 6a. Spatial distribution of SWI from MODIS over agricultural settings of Darkhan-Uul Province of Mongolia during 2015
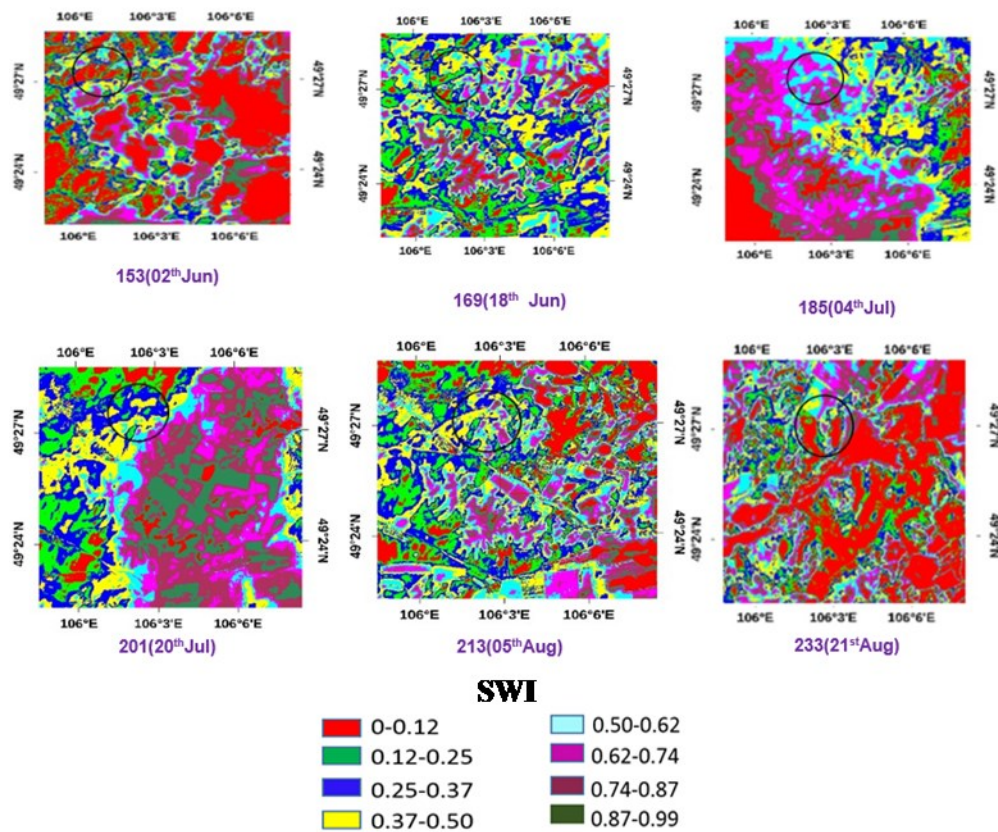
Figure 6b. Spatial distribution of SWI from LANDSAT-8 over agricultural settings of Darkhan-Uul Province of Mongolia during 2015
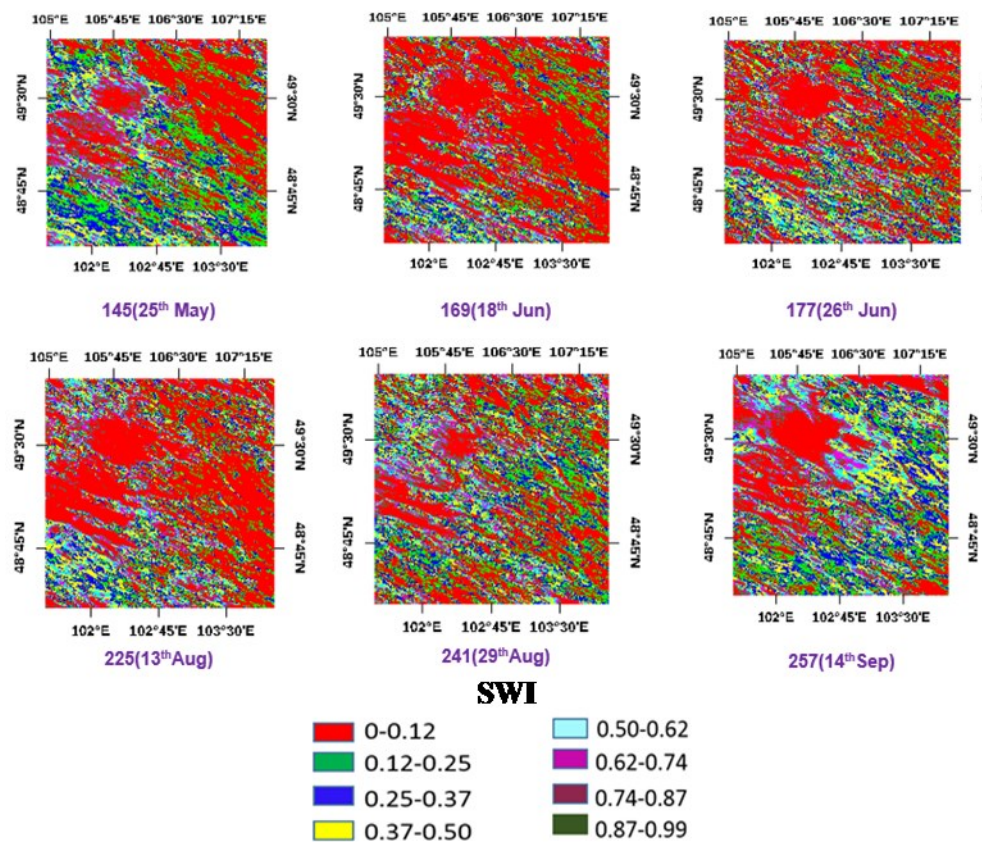
Figure 6c. Spatial distribution of SWI from MODIS over agricultural settings of Darkhan-Uul Province of Mongolia during 2016
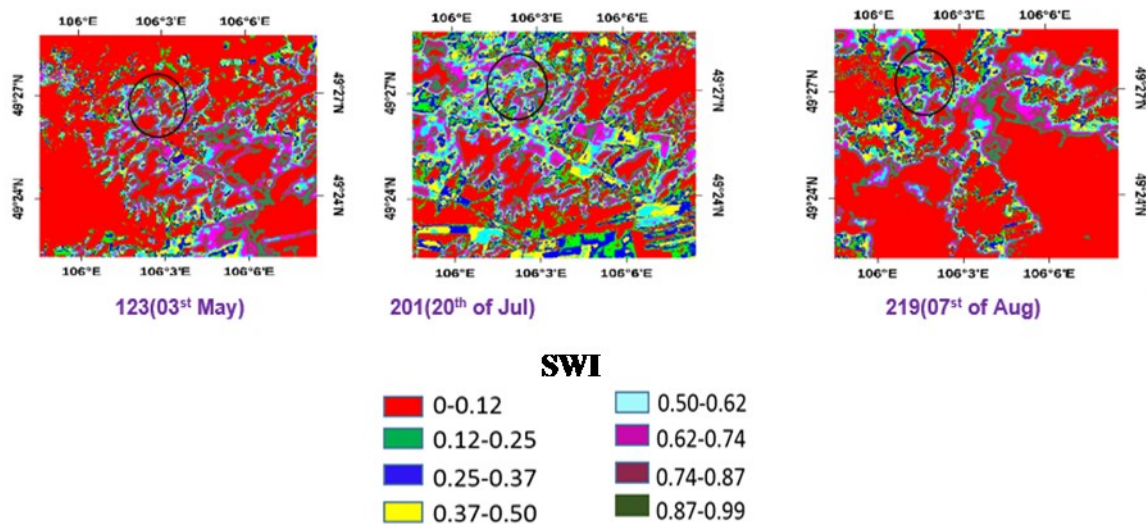
Figure 6d. Spatial distribution of SWI from LANDSAT-8 over agricultural settings of Darkhan-Uul Province of Mongolia during 2016

4.5. Temporal variation of SWI with *in situ* rainfall

The temporal SWI over known agricultural station is exracted from the SWI images of MODIS and LANDSAT for two consecutive years and plotted against the measured ground rainfall over that station. In 2015 the estimated SWI showed high SWI (0.4 to 0.5) during initial crop phase of the crop when crop water requirement is less and it receives frequent rainfall as shown in Fig. 7 a. In vegetaive stage the SWI showed low value between 0.30 to 0.35 due to high transpirational requirement of the crop in that stage. In latter stage of physiological maturity when crop transpiration is less the SWI start increasing. The high resolution LANDSAT data over agricultural station further showed (Fig. 7 b) that in early and late crop season the SWI able to pick the rainfall signature quite well and during vegetative stage and the low SWI value coincide with low rainfall during crop season. Then futher rise in SWI after 217 days also matched well with rainfall received at that station. In 2016 the estimated SWI showed high value (0.1 to 0.2) during initial crop phase of the crop when crop water requirement is less eventhough the station received frequent rainfall as shown in Fig. 7 (c) . In vegetaive stage the SWI showed low value between 0.3 to 0.4 due to high transpirational requirement of the crop. In latter stage of physiological maturity when crop transpiration is less the SWI start increasing. The estimated SWI showed that rise

and fall of SWI matches well with water requirement at each crop growth stage and rainfall. During initial phase at 123 calender day when there is no crop rainfall effect is well captured in surface moisture and further in SWI. In latter stage due to peak vegetative phase the SWI not increase much with rainfall event due to loss of surface water through transpiration.

The MODIS and LANDSAT intermediate product such LST and NDVI to estimate SWI are compared at 1 km as shown in Table 2. The difference in NDVI and LST is due to sensor response in that particular bands and time of data aqusiation as well as sun and sensor geometry (Teillet et al. 1982). This lead to more difference in NDVI and LST product when evaluated for 1 km X 1 km area. The LANDSAT data showed low σ (Standard deviation, SD) value for NDVI and LST when evaluated for mentioned ROI and it shows that area is a homogeneous. Similarly, in June and July SWI showed low σ due to more soil exposure and low crop growth but with the advancement of crop growth the difference also increases. This may due to difference in slope, aspect, relative proporation of crop fraction and different phenological stages in high resolution data whereas, these parameters are avergaed out in moderate spatial resolution.
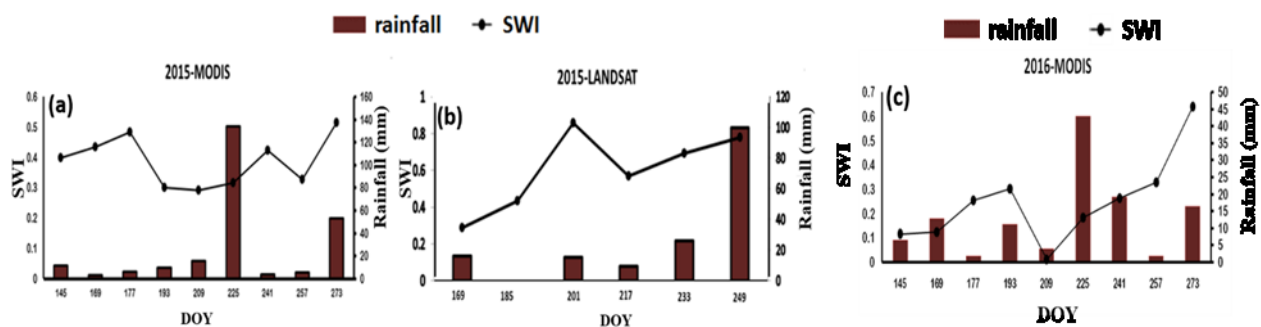

Figure 7. Temporal variation of estimated SWI using MODIS and Landsat-8 data at agricultural station with measured in situ rainfall for year 2015 (a,b) and 2016 (c)

Table 2. Comparison of MODIS and LANDSAT estimated SWI

Variable	MODIS	LANDSAT 8	Standard Deviation (σ)
June			
LST (K)	304.70	308.37	0.86
NDVI	0.35	0.252	0.02
SWI	0.32	0.29	0.01
July			
LST (K)	292.82	284.00	0.47
NDVI	0.72	0.55	0.05
SWI	0.37	0.41	0.12
August			
LST (K)	295.00	286.00	0.25
NDVI	0.64	0.51	0.01
SWI	0.49	0.33	0.19
September			
LST (K)	299.00	292.00	0.34
NDVI	0.78	0.62	0.02
SWI	0.39	0.46	0.02

5. Conclusions

The present study demonstrated the usage of optical (NDVI) and thermal (LST) triangular space to derive surface soil wetness index as surrogate of surface soil moisture in a rainfed region of Mangolia. Non-linear trends in the dry edge at higher NDVI and wet edge are found LST-NDVI scatter. This may due to (i) the attenuation of upwelling longwave radiation from background soil caused by dominant proportion of sunlit canopy at field scale as compared to shaded ones at higher NDVI (Carlson et al. 1990) and (ii) prominent effect of asymptotic increase of NDVI followed by saturation of canopy vigor in the form of leaf area index at peak vegetative phase of the crop. This study showed that the strength of SWI estimates largely depends on dynamic ranges of LST and NDVI, which often may not be sufficient as a result of restricted sampling window size due to low swath in case of finer spatial resolution sensors. This study showed that effectiveness of NDVI-LST triangular scatter will increase in estimation of SWI as the surface heterogeneity increases in sampling domain. The greater dynamics ranges of these two surface variables from a desired sampling widow for larger swath by moderate resolution sensor could lead to relatively low error. The NDVI-LST triangle method showed less error for the intermediate NDVI ranges from 0.3 to 0.7. This work will further be extended to different other rainfed agricultural areas of Mongolia. The spatial soil wetness / moisture in cold rainfed region of Mongolia will be helpful for better crop management and further assimilated in hydrological, crop and NWP models.

References

Brubaker, K. L., and D. Entekhabi (1996). Analysis of Feedback Mechanisms in Land-Atmosphere Interaction. Water Resources Research, 32 (5), 1343-1357.

Carlson, T. N., E. M. Perry, and T. J. Schmugge (1990). Remote Estimation of Soil Moisture Availability and Fractional Vegetation Cover for Agricultural Fields. Agricultural and Forest Meteorology, 52 (1-2), 45-69.

Carlson, T. (2007). An Overview of the "Triangle Method" For Estimating Surface Evapotranspiration and Soil Moisture from Satellite Imagery. Sensors, 7(8), 1612-1629.

De Rosnay, P., G. Balsamo, C. Albergel, J. Muñoz-Sabater, and L. Isaksen (2012). Initialisation of Land Surface Variables for Numerical Weather Prediction. Surveys in Geophysics, 35 (3), 607-621.

Farooq, M., A. Wahid, N. Kobayashi, D. Fujita, and S. M. A. Basra (2009). Plant Drought Stress: Effects, Mechanisms and Management. Agronomy for Sustainable Development, 29 (1), 185-212.

Gillies, Robert R., and T.N. Carlson (1995). Thermal Remote Sensing of Surface Soil Water Content with Partial Vegetation Cover for Incorporation in to Climate Models. Journal of Applied Meteorology, 34 (4), 745-756.

Karthe, D., J. Hofmann, R. Ibisch, S. Heldt, K. Westphal, L. Menzel, S. Avlyush, and M. Malsy (2015). Science-Based IWRM Implementation in a Data-Scarce Central Asian Region: Experiences from a Research and Development Project in the Kharaa River Basin, Mongolia. Water, 7 (12), 3486-3514.

Mallick, K., B. K. Bhattacharya, and N.K. Patel (2009). Estimating Volumetric Surface Moisture Content for Cropped Soils Using A Soil Wetness Index Based on Surface Temperature And NDVI. Agricultural and Forest Meteorology, 149 (8), 1327-1342.

Nigam, R., B. K. Bhattacharya, S. Vyas, and M. P. Oza (2014). Retrieval of Wheat Leaf Area Index from Awifs Multispectral Data Using Canopy Radiative Transfer Simulation. International Journal of Applied Earth Observation and Geoinformation, 32, 173-185.

Rajeshwari, A. and N.D. Mani (2014). Estimation of Land Surface Temperature of Dindigul district using Landsat 8 data. International Journal of Research in Engineering and Technology, 3(5), 122-126.

Sandholt, I., K. Rasmussen, and J. Andersen (2002). A Simple Interpretation of The Surface Temperature/Vegetation Index Space for Assessment of Surface Moisture Status. Remote Sensing of Environment, 79(2-3), 213-224.

Singh, R. and R. B. Alderfer (1966). Effects of soil-moisture stress at different periods of growth of some vegetable crops. Soil Science, 101(1), 69-80. doi:10.1097/00010694-196601000-00014.

Stisen, S., I. Sandholt, A. Nørgaard, R. Fensholt, and L. Eklundh (2007). Estimation of Diurnal Air Temperature Using MSG SEVIRI Data in West Africa. Remote Sensing of Environment, 110(2), 262-274.

Teillet, P.M., B. Guindon, and D.G. Goodenough (1982). On the Slope-Aspect Correction of Multispectral Scanner Data. Canadian Journal of Remote Sensing, 8(2), 84-106.

Use of GIS and sound signal processing for remote monitoring of a data centre for smoke / fire

Rajendra N. Gaikwad[*] and M. P. Oza
Space Applications Centre, Ahmedabad, India
Email: g_rajendra@sac.isro.gov.in

Abstract: Research Centres and Institutes generating or using important civilian, environmental and strategic data are well equipped with high-computing devices and secured with fire safety equipment. This paper describes how amalgamation of fire alarm signals (i.e. sound waves) and Geographical Information System (GIS) is useful in locating origin of alarm signal and communicating it to the identified management teams. Sound signals from smoke / fire hooter are captured using in-built sound recorder of a computing device (voice recorder like microphone) and processed using R Script / Library at source. The sound wave signals generated at data centre are then processed and transferred to the web / disaster recovery (DR) server with location information. An alert is generated with spatial data and maps at server or DR site are transmitted through web services for necessary follow up. Decision makers will be able to identify the exact computer system responsible for causing alert. This information is useful for deciding further course of action. Once samples of possible sound producing sources and their signals at the data centre are captured, remaining part of method developed is a fully automated and avoids any human interaction. This paper illustrates how the fusion of sound waves, 3D graphics and java script for web GIS solution can produce useful system for remote monitoring of a data centre.

Keywords: Sound wave, GIS, emergency, processing

1. Introduction

In the present era, data are precious and critical. Recent times are witnessing challenges in efficient storage, archival and retrieval systems to facilitate safe yet fast access to recent as well as past data. Research Centres and organizations / institutes generating or using civilian, environmental and strategic data are well equipped with high-end computing devices. They typically have a data centre which serves 24 x 7 and are secured with cyber safety equipment. One of the risk factors to safety of data is possibility of fire taking place (possibly due to short circuits and / or environmental conditions such as extreme heat and / or moisture) at such premises. So they are also equipped with alert mechanism of triggering hooter, which produces sound waves, in case of smoke / fire to prompt further immediate action to be taken by concerned team. In the present trend of digital world, there is a need to have soft repository of events, which help to remote monitor and trace the events taking place or took place at the data centres.

If the sound signal of alarm could be integrated with GIS techniques, it should be great help to manage premise remotely yet efficiently. There are at least two compelling factors to jointly use GIS and sound waves. First, to collect and categorise appropriate sound information and second, to visualize through client server for decision making. It must be recognized that it is easier to record sound but not so easy to process them. It is generally agreed that joint use of sound and pictures provide vivid description of activities happening and catch attention for various on-site / off site care takers.

The technological advances in geospatial data collection and sensor networks have motivated new applications that handle spatio-temporal information. To support these applications, there is a growing demand for GIS to deal with such information (Ferreira et al., 2012). Moving object is a well-known category of spatio-temporal data (Erwig et al., 1999). In this paper, changing time is used as surrogate for a moving object. It is noted that there is no accepted standard way to represent them in data files or database systems. There is a requirement to have automatic data analysis with interactive visualization techniques (Andrienko et al., 2011; Kopanakis and Theodoulidis, 2003). With the availability of technologies such as JavaScript, signal processing libraries, it is possible to develop web interface to facilitate displaying location of lab / computer on web pages. The present study, therefore, focuses on providing a system that performs automatic data analysis and visualize using web services in 3D object representation. The present work reports development of a prototype system for achieving such fusion.

2. Objective

The goal of this work is to demonstrate how sound signals of smoke / fire alert sensors can be captured, processed and integrated with GIS to produce web Map to support during smoke or fire.

3. Data

The following data are used for the present study:
(1) High Resolution Satellite (static) data of organization for background reference.
(2) Library of typical sound signals emanating from sources of noise including of alert systems at a data centre.
(3) GIS layers (or CAD / CAM drawing) of campus / organization / institute - used for geographical location of origin of alert signal sound. It is necessary that CAD drawing have location as well as IP of client machines. So while creating geojson database, attributes with

location and IP are linked and available. IP of the machine are stored in server database. R script uses IP of computers (on client side) which gets appended along with timestamp as an attribute and sent to server.

4. Development of prototype system

It is possible to capture sound waves from the in-built hardware sensors and analyse the signal through open source libraries, to identify loudness and location of origin of signal. The work flow of the study presented in this paper is described in three stages, (1) Sound wave capture and processing (2) Server side scripting for web GIS solution and (3) Client web interface for decision makers/disaster management team.

4.1 Sound capturing and processing

Sound signals are captured using in-built recording device, Conexant HD device, of a computer. The sampling rate for generating audio file can be initially defined as desired. User needs to specify sampling rate and audio driver to capture sound signals using R audio package (Urbanek, 2018) library. Base library of R package is utilized to collect other parameters like date stamp with time and concatenating string with audio file and sound amplification. This library creates R object for audio signal, each object containing five slots i.e., left, right, sampling rate, stereo and bit. Left slot vector contains samples for left channel. Six basic properties of sound signal, namely Frequency / Pitch, Amplitude / Loudness, Spectrum / Timbre, Duration, Envelope, Location, help to study sound information for various applications and R libraries help to study these fundamental characteristics in signal processing (Lauren et al., 1982). The amplitude of a sound wave helps to determine its relative loudness. Two sound waves having the same frequency but different amplitude are analysed to set threshold for identifying loudness of (alert-) sound signal. This is important as it permits to set an appropriate threshold to eliminate background noise and restrict false alarms. Importance of comparing parameters for alert generation and implementation is described in methodology with example.

An audio wave file is generated using function "record". The audio signal is tagged with other relevant parameters like IP, date stamp attached with geojson, representing simple geographical features based on JSON (JavaScript Object Notation) – a file that contains geographic location of the site and is sent to web server using local network. Seewave, a command-line driven library devoted to sound analysis and synthesis, was used sounds signal processing (WAV files). This procedure is schematically summarized in figure 1. This process helps to collect the site detail information and may be helpful for other than fire incident / situation like manmade disaster.

Such sound frequencies of various possible sources of noise such as telephone / mobile ring tone, noise of AC / fan, door closure are analyzed to set threshold level due to environmental noise level of study data center. Table 1 lists sound signal output for various features like "tap on

table", "Phone dial" and "Fire alarm" with plots derived with the help of five slots of R object described above. Fire alarm audio file played using player and used for sound wave signal study, where audible fire alarm notification appliances used in the public mode must be a minimum of 15 dB (decibels) above average ambient sound levels (NFPA 72®, 2016), but in practical the decibel value goes between 50-60 dB.
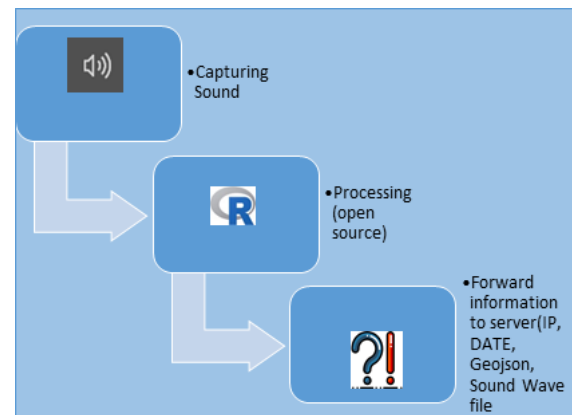
Figure 1. Capturing and processing Sound wave

To utilise capabilities of R package for handling sound signal, a graph is generated as shown in figure 2 which helps in report generation of a site.
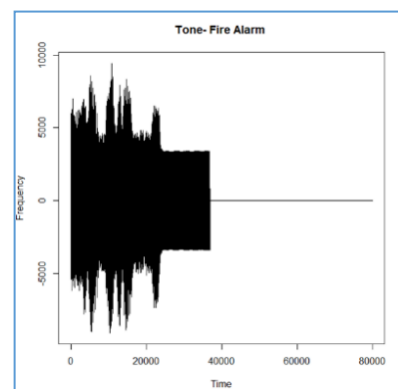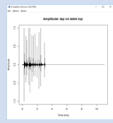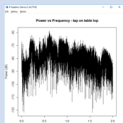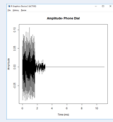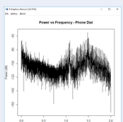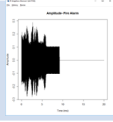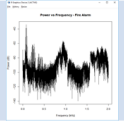
Figure 2. A sample of captured sound wave of fire alarm hooter

4.2 Server side processing

Information received from client site is processed using server side scripting. Web services are important to disseminate the required information / services to end users. In this study, apache tomcat server was used for web services along with java script for handling GIS datasets and 3D graphics information. Visualization techniques provide a powerful way (Andrienko et al., 2011; Kopanakis and Theodoulidis, 2003) for web GIS. This part of the process is shown in figure 3. GIS helps to locate exact location of required features on web pages. To showcase various sites, 3D graphics was generated to show different site clients location (i.e., site where client side sound capturing and processing took place). With the help of CesiumJS, an open-source JavaScript library for world-class 3D globes and maps, a few lines of code produce virtual globe into html (Cesium Consortium, 2016). This facilitates to produce web map using 3D graphics of campus / sites. This is shown in Figure 4.

Table 1. Illustrative representation of typical sound signals

Power (dB)	Amplitude (m)	Feature Type	Amplitude vs time	Power vs Frequency
-54.77606	0.106781	Tap on table		
-58.62353	0.9999695	Phone Dial		
-33.9439	0.2878723	Fire alarm		
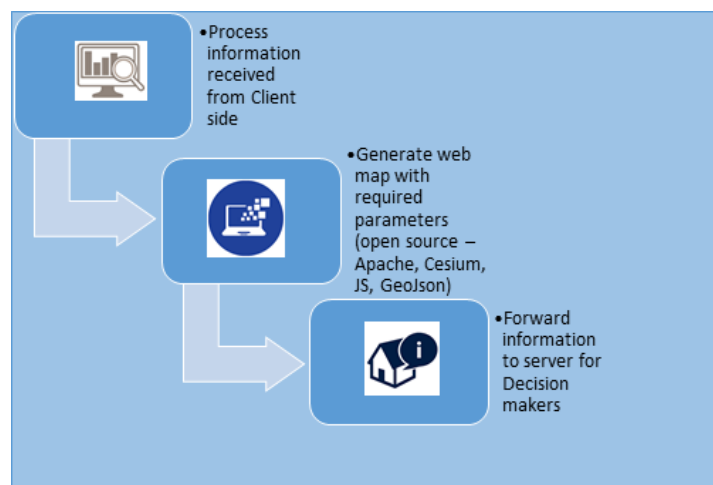
Figure 3. Server side major processing steps
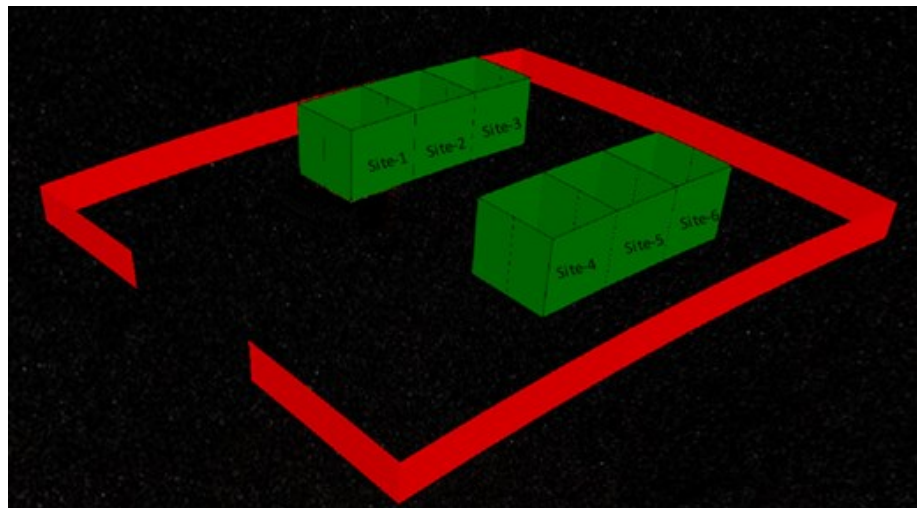
Figure 4. A sample of site map generated as a 3D graphics web page

Such graphics are presented to avoid any geographical mismatch in identification. Cesium has capability to showcase GIS layer in 3D feature. An illustration of 3D map using CesiumJSis presented in Figure 5.

4.3 Web interface
The web interface is broadly having two main interfaces/sections i.e., Alert and Visualization sections.

The picture shows in figure - 6 describe the user interface of alert generated during emergency. The Alert section shows blink message regarding the location of the fire / incident. Second section shows 3D GIS visualization of the location with fire animation image, this section helps to visualize the location in 3D viewer on web and name of the building on right hand side when user select the object on web. Top Section shows images related to emergency messages which appear on screen.
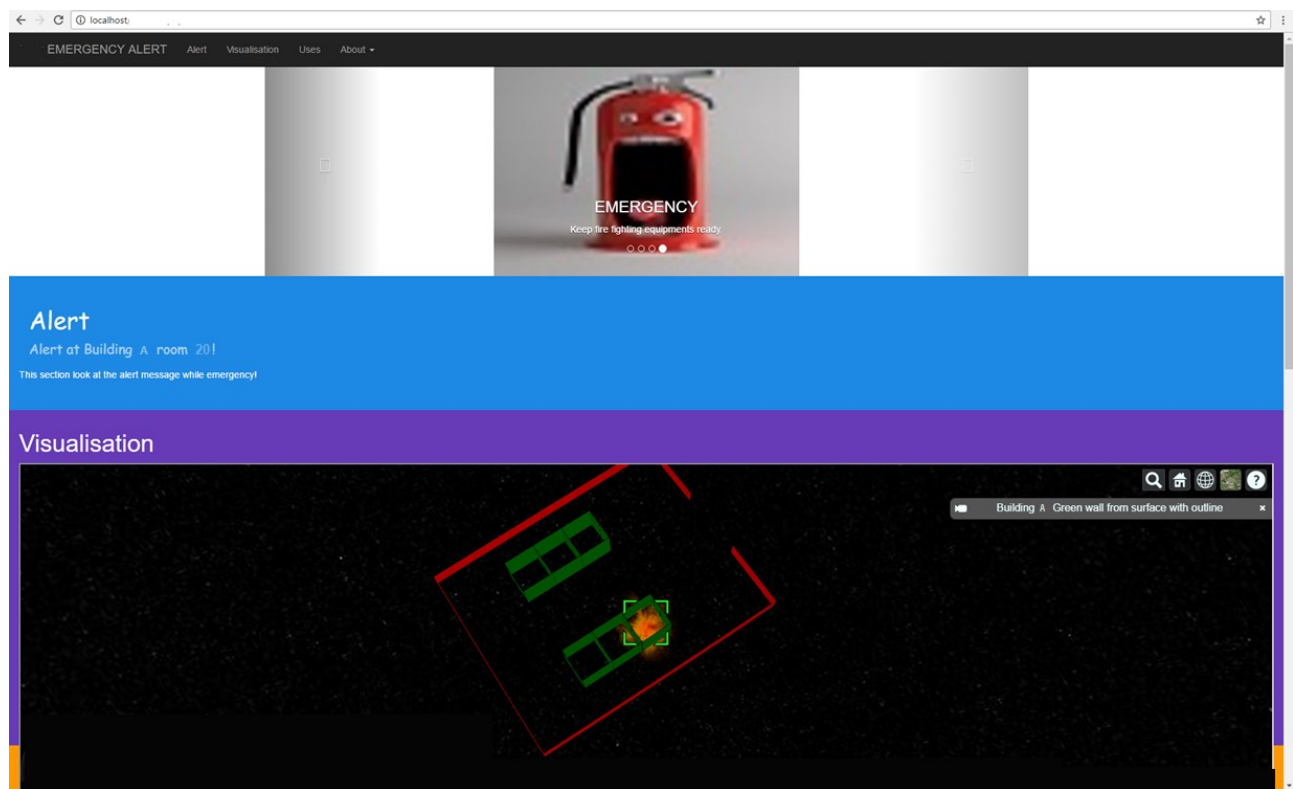
Figure 6. User interface of prototype developed

Sound signal information collected from site is processed at web server. Processing involves decrypting geojson and sound wave details to generate web interface. This is done using java script to notify site location where sound wave was generated. These are integrated to depict a spatial scenario along with appropriate representation of geospatial object (Ferreira et al., 2012) for simpler and visually appealing communication to disaster management team. A web 3D map generated of site is shown in figure 7, which contains fire animated image which continuously appears, until human intervention, at web site to assist disaster team. Such 3D maps help to identify exact location

5. Conclusions

The study utilised sound waves captured by in-built sensors of computer hardware and fused it with GIS technologies to develop a prototype system that could be used to identify geolocation or IP of system culprit for generating smoke / fire alarm at a data centre. The resultant web GIS solution is arrived at using capability of sound signal processing and GIS functionality of R Package. It is demonstrated that such solution provides a useful alternate remote way for alarming the smoke / fire situation at a data centre to the relevant team through web map services.

Figure 5. A template 3D map generated using CesiumJ
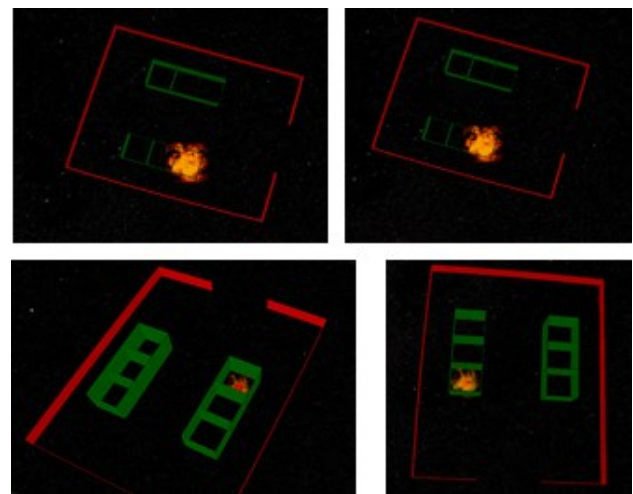
Figure 7. Web 3D maps showing simulated incident at site

References:

Andrienko, G., N. Andrienko, D. Keim, A.M. MacEachren and S. Wrobel (2011). Challenging problems of geospatial visual analytics Journal of Visual Language Computing, 22, 251-256.

Cesium Consortium, (2016). CesiumJSis developed by an open-source community, with support from the Cesium Consortium, founded by Analytical Graphics, Inc., Bentley Systems, and Rafael.

Erwig, M., R.H. Güting, M. Schneider and M. Vazirgiannis (1999). Spatio-Temporal Data Types: An Approach to Modeling and Querying Moving Objects in Databases. GeoInformatica, 3(3), 265–291. (https://doi.org/10.1023/A:1009805532638)

Ferreira, K.R., L. Vinhas, A.M.V. Monteiro and G. Câmara (2012). Moving objects and spatial data sources. RevistaBrasileira De Cartografia, 64, 796–806.

Kopanakis, I. and B. Theodoulidis (2003). Visual data mining modeling techniques for the visualization of mining outcomes, Journal of Visual Language Computing, 14(6), 543-589.

Lauren, E. K., R.F. Austin, B.C. Alan and V.S. James (1982). Fundamentals of acoustics; John Willey & Sons, New York.

NFPA 72® (2016). https://www.nfpa.org/codes-and-standards/all-codes-and-standards/list-of-codes-and-standards/detail?code=72

R Core Team, (2013). R: A language and environment for statistical computing. R Foundation for Statistical Computing, Vienna, Austria. URL http://www.R-project.org/.

Urbanek, Simon (2018). https://cran.r-project.org/package=audio.

Comparison and Validation of DEMs through Topographic Parameters: A Case Study for Micro Watershed of Cauvery River Basin

N. Shenbagaraj*, K. Senthil Kumar, J. Leo Stalin, M. Naresh Kumar and C. Divya
Madras Institute of Technology, Chennai – 600 044,
Email: shenba.gis2009@gmail.com

Abstract: It is inevitable for both present and future, various innovations require hydrological model research to secure and sustainable water resources. Any type of hydrological model can be contributed to the Digital Elevation Model (DEM). The accurate hydrological model depends on the precision of the DEM. In this study, one arc-second resolution of various satellite-derived DEM viz., Cartosat and Shuttle Radar Topographic Mission (SRTM) and 30 m resolution of Advanced Land Observing Satellite (ALOS) Digital Surface Model (DSM) were used. Bentley MicroStation software was used to remove the above and below ground points of DSM. This study mainly has focused to identify sensors for providing more precise DEM. derived DEM from Different sources has been validated through the topographical parameters (elevation, slope, flow direction, flow accumulation, Topographic Wetness Index (TWI) and Stream Power Index (SPI)) using Reference DEM, which was generated from the contour extracted from the 1:25,000 scale of the survey of India (SOI) topographical map. This study has concluded that the SRTM DEM gives more precise result.

Keywords: DEM, DSM, DEM comparison, TWI, SPI and Topographical parameters

1. Introduction

Digital Elevation Model (DEM) represents the horizontal and vertical dimensions of the earth's land surface (Kwanchai Pakoksung and Masatka Takagi 2016). It is an important factor in digital topography analysis including slope, flow direction, flow accumulation, curvature, roughness and its derivatives. The derived parameters from DEMs have normally utilized in various applications such as flood simulation (Wang et al. 2008; Shahapure S. S et al. 2010; Kwanchai Pakoksung and Masataka Takagi 2016) landslide susceptible mapping (Dhakal A.S et al. 2000; Le Lin et al. 2017) and seismic wave propagation (Lee S.J et al. 2009). DEM is publically available from the space-based measurements such as the SRTM DEM data (Farr and Kobrick 2000), the Advanced Spaceborne Thermal Emission and Reflection Radiometer (ASTER) DEM (Meyer D et al. 2013; Tachikawa T et al. 2011) and ALOS Global DSM. DEM is required for hydrology modelling because the trees and buildings modify the natural surface runoff (Polidori, L and El Hage M 2020). DEMs can also be derived from DSM and generated from multiple sources using various methods of processing, including contour map digitisation, interpolation from spot height measurements, collected by using various methods for example conventional survey methods (Global Positioning System (GPS) or Global Navigation Satellite System (GNSS)) and processing of radar/ laser measurement data (Hebeler F and Purves R.S 2009).

Every method in DEM derivation has the limitations of cost involved, accuracy, sampling density, pre-processing requirements (Kwanchai Pakoksung and Masatka Takagi 2016). Four steps were followed to produce a DEM product viz., (i) acquisition of data (ii) resampling for grid spacing (iii) spot height interpolation and DEM representation, and (iv) process repeating and accuracy assessment. The error in DEM generation contributed by all of the above-mentioned steps. These errors were examined in gridded DEM data, which had classified into three categories: gross errors, systematic errors and random errors (Fisher P. F and Tate N. J 2006). The justifications were broadly investigating the blunder of a few DEMs, its importance and the vertical exactness of DEMS would be impacted by various factors, for example, sensor types, landscape type, matrix separating, calculation and attributes (Hebeler and Purves 2009). The error-free DEMs were provided with a more precise outcome in topographic analysis and various disaster applications.

SRTM and ASTER DEMs were compared and validated through the reference DEM, which was generated by using hypsographic and hydrographic data from a 1:50,000 scale of topographical map (Gerald Forkuor and Ben Maathuis 2012). Al-Fugara A. 2015, compared and validated the freely available DEMs of the Global ASTER and SRTM with derived DEM from the elevation points of topographic maps and stereoscopic pairs of aerial images. The accuracy variation of a DEM depends on the location. It could be assessed by using the comparison between the DEM and the corresponding reference point which was measured by the high precision equipment of GPS (Jarvis A et al. 2004; Miliaresis G. C and Paraschou CVE 2005; Nikolakopoulos K. G et al. 2006; Hirt C et al. 2010; Gerald Forkuor and Ben Maathuis 2012; Kolecka N and Kozak J 2013; Antonios Mouratidis and Dimitrios Ampatzidis 2019).

The accuracy of DEM assumes a crucial part in a few applications and the result is to analyse their sensibility relies upon factual estimation for specific applications (Kwanchai Pakoksung and Masataka Takagi 2016). Therefore, assessing the vertical accuracy of DEM is an important task. Hence, in this study, the accuracy of freely available DEM products was compared and validated with DEM, which were derived from SOI toposheets as referenced DEM.

2. Methodology

2.1 Study Area
A micro watershed of the Cauvery River basin was selected as the study area (Figure 1) which is ~ 903 ha of area. It is located in the Coimbatore district, of Tamil Nadu state. It consists of ridges, valley and, plain surface.
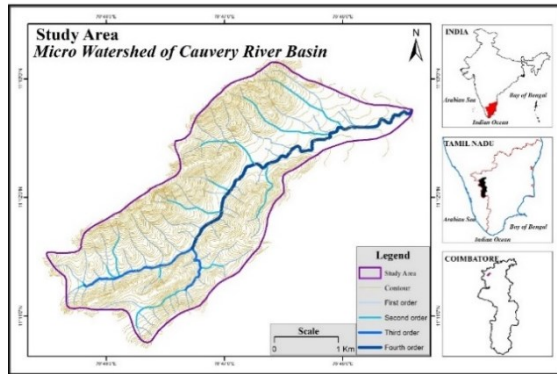
Figure 1. The Location of the Study Area

It is geographically located in between the longitude 76° 45' 32.337" E to 76° 48' 36.758" E and latitude 11° 10' 45.276" N to 11° 13' 12.572" N. The principal land cover type is forest situated on mountain slopes.

3. Data Used

3.1 Digital Elevation Model
Different resolutions of DEMs and DSMs viz., one arc-second resolution of CARTOSAT DEM, SRTM void filled version 3 DEM and ALOS DSM were produced by the Indian Space Research Organisation (ISRO), United States Geological Survey (USGS) and Japan Aerospace Exploration Agency respectively and the reference DEM had derived from the 1:25,000 scale of SOI topographic maps were used for comparison. The metadata of used DEMs and DSM were listed in (Table 1).

3.1.1   CARTOSAT DEM
Bhuvan is a web mapping service that allows downloading the 2D and 3D spatial data of the earth surface. Cartosat-1 was launched on 5th May 2005 by ISRO, which provides stereo data for the entire India. One arc-second resolution of DEM had generated countrywide by using digital photogrammetric techniques (ISRO 2011). For generating
.

seamless DEMs, photogrammetric blocks were formed with fewer break-lines; edge-matching process carried out across the scenes. Ground points through dense feature matching, Triangulated Irregular Network (TIN) modelling and automated strip mosaicking methods had used to generate the automatic process of seamless DEM (Muralikrishnan S 2012). The quality of the DEMs verification process was completed by panning and draped visualization to delineate distortions (Muralikrishnan S et al. 2012).

3.1.2   SRTM DEM
Recently, one arc second resolution of NASA SRTM Global data set released additional tiles for Asia and Australia by the Land Processes Distributed Active Archive Center (LPDAAC). This newly processed area DEMs released by the United States Geological Survey (USGS) in 2015, available through Earth Explorer. ASTER Global Digital Elevation Model 2 (GDEM2), USGS National Elevation Dataset (NED) and USGS Global Multi-resolution Terrain Elevation Data (GMTED) 2010 used for Global 1 arc second resolution of SRTM dataset.

3.1.3   ALOS DSM
The ALOS DSM dataset consists of one arc-second horizontal resolution by the Panchromatic Remote Sensing Instrument for Stereo Mapping (PRISM) on board of ALOS Satellite. In May 2015, the 30 m resolution of ALOS World 3D (AW3D30) was released. No data or low quality of an area from 60° N to 60° S filled with version 1.1, 2.1 and 2.2 had released in March 2017, April 2018 and April 2019 respectively. Version 2.2 has an improved version of the northern region over 60° N.

3.1.4   Reference DEM
For this study area, a topographical map collected from the Survey of India (SOI), Guindy. Then geo-referenced with the corresponding coordinates and assigned the Universal Transverse Mercator (UTM) projection with the World Geodetic System (WGS). The National Imagery and Mapping Agency has provided the transformation parameters ($\Delta x = 295$, $\Delta y = 736$, $\Delta z = 257$) that help to convert the Everest Modified datum to WGS 84 (Srivastava B. K. and Ramalingam K. 2009). the elevation points extracted from the SOI toposheets that helps to derive the DEM. It has been used as the reference DEM

Table 1. Metadata of Used DEM and DSM of this Study

Data	CARTOSAT	SRTM	ALOS DSM	Reference DEM
Data Source	Bhuvan	Earth Explorer	ALOS World 3D	SOI
Generator and Distributor	ISRO	USGS	JAXA	GOI
Releasing Year	2015	2015	2016	1996
Resolution/ Scale	1 arc second	1 arc second	1 arc second	1:25,000

4. Data Preparation

The collected all DEMs transformed into the same projection of Reference DEM - UTM 43 N zone and WGS 1984 was selected as both datum and spheroid. The ALOS DSM dataset had converted to the Lidar point file (.las) in the 5 m interval. Hereafter, Bentley MicroStation software used to remove the high and low points from the Lidar point dataset and then created the surface for ground Lidar points which were exported to the 30 m resolution of DEM file format with the help of Global mapper software. It could be used as the DEM data for hydrological studies. The micro watershed area delineated manually using the SOI topographic maps with the same projection and datum to take as the study area. This study area based mask all DEMs (CARTOSAT DEM, SRTM, ALOS DSM and Reference DEM). The fill tool was run for all used DEMs to remove peaks and fill the sink in the DEM.

4.1 Comparison of DEMs
For this study, two main approaches were used to compare and validate the elevation datasets against the reference DEM. The first approach has determined the accuracy of the elevation values of the products and the other one was to determine the accuracy of terrain derivatives like slope, flow direction, flow accumulation, TWI and SPI.

4.2 Accuracy of Elevation Values
In this study, the accuracy of elevation values has achieved by three-way of performing. These are (i) DEM differencing (ii) Profiling and (iii) correlation Plots.

4.2.1 DEM Differencing
 It was deriving from the elevation errors of the used Different DEMs in this study. Root Mean Square Error (RMSE) is a common measurement to quantify the vertical accuracy of a DEM. In this study, thousand random points were generated to the training sites. For these points, elevation values were extracted from all used DEMs in this study. The given below equation (1) was used to derive the RMSE for all error DEM.

$$\text{RMSE} = \sqrt{\sum_{i=1}^{n} \frac{(Oi - Pi)^2}{n}} \quad \text{--------- (1)}$$

Where, Oi - Observed elevation value from Reference DEM; Pi - Predicted elevation value from error DEM;   n - Number of sample points

4.2.2 Profiling
 Surface Profiles were created for ALOS, Cartosat and SRTM DEMs, which compared and validated against the reference DEM. For this study, the validation purpose had created profile length was 5423 m. An elevation graph generated against distance from the source for all used DEMs in this study.

4.2.3 Scatter Plots Correlation
 It performed to assess the level of correlation between the reference and error DEM. It was a very difficult process because each DEM has more than 50,000 pixels. For this reason, the scatter plots were created based on randomly created points/ pixels. For this purpose, 1000 points/ pixels randomly selected from each DEM. The linear regression

equation and coefficient of determination (R^2) values were generated for all correlation scatter plots.

4.2.4 Accuracy of the Terrain Derivatives
a) Slope: Slope means the ratio of the altitude change to the horizontal distance between any two points on the line. It was widely used as one of the factors in hydrology related studies. It is one of the derivative product of filled DEM. The slope of the training site calculated from each triangle created in the TIN surface. The slope tool calculated for each cell, the maximum rate of change in value from its neighbour's cells. The output slope map generated in the raster format containing the slope value at each cell. The lowest slope value is flattered the terrain and the highest slope value is steeper in the terrain. The slope derived based on the degree.

b) Flow Direction and Accumulation: Determining the direction of flow of water through each cell of DEM and is useful for finding drainage networks and drainage divides. The direction of the flow determined by the elevation of the surrounding cells. The cell has the lowest elevation value compared to the surrounding cell; the water can flow only into one cell. The sink is not there the water can be flow into one other cell. Flow accumulation used to generate a drainage network, based on the direction of flow of each cell. By selecting cells with the greatest accumulated flow, we can create a network of high-flow cells. Output cells with a high flow accumulation are areas of concentrated flow and used to identify stream channels.

c) Topographic Wetness Index (TWI): It is a steady-state wetness index, which also known as Compound Topographic Index (CTI). Generally, it used to study the effects of topography on the hydraulic process (Wolock D. M and McCabe G.J 1995; Sorensen R, et al., 2006) and to describe the spatial pattern of soil moisture (Burt T and Butcher D, 1986; Moore I. D et al., 1991). The TWI, ln ((A + 0.001)/ ((B/ 100) + 0.001)), is the natural logarithm of the ratio of the specific upstream contributing area (A) to the ground surface slope (B). The surface slope generated

from DEM. The specific flow accumulation of training sites evaluated from the flow direction derived from DEM. The continuous TWI range obtained for each of the DEM classified into integer classes and scatter plotted against percentage per class for comparison purpose.

d) Stream Power Index (SPI): It could be used as an algorithm to assess the erosive power of flowing water (De Risi R, 2013) by using the slope and upstream contributing area. Besides, it used to examine the effects of topography on the hydraulic process. For example, SPI helps to identify the approximate location of gullies forming area due to the water flow based on the training sites. The SPI, ln ((P+ 0.001) * ((Q /100) + 0.001)), is the natural logarithm of the product of a specific stream contributing area (P) to the ground slope (Q). The continuous SPI range obtained for each of the DEM classified as an integer class and plotted for comparison purpose. Table 2 represents the statistical summary of the analyzed DEM's elevation and derived topographic parameters.

5. Results and Discussion

5.1 Accuracy of Elevation Values

Table 2 represents the errors statistics of each DEM of the study area, whereas Figure 2 (a-c) portrays the spatial distribution of the different range (each DEM and reference DEM) and the percentage of the pixel, which belongs to the different error ranges. Table 3 consists of the Minimum, Maximum, Mean, Standard Deviation (SD) and RMSE of the difference map. The vertical accuracy of a DEM evaluates based on the RMSE. Table 3 further reveals that the compared out between SRTM and Reference DEM has been very less RMSE value (10.79) compared to an error map of ALOS DEM and Cartosat DEM.

Figure 2 (a), 2 (b) and 2 (c), and show the spatial distribution of error map ALOS DEM, Cartosat DEM and SRTM respectively. The graphical representation and statistics of the error map indicate that the SRTM DEM is close to reference DEM.

Table 2. Analysed DEM's Summary of Error Statistics of Training Sites

Dataset	Description	Minimum	Maximum	Mean	Standard Deviation
Reference DEM (SOI)	Elevation (m)	420	970	587.68	96.49
	Slope (degree)	0	69.81	17.36	10.72
	Flow Direction	1	248	22.77	35.34
	Flow Accumulation	0	10129	81.248	641.55
	TWI	-6.55	16.11	1.94	4.03
	SPI	-13.81	6.47	-2.27	3.94
ALOS DSM to DEM	Elevation (m)	427	921	593.68	93.98
	Slope (degree)	0	44.32	16.72	10.26
	Flow Direction	1	193	23.13	35.93
	Flow Accumulation	0	2894	24.23	138.82
	TWI	-6.06	12.65	0.90	4.18
	SPI	-13.81	5.78	-3.22	4.30
CARTOSAT DEM	Elevation (m)	430	748	583.67	74.72
	Slope (degree)	0	44.05	10.32	6.97
	Flow Direction	1	128	27.48	40.99
	Flow Accumulation	0	674	9.41	31.29
	TWI	-5.94	10.58	0.80	4.17
	SPI	-13.32	357	-4.23	4.43
SRTM DEM	Elevation (m)	431	917	593.81	94.74
	Slope (degree)	0	50.17	15.58	9.62
	Flow Direction	1	208	22.93	35.468
	Flow Accumulation	0	2360	21.78	115.376
	TWI	-6.08	13.70	1.29	4.01
	SPI	-13.8	5.39	-2.96	4.19

Table 3. DEM Difference Statistics of this Study Area

Difference Map	Min	Max	Mean	SD	RMSE
ALOS DEM - Reference	-51	47.81	5.86	10.85	12.31
Cartosat DEM - Reference	-218.45	134.47	-4.67	44.70	110.19
SRTM DEM - Reference	-118	50.66	6.10	8.69	10.79

(a)

(b)

(c)

(d)
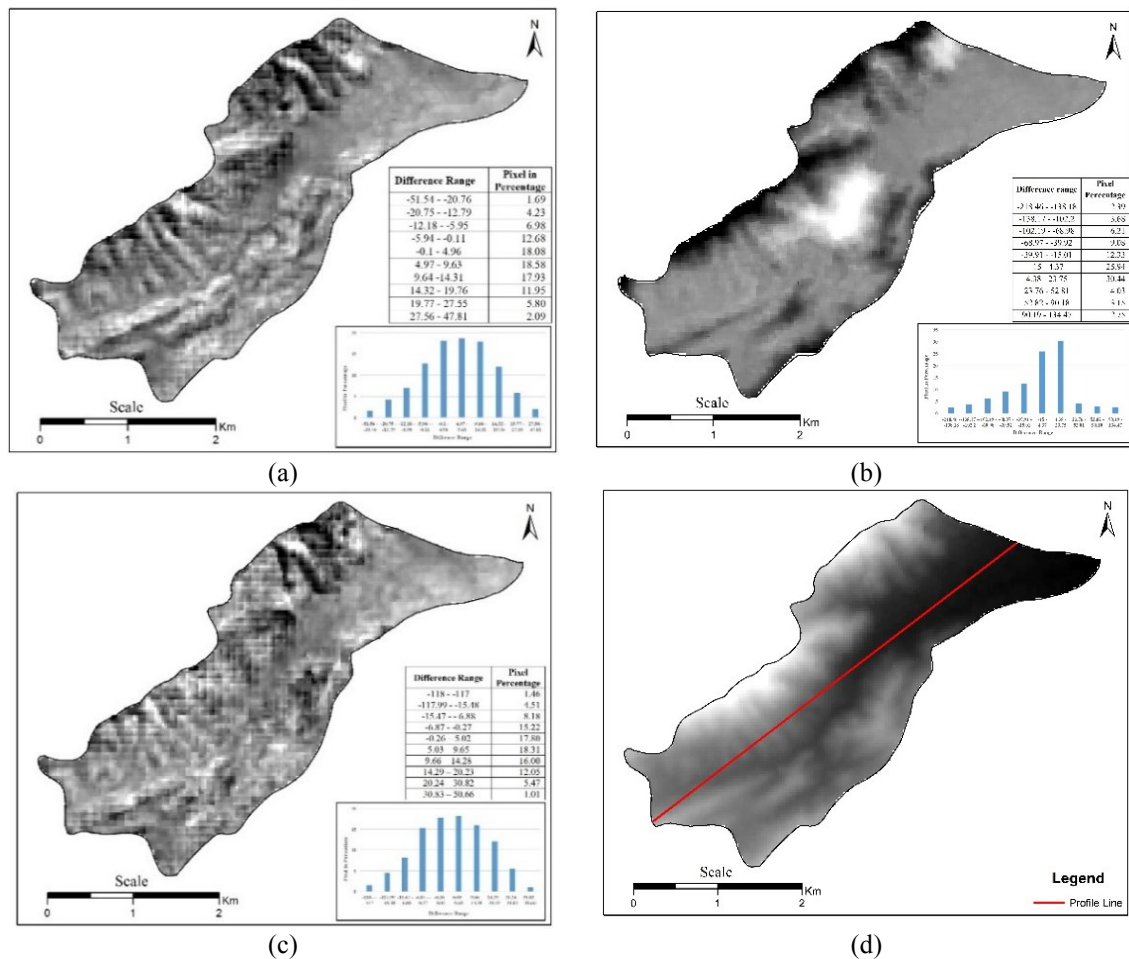
Figure 2. DEM Difference Map computed for the Study Site (a) ALOS minus Reference (b) Cartosat minus Reference (c) SRTM minus Reference (d) Surface Profile Line
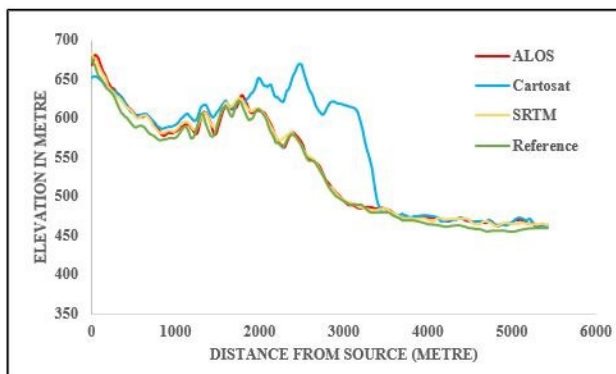
Figure 3. Surface Profiles Derived from Four Different DEM

Apart from generating error maps, statistics and graphs, the surface profile was created for each DEM's for a common line feature by using Global Mapper software and the data exported to the .csv format. All DEM's surface profile statistical data had used to make a graph that was used to identify the accuracy of DEM through the

.

reference DEM's surface profile. Figure 2 (d) represents the created line for surface analysis and the obtained result of the surface profile for this training site further confirmed the earlier findings of elevation difference. A visual inspection of figure 3 clearly shows SRTM and generated DEM from ALOS DSM were very closer to the reference DEM.

Figure 4 (a-c) represents the obtained scatter plots of the training site. The scatter plots were created for (as stated earlier) 1000 random points. The linear regression equation and coefficient of determination (R^2) value for all created correlation scatter plots were seen the SRTM DEM was very closer to reference DEM. Figure 4 (a) shows the scatter plot between reference DEM and ALOS DEM whereas the R^2 value of that scatter plot has 0.9706. Figure 4 (b) expresses the graphical representation of the scatter plot of reference DEM and Cartosat DEM of its R^2 value is 0.8523. Figure 4 (c) portrays the scatter plot between reference DEM and SRTM DEM of its R^2 value is 0.9909, which was very near to one. Hence, SRTM DEM was very closer to the reference DEM

(a)

(b)

(c)
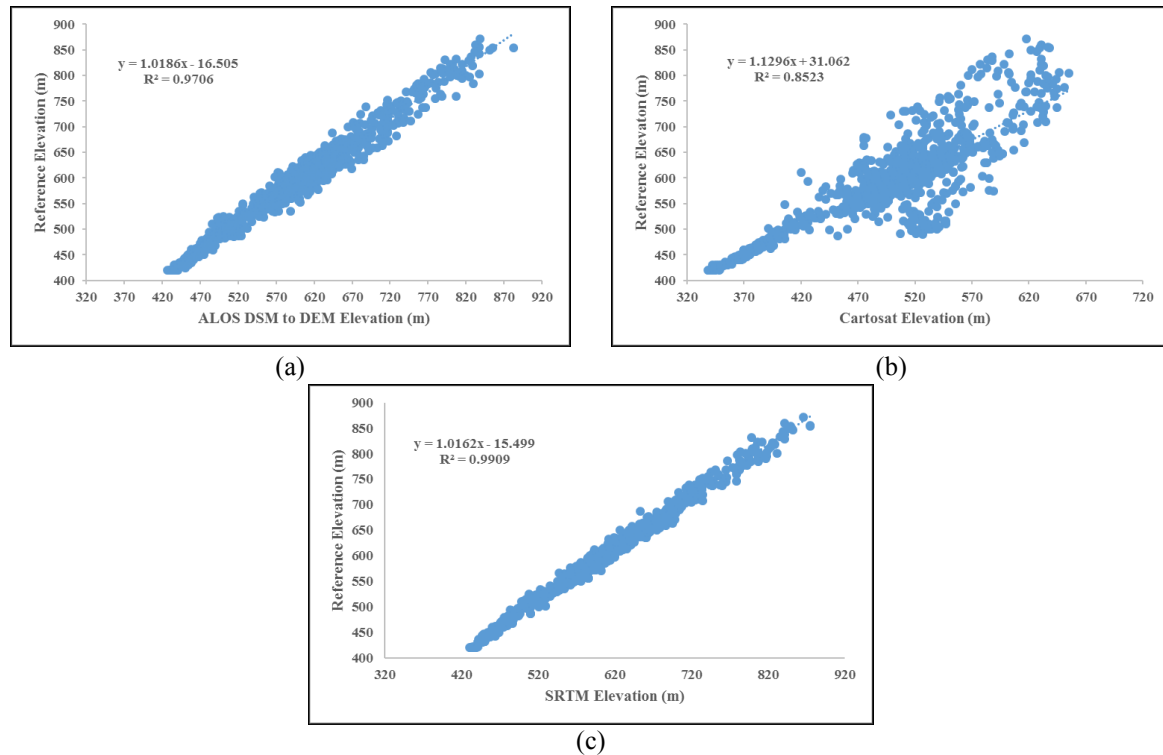
Figure 4. Correlation plots of this study sites (a) DEM derived from ALOS DSM versus Reference DEM (b) Cartosat DEM versus reference DEM (C) SRTM versus Reference DEM

5.2 Accuracy of Terrain Derivatives

In this study, five topographic derivatives such as slope, flow direction, flow accumulation, TWI, and SPI were used to compare and validate the accuracy of used four different DEM against the reference DEM. Each derivative of the four DEM's SD had seen SRTM DEM that was very closer than other DEMs with the reference DEM. The accuracy of terrain derivatives was used for validating the accuracy of different DEMs. The outcome of this study, SRTM DEM gives better accuracy compared to the used other DEM.

Figure 5 shows the graphical representation of TWI for four different DEM's including the reference DEM. The graph was created in between the TWI value and percentage per class. After visually analysing Figure 5 the TWI of SRTM DEM had very near to the reference DEM then next derived DEM from ALOS DSM been matched the reference DEM and the Cartosat DEM's maximum percentage per classes were underestimated in TWI.
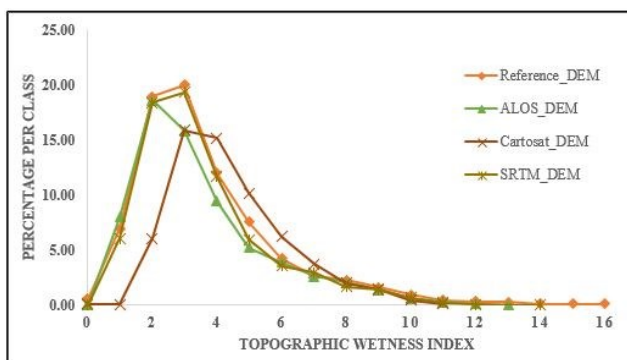
Figure 5. Comparison of TWI Classes for the DEM's

Figure 6 represents the pictorial of SPI of four differently used DEMs in this study, which also included the reference DEM. The graph generated between the SPI value and percentage per class. The graph clearly shows to visualize and identify the similar pattern of SPI curves of used DEM's. The SRTM DEM graph line is very near to the reference DEM line of SPI graph.
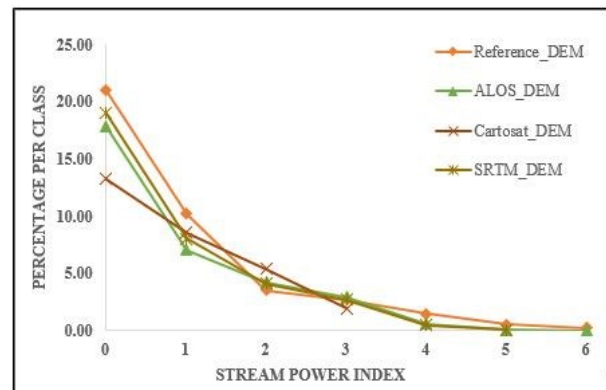
Figure 6. Comparison of SPI Classes for the DEM's

In other words, SRTM DEM and reference DEM have produced a similar SPI curve. After SRTM DEM, converted DEM from DSM was been the maximum percentage of class pixels that comes similar to the reference DEM. SPI of Cartosat DEM in maximum percentage per class pixels falls underestimates.

6. Conclusions

In this study, four different DEMs were compared and validated against the reference DEM. The reference DEM generated by contours had derived from the 1:25,000 scale

of the SOI topographic map. DEM differencing, profiling, correlation plots methods and derived topographic parameters (slope, flow direction, flow accumulation, TWI and SPI) were used to identify the accuracy of the DEM comparison process.

The obtained DEM comparison result of this study has indicated that the training site, the SRTM showed higher vertical accuracy (in terms of RMSE) than the converted DEM from DSM and Cartosat DEM. The RMSEs of the SRTM were converted DEM from DSM and Cartosat DEM have 10.79, 12.31 and 110.19 respectively. The previous SRTM DEM and ASTER DEM comparison study proved that SRTM has greater vertical accuracy than the ASTER (Gerald Forkuor and Ben Maathuis, 2012). The outcome of the surface profile for a common line feature in all DEM's has visualized the SRTM profile was nearly matched to the reference DEM. In the relative accuracy assessment, scatter plots were revealed the R^2 value of SRTM (0.9909) nearly one. Hence, the SRTM has higher vertical accuracy while compared to the other DEM. The statistical and graphical outcomes of all topographic derivatives of these training sites were also revealed that SRTM has more vertical accuracy than the other DEM.

In summary, this study discovered that SRTM has very similar to the Reference DEM to the ALOS and Cartosat, even though all products of DEMs are useful but SRTM was an excellent replacement for the derived DEM from the 1:25000 scale of SOI Data. The Global DEM datasets have the greatest asset of geomorphologists. Because it used in the various surface analysis process. In this study, a relative assessment conducted mainly focused on the hydrological processes, which is one of the terrain processes in geomorphology.

References

Al-Fugara, A. (2015). Comparison and Validation of the Recent Freely Available DEMs over Parts of the Earth's Lowest Elevation Area: Dead Sea, Jordan, International Journal of Geosciences, 6, 1221-1232.

Antonios Mouratidis., and D. Ampatzidis. (2019). European Digital Elevation Model Validation against Extensive Global Navigation Satellite Systems Data and Comparison with SRTM DEM and ASTER GDEM in Central Macedonia (Greece), ISPRS International Journal of Geo-Information, 8(3), 108.

Burt, T., and D. Butcher (1986). Stimulation from simulation – a teaching model of hillslope hydrology for use on microcomputers, J. Geogr. Higher Educ., 10, 23–39.

De Risi R. (2013). A probabilistic bi-scale framework for urban flood risk assessment. Naples (Italy): University of Naples Federico II.

Dhakal, A. S., T. Amanda and M. Aniya (2000). Landslide hazard mapping and its evaluation using GIS: an investigation of sampling schemes for a grid-cell based quantitative method, Photogramm Eng Remote Sens, 66, 981–989.

Fisher, P. F., N. J. Tate (2006). Causes and consequences of error in digital elevation models, Progress in Physical Geography, 30, 467-489.

Gerald Forkuor and B. Maathuis (2012). Comparison of SRTM and ASTER Derived Digital Elevation Models over Two Regions in Ghana - Implications for Hydrological and Environmental Modeling, Studies on Environmental and Applied Geomorphology, Tommaso Piacentini and Enrico Miccadei, IntechOpen, DOI: 10.5772/28951.

Hebeler, F. and R. S. Purves, (2009). The influence of elevation uncertainty on derivation of topographic indices. Geomorphology, 111, 4–16.

Hirt, C., M. S. Filmer and W. E. Featherstone, (2010). Comparison and Validation of the Recent Freely Available ASTER-GDEM ver1SRTM Ver4.1 and GEODATA DEM-9 s Ver3 digital elevation models over Australia, Australian Journal of Earth Science, 57, 337–347.

Indian Space Research Organisation (2011). Evaluation of Indian National DEM from Cartosat-1, National Remote Sensing Centre, Hyderabad-625. September 2011.

Jarvis, A., J. Rubiano, A. Nelson, A. Farrow and M. Mulligan (2004). Practical use of SRTM data in the tropics – Comparisons with Digital Elevation Models Generated from Cartographic Data, Working Document No. 198, 32 (Cali, Columbia: CIAT).

Kolecka, N. and J. Kozak (2013). Assessment of the accuracy of SRTM Cand X-Band high mountain elevation data: a case study of the Polish Tatra Mountains, Pure appl Geophys, DOI: 10.1007/s00024-013-0695-5.

Kwanchai Pakoksung and T. Masatka (2016). Digital elevation models on accuracy validation and bias correction in vertical, Model Earth System and Environment, 2, 11.

Le Lin., Q. Lin and Y. Wang (2017). Landslide Susceptibility Mapping on a Global Scale using the Method of Logistic Regression, Nat. Hazards Earth Syst. Sci., 17, 1411-1424.

Lee, S. J., D. Komatitsch, B. Huang and J. Tromp (2009). Effect of Topography on Seismic-wave Propagation: An example from North Taiwan, Bull Seismol Soc Am, 99, 314–325.

Meyer, D., T. Tachikawa, M. Kaku, A. Iwasaki, D. Gesch, M. Oimoen, Z. Zhang, J. Danielson, T. Krieger, B. Curtis, B et al. (2011). Summary for Policymakers. In Climate Change 2013 - The Physical Science Basis; Intergovernmental Panel on Climate Change, Ed.; Cambridge University Press: Cambridge, UK, 1–30. ISBN 9788578110796.

Miliaresis, G.C. and C.V.E. Paraschou (2005). Vertical accuracy of the SRTM DTED level 1 of Crete, Internation Journal of Applied Earth Observation and Geoinformation, 7, 49–59.

Moore, I. D., R. B. Grayson and A. R. Ladson (1991). Digital terrain modeling – a review of hydrological,

geomorphological, and biological applications, Hydrolological. Process, 5, 3–30.

Muralikrishnan, S. (2012). Validation of Indian National DEM from Cartosat-1 Data, Journal of the Indian Society of Remote Sensing, 41 (1), 1-13.

Muralikrishnan, S., P. Abhijit, B. Narender, S. Reddy, V. Raghu. Venkataraman and V. K. Dadhwal (2012). Validation of Indian National DEM from Cartosat-1 Data, Indian Society of Remote Sensing.

Nikolakopoulos, K.G., E. K. Kamaratakis and N. Chrysoulakis (2006). SRTM vs. ASTER Elevation Products Comparison for Two Regions in Crete, Greece, International Journal of Remote Sens, 27, pp. 4819–4838.

Polidori, L., and M. Hage (2020). Digital Elevation Model Quality Assessment Methods: A Critical Review. Remote Sensing, 12(21), 3522.

Shahapure, S.S., T. I. Eldho and E. P. Rao (2010). Coastal Urban Flood Simulation Using FEM, GIS and Remote Sensing, Water Resour Manage, 24, 3615-3640. https://doi.org/10.1007/s11269-010-9623-y.

Siting Xiong., J. Muller and G. Li (2017). The Application of ALOS/PALSAR InSAR to Measure Subsurface Penetration Depths in Deserts. Remote Sensing, 9, 638.

Sorensen, R., U. Zinko and J. Seibert. (2006). On the Calculation of the Topographic Wetness Index: Evaluation of Different Methods based on Field Observations, Hydrology and Earth System Sciences, 10, 101-112, DOI: org/10.5194/hess-10-101-2006.

Srivastava, B.K., and K. Ramalingam (2009). Error Estimates for WGS-84 and Everest (India - 1956) Transformationm, Geospatial World. https://www.geospatialworld.net/article/error-estimates-for-wgs-84-and-everest-india-1956-transformation/.

Tachikawa, T., M. Hato, M. Kaku and A. Iwasaki (2011). Characteristics of ASTER GDEM version 2, In Proceedings of the International Geoscience and Remote Sensing Symposium (IGARSS), Vancouver, BC, Canada, 24 - 29 July 2011, 3657–3660.

Wolock, D. M. and G. J. McCabe (1995). Comparison of single and multiple flow direction algorithms for computing topographic parameters, Water Resources Research, 31, 1315–1324.

Digitalization of Various Utility Management System using Quantum GIS

Rajeshkumar J. Ajwaliya*, Sanjeev Kumar, Mayursinh A. Rahevar and Jugal V. Gandhi
Space Applications Centre (ISRO), Ahmedabad, Gujarat, India-380015.
Email: rjajwaliya@sac.isro.gov.in

Abstract: With all the technological advancement at a record pace, man-made ecosystems are becoming more complex and need efficient resource management. This paper presents the development of a utility management system for an Institute using GIS and NavIC device for planning and preventive maintenance. In this software-based development of GIS, all physical information such as Campus boundary, Peripheral Roads, Existing Buildings, Roads within the campus, Underground sumps, Underground fuel storage tanks, Solar panels, Electric poles and street lights, Trees, Power supply network, Substation, Hazardous Zones etc. were converted into digital form by developing multiple layers. Open Source-Quantum GIS software is used to utilize and maintain all the utility database at a single platform.

1. Introduction

GIS is a versatile and powerful technology platform that enables organizing information in form of layers for particular data linked with specific layer. Advances in GPS system like NavIC play an important role in geospatial technology. Geo-spatial data are intently structured in four ways that is latitude and longitude, position above ground level, dimension of the data. The GIS is an integrated system of the hardware, software, people participation, data and methods involved (Figure 1).
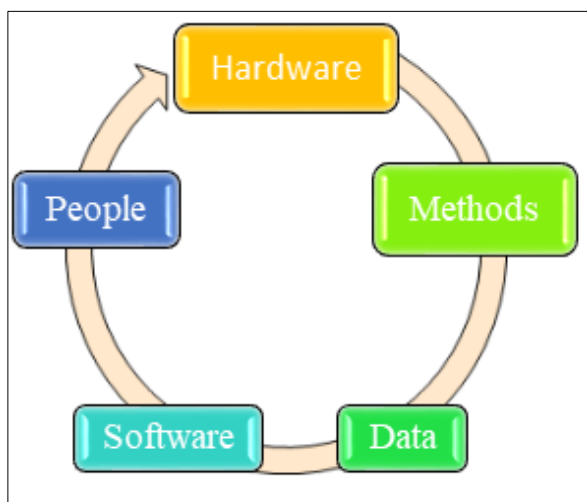
Figure 1. Components of GIS [Sameer et al., 2016]

A GIS can be used to store the position and attributes of infrastructure such as electric assets, water supply line, and nursery, pumps, and Sewage Treatment Plants etc. covers displaying them on a computerized map. These data can accumulate from various source such as documents, maps, images, modelling and analysis and other source (Figure 2). Once all the desired data have been entered into the database of GIS, they can be combined to produce the individual layers-based data for further analysis.

Traditionally, all the data regarding these assets were managed with analogue method such as Electrical network, AC & mechanical network, civil network,

Horticulture network etc. So, spatial database management become more important at a time of emergency and new facilities development. The paper demonstrates the methodology of using GIS and indigenous NavIC system for development of utility database at single platform.
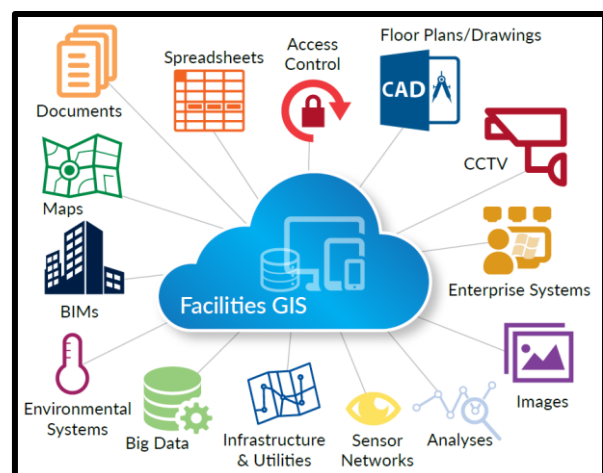
Figure 2. Components of GIS Database [Sameer et al., 2016]

2. 2. Characteristics of existing system

1. All information regarding Electrical, Civil and Mechanical Engineering such as substations, distribution panels, building, roads, power supply line, AC points, Biometric access points etc. are maintained by analogue methods.
2. In this traditional method, the data are available in hard copy and not been able to analyzed at the time of emergency or planning new assets.
3. The data for buildings, rooms in building, roads, street lights etc. are maintained through map sheets with facilities data printed in text form. These maps are rarely updated and there is a lack of linkage between spatial and non-spatial data.
4. All these data exist in hard copy format and are not centralized and hence it is very difficult to update each of the data for upgradation.
5. It is very difficult to directly get the data for length of roads, dimension of building, length of power cable etc.

6. There is no availability of database of all the work of different wings at a single point for ease of decision making during situation.

Thus, for efficient management of utilities and providing instant information access and minimize time for locating any lines, building and efficient planning and for preventive maintenance, development of GIS based Utility Management System for study area is very essential.

3. Objective

The objective is to digitalize and develop a Utility Management System using GIS and NavIC device for data visualization, query and analysis. The detailed objectives are:

1. Collect the data from all the wings for creating the database for 39-Acres' Bopal campus, Ahmedabad.
2. Customization of the software to fulfill the application needs.

4. Study Area

A research lab well equipped with all the utilities of area 39 acres' land at Bopal, Ahmedabad approximately 8 Km. west from main SAC campus is taken as a study area. The campus consists of Auxiliary building, Kiosk building, CISF & PRO building, GIS (Gas Insulated Substation) building, , Vendor complex, GLR & Pump house (Figure 3) etc.

Figure 3. Study area

5. Data and Metrical

- Geocoded cloud free high resolution, ortho-rectified / merged (NCC/FCC) satellite data - 60cm PAN and 1.6m MX sensors of Kompsat satellite data.
- AutoCAD drawing files/maps which can be superimposed on satellite data with correct coordinates showing all existing buildings/facilities, buildings under construction as well as buildings planned for future.

- Information collected from field survey (Buildings, power supply lines, water supply lines, water harvesting structures, trees, roads, walkways, etc.,)
- Open source – Quantum GIS (QGIS), LnKscope, and AutoCAD.
- Dual navigation positioning enabled NavIC device.

6. Navigation System for GIS Functions

The Global Positioning System (GPS) and Indian Regional Navigation Satellite System: NavIC are useful technology which provides accuracy and flexibility for collecting coordinates of stationary or moving objects. Dual positioning enabled device is mainly used for navigation, surveying, remote sensing, mapping and geodetic positioning of study area.

The NavIC or Navigation with Indian Constellation is an autonomous regional satellite navigation system developed by Indian Space Research Organization(ISRO). The Global Positioning System (GPS) is a satellite-based navigation system made up of a complex network of 31 operating satellites placed into inclined orbits by the U.S. Department of Defense Government.
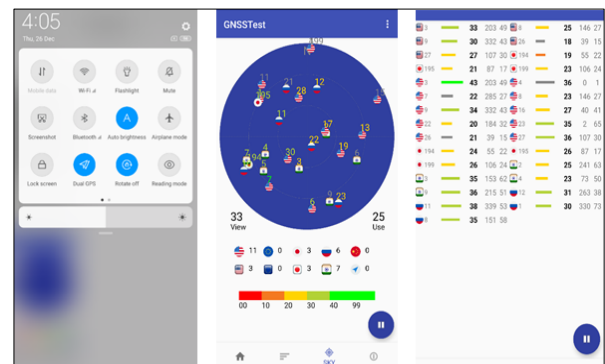
Figure 4. Screenshot for GNSS Tester application (a) Application using dual navigation (b) Application using 7 Indian satellite along with other foreign satellite (c) SNR

In distribution system, geo-data are being used for getting the location of objects such as buildings, roads, pump houses, wells, trees, electric cables, substations, tracking of routes and street light poles etc. Navigation system provides the latitude and longitude, which can directly be used for GIS work.

Thus, Redmi make Note 8 device is used by implementing the NavIC (Figure 4) and GPS based dual positioning system that helps in several aspects of construction of GIS accurate and timely for finding location of an object using two navigation systems i.e. GPS of USA network of 31 satellites covering this planet and IRNSS of INDIA network of 7 satellites. Study area comprises of power supply lines, firefighting lines, drainage lines, cable lines, poles, substations, DG sets, roads, wells and trees etc. Layers extracted from existing AutoCAD map Layers and GPS and IRNSS combined survey.

7. Methodology
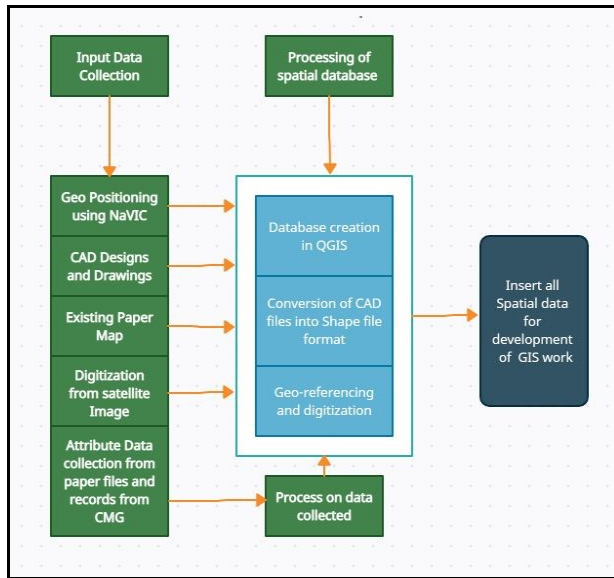
Figure 5. Flow chart for Database creation

Methodology is described in two major parts as (1) GIS database preparation and (2) GIS Application Development. The GIS-mapping involved a participatory approach, where each and every layer should have accurate spatial information associated with attribute information. Methodology for database creation / preparation involves in different steps like base layer creation with geo-referencing then assets mapping in different layer types like (a) all electric poles, bore point - point layer, (b) all lines including roads, cables, pipe lines- line layer and (c) all building, pump house and sub-stations etc. – Polygon layer etc.

Methodology for the GIS based utility Management project execution is described in figure-5, where the first step describes the input data collected from field, CAD map and existing paper maps. second step about to, entire database has been converted into spatial format and geo-referenced. Step three describes about the integration of collateral information within GIS.

8. GIS Databases

For developing a GIS map for utility Management system, a NavIC survey becomes necessary for geo-referencing and mapping the relevant utility assets on the digital base map. GIS mapping, indexing and codification of utility assets with defined schema has been carried out for collection and updating of spatial and non-spatial databases. The collateral data has been converted into compatible GIS format and organized as part of integrated GIS database. The following steps were involved for database preparation:

1. Remote sensing image was acquired from National Remote Sensing Center (NRSC), Hyderabad.
2. AutoCAD layer exported into shape file format and georeferenced with image for Bopal campus boundary Map.

3. Utility layers from existing paper map and CAD map converted and geo-referenced into spatial formats.
4. Measurements of locations of buildings, electric poles, trees etc. using NavIC device.
5. Non-spatial data collected from field records and GIS join analysis carried out to associate it with spatial features.
6. Different data such as power flow line, water supply, firefighting lines, electric lines, etc. were collected from CMG's existing database and converted it into spatial formats.

9. Application Development

The utility management application was developed in QGIS (Quantum GIS) environment. It is a free and open-source cross-platform desktop geographic information system (GIS). QGIS offers a wealth of GIS functions, provided by core features and plugins. QGIS functions as geographic information system (GIS) software, allowing users to analyse and edit spatial information, in addition to composing and exporting graphical maps. The QGIS is used for the development of the attribute information for various features such as civil structure, electrical structure, AC plants and other features along with their metadata as shown in table 1-4. These metadata consist of the various information related to structures and their accessories.

Table 1. Attribute data table for Architecture & Civil wing

Layer	Description
Existing Buildings	Total no of building, Name, location, year of construction, no of floors, Type of construction etc.
GLR	Location, Purpose, Type of Construction, Capacity, Source From
Buildings under construction	Total no of building, Name, location, year of construction, no of floors, Type of construction, Facilities etc.
Roads within the campus	Length of road, width of road, no of lane, Road with footpath etc.
Underground sumps	Number of existing & planned sumps, Location, Size of sumps etc.
Bore wells	Location, Type, Purpose, Depth, year of construction, cleaned on etc.
Rain Water Harvesting (RWH) structures	Number of existing RWH, Type of RWH, Area of existing RWH, Capacity of existing & planned RWH etc.

Roof top Rain Water Harvesting (RRWH)	Location, Number of existing RRWH, Type of RRWH, Area of existing RRWH, Capacity of existing & planned RRWH etc.
Storm water network	Location, Number of existing Storm water network, Name of existing & planned Storm water network etc.
Sewerage network	Location, Number of existing Sewerage network, Name of existing & planned Sewerage network etc.

Table 2. Attribute data table for Electrical wing

Layer	Description
HT Yard	Location, Safety Features, Fire hydrant system, Lightning protection Source voltage etc.
Substation	Year of Commissioning, Area, Incomer cable details, No of Transformers Transformer capacity kVA, No of DG sets with capacity etc.
LT & HT Panel	Location, Rated voltage kV, Short-circuit MVA, Type of Breaker, No of Incoming and Outgoing, Service details etc.
Transformer	Location, Capacity kVA, Vector Group, Cooling Type, Percentage tapping, Year commissioning, IR value etc.
DG set	Location, Engine make, Engine capacity BHP, Cooling Type, Alternator capacity kW etc.
UPS & Battery Bank	Location, Battery-Details, Voltage DC, No of Banks, Year commissioning etc.
Street Light	Location, Material of pole, No of Arms, Wattage, Solar /Conventional etc.
Bollard	Type of bollard, Material of pole, Type of luminaire, Make, Wattage, Timer controlled etc.
EP & SL	Number of existing electric pole, Length of existing & planned power lines, Number of existing & planned street light poles etc.
Substation	Coordinates of existing sub stations, Number of existing sub stations, Number of planned sub stations etc.

Table 3. Attribute data table for AC wing

Layer	Description
Cooling Tower	Make, Capacity, Draft type, Body material, No of fans, Fan capacity, Year of commissioning etc.
AC Chiller	Chiller make, No of compressors, Capacity, Refrigerant, Type of Cooling etc.
AC Plant	Type of construction, No of floors, Fire extinguishers, Type, No of chillers, Plant capacity etc.
Chilled water line	Material of pipe, Pressure bar, Temperature ºC, Insulation material, Insulation protection, Year of laying etc.
Valves	Purpose, Nominal Bore, Material of valve, Valve type, Connected to, Year of installation etc.

Table 4. Attribute data table for miscellaneous data

Layer	Description
Fire stations	Location, No of existing & planned fire station etc.
Watch Towers	Location, No of existing & planned watch tower
Hazardous Zones (HZ)	Location, Area of existing & planned HZ, Location, No of existing & planned HZ etc.
Security fencing	Location, Length of existing & planned security fencing etc.
Biometric / card access	Location, No of existing & planned biometric access points

The QGIS is also used to compose various maps, which includes the boundary layer, internal roads, buildings, AC plants, chillers, cooling towers. The composed maps are shown in Figure 6-8. The analysis is developed by utilizing the data manager, Identification and query tools and has shown in figure 9-11.
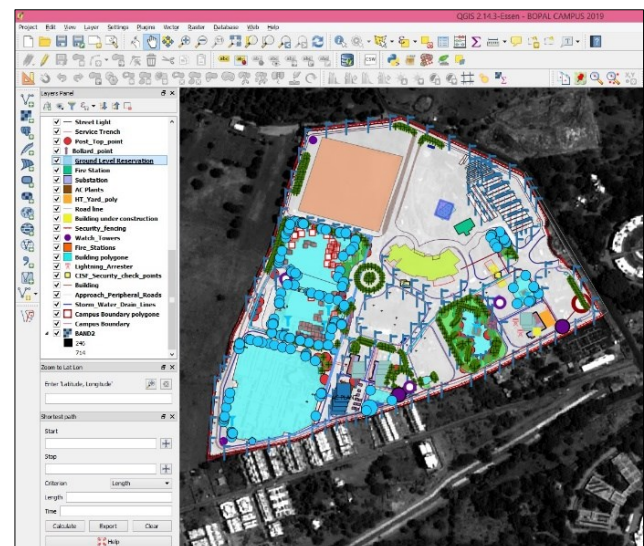
Figure 6. Display of All layers at a time
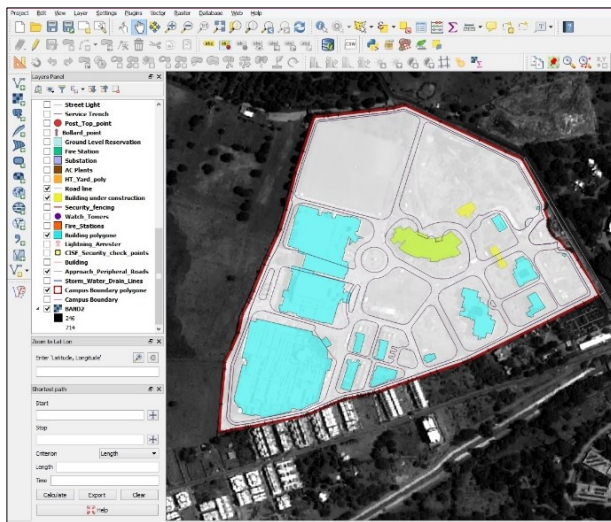
Figure 7. GIS for road, building, building under construction and campus boundary
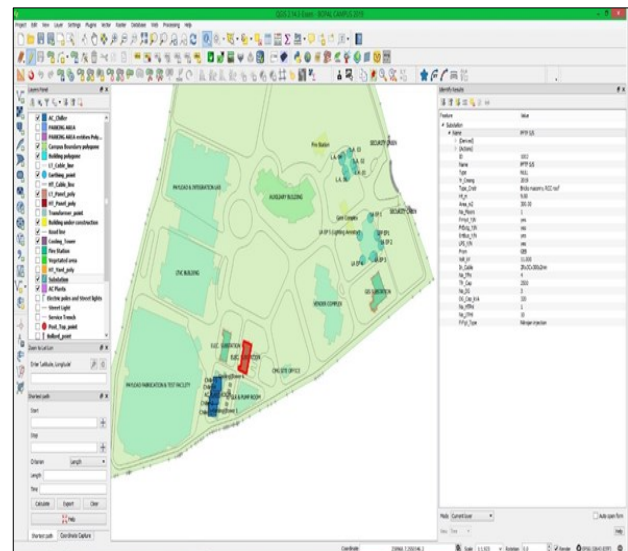
Figure 10. Identify Features for substation layer
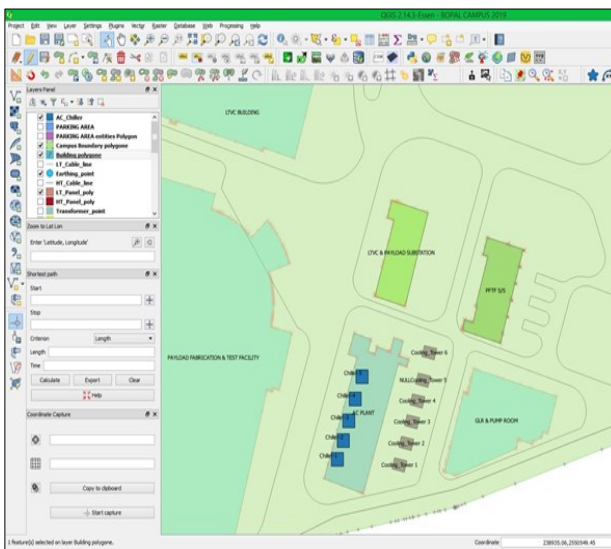
Figure 8. AC plant, AC chillers, Colling tower
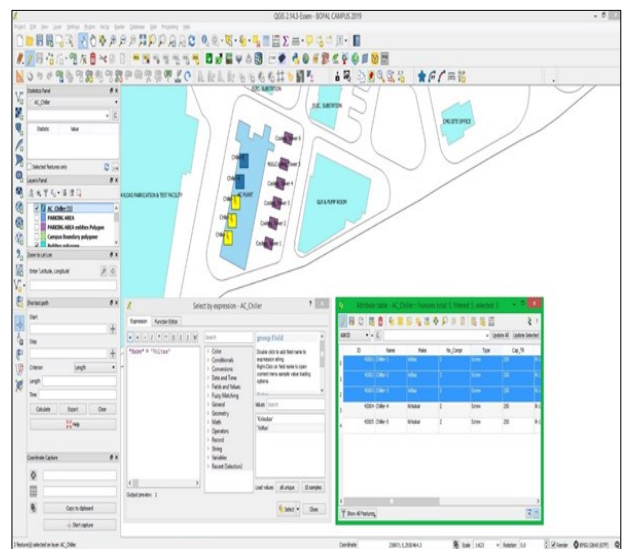
Figure 11. Query generation for AC Chiller Layer

10. Conclusions

Utility management application developed using QGIS at single platform for planning of resources. Geospatial database was found very useful in addressing various management and maintenance related work. Developed Quantum GIS model has been designed to manage utilities for 39 acres' land at Bopal Campus.

Strength of GIS and GPS is integrating geospatial data and preparing it for analysis or modeling makes it an important tool for the planning and decision making.

Figure 9. Data Manager for particular Layer

References

ESRI (1996). Building applications with mapobjects.

Gao, S., F. Mioc and D. J. Coleman (2009), Online GIS services for mapping and sharing disease information, International Journal of Health Geographics, 8(3), 1-16. doi:10.1186/1476-072X-8-3

Nawaz-ul-Huda, S., F. Burke, M. Azam, and S. Naz (2012), GIS for power distribution network: A case study of Karachi, Pakistan, GEOGRAFIA Online, Malaysia Journal of Society and Space, 8(1), 60 - 68

Salawudeen, O.S and U. Rashidat (2006), Electricity Distribution Engineering and Geographic Information System (DeGIS) Shape the Change XXIII FIG Congress Munich Germany, TS 72 – GIS Application – Planning Issues.

Sidda, N. K., D. Boddu and R. M. K Rao (2011). An Eclectic mapping approach for Non-Spatial Data, International Journal of Geomatics and Geosciences, 2(2)

Sameer S., H. S. Prabhakar, A. Verma, G. K. Kota, A. Srivastava, P. K. Gupta, A. K. Jha, K. Oberai, H. Pande, P. Seth, T. S. Raghvendra, K. Pandey, S. Kannaujia and M. Mahadevaswamy (2016), GIS Based Utility Mapping of ISRO/DOS Campuses. June 20-24, 2016.Geoinformatics department, IIRS.

Development of a Crop Residue Burning Information and Management System using Geo-Spatial Technologies

Shashikant Patel[*], Amardeep Singh, Pradeep Kumar Litoria, Anil Sood, Samandeep Kaur, and Brijendra Pateriya
Punjab Remote Sensing Centre, Ludhiana-141004, Punjab
[*]Email: shashikant.p@prsc.gov.in

Abstract: India is the second biggest agro-based economy with all year crop cultivation. Punjab state is one of the major food grains producing state in India. Crop residue burning has become a major environmental problem causing health issues. The government of Punjab has attempted to curtail this problem, through numerous measures and campaigns designed to promote sustainable management methods. The developed Crop Residue Burning Information and Management System (CRBIMS) collects the relevant data from various sources and formats, analyses and manages it with geographical information system at the backend. This system is developed for better understanding and decision making by providing geographical information available along residual burning points, date of burning, geographical locations with administrative boundaries. WebGIS open source technology is used for residual burning points distribution and rendering. This WebGIS based system is easy to understand and has a user-friendly interface. This paper illustrates about technological implementation and conceptual workflow of the developed system. The developed CRBIMS contain various modules like interactive map visualization with user-friendly data selection facility, Dashboard, Report generation and analytics to decision makers, and government officers for historical and present dataset with respect to the residue burning events.

1. Introduction

India is an agrarian country and produces an immense measure of farming wastes. This quantum of farming waste will increase with increase in population. Biomass burning can lead to poor air quality around the globe (Bruce et al., 2000). Air contamination in Indian subcontinent has been identified as a basic issue that is lastingly affecting general wellbeing and death rates (Ghude et al., 2016; Laumbach and Kipen, 2012; Sarkar et.al, 2018). Agricultural residues are the biomass left in the field after harvesting the economic yield. Huge amounts of crop residues are created each year, as cereal straws, woody stalks, and sugarcane leaves/tops during harvest periods. Crop Residue Burning began during the decade of 80s when automated mechanized harvesting for wheat (in the long stretch of April–May) and rice (in the period of October–November) started (Kaskaoutis et al., 2014; Singh and Kaskaoutis, 2014). In India, Significant residue burning happenesin rice growing states like Punjab, Haryana and Uttar Pradesh, situated in the Indo-Gangetic Plain (IGP) (Badarinath, et.al. 2009; and Chhabra et.al. 2019). The disposal of such a large amount of crop residues is a major challenge to clear the field rapidly and inexpensively and allow tillage practices for next crop. Farmers select burning in light of the fact that it is a brisk and simple approach to deal with the enormous amounts of harvest deposits and set up the field for the next crop well in time.

Geographic Information Science (GIS) is the science underlying geographic concepts, applications, and systems (Goodchild, 2010; Patel et.al. 2016; Ajwaliya et.al. 2017). GIS is an important tool for integrating spatial (geo-referenced data) and non-spatial information from different sources or disciplines (Kaur et.al, 2018). Since the progression of web and geospatial innovations, different endeavours have been made to produce data and usage of these methods for the prosperity of society. Today in the advancement of Web technology, various management systems have been developed for utility mapping, power distribution, Earth data and planetary data dissemination and archival. Various applications have been developed using web GIS techniques for decision making and planning prospective viz. Public Transport Management System, Emergency Response System, Livestock Information and Management System, Urban Planning, Utility Management System etc. (Mansourian et al., 2011; Otieno and Nigigi, 2014; Baucic and Medak, 2015; Ranade and Mishra, 2015; and Ajwaliya et.al. 2017)

Web GIS is a powerful tool and technique to distribute spatial data or information on Web with quality, authenticity, and advantages along with interactive representation. At first, it is important to understand the GIS based information and management systems for agriculture and environment management. From the prospect of Air pollution and wellbeing concern, it is important to hinder crop residual burnings in India, especially in Indo-Gangetic Plain (IGP) regions. In continuation of prevention process, Government of Punjab has taken initiatives for near real-time mapping and monitoring of active fire events and information distribution to the all concern officials at Village level, Tahsil level, District level and State managers or planners. The technologies namely GIS and IT have been used in a collaborative way to develop innovative solutions for various problems. Information Technology has already proved it's vast potential to serve the needs in various sectors of development as solution providing tool for various problems.

A web application is a distributed application, which runs on more than one PC and imparts through an organization of worker. Web applications generally run on the Internet or an Intranet and it has become a significant piece of the business world as of late. With the expanding number of clients of the Internet and World Wide Web, more refined Internet and web applications have arisen.

This paper focus on the e-Governance initiative by Punjab Government for better planning and resolving the environmental air pollution problems occurred due to burning of Crop Residue in the Punjab area. Apart from contributing to air pollution stubble burning deteriorates the soil's organic content, essential nutrients and microbial activity – which together will reduce the soil's long-term productivity

This manuscript describes the concept and technical implementation of a web GIS based Crop residue Burning Information and Management System (CRBIMS). The Developed system facilitates user/ decision makers for interactive visualization of daily active fire events (Crop Residue Burning Events). An Interactive and Dynamic Dashboard has been developed for the Government officers and decision makers to get the glimpse and comparative analysis of Crop Residue burning events at State, District, Block and Village level.

2. Objectives

The objective of the study is to develop a web GIS based Crop Residue Burning Information and Management System (CRBIMS) to act as a common platform for the representation of detailed spatial and non-spatial information pertaining to Daily Active Fire events (Crop Residual Burning Events) at various geographical levels

for entire Punjab State. Development of the system includes development of centralised database, Role based login for information visualization and report visualization of actions taken against each burning points.

3. Study Area

Punjab is a state in northern India. Punjab is surrounded by the Indian union territory of Jammu and Kashmir to the north, and Indian states of Himachal Pradesh to the east, Haryana to the south and southeast, and Rajasthan to the southwest. It is bordered by the Pakistani province of Punjab to the west. The state covers an area of 50,362 square kilometres, 1.53% of India's total geographical area. Punjab is the 16th-largest state by population, comprising 22 districts. The five tributary rivers of the Indus River from which the region took its name are Sutlej, Ravi, Beas, Chenab and Jhelum Rivers; Based on Geographical and climatic conditions, Punjab is the state of major food providing state in India. Fig.1. shows the geographical location of the study area and the district boundaries of Punjab State.

4. Data Acquisition and Pre-processing

Daily Active Fire points have been downloaded from NRT VIIRS 375 m Active Fire product VNP14IMGT distributed from NASA FIRMS, available online (https://earthdata.nasa.gov/firms). Daily Active fire points were pre-processed with present land use in geographical regions to separate out fire points, which are within the agricultural fields. Spatial overlay analysis has been carried out to identify the spatial locations (Village, Tehsil, and District) of the active fire points. Daily active fire events are stored in the database as spatial information.
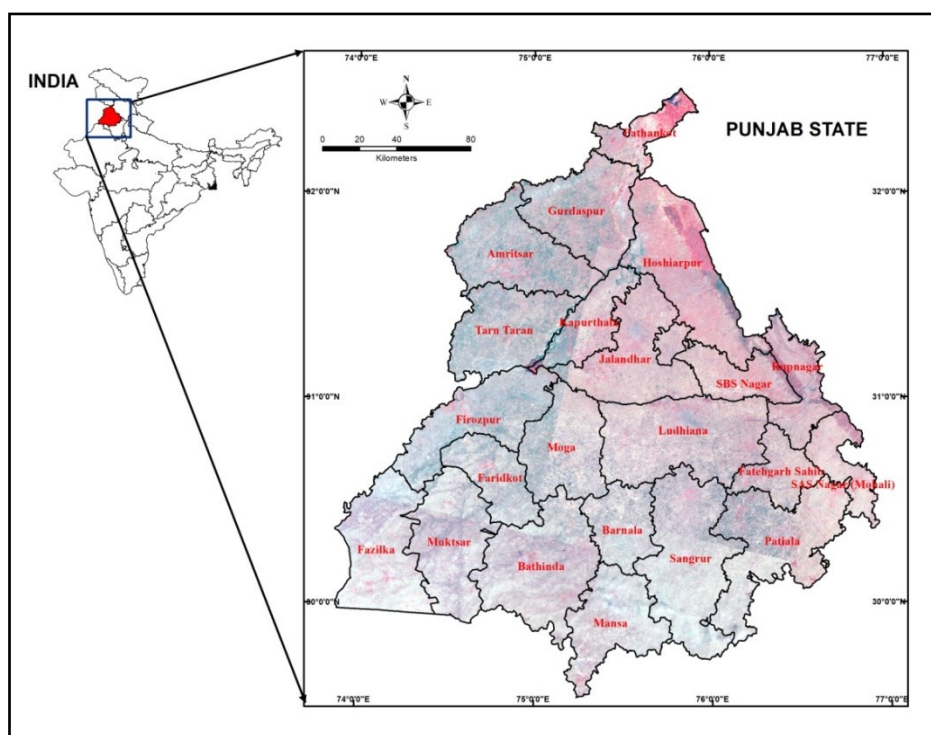

Figure 1. Study area with district boundaries

5. Design and Development of CRBIMS

There are several decisions to be made when developing GIS based web applications (for example; types of data representation, types of data interaction and user's controls in determining the data are retrieved and presented, Processing at client end and Server side). With these broad aspects this research is also subdivided into to two basic categories namely (i) data pre-processing and spatial analysis and (ii) development of CRBIMS. System development further classified into the two major parts MIS information processing and distribution and another is to represent the spatial information as interactive and dynamic maps with user's flexibility.

The conceptual block diagram of the developed CRBIMS system is represented in figure 2. The architecture of the system describes clusters of database created to store, manipulate and update the information on daily basis and requirement basis. Three separate relational tables have been designed to store daily active fire events, officer's information for login and jurisdiction identification, and other spatial and non-spatial data.

Daily active fire dataset injected to database for spatial join to the officer's information for the defined jurisdiction. An automated massage alert system has been setup to send messages to the concerned officers and decision makers. The message information contains the number of active fire events in respective officer's jurisdiction with geographic locations. State level officers, decision makers and planners get the daily active fire event information for the entire Punjab state.

CRBIMS dashboard facilitates users with dynamic charts for daily, seasonal and yearly active fire event statistics and profile visualization and analysis. Highcharts libraries are integrated with the CRBIMS for the graphical representation. District level, Tehsil Level, and Village level information about the daily active fire events is also represented as tabular information.

The server infrastructure consists of several components mainly data acquisition, pre-processing, data retrieval, archival, information processing, and finally information distribution through CRBIMS.

Information gap occurs when decision makers and scientific communities working separately for the identified assignment. This manuscript describes how to fill this space, for the planning and decision making process. Daily continuous dataset is processed into knowledge base for further decision making and prevention protocols development. Fig.2. describes the conceptual block diagram of the developed system.

5.1 Tools and Technologies
The development architecture of the CRBIMS is shown in figure 2. Various tools and technologies have been used in the system development are illustrated here:

Microsoft visual studio: Visual Studio is a complete set of development tools for building ASP.NET Web applications, XML Web Services, desktop applications, and mobile applications (https://visualstudio.microsoft.com/).

ASP.NET is a web development platform, which provides a programming model, a comprehensive software infrastructure and various services required to build up robust web applications (https://dotnet.microsoft.com/learn).

Microsoft SQL is a Relational Database Management System (RDBMS) developed by Microsoft (https://www.microsoft.com/en-us/sql-server).Structured Query Language (SQL) is standard language for relational database management systems. Most of the relational database Management Systems (RDBMS) likes Oracle, Sybase, Microsoft SQL Server, PostgreSQL and Microsoft Access etc .uses SQL or its variant. However, the standard SQL commands such as "Select", "Insert", "Update", "Delete", "Create", and "Drop" can be used to accomplish almost everything that one needs to query or manage a database (https://www.w3schools.com/sql/sql_intro.asp).

Hyper Text Markup Language (HTML) is used for front-end web pages development Inclusion of CSS defines the look and layout of content.HTML elements are the building blocks of HTML pages. They provides a means to create structured documents by denoting structural semantics for text such as headings, paragraphs, lists, links, quotes and other items. HTML elements are delineated by tags, written using angle brackets (https://www.w3schools.com/html/).

Cascading Style Sheets (CSS) is a style sheet language used for describing the presentation of a document written in a mark-up language. CSS is the language for describing the colours, layout, and fonts of web pages. CSS is independent of HTML and can be used with any XML-based mark-up language (https://www.w3schools.com/css/css_intro.asp).

JQuery is a fast, small, and feature-rich JavaScript library. The modular approach of the JQuery library allows the creation of powerful dynamic web pages and Web applications. It is not a language, but it is a well-written JavaScript code. **AJAX** is a set of web development techniques used by client-side frameworks and libraries to make asynchronous HTTP calls to the server. AJAX stands for Asynchronous JavaScript and XML.

We used .NET and SQL Database Technologies to acquire fire-point data set along with spatial co-ordinates, village officer data set along with contact information and village geo spatial data set for mapping fire-point co-ordinates with specific village geography.

Open Geospatial Consortium (OGC) standard, Web Map services (WMS) has been generated using open source Geoserver; The Geoserver, an Open Source platform for publishing spatial data and interactive mapping to the web have been used as spatial data server. It creates

maps, images from spatial information stored in digital format. It can handle both vector and raster data. Open Layers libraries are used to render the spatial maps over the web with GIS functionality. A highly customizable and adaptable environment for deploying and managing Web mapping applications is used to design and Graphic User Interface of WebGIS.
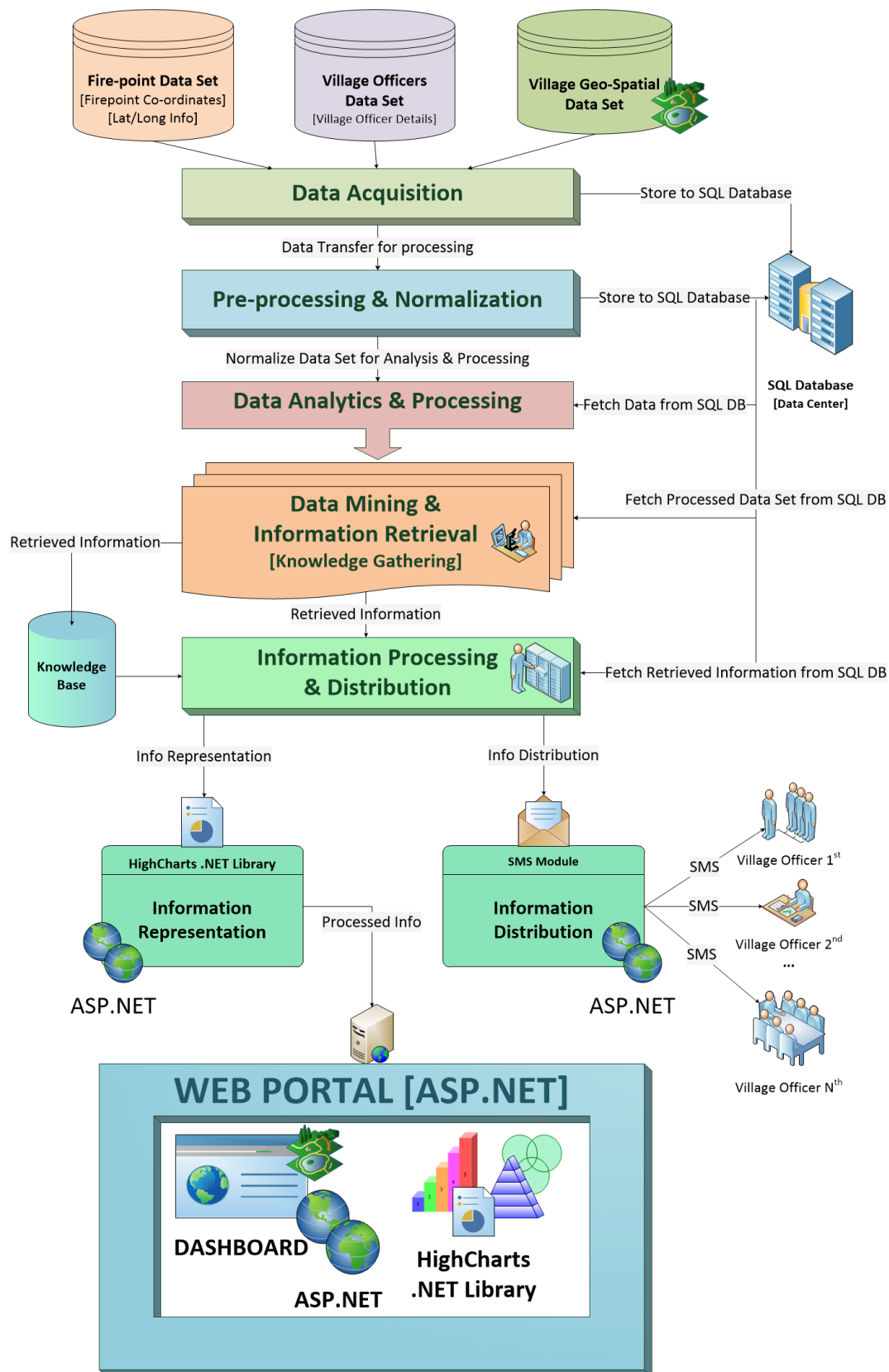

Figure 2. Block Diagram of Crop Residue Burning Information and Management System (CRBIMS)

6. Results and Discussion

The Developed system contains the daily statistics in the form of dashboard with interactive graphical interface. Fig.3. illustrates the dashboard of statistics for daily active fire events observed from the satellite data over the study area. Dashboard provides the daily information about the total observed active fire locations, district-wise statistics for the particular day, cumulative sum of the active fire events in the season, and the state level comparative statistics for the season up to the particular date. Dynamic and interactive dashboards also represent the district with maximum and minimum active fire events observed in a specific day. The dashboard represents the basic statistics for the season and represents comparative chart from the year 2016 for the same season. As figure 3 shows, total 76590 active fire events observed in year 2020 during cropping year (June -May), where as in year 2016, 2017, 2018 and 2019; total observed active fire events were 81042, 46837, 51578, and 55405 respectively. The Comparative analysis represents that the year 2016 was highest observed year and year 2017 was the lowest observed year.

The Menu bar was integrated with the system. Menus are classified in four broad categories (viz. Dashboard, Statistics, Help, and Login). Dashboard menu includes sub menus Home page, Map Page, Daily Reports. Home page is landing page, report submenu facilitates to download statistical reports in Portable Document Format (PDF).As illustrated in fig.4, Map page contains the facility to visualise and analyse daily active fire events geographically over the dynamic and interactive map window. Selection of date and year facility has been

provided to the users for the dynamic rendering. It also provides the Geospatial functions with map window like Pan, Zoom-In, Zoom-Out, Full-Extent, Length measurement, area measurement, and feature attribute information etc. within the overlay tab user can select the administrative layers (viz. Village boundary, Tehsil boundary, District boundary, and other raster or vector layers) which can be rendered over the map.

Action taken against each reported fire point reporting and visualization module has been developed for government officers based on the login credentials for their respective spatial jurisdiction. As illustrated in fig.5, Action Taken Report Module has been developed as per the functional hierarchy. This module has been classified based on the functional responsibilities of the officers like Nodal (Village level), Patwari (one or more than one village), Cluster (cluster of 3-4 villages), Tahsildar (Tehsil level officer), Sub-district Magistrate (SDM), Additional District Commissioner (ADC), District Commissioner(DC) and State level (State government decision makers, Planners) officers. This Module describes number of Crop residue burning points in the jurisdiction of specific officer and out of total CRB points action taken / pending against the specified points. Login based dashboard for the officers has been developed to visualise all the historical and present action taken points with interactive graphical representation and tabular form. User can also download and print the summary and complete report from CRBIMS. Action Taken Report (ATR) module for state level officers provides all statistical and spatial summaries for the entire state to decision makers and planners.
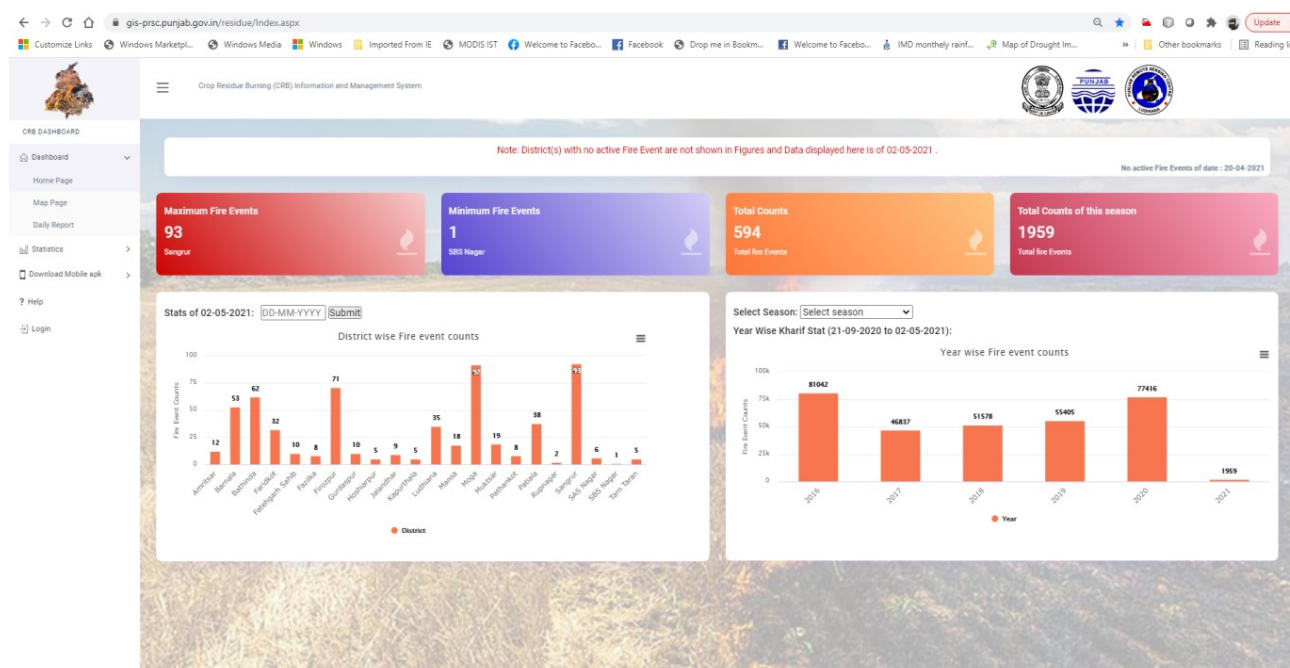
Figure.3. Landing Page/ Home page of Dashboard
(https://gis-prsc.punjab.gov.in/residue/Index.aspx)
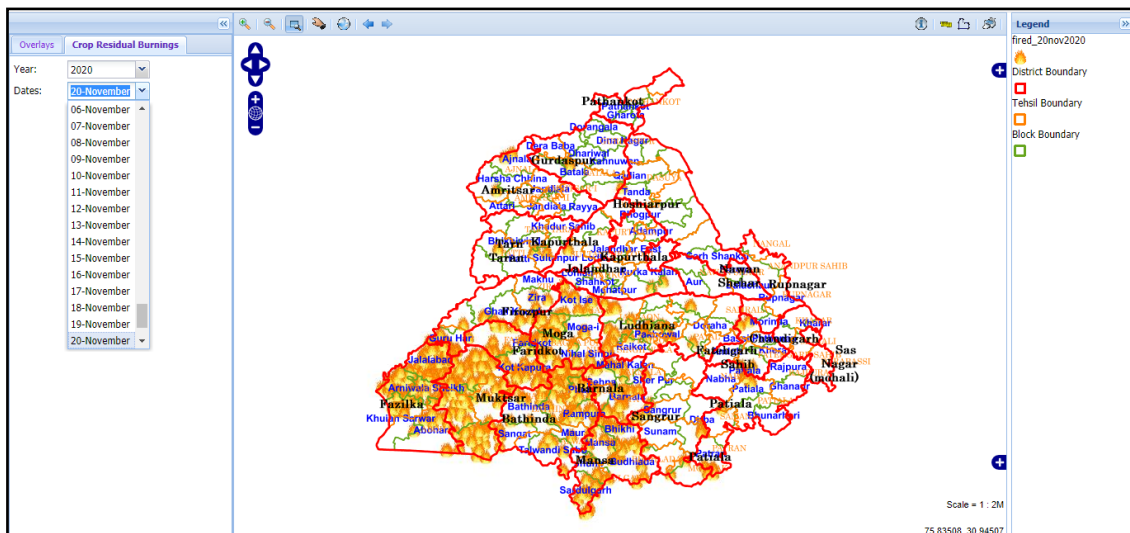
Figure 4. Dynamic Map Page with spatial Locations of Active fire Events on Selected date
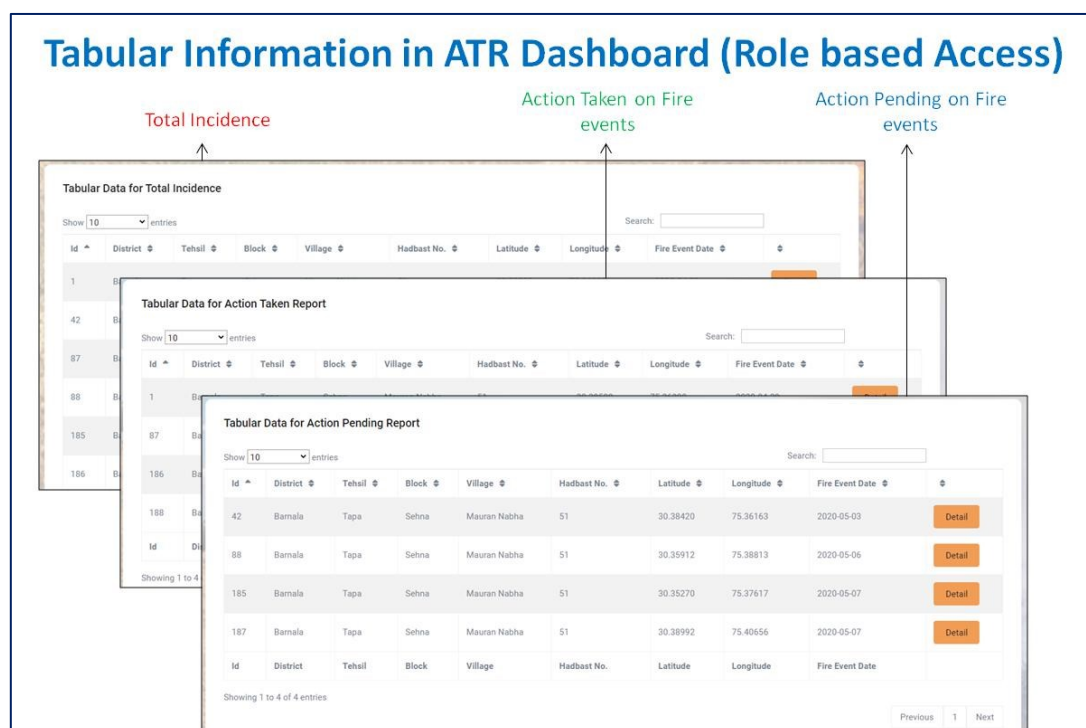
Figure 5. Login based action taken reporting and visualization module

7. Conclusions

The Web-GIS based CRBIMS is regarded as an effective tool to help decision makers and planners. The usefulness and flexibility of the system have been illustrated in the application. In addition to its powerful capabilities in analysing, and visualization which have been used effectively to present crop residual burning events and give solutions to the pollution control board of Punjab and decision makers. Therefore, the use of GIS and remote sensing improves not only the analytical capabilities for crop residual burnings and its management but also increased our ability to share information with stakeholders, decision makers and the public in general. The system is able to support and facilitate visualization and analytical analysis at various geographical levels. The developed system named as CRBIMS needs many experts cooperation such as

environmentalist, climate, agriculture expert, GIS scientist, computer engineers, for this reason; still there is scope to enhance the capabilities of the system.

The methodology taken here accepts that the GIS-based decision support system for crop residue burning can be viewed as an assortment of subsystems as open and adaptable design. The framework is built somewhat in top-down and part of the way in base up style. The goal is to satisfy the requirements of end-clients for wise framework uphold and to show the usefulness and architecture of GIS-based frameworks for this reason.

Additionally, CRBIMS generated data from the system is able to provide enough information for day-to-day monitoring. Capabilities of the developed system can be enhanced to generate and integrate some additional information in environmental aspect (air quality monitoring, Air pollution, PM2.5, Gaseous compositions,

crop conditions and relation between crop residues burning with air pollution). The developed software tool provides useful information for decision-making and planning. Future scope of the CRBIMS can be enhanced with more historical dataset, more remotely sensed data with respect to the Environmental pollutions. The developed system is useful for various management and planning practices especially for environmental studies, and agricultural monitoring. The future advancement in the system capability can be also enhanced by adding some analytical modules in account to decision-making process to prevent residual burning and management practices.

References:
Ajwaliya, R. J., Patel, S. and Sharma, S.A. (2017), "Web-GIS based Application for Utility Management System". Journal of Geomatics, 11(1), 86-97.

Badarinath, K., Kharol, S. K., & Sharma, A. R. (2009). Long-range transport of aerosols from agriculture CRB in Indo-Gangetic Plains—A study using LIDAR, ground measurements and satellite data. Journal of Atmospheric and Solar-Terrestrial Physics, 71(1), 112–120. https://doi.org/10.1016/j.jastp. 2008.09.035.

Baucic, M. and Medak, D. (2015). Web GIS for airport emergency response - UML model. Promet – Traffic & Transportation, 27(2), 155-164.

Bruce, N., Perez-Padilla, R., Albalak, R. (2000). Indoor air pollution in developing countries: a major environmental and public health challenge. World Health Organ. 78 (9), 1078–1092.

Chhabra, A., Sehgal, V.K., Dhakar, R., Jain, N., Verma, R. (2019). Monitoring of active fire events due to paddy residue burning in indo-gangetic plains using thermal remote sensing, the International Archives of the Photogrammetry, Remote Sensing and Spatial Information Sciences, XLII-3/W6.

Geoserver. http://geoserver.org/.

Ghude, S. D., Chate, D. M., Jena, C., Beig, G., Kumar, R., Barth, M. C., &Pithani, P. (2016). Premature mortality in India due to PM2.5 and ozone exposure. Geophysical Research Letters, 43, 4650–4658. https://doi.org/10.1002/2016gl068949

Goodchild, M.F. (2010). Twenty Years of Progress: GIScience in 2010. Journal of Spatial Information Science 1:3-20 (494).

Kaskaoutis, D. G., Kumar, S., Sharma, D., Singh, R. P., Kharol, S. K., Sharma, M., et al. (2014). Effects of CRB on aerosol properties, plume characteristics, and long-range transport over northern India. Journal of Geophysical Research: Atmospheres, 119, 5424–5444. https://doi.org/10.1002/2013jd021357

Kaur, R., Jain, A.K., and Singh, H. (2018).Development of village information system for Faridkot district using remote sensing and geographic information system. 2018, International Journal of Information Technology. DOI: 10.1007/s41870-018-0180-6.

Laumbach, R. J., & Kipen, H. M. (2012). Respiratory health effects of air pollution: Update on biomass smoke and traffic pollution. Journal of Allergy and Clinical Immunology, 129(1), 3–11. https://doi.org/10.1016/j.jaci. 2011.11.021

Mansourian, A., Taleai, M. AndFasihi, A. (2011). A web-based spatial decision support system to enhance public participation in urban planning processes. Journal of Spatial Science, 56(2), 269–282.

Otieno, E.O. and Ngigi, M.M. (2014). Web based public transport management system: A prototype PSV tracking system for Nairobi city. International Journal of Science and Research (IJSR). 3(6), 922-926. (online): 2319-7064.

Patel, S., Khopkar, P.S., Mishra, S., Sharma, S.A., Chaudhary, K.N., and Oza, M.P. (2016). Web GIS based Vegetation Monitoring System (WGVMS). Technical Report. Space Applications Centre-ISRO: SAC/EPSA/VRG/CGDD/TR_02/July-2016.

PostGIS. http://postgis.refractions.net/

PostgreSQL. www.postgresql.org/

Ranade, P. and Mishra, A. (2015). Web-GIS based livestock information management system (WGLIMS): Review of Indian scenario. Int. Journal of Applied Sciences and Engineering Research, 4(2), 2277-9442.

Sarkar, S., Singh, R. P., & Chauhan, A. (2018). Crop residue burning in northern India: Increasing threat to Greater India. Journal of Geophysical Research: Atmospheres, 123. https://doi.org/10.1029/2018JD028428

Singh, R. P., & Kaskaoutis, D. G. (2014). CRB: A threat to South Asian air quality. Eos, Transactions American Geophysical Union, 95(37), 333–334. https://doi.org/10.1002/2014eo370001

Long-term observation and modelling on the distribution and patterns of alpine treeline ecotone in Indian Himalaya

C. P. Singh[1,*], Jakesh Mohapatra[1,9,#], Jincy Rachel Mathew[1,10], Anzar A. Khuroo[2], Maroof Hamid[2], A. H. Malik[2], Rameez Ahmad[2], Amit Kumar[3], Anirudh Verma[3], Mohan C. Nautiyal[4], Sudeep Chandra Semwal[4], Ankit Singh[4], Subrat Sharma[5], Swati Naidu[5], Dhiren G. Shrestha[6], Narpati Sharma[6], Bandan Gajmer[6], O. P. Tripathi[7], Ashish Paul[7], Sayed Ali[7], Rajesh Bajpai[8], K. K. Rawat[8], D. K. Upreti[8], Himanshu A. Pandya[9], Hitesh Solanki[10], Nishith Dharaiya[11], R. P. Singh[1] and B. K. Bhattacharya[1]

[1]EPSA, Space Applications Centre (SAC), ISRO, Ahmedabad, Gujarat, India
[2]Centre for Biodiversity and Taxonomy, University of Kashmir, Srinagar, Jammu and Kashmir, India
[3]CSIR-Institute of Himalayan Bioresource Technology (IHBT), Palampur, Himachal Pradesh, India
[4]HAPPRC, H.N.B. Garhwal University, Srinagar, Garhwal, Uttarakhand, India
[5]G.B. Pant National Institute of Himalayan Environment, Kosi-Katarmal, Almora, Uttarakhand, India
[6]Sikkim State Council of Science and Technology, Deorali, Gangtok, Sikkim, India
[7]North Eastern Regional Institute of Science and Technology, Nirjuli, Arunachal Pradesh, India
[8]CSIR-National Botanical Research Institute, Lucknow, Uttar Pradesh, India
[9]Dept. of Botany, Bioinformatics, and Climate Change Impacts Management, Gujarat University, Ahmedabad, Gujarat
[10]Department of Environmental Sciences, Gujarat University, Ahmedabad, Gujarat, India
[11]WCB Research Lab, Hemchandracharya North Gujarat University (HNGU), Patan, Gujarat, India
[#] Present Affiliation: North Eastern Space Applications Centre, DoS, Umiam, Meghalaya, India
Email: cpsingh@sac.isro.gov.in

Abstract: High elevation ecosystems of the Himalaya have warmed more rapidly in recent decades than other areas of the globe. Alpine life zones are areas lying between the elevational climatic treeline and the snow line. The limit of alpine treeline elevational position in Himalaya is temperature dependent. Satellite remote sensing of delineating Himalayan alpine treeline position and its dynamics can give insight regarding climatic variability. Resourcesat-1/2 Linear Imaging Self Scanning Sensor (LISS-III) and Landsat-1/2/3 Multispectral Scanner (MSS) were used to evaluate the long-term (1970s to 2014) treeline dynamics in high elevations (>3500 m) of Himalaya. The mean elevation of treeline position has shifted vertically 381 ± 73 m in over four decades at a rate of c. 95 m decade^{-1} in the entire Indian Himalaya. The highest shift (452 ± 74) in the treeline position was observed in Arunachal Pradesh Himalaya. We have also predicted through future climate model simulations, that there will be overall vertical shift in the niche area of treeline tree species (*Betula utilis*) in general and more towards eastern Indian Himalaya, in particular. The highest rate of upward shift in niche was observed in Sikkim Himalaya (c. 109.9 m decade^{-1}) and the lowest magnitude of shift (c. 20.8 m decade^{-1}) in Jammu and Kashmir Himalaya. The significant elevational shifts of the treeline ecotone is a fingerprint of climate change impact in Indian Himalayan alpine ecosystem.

Keywords: alpine ecosystem; mountain; climate change; elevation; NDVI

1. Introduction

High elevation ecosystem of the Himalayan mountain ranges are the pristine environment that enables climate change studies. In the recent decades, Himalaya have warmed up more rapidly than other areas of the globe (Field and Barros, 2014). The warming effect is seen in the treeline ecotone where trees struggle to survive under cold stress in mountain summits (Butler et al., 2009). The alpine ecosystem is the zone where along the elevational gradient woody vegetation changes from lowland to dwarf shrubs, grasses, sedges, mosses, and finally to the snow line. An imaginary line connecting the uppermost patches of short stature trees (*krummholz*) and the lower most limit alpine vegetation is called the treeline (Körner, 2012). This imaginary line can be well visualized and delineated at landscape level with the help of biophysical and environmental thresholds (e.g. temperature). Temperature reduction with increasing elevation is a primary driver of species biodiversity and the formation of treelines (Mayor et al., 2017) in alpine ecosystems. The treeline is shifting upward to higher elevation primarily because of the

warming (Grabherr et al., 1994; Walther et al., 2005; Schickhoff et al., 2015). Along the elevation gradients, the number of vascular plant species decreases as harsher cold environment prevails towards the nival zone (Mohapatra, 2015). Temperature and precipitation are essential environmental parameters that govern the treeline dynamics.

Investigating the long-term dynamics of treeline only through field study is difficult. Remoteness, ruggedness of the terrain and extreme weather conditions in the high elevation region of Himalaya, is a challenge for field-based research. Remote sensing and Geographic Information System (GIS) with high-resolution data is useful in delineating treeline ecotone at the landscape scale. Resourcesat and Landsat imageries provide medium resolution multispectral data with the synoptic view of the earth surface at a regular interval of time. The Resourcesat-1/2 Linear Imaging Self Scanning Sensor (LISS-III) with a spatial resolution of 23.5 m is appropriate for studying vegetation dynamics at a landscape level. Landsat-1/2/3 Multispectral Scanner (MSS) with a spatial resolution of

60 m provides a long-term historical medium resolution multispectral data record at a global scale from 1972 at a regular interval of time. It provides long-term records widely used for studying the impact of climate change on natural vegetation. These satellites have previously been used by many researchers for studying the impact of climate change on treeline ecotone (Lal et al., 1991; Panigrahy et al., 2010; Singh et al., 2011, 2012).

Vegetation indices from satellite remote sensing provides landscape scale physiological status of plant species. Normalised Difference Vegetation Index (NDVI) is the normalised difference of Near Infrared and Red wavelengths that correlates with the absorption of photosynthetically active radiation by the vegetation. Identification of the suitable geographical space that supports the survival of treeline species over time is essential for the purpose of species conservation in Himalaya. Niche modelling of the treeline species give inference on the probable habitat in the high elevation of Himalaya. Bioclimatic data provides the scope for determining the fundamental niche of species. There is upward shift of *Betula utilis* D. Don to higher elevation in Himalaya, in which temperature and precipitation are the most important variables for the prediction (Bobrowski et al., 2017). Niche modelling predicts an upward shift of *B. utilis* in the future (Singh et al., 2013), at the rate of 184 m in seven decades (Singh et al., 2011). Natural and anthropogenic factors determine the level of forcings in climate projections. The Representative Concentration Pathways (RCPs) in the Intergovernmental Panel on Climate Change Fifth Assessment (IPCC$_5$) Report (IPCC, 2013) describe the 21st century evolution of atmospheric greenhouse gas concentrations, land-use changes and emissions of air pollutants under four very different futures.

There have been a few studies on the impact of climate change on treeline position in Himalaya (Dutta et al., 2014) through field observations and incidental historical data. It had been studied through past photography (Baker and Moseley, 2007), or field inventory data (Dubey et al., 2003). Studies on the treeline shift in Himalaya solely on the basis of field study is challenging and is limited only to specific area or community. It is time consuming, costly and is limited to a specific period. Inaccessibility and remoteness make remote sensing an attractive method for conducting research in the alpine ecosystem of the Himalaya.

Past records of Landsat data are advantageous in providing large time scale for observing the dynamics of treeline ecotone in response to climatic variability. For climate change monitoring in Himalaya, higher resolution systems can provide the best possible spatial details, but their revisit periods are longer and cloud cover limits usability of data. Therefore, it is essential to combine data from more than one observing system in order to fill the gaps in observation. It is valuable to compare high-resolution measurements of vegetation with more frequent measurements made by lower resolution systems (Steven et al., 2003). For studying the treeline responses to climate change, continuity and consistency of observations are essential through long time series of data. In many

previous studies, it has been observed that there is densification of treeline with the shift in its position to the higher elevation (Singh et al., 2011) and also densification with no shift (Zhang et al., 2009).

Delineating treeline ecotone and studying their dynamics by image classification is not an efficient technique in the sparse vegetation area of alpine ecosystem (Zhang et al., 2009). Treeline shift happens not as a whole patch but rather in the form of spreading of individual trees. Therefore, the absolute boundary of classified vegetation type cannot detect the small continuous migration of treeline ecotone. NDVI could track the continuous changes in the vegetation distinguishing dense vegetation, sparse vegetation and bare area. The present study is based on the technique of delineating both past and current treelines at the landscape level by combining both remote sensing and field survey. It involves a semi-autonomic approach for delineating treeline using NDVI as the functional difference between treeline and the high elevation pasture, which is through known NDVI values of treeline locations on the ground. This study has two main parts. First, moderate resolution multispectral satellite imageries separated by around four decades were used to delineate and evaluate the alpine treeline ecotone shifts. Second, niche modelling of *B. utilis* was performed and the changes were evaluated from the current to future IPCC scenario.

2. Materials and methods

2.1 Study area
The study was carried out in the Indian Himalaya (Figure 1) featuring a complex terrain and highly dense forest. This includes Jammu and Kashmir (J&K), Himachal Pradesh (H.P.), Uttarakhand, Sikkim and Arunachal Pradesh. The area is topographically complex with elevation reaching up to 8564 m a.m.s.l. (above mean sea level) and slope varying between 0º to 82º derived from digital elevation model. There is dominance of forest cover in all the Himalayan states *viz*. Jammu and Kashmir (10.34%; percentage of total geographic area), Himachal Pradesh (26.40%), Uttarakhand (45.32%), Sikkim (47.31%), and Arunachal Pradesh (80.30%) (SFR, 2015). The regions of Indian Himalaya have many endemics plant species with enormous biodiversity being considered as one-biodiversity hot spots on the Earth.

Climatic conditions are related closely to the elevation, which causes steep environmental gradients in the Himalaya. Micro-climatic diversity in the region leads to remarkable differences in vegetation over short distances. In the south, it has moist tropical forest and in the north cold desert within a very short distance (Rawat and Tambe, 2011). There is generally a sharp decrease in the NDVI value after a certain elevation representing the treeline ecotone. Further decrease in the NDVI value represented other vegetation line. The area between the treeline and snow cover is the high elevation pasture. Heavy and long-duration precipitations in both the winter and summer season results into a luxuriant vegetation.

2.2 Methodology

2.2.1 Data used
The list of satellite data used is given in Table 1.

2.2.2 Treeline position delineation
Terrain corrected, orthorectified (UTM WGS84 projection), cloud-free Resourcesat-1/2 LISS-III image was acquired from National Remote Sensing Centre (NRSC), Hyderabad (https://nrsc.gov.in/Search_and_Order_Data).

Resourcesat-1 and Resourcesat-2 operates in sun-synchronous near-polar orbit since 2003 and 2011, respectively. Landsat data have been available since the 1970's. Landsat-1, Landsat-2 and Landsat-3 with MSS sensor were launched in the year 1972, 1975 and 1978, respectively. Landsat-1/2/3 MSS images of the past period were acquired from Global Land Cover Facility (GLCF, www.landcover.org). MSS and LISS-III data were used for the demarcation of treelines in respective periods. Digital numbers (DN) in the imagery were converted to radiance using the Equation (1) (Chander and Markham, 2003),

$$L^* = \frac{(L_{max} - L_{min})Q_{cal}}{Q_{calmax}} + L_{min} \qquad (1)$$

where L^* is the spectral radiance at the sensor aperture in W m^2 sr^{-1} μm^{-1} unit, L_{max} and L_{min} are the scaled spectral radiance, Q_{cal} is the calibrated DN, and Q_{calmax} is the maximum possible DN value. L_{max} and L_{min} values of the sensors were extracted from the metadata files.

Resourcesat-1/2 LISS-III multispectral images were atmospherically corrected using the Fast Line-of-Sight Atmospheric Analysis of Spectral Hypercube (FLAASH) (Matthew et al., 2000), and Landsat-1/2/3 MSS image using Dark Object Subtraction (DOS) method (Chavez, 1988) to retrieve surface reflectance. For the atmospheric correction of Resourcesat-1/2 LISS-III, we used the FLAASH technique implemented in the ENVI software

that was the best possible method available. However, for Landsat-1/2/3 MSS, the method of FLAASH correction is not available in the ENVI software. For the use of the FLAASH technique of atmospheric correction of Landsat-1/2/3 MSS, it is necessary to define the sensor's spectral response functions, which was not available. Therefore, the DOS method was the best possible option for the atmospheric correction of Landsat-1/2/3 MSS imagery. For long-term climate change studies, data from multiple sensors were used, which needed to be inter-calibrated as the sensors differ in their bandwidth and radiometric resolution. Vegetation indices are most sensitive to such difference and therefore normalization of MSS-derived NDVI data with respect to LISS-III derived NDVI were carried out as per the coefficients developed by Steven et al., (2003) (Equation (2)).

$$NDVI_{RS2} = -0.020 + 1.065 \times NDVI_{LandsatMSS} \qquad (2)$$

MSS-derived NDVI were adjusted to match a standard based on LISS-III derived NDVI. According to Steven et al. (2003), the conversion coefficients from MSS derived NDVI to LISS-III derived NDVI are not exactly the inverse of the coefficients from LISS-III derived NDVI to MSS derived NDVI. To validate the normalisation and to further increase the precision, a linear regression model of pseudo-invariant features (Anderson et al., 2011) was carried out. Values of NDVI derived from both the sensors were sampled from the common pixels for which dense vegetation, sparse vegetation and bare land were taken into account. The linear regression model showed significantly (p-value < 0.001) positive correlation (r = 0.87) between both the images. The mean slope and intercept between the NDVI values were calculated and the resulting regression equation was then used to inter-calibrate MSS-derived NDVI to a LISS-III-derived NDVI equivalent.
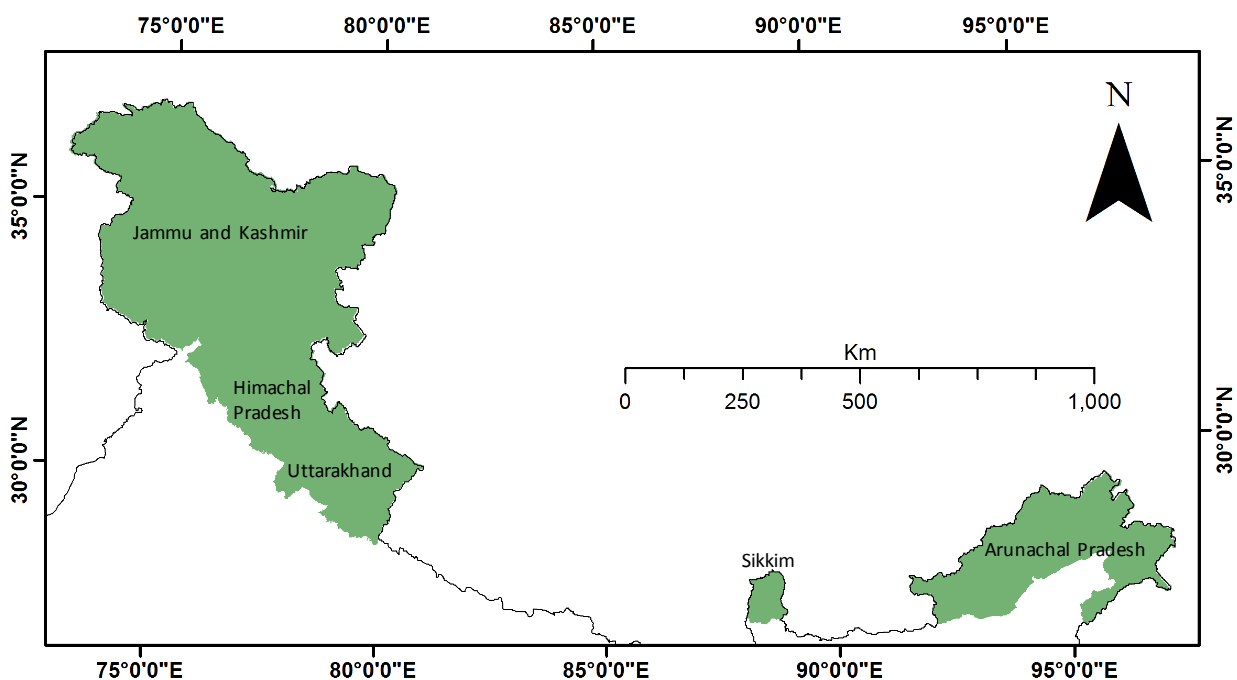

Figure 1. Study area (shown in shade)

Table 1. Satellite Data used for Past (Landsat) and Current (Resourcesat) Treeline delineation

S. No.	Himalayan State	Satellite / Sensor	Acquisition (Month/Year Range)
1	Jammu & Kashmir	Resourcesat-1/2 (LISS-III*) – 31 Scenes	Aug.-Dec., 2012-2014
2		Landsat-2/3 (MSS**) – 10 Scenes	June-Feb., 1976-1979
3	Himachal Pradesh	Resourcesat-1 (LISS-III) – 6 Scenes	Oct.-Nov., 2014
4		Landsat-1/2/3 (MSS) – 5 Scenes	Sep.-Jan., 1972-1979
5	Uttarakhand	Resourcesat-1/2 (LISS-III) – 10 Scenes	Oct.-Dec., 2012-2014
6		Landsat-1/2 (MSS) – 4 Scenes	Oct.-Dec., 1972-1976
7	Sikkim	Resourcesat-1 (LISS-III) – 4 Scenes	Nov.-Dec., 2012-2014
8		Landsat-2 (MSS) – 1 Scene	Jan., 1977
9	Arunachal Pradesh	Resourcesat-1 (LISS-III) – 13 Scenes	Oct.-Dec., 2012-2014
10		Landsat-1/2/3 (MSS) – 9 Scenes	Oct.-Feb., 1973-1978

* Resourcesat-1/2 (LISS-III) having 23.5 m spatial resolution, 140 km swath and 10 bit radiometric resolution with 4 bands (0.52 – 0.59 µm, 0.62 – 0.68 µm, 0.77 – 0.86 µm, 1.55 – 1.70 µm)
** Landsat-1/2/3 (MSS) having 60 m spatial resolution, 185 km swath and 6 bit radiometric resolution with 4 bands (0.5 – 0.6 µm, 0.6 – 0.7 µm, 0.7 – 0.8 µm, 0.8 – 1.1 µm)

The past and the current treeline delineations were done using automatic contour delineation method in ArcGIS (ESRI, 2016). The field records of high elevation treeline locations, as well as ancillary data (digital forest map of SFR, 2015), were used for ascertaining the NDVI value (0.45) over the treeline. Connection with iso-NDVI-line based on bi-cubic spline interpolation and filtering small spurious contours automatically generated on a defined threshold derived the treeline. Manual on-screen digitization was done in addition to the automatic process to correct temporary snow pixels, hill shadow, and treeline areas affected by landslides and avalanches. The treeline that gets unnoticed in the automatic process due to the presence of temporary snow cover in the image are manually digitized taking into reference the forest cover map of the Forest Survey of India (SFR, 2015). The landslides and avalanches are a onetime process. This problem is taken care because we are making contour over threshold NDVI (iso-NDVI-line) which was edited to follow its contour line if it goes abruptly downward due to such disturbances. This process ensures that we capture realistic climate-driven treeline ecotone. Such abrupt changes in the NDVI caused due to landslides and avalanches were verified in the FCC imagery

2.2.3 Treeline position elevation and uncertainty assessment

The elevations at the past and current treelines were extracted from orthorectified Cartosat-1 DEM, which is available at the spatial resolution of 1/3 arc-second. Station points at every 10 m were generated at both the past and current treeline ecotones. The elevation values (in meters) were extracted using Cartosat-1 DEM for each station point. The mean and maximum level of the past and current treeline with their elevation shift was computed. Different sets of satellite data and products were used for delineating the treeline positions and its elevation; therefore, the estimates were subjected to inherent errors associated with each step of the process and data used. The elevation and planimetric DEM accuracies are 8 and 15 m, respectively at statistically 90% confidence level (Muralikrishnan et al., 2011). Both planimetric and elevation errors in the DEM can contribute to elevation errors in the position of the treeline, therefore mapping uncertainty of the treeline was estimated by combining all possible error sources. The horizontal or spatial

uncertainty of the past and current treeline was calculated as the quadratic sum of uncertainties (Taylor, 1997) using the Equation (3),

$$\delta\varepsilon_x = \sqrt{(\delta x)^2 + (\delta z_x)^2} \qquad (3)$$

where $\delta\varepsilon_x$ is the horizontal uncertainty, δx is the horizontal error of the data used for mapping treeline position, and δz_x is the horizontal error of the elevation data. DEM affects the treeline vertical position accuracy through the effect of horizontal treeline mapping error (Fissore et al., 2015). In a highly steep mountainous region like that of Himalaya, a small horizontal shift due to the error may result in a momentous vertical shift. The vertical uncertainty of the treelines caused by the covariation of horizontal error and slope were estimated using the Equation (4),

$$\delta\varepsilon_y = \delta\varepsilon_x \times \tan\theta \qquad (4)$$

where $\delta\varepsilon_y$ is the vertical uncertainty and θ is the terrain slope in radian unit. The combined vertical uncertainty of both the treelines was obtained using Equation (5),

$$\delta\varepsilon_{yc} = \sqrt{(\delta\varepsilon_y)^2 + (\delta z_y)^2} \qquad (5)$$

where $\delta\varepsilon_{yc}$ is the combined vertical uncertainty and δz_y is the vertical error of the elevation data. Since the mapping implicates treeline shift over time, the overall uncertainty was calculated as the propagation of error using the Equation (6),

$$\delta\varepsilon = \sqrt{(\delta\varepsilon_{yca})^2 + (\delta\varepsilon_{ycb})^2} \qquad (6)$$

where $\delta\varepsilon$ is the combined uncertainty of treeline shift; $\delta\varepsilon_{yca}$ and $\delta\varepsilon_{ycb}$ are the combined vertical uncertainty of past and current treeline, respectively. The actual elevation is related to the spatially paired DEM elevation and uncertainty by Equation (7) (Wheaton et al., 2010),

$$Z_{Actual} = Z_{DEM} \pm \delta\varepsilon \qquad (7)$$

where Z_{Actual} is the true value of elevation, Z_{DEM} is the spatially-paired DEM elevation, and $\delta\varepsilon$ is the overall uncertainty in the treeline elevation. Assessment of the positional accuracy of the treeline using true or reference location on the ground was not possible for the entire study area due to its inaccessibility. In addition, uncertainty with respect to higher resolution imagery compared to the resolution used in this study as reference was not considered because of the non-availability of higher

resolution images in 1970s. Since, it has not been possible to quantify the uncertainty in the NDVI-based classification of the treeline, this is an added source of error that has not been quantified. Thus, the estimates of the error provided in the paper likely underestimate the total error.

2.2.4 Ground survey and validation

Field validations were conducted in all the states *viz.* Gulmarg, Jammu and Kashmir; Chansal, Himachal Pradesh; Tungnath and Pakhwa, Uttarakhand; Gnathangand Kabi-Tingda, Sikkim; and Tawang, Arunachal Pradesh. These areas are rich in endemic alpine plant species. The vegetation along the elevational gradient range from closed montane forest to high elevation alpine pasture. Three summits were selected along the elevation gradient at each location. These sites experience little influence of anthropogenic activities. Permanent plots were established in all the summits to detect long-term climate change (Singh, 2015). The elevation and geolocations of the treeline species were noted (61 points, Table 3 - 7) along the elevation gradient for the validation of the satellite-derived treeline position. The geolocation points belonging to *Betula utilis* were also used as presence records for niche modelling.

2.2.5 Niche modelling of treeline species- Betula utilis

The niche (habitat) modelling is an effort to simulate the conducive environmental condition based on a set of bioclimatic parameters that allow a given species in question to survive, reproduce and grow. However, a species can occupy only a part of its fundamental environmental niche in a particular ecosystem because of absence of other local conditions. The niche models mainly provide a detailed prediction of distributions of a species by relating presence of the species to environmental predictors. The primary aim of this experiment was to evaluate the fate of treeline tree species in future climatic scenarios. The alpine treeline ecotone is majorly populated with Himalayan birch (*Betula utilis*) also known locally as "*Bhojpatra*", forming present-day alpine treeline in conjunction with *Abies* sp. and *Rhododendron* sp. Species sampling in high elevation region of Himalaya is climatically and logistically difficult and therefore, it was possible to gather smaller number of samples from field. Occurrence records were collected using handheld Global Positioning System (GPS) around the summits of Gulmarg, Jammu and Kashmir; Chansal, Himachal Pradesh; Tungnath, Uttarakhand; and Kabi Tingda, Sikkim. These sites have been established for the long-term monitoring of alpine treeline dynamics in Himalaya (Singh, 2015). More occurrence records were downloaded from Global Biodiversity Facility (GBIF, 2018) and out of the total (47) treeline species locations, 70% were used for model calibration and 30% were kept as an independent dataset for presence-only evaluation metrics or model testing (external evaluation). In the process of repeated cross-validation, 70% of data for model fitting and 30% data for model validation were randomly selected from calibration dataset.

The digital elevation model (DEM) and bioclimatic data have been used for the prediction of the *B. utilis* distribution. The 19 bioclimatic variables and 3 topographic variables had spatial resolution of 1 km × 1 km. Current (1970-2000; version 2; Fick and Hijmans, 2017) and future (2061-2080; version 1; Hijmans et al., 2005) bioclimatic data and DEM were acquired from WorldClim (www.worldclim.org). The bioclimatic data were derived from the monthly temperature and precipitation data representing seasonality and extreme environmental factors. The 2061-2080 climate projection RCP8.5 used in the IPCC$_5$ is the possibility of a continuous rise in the greenhouse gas emission throughout the 21st century. The common downscaled, bias-corrected global climate model (GCM) dataset for LIG and HadGEM2-AO (Baek et al., 2013) was used for 2061-2080. The DEM data for niche modelling purpose was used from Shuttle Radar Topography Mission - SRTM (USGS, 2006) at 1 km spatial resolution. The details of the variables used in the present study have been provided in Table 2.

The check of collinearity in the predictor variables is necessary before habitat suitability modelling (Dormann et al., 2013). The collinearity in the bioclimatic and topographic variables was checked using Pearson's linear model and one of the ecologically meaningful variables was selected of the two variables that have correlation coefficient more than 0.7. Additionally, variance inflation factor (VIF) was also checked and the variables were selected that have VIF less than 10 (Naimi et al., 2014). DEM was also used (after the modelling and predictions) to get information about the elevation ranges and shift of habitat suitability. Random Forest (RF) machine learning technique was used in niche modelling. For RF algorithm pseudo-absences or background data (Barbet-Massin et al., 2012) is necessary (Liu et al., 2016), that allows predicting the probability of presence (Merow et al., 2013). We have used presence-background data for niche modelling (Guillera-Arroita et al., 2015). The '*biomod2*' package (Thuiller et al., 2016) of the 'R' programming language (R Core Team, 2018) has been used for the analysis.

The repeated cross-validations during ensemble modelling (bootstrap aggregation) in RF were performed using true skill statistics (TSS). A 2 × 2 confusion matrix was constructed having records of the number of true positive (a), false positive (b), false negative (c), and true negative (d). Specificity is the probability that the prediction model correctly classify absence. Sensitivity is the probability that the prediction model correctly classify presence. The model sensitivity, specificity and the TSS were estimated using training dataset. Since the predictions are based on a probabilistic statistical model, these need to be transformed to the scale of real observations in terms of high to low suitability. The continuous probability of occurrence data was truncated to three classes (highly, moderately and less suitable habitats) using 0.33 and 0.66 cut-offs (thresholds). Presence-only evaluation metrics like sensitivity (Allouche et al., 2006; Fielding and Bell, 1997), false negative rate (Fielding and Bell, 1997) and continuous Boyce index (Hirzel et al., 2006) were computed using the independent dataset to properly assess the model's ability to predict niche areas. Continuous Boyce index was computed using '*ecospat*' package (Broennimann et al., 2018) in the 'R' programming language. All statistical analysis was done using the '*stats*' package in 'R'.

Table 2. Bioclimatic and topographic data used for niche modelling of *Betula utilis*

Code	Environmental and topographic variable
BIO1	Annual Mean Temperature
BIO2	Mean Diurnal Range (Mean of monthly (max temp - min temp))
BIO3	Isothermality (BIO2/BIO7) ($\times$ 100)
BIO4	Temperature Seasonality (standard deviation $\times$ 100)
BIO5	Max Temperature of Warmest Month
BIO6	Min Temperature of Coldest Month
BIO7	Temperature Annual Range (BIO5 - BIO6)
BIO8	Mean Temperature of Wettest Quarter
BIO9	Mean Temperature of Driest Quarter
BIO10	Mean Temperature of Warmest Quarter
BIO11	Mean Temperature of Coldest Quarter
BIO12	Annual Precipitation
BIO13	Precipitation of Wettest Month
BIO14	Precipitation of Driest Month
BIO15	Precipitation Seasonality (Coefficient of Variation)
BIO16	Precipitation of Wettest Quarter
BIO17	Precipitation of Driest Quarter
BIO18	Precipitation of Warmest Quarter
BIO19	Precipitation of Coldest Quarter
DEM	Digital Elevation Model
Slope	Slope in degree unit
Aspect	Aspect in degree unit

3. Results and Discussion

3.1 Treeline position elevation and upward shift

The mean elevation of the current treeline position in Jammu and Kashmir, Himachal Pradesh, Uttarakhand, Sikkim and Arunachal Pradesh Himalaya was 4121 m, 3520 m, 3615 m, 3542 m and 4136 m a.m.s.l., respectively (computed from Cartosat-1 DEM). The past and current treeline position for Himalayan states under the study has been shown in Figure 2 to 6. The environmental constraints (mainly temperature) prevent the tree growth beyond this elevation, which yields low stature vegetation. The most dominant treeline species found in the treeline zone in Indian Himalaya is shown in Table 3-7. *Rhododendron* L. is the most dominant treeline species associated with *Viburnum* L., *Abiesdensa* Griff., and *Betula utilis* D. Don. In eastern Himalaya, large trees species of *Rhododendron* L. (tree height *c.* 7.5 m) dominated at the lower elevation (*c.* 1940 m to 3150 m a.m.s.l.). Whereas, at a higher elevation of *c.* 3150 to 3900 m a.m.s.l, dwarf shrubs of *Rhododendron* sp. (*krummholz*) of heights of *c.* 3 m were dominant.

The dominant *Rhododendron* sp. in the *krummholz* zone (3500 to 4200 m a.m.s.l.) were *R. campanulatum* D. Don, *R. lanatum* Hook. f., *R. hodgsonii* Hook. f., *R. thomsonii* Hook. f., *R. wightii* Hook. f., and *R. fulgens* Hook. f. (Rawat and Tambe, 2011). The high elevation pastures were mostly dominated by by species of *Prunus* L. (low-

shrub), *Aconitum* L., grasses, ferns, bryophytes, and lichens.

The comparison of treeline between the years past to current showed significant changes in the ecotone elevation in the past four decades (Table 8; Figure 2 to 6). The overall vertical shift in the alpine treeline ecotone was 381 ± 73 m in over four decades at a rate of c. 95 m decade^{-1} in the entire Indian Himalaya. The highest shift in the treeline was observed in Arunachal Pradesh Himalaya. In the past, the mean elevation of treeline positon in Jammu and Kashmir, Himachal Pradesh, Uttarakhand, Sikkim and Arunachal Pradesh was 3680 m, 3219 m, 3204 m, 3241 m, and 3684 m a.m.s.l., respectively. In Sikkim Himalaya, the maximum elevation of 4579 m has shifted upward to attain the maximum elevation of 4804 m in year 2014.

Comparing both the past and current mean elevation status of the treeline, it was observed that the mean upward shift in the treeline is 301 ± 66 m in Sikkim Himalaya i.e., approximately 81 m decade^{-1}. The treeline position and their upward shift are variable throughout the mountain because of various factors responsible for the treeline species growth like topography, macro- and micro-climate, and other ecological conditions.

Alpine treeline dynamics is an indicator of climate change mainly due to long-term changes in temperature regime (Zhang et al., 2009). In Sikkim Himalaya, the annual mean minimum temperature varies from 15.26 ℃ to 17.22 ℃ and annual cumulative precipitation from 1418.7 mm to

4061.5 mm based on 37 years (1977-2013) of gridded climate dataset (Singh et al., 2018). At a rate of 0.3 ℃ decade[-1], the minimum air temperature would have gone up by *c.* 1.1 ℃ (in the observation period), making the treeline position to shift *c.* 301 ± 66 m upward. In Himalaya, 1 ℃ increase in temperature led to 250-300 m elevation shift of treeline species (Kumar, 2012). Similarly, an upward shift of treeline but with lesser magnitude was observed in Himachal Pradesh (1860 to 2000) for Himalayan pine with 19 m decade[-1] upward shift on the south and 14 m decade[-1] shift on the northern slope (Dubey et al., 2003). A repeat photography study (1923 to 2003) of Yunan, China region showed a rising trend of 8 to 15 m decade[-1] (Baker and Moseley, 2007). However, in a previous study based on satellite remote sensing in western Himalaya (1976 to 2006), a greater shift of 110 m decade[-1] was observed (Singh et al., 2011). The current study also brought a similar rate of change of 81 m decade[-1] that highlighted the importance of baseline data.
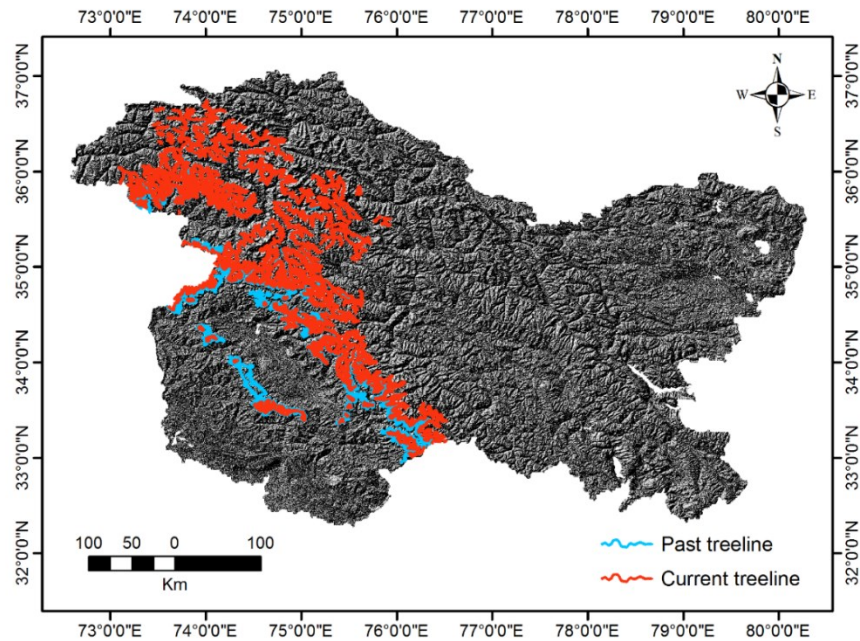
Figure 2. Alpine treeline ecotone position in Jammu and Kashmir Himalaya
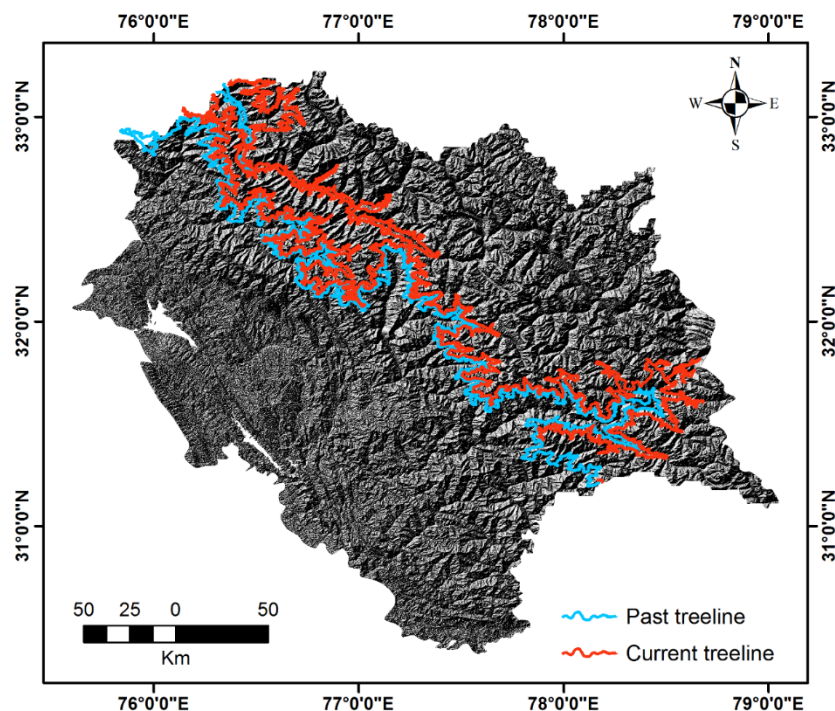
Figure 3. Alpine treeline ecotone position in Himachal Pradesh Himalaya
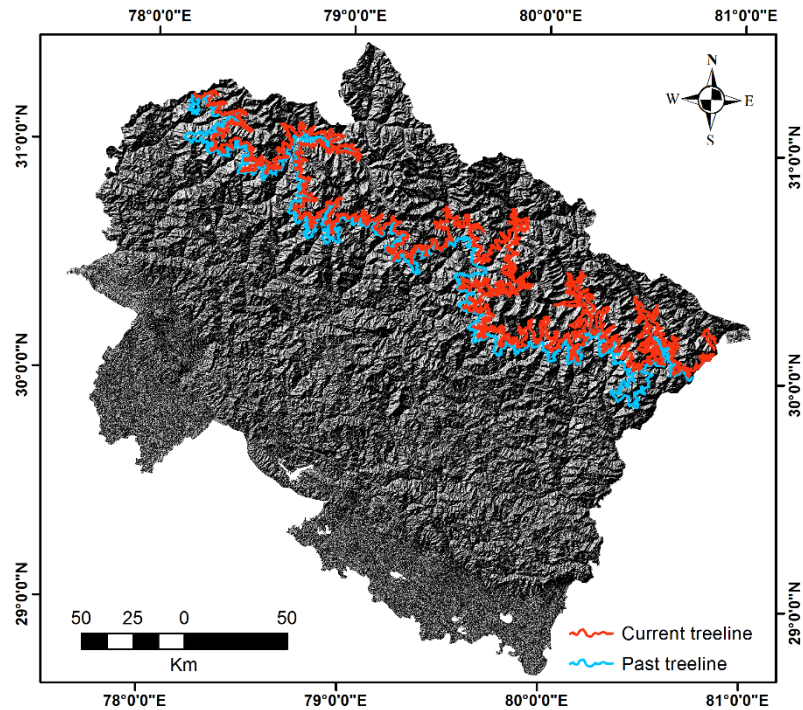
Figure 4. Alpine treeline ecotone position in Uttarakhand Himalaya
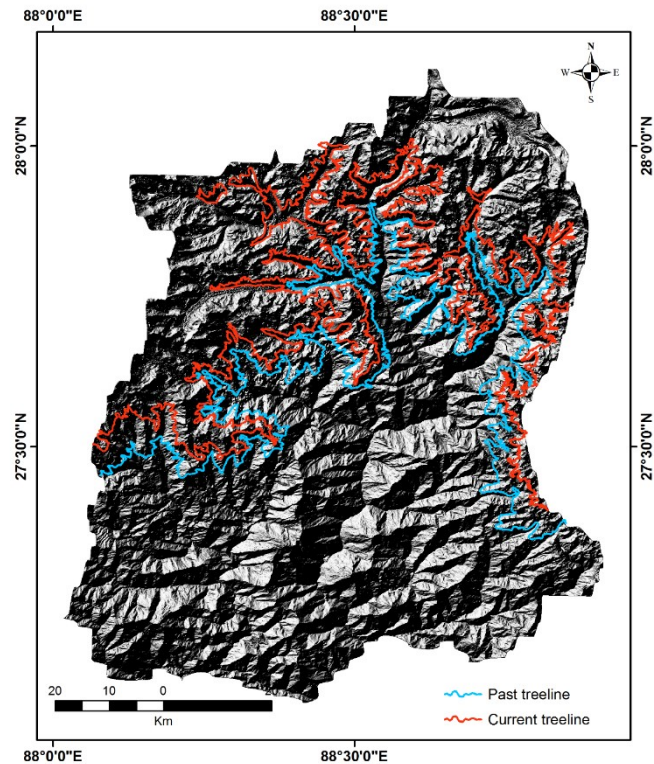
Figure 5. Alpine treeline ecotone position in Sikkim Himalaya
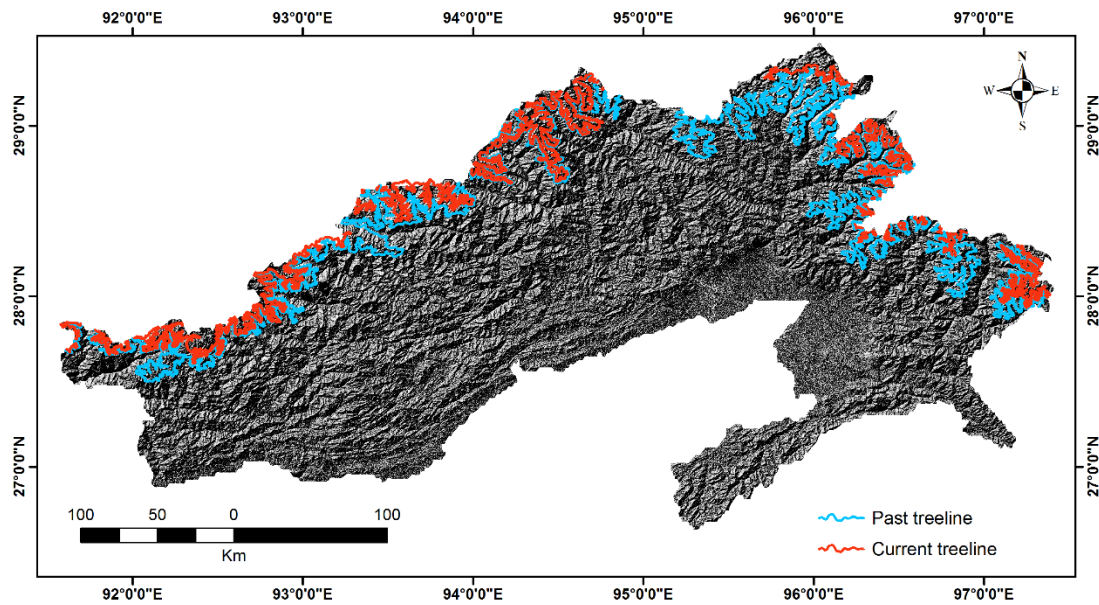
Figure 6. Alpine treeline ecotone position in Arunachal Pradesh Himalaya

Table 3. Treeline species locations and elevations in Jammu and Kashmir Himalaya

Treeline species	Latitude (°N)	Longitude (°E)	Elevation (m)
Abies pindrow	34.298	75.271	2757
Abies pindrow	34.291	75.269	2770
Abies pindrow	34.293	75.315	2844
Abies pindrow	34.291	75.319	2722
Abies pindrow	34.287	75.321	2787
Abies sp.	34.300	75.300	2400
Abies sp.	34.050	74.380	2721
Betula utilis	34.380	76.370	3337
Betula utilis	34.080	74.820	3048
Betula utilis	33.850	77.100	4070
Betula utilis	33.260	77.420	4230
Betula utilis	34.291	75.224	3005
Betula utilis	34.288	75.278	3016
Betula utilis	34.298	75.326	2989
Betula utilis	34.255	75.423	2914
Betula utilis	34.291	75.224	2963
Rhododendron sp.	34.370	75.600	3658
Rhododendron sp.	33.380	74.300	2743
Rhododendron sp.	32.867	76.860	3700

Table 4. Treeline species locations and elevations in Himachal Pradesh Himalaya

Treeline species	Latitude (°N)	Longitude (°E)	Elevation (m)
Abies sp.	31.980	77.430	2100
Betula utilis	31.087	77.279	3048
Betula utilis	33.130	76.350	4267
Betula utilis	31.350	78.443	3400
Betula utilis	31.721	77.986	3286
Betula utilis	31.409	78.331	3020
Betula utilis	32.328	77.205	2850
Betula utilis	33.144	76.449	3228
Betula utilis	31.413	78.332	3456
Rhododendron campanulatum	31.541	77.372	3169
Rhododendron campanulatum	32.414	77.234	3141
Rhododendron sp.	32.370	77.250	4004

Table 5. Treeline species locations and elevations in Uttarakhand Himalaya

Treeline species	Latitude (°N)	Longitude (°E)	Elevation (m)
Abies sp.	30.430	78.070	2100
Abies sp.	30.606	79.216	2673
Abies sp.	30.080	79.230	3600
Abies sp.	30.127	79.979	3439
Betula utilis	30.124	79.977	3355
Rhododendron barbatum	30.126	79.979	3440
Rhododendron campanulatum	30.127	79.978	3418
Rhododendron campanulatum	30.126	79.979	3421
Rhododendron sp.	30.411	78.285	2550
Rhododendron sp.	30.702	77.870	3353
Rhododendron sp.	30.127	79.978	3432

Table 6. Treeline species locations and elevations in Sikkim Himalaya (Singh et al., 2018)

Treeline species	Latitude (°N)	Longitude (°E)	Elevation (m)
Abies densa	27.425	88.709	3570
Betula utilis	27.830	88.700	3658
Betula utilis	27.900	88.530	3658
Betula utilis	27.896	88.537	3682
Betula utilis	27.901	88.530	4210
Betula utilis	27.895	88.527	4136
Betula utilis	27.884	88.526	4331
Rhododendron sp.	27.425	88.716	3904
Rhododendron sp.	27.422	88.706	3537
Rhododendron sp.	27.425	88.716	3900
Rhododendron sp.	27.750	88.500	3810

Table 7. Treeline species locations and their elevations in Arunachal Pradesh Himalaya (Mohapatra et al., 2019b)

Treeline species	Latitude (°N)	Longitude (°E)	Elevation (m)
Rhododendron sp.	28.35	96.61	3810
Rhododendron sp.	28.33	96.62	3810
Rhododendron sp.	27.80	96.90	4119
Rhododendron crinigerum	27.80	96.90	4119
Rhododendron sidereum	27.80	96.90	4119
Rhododendron ramsdenianum	27.80	96.90	4119
Rhododendron arizelum	27.80	96.90	4119
Rhododendron pudorosum	27.70	92.20	4375

Table 8. Mean upward shift of alpine treeline ecotone in Indian Himalaya from 1972 to 2014

State	Mean shift (m) ± uncertainty
Jammu and Kashmir	441 ± 71
Himachal Pradesh	301 ± 77
Uttarakhand	411 ± 79
Sikkim	301 ± 66
Arunachal Pradesh	452 ± 74

3.2 Fundamental niche dynamics of Betula utilis

The sensitivity, specificity and TSS of the RF ensemble model evaluated using the training set (internal evaluation) were 0.91, 0.70 and 0.61, respectively (Mohapatra et al., 2019a). The continuous Boyce index that is the Spearman's correlation between Predicted to Expected (P/E, P/E = 1 indicates a completely random model) and habitat suitability classes was 0.92 indicating ascending curve, indicating a non-random model (Hirzel et al., 2006)

with better predictive accuracy. The variables that RF identified as most important for classifying *B. utilis* occurrence was mean diurnal range, followed by mean temperature of driest quarter, slope, the mean temperature of wettest quarter; precipitation of warmest quarter; isothermality, precipitation seasonality, precipitation of coldest quarter; aspect, and precipitation of driest month. This indicates that temperature is a major factor compared to other variables that govern the distribution of *B. utilis* in

Himalaya. Compared to aspect, the slope is a better determinant of a suitable niche for *B. utilis*. The projected potential distribution of *B. utilis* in 1970-2000 for different Indian states are shown in Figures 7-11. Niche modelling showed that *B. utilis* had shifted to higher elevation (Table 9) in response to projected climate change. This is because of increase in temperature at higher elevations zones in the Himalaya. While in 1970-2000, the highly suitable niche of *B. utilis* was found to have reached up to 4000 m a.m.s.l.

in Sikkim Himalaya. Similarly, Körner (2012) reports the current presence of *Betula* species at an elevation of 4010 m in Langtang, northern Nepal. In 2061-2080, there has been further advancement of a highly suitable niche to a higher elevation, reaching up to 5000 m elevations. This indicates that the shift in the *B. utilis* niche is importantly more along elevation than latitude or longitude when studied at a smaller detailed scale (Mohapatra et al., 2019a) .
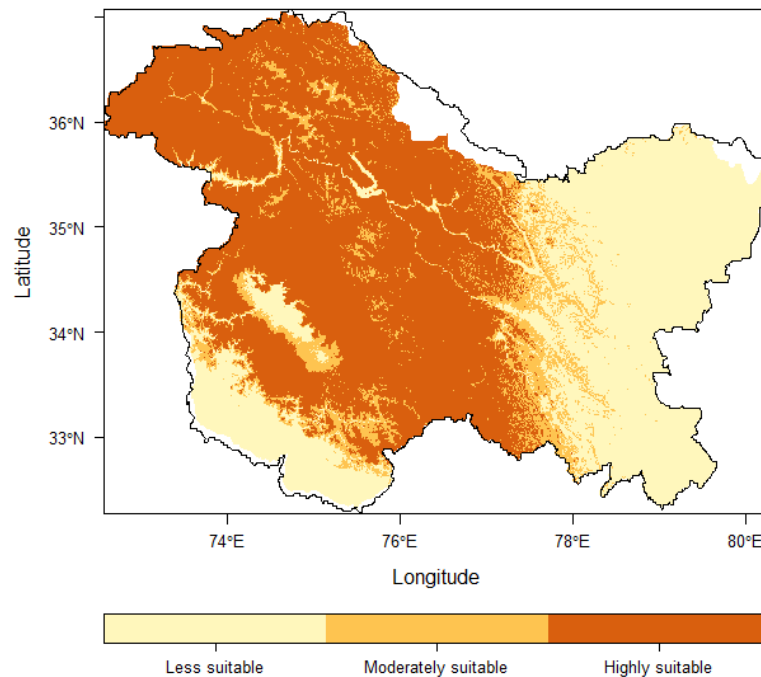

Figure 7. Potential distribution of *Betula utilis* in Jammu and Kashmir Himalaya in 1970-2000
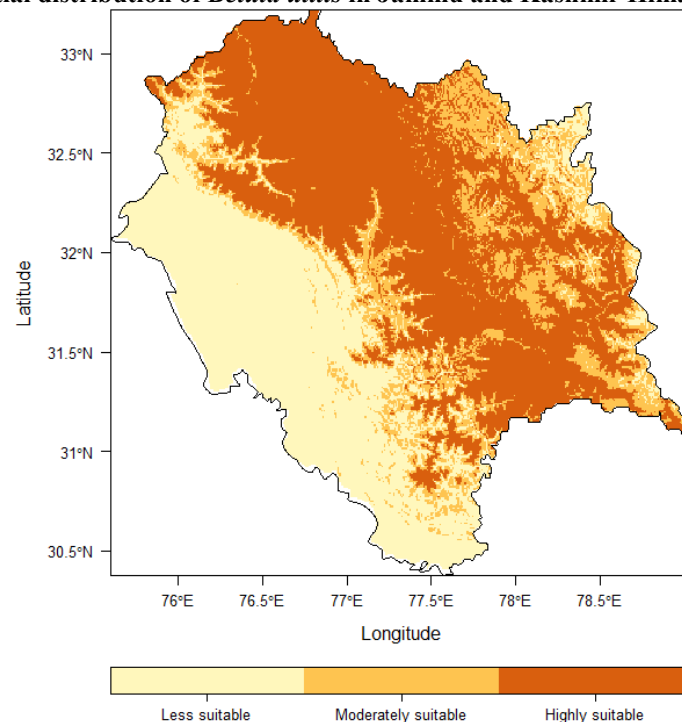

Figure 8. Potential distribution of *Betula utilis* in Himachal Pradesh Himalaya in 1970-2000
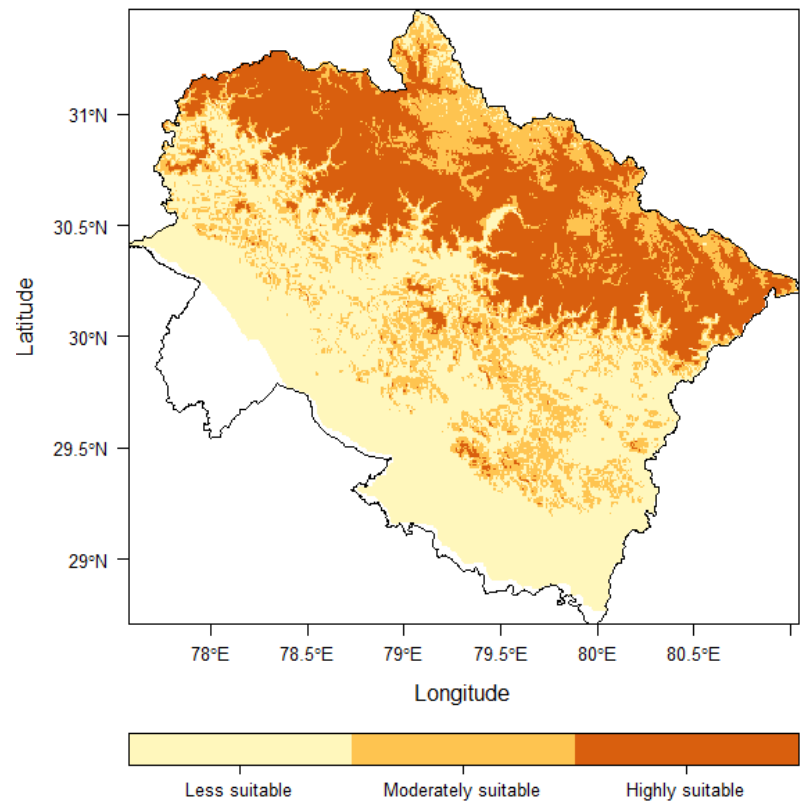
Figure 9. Potential distribution of *Betula utilis* in Uttarakhand Himalaya in 1970-2000
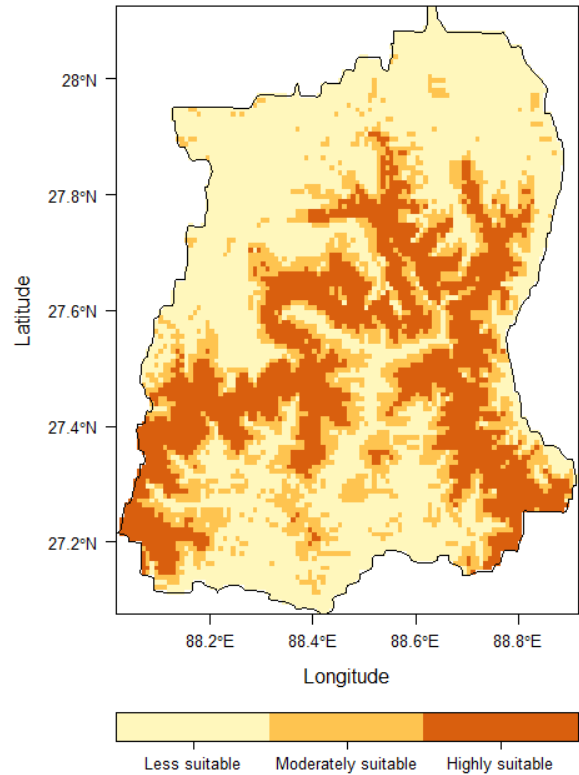

Figure 10. Potential distribution of *Betula utilis* in Sikkim Himalaya in 1970-2000
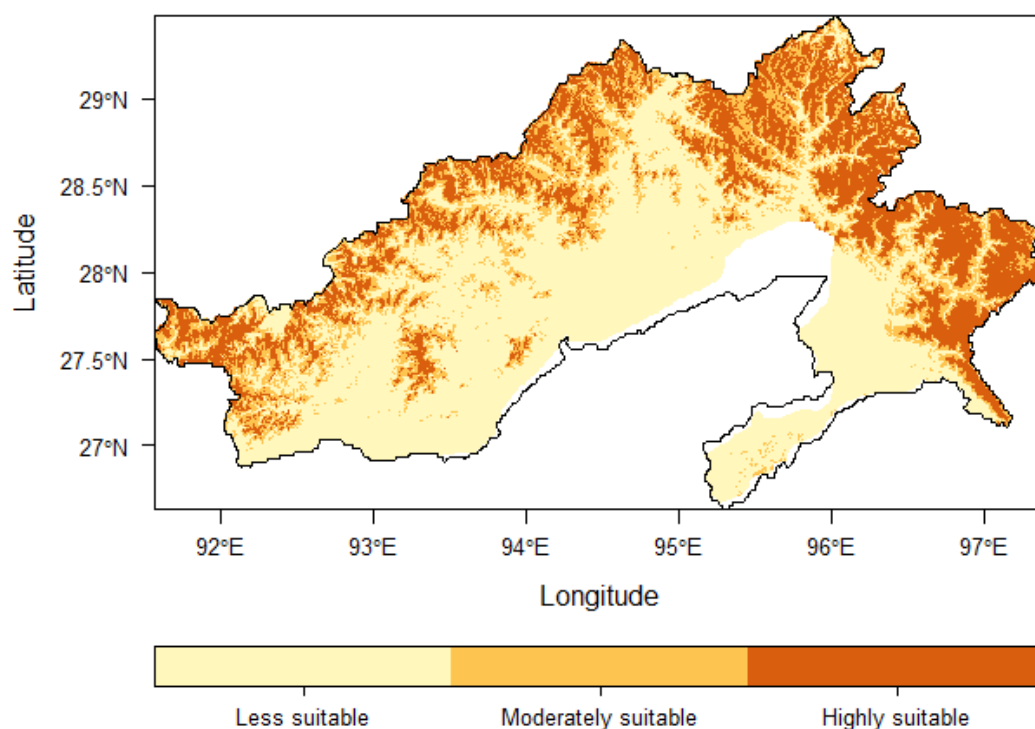
Figure 11. Potential distribution of *Betula utilis* in Arunachal Pradesh Himalaya in 1970-2000

The shift of treeline in Himalaya is more elevation driven compared to other global climatic treelines that are more latitude driven towards the pole. There is a chance of competition (for space and other resources) between the tree species like *B. utilis* and the alpine herbs and shrubs that dwell above the treeline in the mountain peaks of Himalaya, and therefore a greater chance of species extinctions, if the warming as projected in RCP8.5 continues.

This signifies that the projected future temperature change has caused noticeable deviation of *B. utilis* niche. There has been a decrease in a highly suitable niche area in the elevation zone of 2000 to 2600 m from past to future scenarios. The lower elevation ranges of the Himalayan mountain zones limits the suitable bioclimate for *B. utilis*. Similar observation of *B. utilis* niche shift to higher elevation was observed in Uttarakhand, India, western Himalaya by Singh et al. (2011). There is an observation of the invasion of the thermophilic species to the higher elevation (Gottfried et al., 2012; Hamid et al., 2020).

There has been an increase in the highly suitable habitat for *B. utilis* from the past to future along the elevational, latitudinal and longitudinal gradients. Comparing the mean elevation of highly suitable niche showed that the difference is higher from 1970-2000 to 2061-2080. From 1970-2000 to 2061-2080 (in *c.* eight and half decades), the mean upward shift of *B. utilis* niche in Jammu and Kashmir, Himachal Pradesh, Uttarakhand, Sikkim and Arunachal Pradesh were *c.* 21 m, 46 m, 78 m, 110 m and 45 m decade[-1], respectively (Table 9; Mohapatra et al., 2019a). This rate of the upward shift has been estimated taking the difference of the mean elevation of the highly suitable niche of 1970-2000 and 2061-2080. The difference was then further divided with the time gap (86

years) from the year 1985 to 2071 (the mid-years of the climate normal of current and future time, respectively).

In all the states of Indian Himalaya, there has been a shift of *B. utilis* niche to higher elevation from current and then to future scenario. The highest rate of upward shift in niche was in Sikkim Himalaya *c.* 109.9 m decade[-1], which was higher than the actual treeline shift (*c.* 81 m decade[-1]) studied using satellite remote sensing (Singh et al., 2018). The lowest magnitude of shift (*c.* 20.8 m decade[-1]) has been observed in Jammu and Kashmir Himalaya. There has been no contraction of highly suitable *B. utilis* niche along the elevational gradient. This rate of niche shift has been shown from current to future time rather than from past to current or future scenarios.

Climatic variations in Himalaya not only cause the shift of *B. utilis* to higher elevation zones but also to higher latitude and longitude areas in many regions. *B. utilis* has become dominant in the eastern Himalaya during 1970-2000 and is likely to be found more towards eastern side in 2061-2080. Along the longitudinal gradient, the magnitude of niche shift is higher from current to future than past to current, similar to that along elevation. In the lower longitude regions, the difference in the frequency of suitable habitat for *B. utilis* from 1970-2000 to 2061-2080 is less. There was a decrease in the mean slope of highly suitable niche from the past to future. During the field survey, *B. utilis* was observed to be the most dominant species in the treeline ecotone at the western Himalaya, while it was scarce and mixed with other species (like *Rhododendron* sp.) in the treeline ecotones of eastern Himalaya. This means that conditions in western Himalaya are better than the eastern Himalaya for the establishment and growth of *B. utilis*. There has been least contraction of highly suitable habitat of *B. utilis* along elevation, latitude, and longitude in Himalaya from current and future time.

Table 9. Mean elevation (in meter) of the realized and fundamental niche of treeline (including *B. utilis*) in the Indian Himalaya. The rate of shift is in meter decade^{-1}

Data / Model	Period	J&K	H.P.	Uttarakhand	Sikkim	Arunachal Pradesh
Landsat-1/2/3	1972 - 1979	3680	3219	3204	3241	3684
Resourcesat-1/2	2014	4121	3520	3615	3542	4136
Rate of Treeline Shift		116	79	108	81	113
Bioclimatic Niche	1970-2000	4048	4029	3751	3150	3342
IPCC$_5$ Scenario based Niche (RCP 8.5)	2061-2080	4227	4426	4421	4095	3731
Rate of B. utilis Niche Shift		21	46	78	110	45

The region of highly suitable niche area of *B. utitis* had moderate to no constraints on the nutrient retention capacity of soil (Fischer et al., 2008). Higher importance of temperature variables indicates that it is a more important predictor of *B. utilis* niche compared to precipitation parameters. Paulsen and Körner (2014) reported that the distribution of treeline species over the globe is temperature dependent and drought is a rare phenomenon at the alpine treeline ecotone. Using the climatic database, Paulsen and Körner (2014) modelled that water plays a potential constraint in determining the minimum length of the growing season during which the thermal conditions permit tree growth. The most active period of the growth of high elevation treeline species is monsoon during which availability of water is maximum. The growth of high-elevation treeline species requires a minimum length of the growing season of 94 days having a mean temperature of 6.4 °C across all growing season (Paulsen and Körner, 2014). Bobrowski et al. (2017) report that the bioclimatic variables like the mean temperature of the wettest quarter, temperature annual range, precipitation of the coldest quarter, average precipitation of March, April and May and precipitation seasonality are the most important variables in predicting the potential distribution of B. utilis in Himalaya.

Niche expansion of treeline species in the high elevation zones of Himalaya could cause the alpine species to become vulnerable to 21st century climate changes because of competition for space. Rapid snow and glacier melting due to global warming may give the alpine species a chance to gain ground and proliferate. Schickhoff et al. (2015) predicted a shift in the potential habitat of *B. utilis* from lower to higher elevation and expansion into the north of the Himalayan ranges. Singh et al. (2013) also observed the dominance of *B. utilis* as a treeline species using presence-only occurrence data by Generic Algorithm for Rule-set Production (GARP) model in Uttarakhand. In Himalaya, seedlings and saplings of *Betula* sp. were found along vertical transects at a distance of 50 m above the treeline (Schickhoff et al., 2015). This suggested that in response to changing climatic conditions, *B. utilis* has a chance to have a high population in the mountain summits. Future warming may disturb the high elevation montane ecosystems, as the lower plant community (herb and shrub species) reorganisation requires a longer period than the tree species in high elevation (Mayor et al., 2017). Therefore, herbs and shrubs

species will not be able to cope with the rapid treeline advancement to a higher elevation.

In the real world, species may not totally fill its potential distribution (fundamental niche) but rather is more likely to be present where the climate is most suitable (realized niche) for its optimum growth and evolution. Predicted suitability is not proportional to the actual probability of occurrence (Guillera-Arroita et al., 2015). *B. utilis* may fail to colonize the suitable areas in Himalaya predicted in this study because of dispersal inability in the rugged terrain and competition with other dominant treeline species. Many other relevant biotic and abiotic variables could make the species niche modelling more mechanistically meaningful but at the cost of more errors. Deriving more mechanism-oriented variables require advanced spatial modelling (Guisan et al., 2017).

The result of the niche modelling computed in this study is a predictive model assigning a probability of occurrence to each of the grid boxes as a function of the bioclimatic indicators. Therefore, the pixels showing the highest probability of *B. utilis* does not mean that only *B. utilis* would be present there in future. Many other species may also occur with *B. utilis* (niche overlapping), like the *Quercus* sp. and *Rhododendron* sp. (other dominant species at high elevation regions of Himalaya) if the similar bioclimatic and topographic conditions are suitable for the other species. Gaire et al. (2014) observed a stagnant upper distribution limit of *B. utilis* in Nepal Himalaya in the recent decades along with poor regeneration in spite of temperature warming in the area. This indicates that there are many factors that usually limit *B. utilis* to occupy their fundamental niche. Modelling alpine species that survives at a greater elevation than the treelines and studying their overlap for suitable habitats would provide inference on the high elevation species survival.

Detection of *B. utilis* dynamics in Himalaya using Light Detection and Ranging (LiDAR) technology are necessary for more detail evaluation of treeline dynamics measuring the tree height at the landscape scale in 3-dimension. Further research including variables representing the actual functional characteristics of vegetation like land surface phenology, leaf area index, net primary productivity and chlorophyll-*a* fluorescence will make the predictions more accurate in terms of realized niche. The inclusion of more abiotic and biotic variables will strengthen the model. The present evaluation of habitat

suitability in Himalaya at landscape scale would help in the development of management practices for species conservation in the high elevations.

The minimum temperature in the high elevation region is a most critical environmental factor responsible for the growth of vegetation (Gottfried et al., 2012; Gaire et al., 2014). In the major parts of the greater Hindu-Kush Himalaya, the annual mean air temperature has increased by 0.06 °C yr^{-1} from the year 1982 to 2006 (Shrestha et al., 2012). There is positive greening trend and lengthening of the growing season in the current warming scenario (Singh et al., 2018; Mohapatra et al., 2019b). The response of vegetation to warming around the treeline has been reported as increased forest density and increased radial and vertical growth rather than advancing of treeline forests (Payette and Filion, 1985; Kullman, 2007; Zhang et al., 2009).

Since the upward shift of treeline position was c. 10 m yr^{-1}, detecting elevational range shift of treeline in response to climate change every year at the resolution used here is not practical. In addition, the growth of trees requires a longer period, hence, observing yearly changes are not feasible. Usually, treeline changes as climate vary, and climatic changes occur in a long-term and not a year wise change. High spatial and temporal resolution data is needed for better understanding the treeline position dynamics in less than a decade time gap. Nonetheless, the changes at the treeline have occurred and it is significant in terms of numbers. Remote sensing based treeline position upward shift was higher than the shift observed in field studies. Other techniques like lichenometry and dendrochronology may substantiate and add new dimensions towards this element of alpine research. Advance remote sensing technology like LiDAR have potential of defining treeline physiognomy and microwave remote sensing may characterise the structural properties of treeline ecotone (Singh et al., 2015). The effects of slope and aspects on the upward shift of treeline in Himalaya should also be investigated in future. Studying the dynamics of snow line in Indian Himalaya coupled with the alpine treeline ecotone dynamics would provide more insight to climate change response of ecotone. This study provide the evidence of century scale dynamics of treeline ecotone in Himalaya at the landscape scale.

4. Conclusions

The study shows the dynamics of the alpine treeline ecotone in the Indian Himalaya from past status to future projection. Remote sensing of treeline ecotone in over a century scale study reveals that the treeline ecotone position in the Himalaya is sensitive to climatic variability, especially warming. The upward shift in the treeline is about 95 m decade^{-1} which is higher than reported in other countries and that is known through dendroclimatology and theoretical simulations. This also brings an important point of having the oldest baseline records while comparing with the recent observations. The positon of alpine treeline in Himalaya is temperature driven. Increase in the temperature (diurnal temperature ranges) is a major driver for the changes in treeline niche. There has been a niche shift of *B. utilis* to higher elevation regions in the

Indian Himalaya due to an increase in the pace of ongoing climate warming. Shift of tree species to the alpine pastures can cause the extinction of endemic herb and shrub species that dwell in the space and resource limiting mountain summits.

References

Allouche, O., A. Tsoar and R. Kadmon (2006). Assessing the accuracy of species distribution models: prevalence, kappa and the true skill statistics (TSS). Journal of Applied Ecology, 43, 1223-1232.

Anderson, J.H., K.T. Weber, B. Gokhale and F. Chen (2011). Intercalibration and evaluation of ResourceSat-1 and Landsat-5 NDVI. Canadian Journal of Remote Sensing, 37(2), 213-219.

Baek, H.J., J. Lee, H.S. Lee, et al. (2013). Climate change in the 21st century simulated by HadGEM2-AO under representative concentration pathways. Asia-Pacific Journal of Atmospheric Sciences, 49(5), 603-618.

Baker, B.B. and R.K. Moseley (2007). Advancing treeline and retreating glaciers: implications for conservation in Yunnan, P.R. China. Arctic, Antarctic, and Alpine Research, 39(2), 200-209.

Barbet-Massin, M., F. Jiguet, C.H. Albert and W. Thuiller (2012). Selecting pseudo-absences for species distribution models: how, where and how many? Methods in ecology and evolution, 3, 327-338.

Bobrowski, M., L. Gerlitz and U. Schickhoff (2017). Modelling the potential distribution of *Betulautilis* in the Himalaya. Global Ecology and Conservation, 11, 69-83.

Broennimann, O., V.D. Cola and A. Guisan (2018). ecospat: spatial ecology miscellaneous methods. R package version 3.0. https://CRAN.R-project.org/package=ecospat

Butler, D.R., G.P. Malanson, S.J. Walsh and D.B. Fagre (2009). The changing alpine treeline: the example of Glacier National Park, MT, USA. Developments in earth surface processes, 12. United Kingdom (UK): Elsevier.

Chander, G. and B. Markham (2003). Revised Landsat-5 TM radiometric calibration procedures and postcalibration dynamic ranges. IEEE Transactions on geoscience and remote sensing, 41(11), 2674-2677.

Chavez, P.S. Jr. (1988). An improved dark-object subtraction technique for atmospheric scattering correction of multispectral data. Remote sensing of Environment, 24(3), 459-479.

Dormann, C.F., J. Elith, S. Bacher, et al. (2013). Collinearity: A review of methods to deal with it and a simulation study evaluating their performance. Ecography, 36, 27-46.

Dubey B., R.R. Yadav, J. Singh and R. Chaturvedi (2003). Upward shift of Himalayan pine in Western Himalaya, India. Current Science 85(8): 1135-1136.

Dutta, P.K., B.K Dutta, A.K. Das and R.C. Sundriyal (2014). Alpine timberline research gap in Himalaya: A literature review. Indian Forester, 140(4), 419-427.

ESRI (2016). ArcGIS Desktop. Environmental Systems Research Institute. https://desktop.arcgis.com/en/arcmap

Fick, S.E. and R.J. Hijmans (2017). Worldclim 2: New 1-km spatial resolution climate surfaces for global land areas. International journal of climatology, 37, 4302-4315.

Field, C.B. and V.R. Barros (2014). Climate change 2014: Impacts, adaptation, and vulnerability. Part A: Global and sectoral aspects. Intergovernmental Panel on Climate Change (IPCC). USA: Cambridge University Press.

Fielding, A.H. and J.F. Bell (1997). A review of methods for the assessment of prediction errors in conservation presence/absence models. Environmental conservation, 24 (1), 38-49.

Fischer, G., F. Nachtergaele, S. Prieler, H.T. Van Velthuizen, L. Verelst and D. Wiberg (2008). Global agro-ecological zones assessment for agriculture (GAEZ 2008). IIASA, Laxenburg, Austria and FAO, Rome, Italy

Fissore, V., R. Motta, B. Palik and E.B. Mondino (2015). The role of spatial data and geomatic approaches in treeline mapping: A review of methods and limitations. European Journal of Remote Sensing. 48(1), 777-792.

Gaire, N.P., M. Koirala, D.R. Bhuju and H.P. Borgaonkar (2014). Treeline dynamics with climate change at the Central Nepal Himalaya. ClimPast 10: 1277-1290.

GBIF (2018). Global Biodiversity Information Facility. GBIF occurrence download. Accessed 05 November 2018

Gottfried, M., H. Pauli, A. Futschik, M. Akhalkatsi, P. Barančok, J.L.B. Alonso, G. Coldea, J. Dick, B. Erschbamer, M.R.F Calzado, et al. (2012). Continent-wide response of mountain vegetation to climate change. Nature climate change, 2, 111-115.

Grabherr, G., M. Gottfried and H. Pauli (1994). Climate effects on mountain plants. Nature 369, 448

Guillera- Arroita, G., J.J. Lahoz- Monfort, J. Elith, et al. (2015). Is my species distribution model fit for purpose? Matching data and models to applications. Global Ecology and Biogeography, 24, 276-292.

Guisan, A., W. Thuiller, N.E. Zimmermann, V.D. Cola, D. Georges and A. Psomas (2017). Habitat suitability and distribution models. Cambridge University Press: UK. https://doi.org/10.1017/9781139028271

Hamid, M., A.A. Khuroo, A.H. Malik, R. Ahmad, C.P. Singh, J. Dolezal and S.M. Haq (2020). Early Evidence of Shifts in Alpine Summit Vegetation: A Case Study from Kashmir Himalaya. Frontiers in Plant Science, 11:421. doi: 10.3389/fpls.2020.00421

Hijmans, R.J., S.E. Cameron, J.L. Parra, P.G. Jones and A. Jarvis (2005). Very high resolution interpolated climate surfaces for global land areas. International Journal of Climatology, 25, 1965-1978.

Hirzel, A.H., G. L. Lay, V. Helfer, C. Randin and A. Guisan (2006). Evaluating the ability of habitat suitability models to predict species presences. Ecological modelling, 199, 142-152.

IPCC (2013). Climate Change 2013: The Physical Science Basis. Contribution of Working Group I to the Fifth Assessment Report of the Intergovernmental Panel on Climate Change. Intergovernmental Panel on Climate Change. Stocker T.F., D. Qin, G.K. Plattner, M. Tignor, S.K. Allen, J. Boschung, A. Nauels, Y. Xia, V. Bex, P.M. Midgley (eds), Cambridge University Press, Cambridge, United Kingdom and New York, NY, USA, pp 1535.

Körner, C. (2012). Alpine treelines: Functional ecology of the global high elevation tree limits. Basel: Springer.

Kullman, L. (2007). Tree line population monitoring of *Pinussylvestris* in the Swedish Scandes, 1973-2005: Implications for tree line theory and climate change ecology. Journal of Ecology, 95(1), 41-52.

Kumar, P. (2012). Assessment of impact of climate change on Rhododendrons in Sikkim Himalayas using Maxent modelling: Limitations and challenges. Biodiversity and Conservation, 21(5), 1251-1266.

Lal, J.B., A.K. Gulati and M.S. Bist (1991). Satellite mapping of alpine pastures in the Himalayas. International Journal of Remote Sensing, 12(3), 435-443.

Liu, C., G. Newell and M. White (2016). On the selection of thresholds for predicting species occurrence with presence-only data. Ecology and evolution, 6(1), 337-348.

Matthew, M.W., S.M. Adler-Golden, A. Berk, S.C. Richtsmeier, R.Y. Levine, L.S. Bernstein, P. K. Acharya, G. P. Anderson, G. W. Felde, M.P. Hoke, et al. (2000). Status of atmospheric correction using a MODTRAN4-based algorithm. Proceedings of SPIE 4049, Algorithms for multispectral, hyperspectral, and ultraspectral imagery VI (199). doi: 10.1117/12.410341.

Mayor, J.R., N.J. Sanders, A.T. Classen, R. D. Bardgett, J.C. Clément, A. Fajardo, S. Lavorel, M. K. Sundqvist, M. Bahn, C. Chisholm, et al. (2017). Elevation alters ecosystem properties across temperate treelines globally. Nature, 542, 91-95.

Merow, C., M.J. Smith and J.A. Silander Jr. (2013). A practical guide to MaxEnt for modelling species' distributions: What it does, and why inputs and settings matter. Ecography 36: 1058-1069.

Mohapatra, J. (2015). The changing face of the alpine ecosystem in the Himalaya. ENVIS Newsletter Himayalan Ecology 12(2): 9. ISSN: 2277-9000

Mohapatra, J., C.P. Singh, M. Hamid, A. Verma, S.C. Semwal, B. Gajmer, A. A. Khuroo, A. Kumar, M.C. Nautiyal, N. Sharma and H.A. Pandya (2019a). Modelling *Betula utilis* distribution in response to climate-warming scenarios in Hindu-Kush Himalaya using random forest. Biodiversity and Conservation, https://doi.org/10.1007/s10531-019-01731-w

Mohapatra, J., C.P. Singh, O.P. Tripathi and H.A. Pandya (2019b). Remote sensing of alpine treeline ecotone dynamics and phenology in Arunachal Pradesh Himalaya. International Journal of Remote Sensing, https://doi.org/10.1080/01431161.2019.1608383.

Muralikrishnan, S., B. Narender, S. Reddy and A. Pillai (2011). Evaluation of Indian national DEM from Cartosat-1 data. India: Aerial Services and Digital Mapping Area, National Remote Sensing Centre, Hyderabad.

Naimi, B., N.A.S. Hamm, T.A. Groen, A K. Skidmore and A.G. Toxopeus (2014). Where is positional uncertainty a problem for species distribution modelling? Ecography 37: 191-203.

Panigrahy, S., D. Anitha, M.M. Kimothi and S.P. Singh (2010). Treeline change detection using topographic map and satellite imagery. Tropical Ecology.51(1): 87-91.

Paulsen, J. and C. Körner (2014). A Climate-Based Model to Predict Potential Treeline Position Around the Globe. Alpine Botany, 124, 1-12.

Payette, S. and L. Filion (1985). White spruce expansion at the tree line and recent climatic change. Canadian Journal of Forest Research, 15(1), 241-251.

R Core Team (2018). R: A language and environment for statistical computing. R Foundation for Statistical Computing, Vienna, Austria. https://www.R-project.org/

Rawat, G.S. and S. Tambe (2011). Sikkim Himalaya: Unique features of biogeography and ecology. In: Arrawati ML, Tambe S, editors. Biodiversity of Sikkim: Exploring and conserving a global hotspot. India: Information and Public Relation Department, Government of Sikkim, p. 1-13.

Schickhoff, U., M. Bobrowski, J. Böhner, B. Bürzle, R.P. Chaudhary, L. Gerlitz, H. Heyken, J. Lange, M. Müller, T. Scholten, et al (2015). Do Himalayan treelines respond to recent climate change? An evaluation of sensitivity indicators. Earth System Dynamics, 6, 245-265.

Shrestha, U.B., S. Gautam and K.S. Bawa (2012). Widespread climate change in the Himalayas and associated changes in local ecosystems. PLoSONE 7(5): e36741. doi:10.1371/journal.pone.0036741

Singh, C.P. (2015). Long-term monitoring of alpines of the Himalaya. ENVIS Newsletter Himayalan Ecology 12(2):1-3. ISSN: 2277-9000.

Singh, C.P., J. Mohapatra, H.A. Pandya, B. Gajmer, N. Sharma, and D.G. Shrestha (2018). Evaluating changes in treeline position and land surface phenology in Sikkim Himalaya. Geocarto International, https://doi.org/10.1080/10106049.2018.1524513

Singh, C.P., S. Panigrahy, A. Thapliyal, M.M. Kimothi, P. Soni and J.S. Parihar (2012). Monitoring the alpine treeline shift in parts of the Indian Himalayas using remote sensing. Current Science. 102(4): 559-562.

Singh, C.P, S. Panigrahy, J.S. Parihar, and N. Dharaiya (2013). Modelling environmental niche of Himalayan Birch and remote sensing based vicarious validation. Tropical Ecology. 54 (3): 321-329.

Singh, C.P., J. Mohapatra and N. Dharaiya. (2015). Remote sensing of alpine treeline dynamics. Indian Society of Geomatics Newsletter. 21(4): 3-8. ISSN: 0972-642X.

Singh, C.P., S. Panigrahy and J.S. Parihar (2011) Alpine vegetation ecotone dynamics in Gangotri catchment using remote sensing techniques. International Archives of the Photogrammetry, Remote Sensing and Spatial Information Sciences, XXXVIII-8/W20: 162-169.

SFR (2015). India state of forest report. India: Forest Survey of India, Ministry of Environment, Forest and Climate Change, Government of India. State of Forest Report (India). ISBN: 97881929285-2-4.

Steven, M.D., T.J. Malthus, F. Baret, H. Xu and M.J. Chopping (2003). Intercalibration of vegetation indices from different sensor systems. Remote Sensing of Environment, 88, 412-422.

Taylor, J.R. (1997). An introduction to error analysis: The study of uncertainties in physical measurements. 2nd ed. California (US): University Science Books; p. 45-79.

Thuiller, W., D. Georges, R. Engler and F. Breiner (2016). biomod2: Ensemble Platform for Species Distribution Modeling. R package version 3.3-7. https://CRAN.R-project.org/package=biomod2

USGS (2006). Shuttle Radar Topography Mission, 30 Arc Second, Global Land Cover Facility, University of Maryland, College Park, Maryland. United States Geological Survey, February 2000. United States Geological Survey.

Walther, G.R., S. Beißner and C.A. Burga (2005). Trends in the upward shift of alpine plants. Journal of Vegetation Science, 16, 541-548.

Wheaton, J.M., J. Brasington, S.E. Darby and D.A. Sear (2010). Accounting for uncertainty in DEMs from repeat topographic surveys: Improved sediment budgets. Earth Surf Proc Land. 35: 136-156.

Zhang, Y., M. Xu, J. Adams and X. Wang (2009). Can Landsat imagery detect tree line dynamics? International Journal of Remote Sensing, 30(5), 1327-1340.

Fog characteristics and it's inter annual variability over the Indo-Gangetic Plains during the winter season using satellite data

S.H. Arun[*1,2], Sasmita Chaurasia[1], Atul Kumar Varma[1] and Raj Kumar[3]

[1] EPSA Space Applications Centre, ISRO, Jodhpur Tekra, Ahmedabad- 380 015, Gujarat, India
[2] Department of Physics, Gujarat University, Navrangpura, Ahmedabad- 380 009, Gujarat, India
[3] National Remote Sensing Centre, ISRO, Hyderabad- 500 037, Telangana, India
*Email: arunshphysics05@gmail.com

Abstract: A study on the fog characteristics over the Indo-Gangetic Plains (IGP) during the winter season from 2013 to 2018 have been performed using Indian National Satellite (INSAT-3D) data. Based on the present study, it is observed that the mean monthly frequency of fog is maximum in January followed by December in all the study regions over the IGP. This study brings out different fog prone zones over IGP region (i.e. Low, Medium and High) based on the number of foggy days. In order to study the uncertain pattern of fog in the past winter seasons, a time series analysis has been carried out. The results of the present study such as the inter annual variability and mean monthly frequency of fog, classification of fog prone areas, inter winter seasonal comparisons etc. can be used to better understand the nature of fog over the IGP. Further, this understanding can be used to better predict fog occurrence in future now casting/forecasting applications.

Keywords: Fog, INSAT-3D, Indo-Gangetic Plains, Satellite data, winter season

1. Introduction

Every year, fog routinely develops in the Indo-Gangetic Plains (IGP) during the winter period (November-February). These fog episodes have several disruptions on human activities as well as have an impact on agriculture, general economy, global and regional climate (Badarinath et al., 2009). Reduced visibility associated with the fog period is a major hazard to land, marine and aviation transportation. Numerous accidents have been reported in different parts of the IGP during the peak winter months in 2014 and 2015, claiming life of 69 people distinctly shows the effect of fog on human life and daily activities (Srivastava et al., 2016). Flight cancellation, diversion or delay for hours are common scenarios at various airports of India during the foggy days. A total of 653 hours of dense fog during the winter period from 2011 to 2016 at Indira Gandhi International (IGI) Airport caused an economic loss of approximately 3.9 million USD to the airlines (Kulkarni et al., 2019). The socio-economic loss due to fog is comparable with that of hurricanes, tornadoes, storms, floods and droughts (De et al., 2005; Gultepe et al., 2007). In order to reduce the socio-economic loss as well as to ease disruptions on human life, an improved understanding of fog specifically its formation, spatial extent and dissipation time is needed to be studied in detail.

IGP have extensive dense fog conditions in every winter in which radiation and advection fog are the most common types. It can form in various temporal and spatial scales depending upon the local meteorological conditions and synoptic scale weather systems (Syed et al., 2012; Ghude et al., 2017). The basic requirement of radiation fog to form are temperature inversion, high relative humidity, clear skies and calm winds. IGP experiences minimum surface air temperature and maximum mean sea level pressure during winter season which is an indication of low winds and clear sky conditions. In addition, geographical characteristics, topography and meteorological conditions

play a crucial role on the evolution of fog. The terrestrial structure of IGP consists of low elevation, gradual sloping surfaces of the Indus, the presence of Himalayan ranges, low wind speed and Ganges river basin which are favourable for the prolonged dense fog during the winter season. Several studies have been attempted to investigate the role of natural phenomena and anthropogenic activities on fog formation over the IGP. Western disturbances, an extra tropical storm having large moisture content and cold wave condition are considered to be the major reason for the widespread fog over the IGP (Dimri et al., 2006). Agricultural crop residue which is burned in the Punjab region before the winter season is also considered to be a major contributing factor for fog formation over the IGP (Badarinath et al., 2006; Sharma et al., 2010). Moreover, higher concentration of aerosols in the lower atmosphere contributed by the thermal power plants and air pollution enhances the fog formation over the IGP (Prasad et al., 2006; Badarinath et al., 2007; Jenamani 2007; Nair et al., 2007). Since, many meteorological conditions such as minimum surface air temperature, large moisture content, low wind speed etc. for fog formation are extremely available along with the favourable geographical conditions, IGP is always considered as a prominent region for the fog study.

Fog studies using ground based observations, model and satellite remote sensing have taken place since many years (Ellrod 1995; Teixeira 1999; Bhushan et al., 2003; Underwood et al., 2004; Singh et al., 2007; Chaurasia et al., 2011; Chaurasia et al., 2015; Arun et al., 2018). Simulation of Brightness Temperature Difference (BTD) using two different spectral channels (3.9µm and 10.8 µm) has been used for the nighttime fog detection (Ellrod et al., 1995; Chaurasia et al., 2011). However, BTD technique is not suitable for daytime due to the solar contamination in the MWIR channel which leads to wrong estimation of fog. For the daytime fog analysis, temporal differencing technique and spatial homogeneity test have been

performed (Chaurasia et al., 2015). This technique is fit for any geostationary satellite having visible and thermal infrared channel. Fog detection is made using visible channel whereas thermal infrared channel is used for the elimination of medium/high level clouds and snow. Later, a single algorithm using BTD between 3.9 μm and 10.8 μm has been introduced for both day and nighttime analysis of fog (Chaurasia et al., 2017). In order to reduce the false detection of fog in daytime, spatial homogeneity test has been performed. In addition, thermal infrared, water vapor and visible channel spectral information have been used for better estimation of fog. The results have been validated with the visibility data over various airports in the IGP. All these techniques are found to be suitable for fog detection throughout the day without any spatial and temporal discontinuity with an acceptable false alarm rate. However, certain drawbacks have been observed in these methods. These techniques are not able to detect fog beneath the high clouds as well as not able to differentiate fog from low clouds (Chaurasia et al., 2017). However, the effect of these meteorological parameters has not been researched extensively in the existing techniques. Use of *in-situ* and satellite sounder observations having temperature and humidity profiles of the atmosphere together with surface wind conditions from model observations are more suitable for detection of fog (Wantuch 2001; Song et al., 2013; Arun et al., 2018).

Even though all these studies are able to detect the fog conditions, some difficulties such as the complexity involved in the mechanism of fog formation, its evolution, spatial-temporal variability and dissipation etc. still remain as an open challenge. An accurate and timely forecasting of fog is an essential factor in fog study which can play a significant role in land, marine and aviation sector as well as in agriculture production and public health. The existing fog forecasting system over the IGP is mainly composed of traditional synoptic methods and numerical models (Bhowmik et al., 2004; Ghude et al., 2017). However, prediction of exact characteristics of fog which consist of its time of evolution, intensity, spatial variability, visibility conditions etc. are still a challenging task. To overcome these difficulties, more research work such as fog climatology, trend analysis etc. needs to be done to study the complexity of fog mechanism over the IGP. Several attempts have been made to study the climatological characteristics of fog worldwide during the past years (Meyer and Lala 1990, Tardif and Rasmussen 2007, Cermak et al., 2009). Fog data during the period 1949-1990 over Southern Germany have been investigated (Sachweh and Koepke 1995). In their study, a relation between urban building density and fog frequency has been estimated. An increase in urban building density result in the urban heat island and moisture deficiency which leads to reduction in number of fog days. Teixeira (1999) analysed the mechanism and dissipation of radiation fog using ECMWF model and compared with the climatological data. Moreover, a comparison between the observed and simulated visibility confirmed that the evolution of fog is properly simulated. A 10-year fog climatology over Germany using NOAA-AVHRR data has been presented (Bendix 2002). Maximum and minimum fog frequency along with fog persistence has

been estimated using day and nighttime fog maps. The cloud microphysical parameters such as fog optical depth, cloud effective radius, liquid water content have been computed. The typical features of advection fog are obtained in the coastal regions whereas characteristics of radiation fog have been identified over land area. The variability of meteorological parameters such as surface temperature, relative humidity and wind speed over the IGP has been analysed during the winter season from 1971-2010 (Sawaisarje et al., 2014). The study reported that, over the IGP, surface temperature ranges from 9°C to 15°C, relative humidity varies from 72% to 84% and average wind speed is 0.6 m/s at 03:00 UTC. The long term (1971-2015) characteristics of winter fog in terms of its trend and spatial-temporal variability over the IGP have been investigated by Srivastava et al., 2016 using ground based observations of India Meteorological Department (IMD). An alarming rise in fog frequency was observed over the IGP during the peak winter months of December and January in the past four decades. The study also analysed the average daily persistence of fog over various locations in the IGP which is important to reduce the negative impact of fog on day to day activities. However, monitoring the spatial extent and time period of fog in large scale is a difficult task using the conventional and ground based measurements. In order to analyze the fog climatology in a large spatial extent, satellite observations play a vital role due to its improved spatial, spectral and temporal resolutions. Therefore, a satellite based inter annual variability of fog over the IGP has been investigated in the present study during the winter period from 2013-2018.The monthly frequency of fog, fog prone area classification, time series analysis and inter annual variability of fog over the IGP have been discussed in the present study.

2. Data used

The INSAT-3D is an advanced geostationary weather satellite configured with an improved imaging system and atmospheric sounder, which is operational since July 2013. INSAT-3D carries four payloads i.e. six channel multi-spectral imager, nineteen channel sounder, Data Relay Transponder and Search and Rescue Transponder. INSAT-3D is capable of generating the images of the Earth in six wavelength bands i.e. Visible (VIS), Short Wave Infra-Red (SWIR), Mid Wave Infra-Red (MWIR), Water Vapor (WV), Thermal Infra-Red 1 (TIR1) and Thermal Infra-Red 2 (TIR2). INSAT-3D imager channel specifications are listed in Table 1 (INSAT-3D Algorithm Theoretical Basis Development Document, ATBD 2015). The INSAT-3D imager fog product having a spatial resolution of 4 km and temporal resolution of 30 minutes has been used. This fog product is being generated using the INSAT-3D TIR1 (10.8 μm) and MWIR (3.9 μm) channel data for nighttime and TIR1 (10.8 μm) and visible (0.5-0.7 μm) channel for daytime (Fog product, INSAT-3D ATBD 2015, www.mosdac.gov.in). Fog detection in presence of higher clouds and distinguish in between fog and low clouds are still remains as an open challenge.

3. Study region

The inter annual variability of fog has been carried out during the period from 2013 to 2018 over six different states i.e. Punjab, Haryana, Delhi, Uttar Pradesh, Bihar and West Bengal in the IGP which are mostly dense fog conditions in every winter (November to February). Figure 1 represents the study area.

Table 1. Channel specifications of the INSAT-3D/3DR imager (Source: INSAT-3D ATBD document, May 2015)

Channel Number	Channel	Wavelength (μm)	Spatial Resolution (km)
1	VIS	0.5-0.7	1.0
2	SWIR	1.5-1.7	1.0
3	MWIR	3.8-4.0	4.0
4	WV	6.5-7.1	8.0
5	TIR 1	10.2-11.3	4.0
6	TIR 2	11.5-12.5	4.0

4. Methodology

In order to have a better understanding of fog characteristics over the IGP, the entire period of study has been classified into five winter periods (i.e. 2013-14, 2014-15, 2015-16, 2016-17 and 2017-18). Since, the present study has been carried out in a larger spatial scale, a day is considered as a foggy one only if a minimum of 10% area of the state is covered with fog at least once in a day. The study has been divided into three major parts i.e. monthly frequency of fog, classification of fog prone areas in the IGP and inter annual variability of fog based on time series analysis, which is shown in Figure 2. In the first part, monthly frequency of fog has been estimated for the months of November, December, January and February based on the number of fog days over all the states, which is calculated as follows.

$$\text{Mean frequency of fog (\%)} = \frac{\text{Total number of fog days}}{\text{Total number of days}} * 100 \quad \text{......................}(1)$$

From the results obtained from equation 1, the number of fog days for each month is calculated as below

Monthly frequency of fog (days)= (Mean Frequency of fog X Number of days in a month)/ 100……………………………………………...(2)

For example, the total number of fog days over Punjab for the month of December during the period from 2013-2018 is 97. The corresponding total number of days observed to be 155. From equation 1, the frequency of fog has been estimated to be 62.58 %. By using this information, the monthly frequency of fog in days for the month of December can be estimated from the equation 2, i.e. 19.39 that is nearly 19.
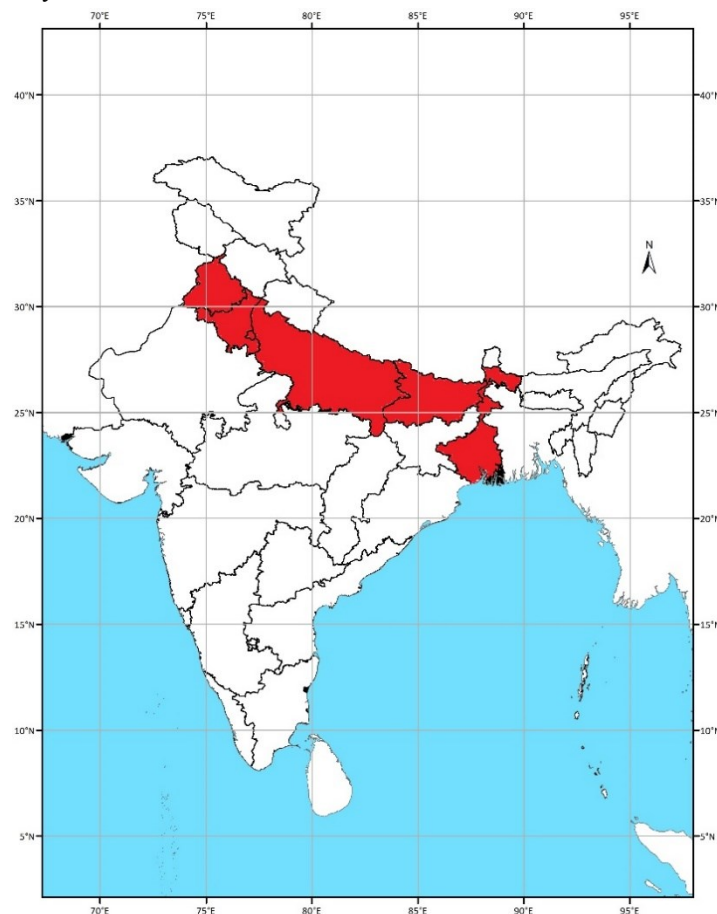

Figure 1. The study region (i.e. Punjab, Haryana, Delhi, Uttar Pradesh, Bihar and West Bengal) is indicated in red color.
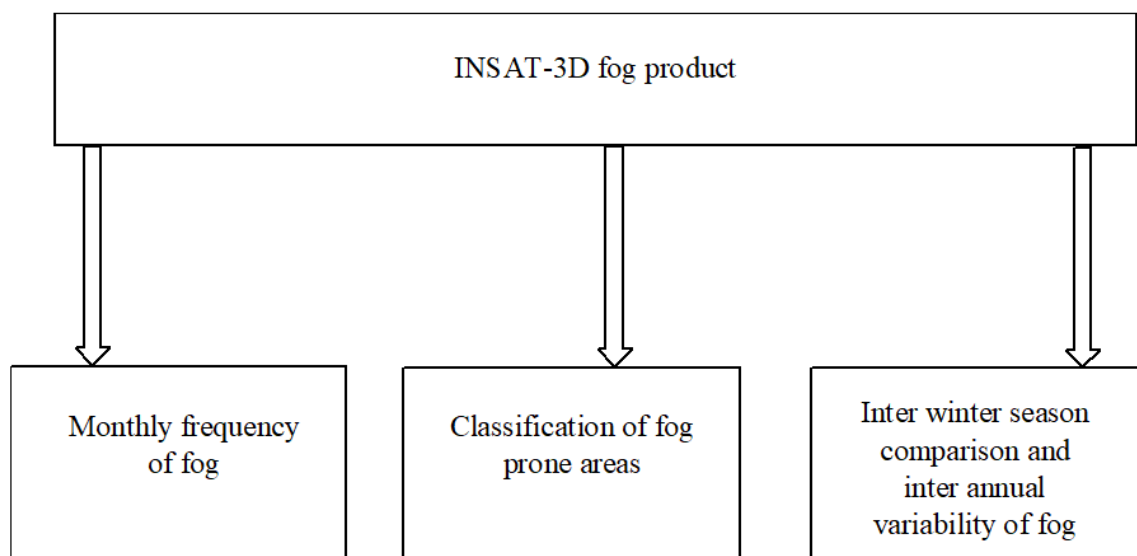
Figure 2. Flowchart of the general methodology

In the second part, the IGP has been classified into three major zones i.e. high, moderate and low fog prone areas based on satellite observations. The classification has been done on the basis of number of fog days in the months of December and January during the period from 2013 to 2018. The region is identified as high fog prone zone, if the number of fog days over that region is more than two thirds of the total number of days (Srivastava et al., 2016). Similarly, Moderate fog prone zone has been classified as the region in which the number of fog days is in between one-third to two-thirds of the total number of days (Srivastava et al., 2016). When the number of fog days lies below one-third of the total number of days, the region is classified as low fog prone zone, i.e. regions were identified based on the criteria adopted by Srivastava et al., 2016. The general methodology of fog prone area classification is shown in Figure 3.

In the final part, time series analysis based on the number of fog days has been performed for inter seasonal comparison of fog for each states during the winter season from 2013 to 2018. Moreover, inter winter seasonal

comparison study can provide a clear scenario of fog occurrence over the IGP in each season. In addition, month wise variability of fog has also been studied in detail by estimating the percentage increase/decrease in fog in comparison to previous winter seasons.

5. Results and discussions
The study has been carried out during the winter period (November to February) of 2013-2018 over six states in the IGP, which are severely affected by fog conditions every year (Table 2). The study period has been divided into five winter seasons (2013-14, 2014-15, 2015-16, 2016-17 and 2017-18) for a better understanding of fog characteristics over various locations in different winter seasons. The detailed analysis is as follows.

5.1 Monthly frequency of fog
The monthly frequency of fog over various regions in the IGP on a monthly basis is illustrated in Figure 4 (a-d). IGP experiences severe fog conditions during the period from December to January.
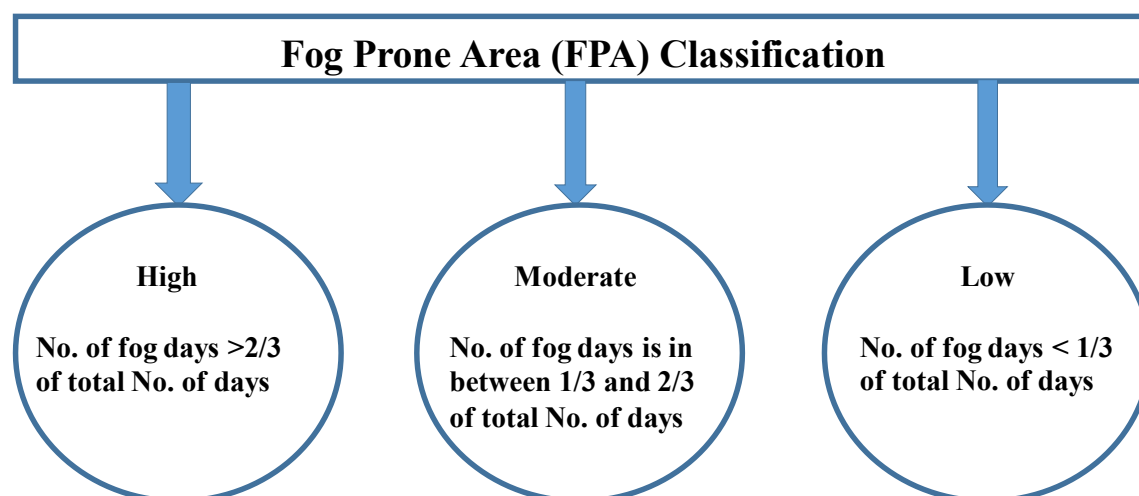
Figure 3. The general methodology for the classification of fog prone areas in the IGP (classification strategy adopted from Srivastava et al., 2016.)

Table 2. Monthly fog frequency over various states over the IGP during the winter season from 2013-2018

State	Month			
	November	December	January	February
Punjab	11	19	20	08
Haryana	13	20	23	09
Delhi	9	17	18	08
Uttar Pradesh	11	23	26	09
Bihar	10	23	26	11
West Bengal	08	18	19	12

The winter fog study over all the regions during the period from 2013 to 2018 revealed that the average frequency of fog is maximum in the month of January (22 days) followed by December (20 days). The average frequency of fog is observed to be less in both November and February (10 days). It has been observed that the monthly frequency of fog over Uttar Pradesh and Bihar is the highest (26) among all the states which is followed by Haryana (23) in the month of January. The corresponding number of fog days over Punjab, Delhi and West Bengal have been observed to be 20, 18 and 19 respectively. Moreover, in the month of December, the fog frequency has been observed to be the maximum (23) in Uttar Pradesh and Bihar region whereas the minimum (17) has been observed over the Delhi region.

Figure 4. Monthly frequency of fog over different regions in the IGP during the winter period from 2013 to 2018 on (a) November, (b) December, (c) January and (d) February.

The regions in the North-Western parts of India, i.e. Punjab, Haryana, Delhi and UP observed to have more number of fog days in November in comparison t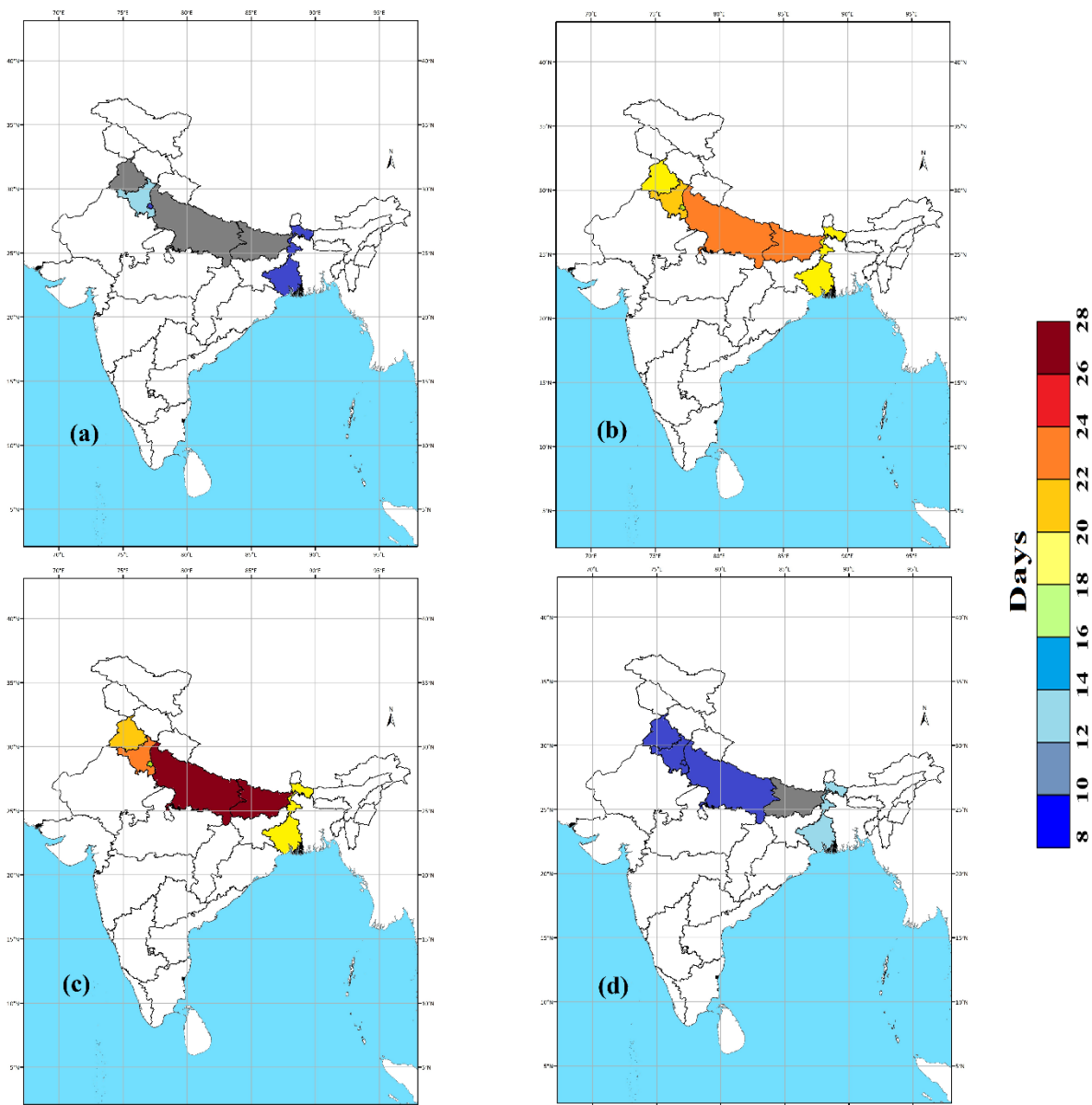o February (Table 3). The Eastern parts of India (Bihar and West Bengal) experiences more number of fog days in February than November. The increase in the number of fog days in November than February over the North-Western parts could be due to the aerosol loading by the agricultural crop burning in the Punjab region. As the fog season progresses, these aerosols have been transported to the Central and Western parts of India where they are trapped due to the presence of the Himalayan ranges. The long range transport of aerosols could be the reason for an increase in fog days in the Eastern parts of India during the month of February than November. Western disturbances which brings mild to heavy rainfall along with cold wave conditions over the IGP also enhances the aerosol transportation from Western to Eastern regions.

5.2 Classification of fog prone areas over the IGP

The fog prone areas over the IGP are classified into three major zones based on the satellite observations. The classification is done on the basis of number of fog days in the months of December and January during the period from 2013 to 2018. The number of fog days over the study regions in December and January during the period from 2013 to 2018 are shown in Figure 5 (a-b).

From the analysis, it can be seen that UP, Haryana and Bihar have number of fog days greater than two-thirds of the total number of days during the period of study and can be considered as high fog prone zone.

Table 3. Number of fog days over various states over the IGP during the months of December and January during the winter period from 2013 to 2018

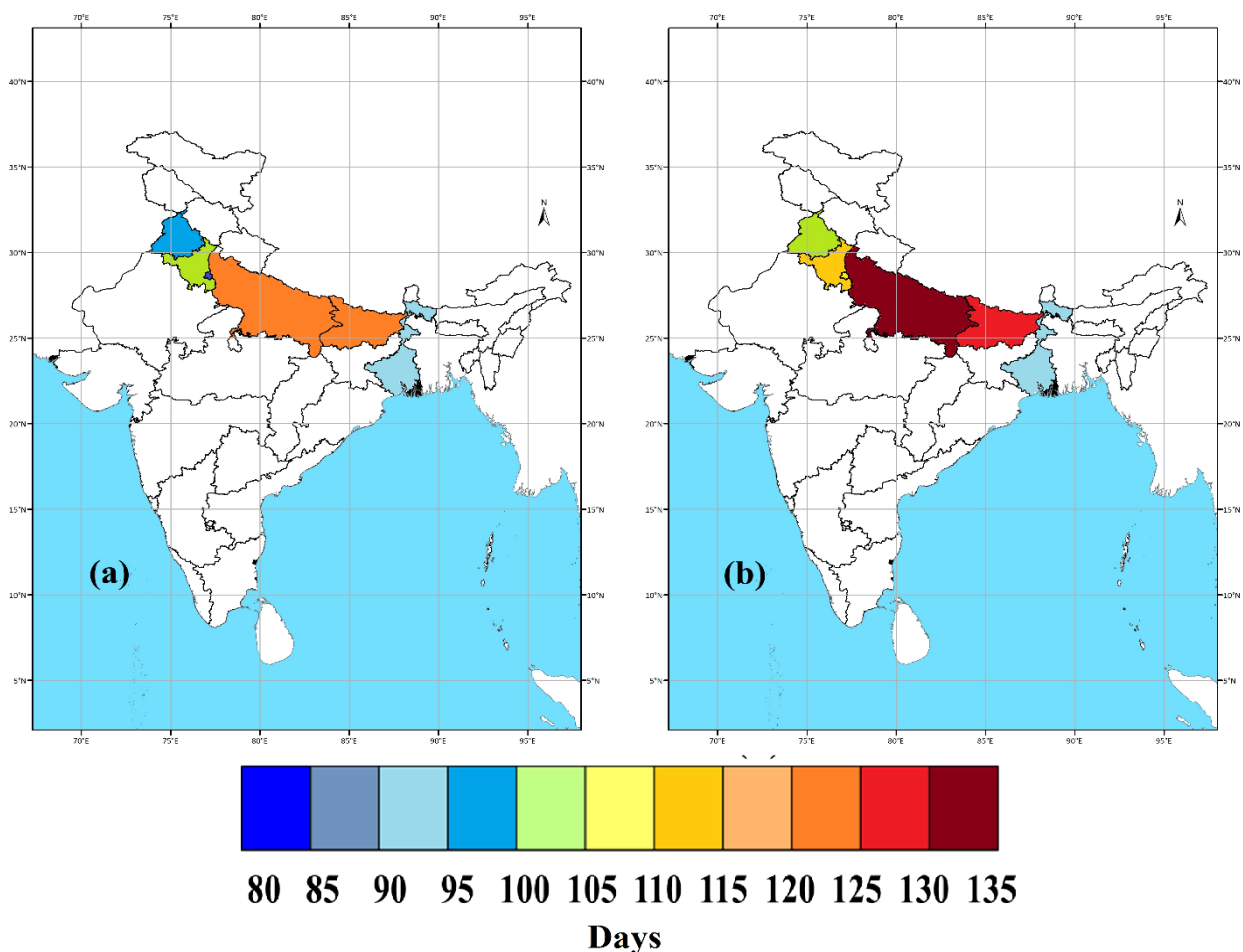| State	Month	
	December	January
Punjab	97	102
Haryana	100	114
Delhi	83	105
Uttar Pradesh	116	132
Bihar	117	128
West Bengal	90	93

Figure 5. Number of fog days in (a) December and (b) January over different regions in the IGP during the winter period from 2013 to 2018.

Out of the 310 days (sum of the number of days of December and January from 2013-2018), UP observed to have 238 fog days (76.77%). The corresponding number of fog days for Haryana and Bihar have been observed to be 214 (69.03%) and 245 (79.03%) respectively. The remaining regions i.e. Punjab (64.19%), Delhi (60.65%) and West Bengal (59.03%) are classified as moderate fog prone zones based on the number of fog days during the winter months of December and January. The analysis also reveals that there is an increase in the number of fog days in January compared to December over all the study region. It has been observed that Delhi has maximum increase in number of fog days (22 days i.e. 14.20%) in January compared to December whereas WB observed to have minimum increase in number of fog days (3 days i.e. 1.94%). The remaining regions i.e. Punjab, Haryana, UP and Bihar observed to have an increase of 3.22%, 9.04%, 10.32% and 7.10% respectively in fog days in January compared to December.

5.3 Inter winter seasons comparison and inter annual variability of fog over the IGP
In order to study the uncertain patterns of fog in the past winter seasons, time series analysis carried out in the recent five winter season from 2013 to 2018 is shown in

Figure 6 (a-e). Time series analysis has been performed on the fog data for the months of November to February during the period from 2013 to 2018.

It has been observed that 2016-17 winter experienced peak fog period with a maximum number of fog days (i.e. 498 (sum of foggy days over all the study regions)). 2013-14 winter observed to have least number of fog days (255) followed by 2015-16 winter (301 days). However, 2014-15 and 2017-18 winter observed to have moderate number of fog days (396 and 427 respectively). From Figure 5 (a-e), it can be observed that a usual fog pattern is repeated in every winter from 2013-14 to 2017-18. An increase of 141 fog days has been observed in 2014-15 winter season compared to 2013-14. A decrease of 95 fog days has been noticed in 2015-16 in comparison to its previous season i.e. 2014-15. The winter season 2016-17 witnessed maximum fog episodes among all the seasons and shown an increase of 197 fog days compared to 2015-16 winter season. The 2017-18 winter season observed to have a decrease in the number of fog days (i.e. 71) in comparison to 2016-17 winter season. Over all, an alternate increase and decrease in the number of fog days in winter season have been clearly identified over all the regions during the period from 2013 to 2018.
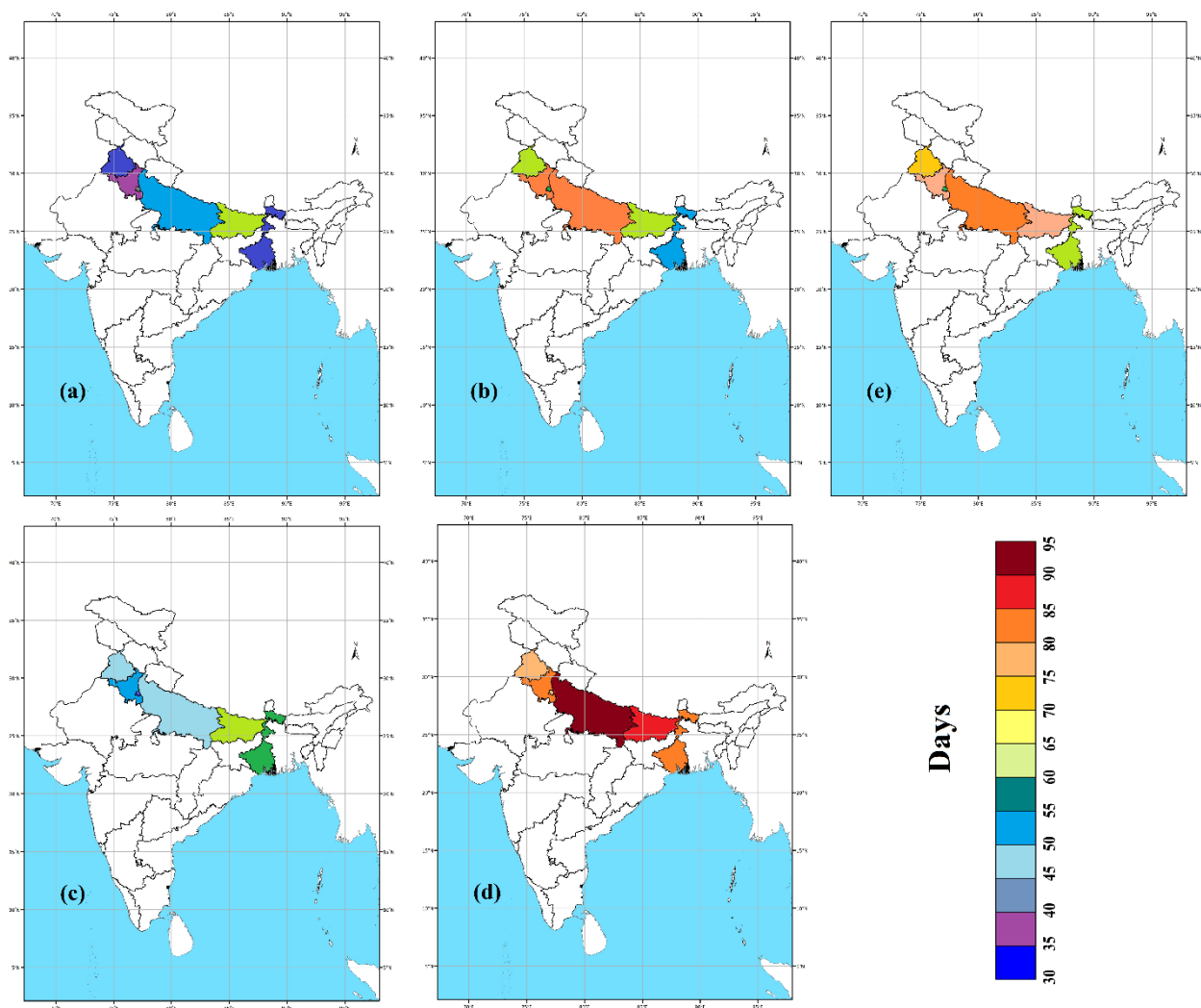

Figure 6. Number of fog days (November-February) during the winter season (a) 2013-14, (b) 2014-15, (c) 2015-16, (d) 2016-17 and (e) 2017-18 over different regions in the IGP

Table 4. Inter annual variability of fog over different winter periods over the IGP from 2013-14 to 2017-18.

Month	Fog (%)				
	2013-14	2014-15	2015-16	2016-17	2017-18
November	7.22	19.44	21.66	68.89	55.00
December	33.87	73.11	37.09	93.01	87.09
January	65.59	82.79	55.91	83.33	74.73
February	33.93	41.07	51.14	27.38	16.07

Table 5. Time series analysis of winter fog (November-February) during the winter season from 2013 to 2018 over different regions in the IGP

State	Winter Season				
	2013-14	2014-15	2015-16	2016-17	2017-18
Punjab	33	65	46	77	74
Haryana	38	77	54	83	76
Delhi	42	59	34	77	60
Uttar Pradesh	52	77	46	93	82
Bihar	60	65	62	87	74
West Bengal	30	53	59	81	61

Inter annual variability of fog has also been studied in detail which is shown in Table 4. In all the months, fog frequency has increased significantly in 2014-15 and 2016-17 in comparison to its previous winter season (i.e. 2013-14 and 2015-16 respectively). During the month of November, fog frequency has increased gradually till 2016-17 winter season and thereafter shown a decrease by 13.89% in 2017-18 winter season. However, in the case of February, fog frequency has shown an increasing trend till 2015-16 winter season followed by a decrease of 23.76% in 2016-17 and 11.31% in 2017-18 winter season. Moreover, during the peak period of fog i.e. December and January, fog frequency has been noticed to show an alternate increase and decrease in comparison to its previous winter season observations. In 2014-15 winter season, an increase of 39.24% and 17.2% has been observed on December and January respectively as compared to 2013-14 winter season whereas the increase in percentage were noticed to be 55.92 and 27.42 in 2016-17 season in comparison to 2015-16 winter season. However, in both 2015-16 and 2017-18 winter season, a decrease in fog frequency on December and January have also been identified. In 2015-16 winter season, decrease in fog frequency has been observed to be 36.02% and 26.88% respectively whereas the decrease in fog frequency in 2017-18 winter season has been observed to be less (8.6% and 11.31%).

6. Conclusions

The present work analysed the fog characteristics over the IGP using INSAT-3D fog product during the winter period from 2013 to 2018. The monthly fog frequency has been observed to be maximum in January followed by December in all the study regions over the IGP. The North-Western parts of IGP have shown more number of fog days in November compared to February whereas the Central-Eastern parts of IGP have shown a reverse characteristic. The fog prone areas in the IGP have been classified into three major zones based on the satellite observations. Based on the number of fog days, UP (76.77%), Haryana (69.03%) and Bihar (79.03%) are classified as high fog prone area whereas Punjab (64.19%), Delhi (60.65%) and West Bengal (59.03%) are listed as moderate fog prone area. Time series analysis has been performed to identify the general trends in the fog characteristics in different winter seasons (Table 5). Maximum number of fog days has been observed in the 2016-17 winter season whereas 2013-14 winter season observed to have minimum number of fog days followed by 2015-16 winter season. Moderate number of fog days has been observed in the 2014-15. Finally, inter annual variability of fog has been discussed on a monthly basis which can provide a better estimation about the increase/decrease in fog percentage during the winter seasons from 2013 to 2018. In all the months, fog frequency has increased significantly in 2014-15 and 2016-2017 winter season as compared to its previous winter seasons i.e. 2013-14 and 2015-16 respectively. The results of the present study can be used for further fog now-casting/ fore-casting purposes.

References

Algorithm Theoretical Basis Development Document INSAT-3D, May 2015.

Arun, S. H., S. K. Sharma, S. Chaurasia, R. Vaishnav and R. Kumar (2018). Fog/low clouds detection over the Delhi Earth Station using the Ceilometer and the INSAT-3D/3DR satellite data. International Journal of Remote Sensing, 39(12), 4130-4144.

Arun, S. H., S. Chaurasia, A. Misra and R. Kumar (2018). Fog Stability Index: A novel technique for fog/low clouds detection using multi-satellites data over the Indo-Gangetic plains during winter season. International Journal of Remote Sensing, 39(22), 8200-8218.

Badarinath, K. V. S., T. K.Chand and V. K. Prasad (2006). Agriculture crop residue burning in the Indo-Gangetic Plains–a study using IRS-P6 AWiFS satellite data. Current Science, 1085-1089.

Badarinath, K. V. S., K. M. Latha, T. K. Chand, R. R. Reddy, K. R. Gopal, L. S. S Reddy and K. R. Kumar, (2007). Black carbon aerosols and gaseous pollutants in an urban area in North India during a fog period. Atmospheric research, 85(2), 209-216.

Badarinath, K. V. S., S. K. Kharol, A. R. Sharma and P. S. Roy, (2009). Fog over Indo-Gangetic plains—a study using multisatellite data and ground observations. IEEE Journal of Selected Topics in Applied Earth Observations and Remote Sensing, 2(3), 185-195.

Bendix, J. (2002). A satellite-based climatology of fog and low-level stratus in Germany and adjacent areas. Atmospheric Research, 64(1-4), 3-18.

Bhowmik, S. K. R., A. M. Sud, and C. Singh (2004). Forecasting fog over Delhi-An objective method. Mausam, 55(2), 313-322.

Bhushan, B., H. K. N. Trivedi, R.C. Bhatia, R.K. Dube, R. K. Giri, and R. S. Negi (2003). On the persistence of fog over northern parts of India. Mausam, 54(4), 851-860.

Cermak, J., R. M. Eastman, J. Bendix and S. G. Warren (2009). European climatology of fog and low stratus based on geostationary satellite observations. Quarterly Journal of the Royal Meteorological Society: A journal of the atmospheric sciences, applied meteorology and physical oceanography, 135(645), 2125-2130.

Chaurasia, S., V. Sathiyamoorthy, S. B. Paul, B. Simon, P. C. Joshi, and P. K. Pal (2011). Night time fog detection using MODIS data over Northern India. Meteorological Applications, 18(4), 483-494.

Chaurasia, S., and B. S. Gohil, (2015). Detection of day time fog over India using INSAT-3D data. IEEE Journal of Selected Topics in Applied Earth Observations and Remote Sensing, 8(9), 4524-4530.

Chaurasia, S., and R. K. Jenamani (2017). Detection of fog using temporally consistent algorithm with INSAT-3D imager data over India. IEEE Journal of Selected Topics in Applied Earth Observations and Remote Sensing, 10(12), 5307-5313.

De, U. S., R. K. Dube and G. P. Rao (2005). Extreme weather events over India in the last 100 years. J. Ind. Geophys. Union, 9(3), 173-187.

Dimri, A. P., U. C. Mohanty, M. Azadi and L. S. Rathore (2006). Numerical study of western disturbances over western Himalayas using mesoscale model. Mausam, 57(4), 579.

Ellrod, G. P. (1995). Advances in the detection and analysis of fog at night using GOES multispectral infrared imagery. Weather and Forecasting, 10(3), 606-619.

Ghude, S. D., G. S. Bhat, T. Prabhakaran, R.K. Jenamani, D.M. Chate, P.D. Safai and M. Rajeevan (2017). Winter fog experiment over the Indo-Gangetic plains of India. Current Science, 767-784.

Gultepe, I., R. Tardif, S.C. Michaelides, J. Cermak, A. Bott, J. Bendix and S. G. Cober (2007). Fog research: A review of past achievements and future perspectives. Pure and applied geophysics, 164(6), 1121-1159.

Jenamani, R. K. (2007). Alarming rise in fog and pollution causing a fall in maximum temperature over Delhi. Current Science, 314-322.

Kulkarni, R., R. K. Jenamani, P. Pithani, M. Konwar, N. Nigam and S. D. Ghude (2019). Loss to aviation economy due to winter fog in New Delhi during the winter of 2011–2016. Atmosphere, 10(4), 198.

Meyer, M. B., and G. G. Lala (1990). Climatological aspects of radiation fog occurrence at Albany, New York. Journal of Climate, 3(5), 577-586.

Nair, V. S., K. K. Moorthy, D. P. Alappattu, P. K. Kunhikrishnan, S. George, P.R. Nair and R. R. Reddy (2007). Wintertime aerosol characteristics over the Indo-Gangetic Plain (IGP): Impacts of local boundary layer processes and long- range transport. Journal of Geophysical Research: Atmospheres, 112(D13).

Prasad, A. K., R. P. Singh, and M. Kafatos (2006). Influence of coal based thermal power plants on aerosol optical properties in the Indo- Gangetic basin. Geophysical Research Letters, 33(5).

Sachweh, M., and P. Koepke (1995). Radiation fog and urban climate. Geophysical Research Letters, 22(9), 1073-1076.

Sawaisarje, G.K., P. Khare, C. Y. Shirke, S. Deepakumar and N. M. Narkhede (2014). Study of winter fog over Indian subcontinent: Climatological perspectives. Mausam, 65(1), pp.19-28.

Sharma, A. R., S. K. Kharol, K. V. S. Badarinath, and D. Singh (2010, February). Impact of agriculture crop residue burning on atmospheric aerosol loading–a study over Punjab State, India. In Annales Geophysicae (Vol. 28, No. 2, pp. 367-379). Copernicus GmbH.

Singh, S., D. Singh and V. U. M. Rao (2007). Fog and dew analysis over Hisar. Journal of Agrometeorology, 9(1), 118-121.

Song, Y., and S. S. Yum (2013). Development and verification of the fog stability index for Incheon international airport based on the measured fog

characteristics. Atmosphere, 23(4), 443-452.

Srivastava, S. K., A. R. Sharma and K. Sachdeva (2016). A ground observation based climatology of winter fog: study over the Indo-Gangetic Plains, India. International Journal of Environmental and Ecological Engineering, 10(7), 742-753.

Syed, F. S., H. Körnich, and M. Tjernström (2012). On the fog variability over south Asia. Climate dynamics, 39(12), 2993-3005.

Tardif, R., and R. M. Rasmussen (2007). Event-based climatology and typology of fog in the New York City region. Journal of applied meteorology and climatology, 46(8), 1141-1168.

Teixeira, J. (1999). Simulation of fog with the ECMWF prognostic cloud scheme. Quarterly Journal of the Royal Meteorological Society, 125(554), 529-552.

Underwood, S. J., G. P. Ellrod, and A. L. Kuhnert (2004). A multiple-case analysis of nocturnal radiation-fog development in the central valley of California utilizing the GOES nighttime fog product. Journal of Applied Meteorology, 43(2), 297-311.

Wantuch, F. (2001). Visibility and fog forecasting based on decision tree method. Idojárás, 105, 29-38

INDIAN SOCIETY OF GEOMATICS: AWARDS

National Geomatics Award for Excellence

This award has been instituted to recognize outstanding and conspicuously important contribution in promoting geomatics technology and applications at the country level. The contributions should have made major impact on the use of this technology for national development.
Areas of contribution considered for the award are:

1. Geographical Information System
2. Global Positioning System
3. Photogrammetry
4. Digital Cartography
5. Applications of Geomatics

The award shall consist of Rs. 50,000/- in cash, a medal and citation.

Eligibility

Any citizen of India, engaged in activities related to geomatics technology and its applications is eligible for this award. The prize is awarded on the basis of work primarily done in India.

The age limit for awardees is 45 years or above as on June 30 of the year of award.

Selection

A duly constituted Award Committee will evaluate all nominations received. The committee shall consist of eminent experts in the field of geo-spatial technology, to be identified by the Executive Council, ISG. The committee shall forward selected name/s to ISG – EC for approval and announcement. Apart from those persons, whose nominations have been received, the Committee may consider any person or persons who, in their opinion, have made outstanding contributions to development of geo-spatial technology and applications.

The award can be withheld in any year if, in the opinion of the committee, no candidate is found suitable in that particular year.

Presentation of the Award

The award shall be presented during the Annual Convention of ISG. Local Hospitality shall be taken care by ISG & Air fare (low cost) may be reimbursed if awardees request for it.

How to make Nomination

The nominations can be proposed by Head of a major research institute/ centre; Vice-Chancellor of a university; Secretary of Government Scientific Departments; President of a National Academy, President, Indian Society of Geomatics / Indian Society of Remote Sensing / Indian National Cartographic Association / ISG fellow or two life members of the society with more than 10 year old membership.

A candidate once nominated would be considered for a total period of two years. Nomination should be sent in the prescribed format to Secretary, ISG.

The last date for receiving nominations shall be September 30 or otherwise extended.

Format for nomination of Geomatics Award for Excellence

1. Name of the Nominee

2. Postal Address

3. Academic Background (Bachelor degree onwards)

4. Field of Specialisation

5. Important positions held (in chronological order)

6. Professional Experience including foreign assignments.

7. Important Awards / Honours

8. Important Publications/Patents: (A set of ten most important publications to be enclosed with this form)

9. Contributions of Nominee based on which the nomination is sent (in 1000 words, also provide a statement in 50 words which may be used for citation.):

10. Other Relevant Information:

Proposer:

Signature
Name
Address
Phone/ Fax
E-mail
Life Membership No. (in case of ISG Member):

Place & Date

Endorsed by (in case nomination is by 2 ISG Life members)

Signature
Name
Address
Phone/ Fax
E-mail
Life Membership No. (in case of ISG Member):

Place & Date
(The proposer should give a brief citation of the nominee's work)

National Geomatics Award

National Geomatics Award to be given each year: a) for original and significant contribution in Geomatics technology, b) for innovative applications in the field of Geomatics. Each award comprises a medal, a citation and a sum of Rs 25,000/- The guidelines for these awards are available on ISG website.

ISG Chapter Award for Best Performance

The best chapter award will be given to an active chapter of Indian Society of Geomatics, which has made significant contribution to further the mandate and goal of the society. The award consists of a citation and medal

President's Appreciation Medal for Contribution to the ISG

This award will be given to a member of the society, who has made noteworthy contribution to the growth of the ISG (its main body or any chapter). The Award consists of a Medal and a Citation.

Prof. Kakani Nageswara Rao Endowment Young Achiever Award

Indian Society of Geomatics instituted a new award from year 2013 named "Prof. Kakani Nageswara Rao Endowment Young Achiever Award", to encourage young researchers/scientists/academicians pursuing research in the field of geospatial technology/applications. The award carries a cash prize of Rs. 10,000/- along with a citation.

NATIONAL GEOMATICS AWARD

Indian Society of Geomatics has instituted two National Geomatics Awards to be given each year for (a) Original and significant contribution in Geomatics technology, (b) Innovative application(s) in the field of Geomatics. Each award comprises a medal, a citation and a sum of Rs. 25,000/-.

The guidelines for the award are as under

Areas of contribution considered for the award (both technology and applications)

1. Geographical Information System

2. Global Positioning System

3. Photogrammetry

4. Digital Cartography

5. Remote Sensing

Eligibility

Any citizen of India engaged in scientific work in any of the above-mentioned areas of research is eligible for the award.

The awards are to be given for the work largely carried out in India.

- First award will be given for original contribution in the field of Geomatics technology supported by publications in a refereed journal of repute.

- Second award will be given for carrying out innovative application(s). Supported by publications in rear reviewed Journals of repute.

- The contribution for the first award should have been accepted by peers through citation of the work.

- Work based on the applications of existing technologies will not be considered for the first award.

- The work should have made impact on the overall development of Geomatics.

How to Send Nomination

Nominations should be sent in the prescribed format, completed in all aspects to the Secretary, Indian Society of Geomatics, Space Applications Centre Campus, Ahmedabad 380 015 by August 31 of the year of award.

Selection Process

An expert committee, consisting of at least three members, constituted by the Executive Council of the Indian Society of Geomatics, will scrutinize the nominations and recommend the awardees' names to the Executive Council. The Council will decide on the award based on the recommendations.

FORMAT FOR AWARD NOMINATION

1. Name of the Candidate:

2. Present Position:

3. Positions held earlier (chronological order):

4. Academic qualifications (Bachelor's degree onwards):

5. Names of at least three Indian Scientists/Technologist in the area as possible referees *:

6. Brief write up on the work (500 words) for which award is claimed:

7. Publication(s) on the above work (reprint(s) to be enclosed):

8. List of other publications of the candidate:

9. Citation of the work for which award is claimed:

10. Impact of the work (for which award is claimed) on the development in the field of Geomatics (500 words):

11. Whether the work has already won any award? If so, give details:

The Applications in the above format (five copies) should be submitted (by Registered Post or Speed Post) to

The Secretary, Indian Society of Geomatics,

Space Applications Centre Campus,

Ahmedabad-380015

so as to reach by September 30 of the year of award

*ISG is, however, not bound to accept these names and can refer the nomination to other experts/peers

INDIAN SOCIETY OF GEOMATICS: FELLOWS

Shri Pramod P. Kale, Pune
Dr George Joseph, Ahmedabad
Dr A.K.S. Gopalan, Hyderabad
Dr Prithvish Nag, Varanasi
Dr Baldev Sahai, Ahmedabad
Shri A.R. Dasgupta, Ahmedabad
Dr R.R. Navalgund, Bengaluru
Shri Rajesh Mathur, New Delhi
Dr Ajai, Ahmedabad
Prof P. Venkatachalam, Mumbai
Dr Shailesh Nayak
Prof I.V. Murli Krishna
Prof SM Ramasamy, Tiruchirapalli
Dr Ashok Kaushal, Pune
Shri A.S. Kiran Kumar, Bengaluru
Prof. P.K. Verma, Bhopal
Maj. Gen. Siva Kumar, Hyderabad
Dr A S Rajawat, Ahmedabad
Dr Shakil Romshoo, Srinagar

INDIAN SOCIETY OF GEOMATICS: PATRON MEMBERS

P-1   Director, Space Applications Centre (ISRO), Jodhpur Tekra Satellite Road, Ahmedabad - 380 015

P-2   Settlement Commissioner, The Settlement Commissioner & Director of Land Records-Gujarat, Block No. 13, Floor 2, Old Sachivalay, Sector-10, Gandhinagar   – 382 010

P-3   Commissioner, Mumbai Metropolitan Region Development Authority, Bandra-Kurla Complex, Bandra East, Mumbai - 400 051

P-4   Commissioner, land Records & Settlements Office, MP, Gwalior - 474 007

P-5   Director General, Centre for Development of Advanced Computing (C-DAC), Pune University Campus, Ganesh Khind, Pune - 411 007

P-6   Chairman, Indian Space Research Organization (ISRO), ISRO H.Q., Antariksha Bhavan, New BEL Road,Bengaluru 560 231

P-7   Director General, Forest Survey of India, Kaulagarh Road, P.O. I.P.E., Dehra Dun – 248 195

P-8   Commissioner, Vadodara Municipal Corporation, M.S. University, Vadodara - 390 002

P-9   Director, Centre for Environmental Planning and Technology (CEPT), Navarangpura, Ahmedabad - 380 009

P-10   Managing Director, ESRI INDIA, NIIT GIS Ltd., 8, Balaji Estate, Sudarshan Munjal Marg, Kalkaji, New Delhi - 110 019

P-11   Director, Gujarat Water Supply and Sewerage Board (GWSSB), Jalseva Bhavan, Sector – 10A, Gandhinagar - 382 010

P-12   Director, National Atlas & Thematic Mapping Organization (NATMO), Salt Lake, Kolkata - 700 064

P-13   Director of Operations, GIS Services, Genesys International Corporation Ltd., 73-A, SDF-III, SEEPZ, Andheri (E), Mumbai - 400 096

P-14   Managing Director, Speck Systems Limited, B-49, Electronics Complex, Kushiaguda, Hyderabad - 500 062

P-15   Director, Institute of Remote Sensing (IRS), Anna University, Sardar Patel Road, Chennai - 600 025

P-16   Managing Director, Tri-Geo Image Systems Ltd., 813 Nagarjuna Hills, PunjaGutta, Hyderabad - 500 082

P-17   Managing Director, Scanpoint Graphics Ltd., B/h Town Hall, Ashram Road, Ahmedabad - 380 006

P-18   Secretary General, Institute for Sustainable Development Research Studies (ISDRS), 7, Manav Ashram Colony, Goplapura Mod, Tonk Road, Jaipur - 302 018

P-19   Commandant, Defense institute for GeoSpatial Information & Training (DIGIT), Nr. Army HQs Camp, Rao Tula Ram Marg, Cantt., New Delhi - 110 010

P-20   Vice President, New Rolta India Ltd., Rolta Bhavan, 22nd Street, MIDC-Marol, Andheri East, Mumbai - 400 093

P-21   Director, National Remote Sensing Centre (NRSC), Deptt. of Space, Govt. of India, Balanagar, Hyderabad - 500 037

P-22   Managing Director, ERDAS India Ltd., Plot No. 7, Type-I, IE Kukatpalli, Hyderabad - 500 072

P-23   Senior Manager, Larsen & Toubro Limited, Library and Documentation Centre ECC Constr. Gp., P.B. No. 979, Mount Poonamallee Road, Manapakkam, Chennai - 600 089.

P-24   Director, North Eastern Space Applications Centre (NE-SAC), Department of Space, Umiam, Meghalaya 793 103

P-25   Progamme Coordinator, GSDG, Centre for Development of Advanced Computing (C-DAC), Pune University Campus, Pune – 411 007

P-26   Chief Executive, Jishnu Ocean Technologies, PL-6A, Bldg. No. 6/15, Sector – 1, Khanda Colony, New Panvel (W), Navi Mumbai – 410 206

P-27   Director General, A.P. State Remote Sensing Applications Centre (APSRAC), 8th Floor, "B" Block, Swarnajayanthi Complex, Ameerpet, Hyderabad- 500 038

P-28   Director, Advanced Data Processing Res. Institute (ADRIN), 203, Akbar Road, Tarbund, Manovikas Nagar P.O., Secunderabad –500 009

P-29   Managing   Director, LEICA Geosystems Geospatial Imaging Pvt. (I) Ltd., 3, Enkay Square, 448a Udyog Vihar, Phase-5, Gurgoan- 122 016

P-30   Director, Defense Terrain Research Limited (DTRL), Ministry of Defense, Govt. of India, Defense Research & Development Organisation, Metacafe House, New Delhi – 110 054

P-31   Chairman, OGC India Forum, E/701, Gokul Residency, Thakur Village, Kandivali (E), Mumbai – 400 101

P-32   Managing Director, ML Infomap Pvt. Ltd., 124-A, Katwaria Sarai, New Delhi – 110 016

P-33   Director, Rolta India Limited, Rolta Tower, "A", Rolta Technology Park, MIDC, Andheri (E), Mumbai – 400 093

P-34   Director, State Remote Sensing Applications Centre, Aizawl – 796 012, Mizoram

Instructions for Authors

The journal covers all aspects of Geomatics – geodata acquisition, pre-processing, processing, analysis and publishing. Broadly this implies inclusion of areas like GIS, GPS, Photogrammetry, Cartography, Remote Sensing, Surveying, Spatial Data Infrastructure and Technology including hardware, software, algorithm, model and applications. It endeavors to provide an international forum for rapid publication of developments in the field – both in technology and applications.

A manuscript for publication must be based on original research work done by the author(s). It should not have been published in part or full in any type of publication nor should it be under consideration for publication in any periodical. Unsolicited review papers will not be published.

The Editorial Board or the Indian Society of Geomatics is not responsible for the opinions expressed by the authors.

Language

The language of the Journal will be English (Indian). However, manuscripts in English (US) and English (British) are also acceptable from authors from countries located outside India.

Manuscript Format

Each paper should have a title, name(s) of author(s), and affiliation of each of the authors with complete mailing address, e-mail address, an abstract, four to six keywords, and the text. The text should include introduction/background, research method, results, discussion, followed by acknowledgements and references. The main text should be divided in sections. Section headings should be concise and numbered in sequence, using a decimal system for subsections. Figures, images and their captions should be inserted at appropriate points of the text. Figures, images and tables should fit in two column format of the journal. If absolutely necessary, figures, images and tables can spread across the two columns. Figures and images, however, should not exceed half a page in height. A title should be provided for each Table, Image and Figure. All figures and images should be in 600 dpi resolution and sized as per column/margin width. Authors must ensure that diagrams/figures should not lose easy readability upon reduction to column size. The SI (metric) units and international quantities should be used throughout the paper. In case measurements are given in any other system, equivalent measurements in SI (metric) units should be indicated in brackets.

Use MS Word with English (UK/US) or English (Indian) dictionary. The page size should be A4 paper, with 2 cm margin on all sides. Title, authors and affiliation should be centred. Abstract should be justified across margins. The manuscript text should be in two columns of 8.2 cm each with a gutter of 6mm between them. Use only Times New Roman fonts. Title should be 12 points bold. Authors and affiliation should be 9 points. All other text including headings should be 10 points. Heading numbering scheme should be decimal e.g. 1, 1.1, 1.2.3, etc. Headings should be in bold.

Normally length of a published paper should be about 6-10 pages in A4 size including figures. Use of illustrations in colour should be restricted and resorted to only where it is absolutely necessary and not for enhancing the look of the paper. If the number of colour illustrations exceeds five, authors' institution may be asked to reimburse the extra cost involved, which at current rates is about Rs. 2500 per coloured figure/diagram/plate/illustration.

Submission of Manuscript

Submissions should be in electronic form via email. The manuscript may be sent by email to editorjogisg@gmail.com. In exceptional cases hard copy submission in camera ready form may be allowed with the prior permission of the Chief Editor. Submission in any other form will be returned to the author. To speed up the review process, authors are advised to provide a list of three probable reviewers with their institutional address and e-mail IDs.

Guidelines for Citing References

Names of all cited publications should be given in full. No abbreviations should be used. Following procedure is to be adopted.

Journal Publications

Bahuguna, I.M. and A.V. Kulkarni (2005). Application of digital elevation model and orthoimages derived from IRS-1C Pan stereo data in monitoring variations in glacial dimensions, Journal of the Indian Society of Remote Sensing, 33(1), 107- 112. (to be referred to in the text as Bahuguna and Kulkarni (2005) or if more than two sets of authors are to be referred to, as (Bahuguna and Kulkarni, 2005; Jain et al., 1994)) When more than two authors are to be referred to, use Jain et al. (1994). However, in References, all authors are to be mentioned.

Publication in a Book

Misra, V.N. (1984). Climate, a factor in the rise and fall of the Indus Civilization – Evidence from Rajasthan and Beyond in Frontiers of the Indus Civilization (B.B. Lal and S.P. Gupta: Chief Editors) Books and Books, New Delhi, pp. 461-489

Papers Published in Seminar/ Symposium Proceedings

Jain, A., A.R. Shirish, M. Das, K. Das, M.C. Porwal, and P.S. Roy (1994). Remote Sensing and Geographic Information System – An approach for the assessment of biotic interference in the forest ecosystem. Proceedings. 15th Asian Conference on Remote Sensing, Bangalore, November 17-23, 1994, pp. 65-72.

Books

Possehl, Gregory L. (1999). Indus Age: The beginnings. Oxford and IBH Publishing Corporation, New Delhi.

Reviewing

Each paper will be reviewed by three peers. Papers forwarded by members of the Editorial or Advisory Boards along with their comments would get processed faster and may be reviewed by two referees only.

Sample format for Authors is available in downloadable form at ISG website: www.isgindia.org/JOG/Sample_format.doc

Copyright

The copyright of the paper selected for publication will rest with the Indian Society of Geomatics. Corresponding author shall be required to sign a copyright assignment form, on behalf of all authors, once the paper is selected for publication. Authors are, however, at liberty to use this material elsewhere after obtaining permission from the Indian Society of Geomatics.

If the authors have used any copyright material in their

manuscript, it is understood that they have obtained permission from the owner of the copyright material and they should convey the same along with the manuscript to the Chief Editor.

Certificate of Original Work

The authors will also provide a certificate that the paper is an original work, not published or being considered for publication elsewhere.

In the event the certificate turns out to be false, the Journal shall ban the author(s) from publishing in the Journal for a period of five years and inform the same to all other related publications.

Reprints

Authors will be allowed to download the (PDF) of their paper from ISG Website www.isgindia.org, No hard copy reprints will be provided.

Journal of Geomatics		
Advertisement Rates		
	1 Issue	**4 Issues**
Back Cover Page in colour	**Rs. 25,000**	**Rs. 80,000**
Inside Cover Page in colour	**Rs. 20,000**	**Rs. 64,000**
Full Page inside in colour	**Rs. 15,000**	**Rs. 48,000**
Full Page inside in B/W	**Rs. 10,000**	**Rs. 32,000**

Advertisement Details

Mechanical Details
Double Spread/Center Spread (42 x 29.7) cm
Full page bleed (21 x 29.7) cm
Full page non-bleed (19 x 27.7) cm

Art Requirements

Negatives: Art must be right reading, emulsion, down. Film must be supplied in one piece per color, each identified by color. Camera-ready art is accepted for black & White adds; however, film is preferred. Electronic Files are also accepted.

Electronic File Requirements: All material must be received before ad close dates.

Software: Adobe illustrator 9.0 (saved as EPS). Adobe Photoshop CS (saved as EPS or TIFF). Please convert higher versions down. If you can only supply an IBM format, the file must be in viewable EPS or TIFF format with fonts embedded as that format.

Colour Ads: Colour separations must be provided, right reading, emulsion down. Please note that files using RGB or Pantone colours (PMS) must be converted to CMYK before we receive files.

To,
The Secretary, Indian Society of Geomatics
6202, Space Applications Centre (ISRO)
AHMEDABAD – 380 058. INDIA

Sir,

I want to become Life Member/ Sustaining Member/ Patron Member of the Indian Society of Geomatics, Ahmedabad. Membership fee of Rs. _____ is being sent to you by Online/ Cash/ DD/ Cheque. (DD/ Cheque/ Transaction No._____ dated_____drawn on Bank _____). **I agree to abide by the Constitution of the Society.**

Date:

Place: **Signature**

- Name: Mr/Ms/Mrs/Dr_____

- Address: _____

_____PIN: _____

Phone: _____   Mobile: _____Email: _____

• Date of Birth _____

•Qualifications_____

- Specialisation: _____

- Designation: _____ Organisation. _____

- Membership in other Societies: _____

- Mailing Address: _____

     _____PIN: _____

Proposed by:
(Member's Name and No)
    Signature of Proposer

For Office Use: A/P/L Member No.		Receipt No.		Date:	

Membership Fees

S.No.	Membership	Life/Patron Membership fees		Annual Subscription
	Category	₹ Indian	US $ Foreign	₹ Indian
1.	Life Member a) Admitted below 45 years of age	2500	250	
	b) Admitted after 45 years of age	2000	200	
2.	Sustaining Member	---	---	2000
3.	Patron Member	50000	3000	---

MEMBERSHIP GUIDELINES

- Online payment to be made to ISG account and transaction number to be mentioned in the form.
  Bank: State Bank of India. **Branch**: Jodhpur Tekra, Ahmedabad
  IFS Code: SBIN0003967 **Account No**:10327867093
- Financial year of the Society is from April 1 to March 31.
- Subscription through DD / Cheque can also be made in the name of 'Indian Society of Geomatics' and payable at Ahmedabad.
- Scanned copy of the filled and signed form may be sent by email
- Any life member of the Society can countersign application as proposer.
- For further details, contact Secretary, Indian Society of Geomatics.
- ISG has chapters already established at the following places. Ahmedabad, Ajmer, Bhagalpur, Bhopal, Chennai, Dehradun, Delhi, Hissar, Hyderabad, Jaipur, Ludhiana, Mangalore, Mumbai, Mysore, Pondicherry, Pune, Shillong, Trichi, Srinagar, Vadodara, Vallabh Vidya Nagar, Visakhapatnam and Trivandrum. Applicants for membership have the option to contact Secretary/Chairman of the local chapter for enrolment. Details can be found at the website of the Society: **www.isgindia.org**.
- Journal of the Society will be sent to Life Members by softcopy only.

IGiS

Geomatics Revealed

Integrated GIS & IP Software

VERSION 2.0

MAKE IN INDIA

National Awards on Technology
By The Former President of India,
Dr. A. P. J. Abdul Kalam

Launch of IGiS Version 2.0
By Padam Shri AS Kiran Kumar, Chairman, ISRO and
Shri Tapan Mishra, DIRECTOR, SAC, ISRO.

What's new in IGiS

IGiS Version 2.0 is full of enhancements which you'll appreciate every day. New advanced GIS/IP and SAR modules are vital now a days. New COM Based Architecture makes you even more productive. The more you do with IGiS Version 2.0, the more you'll wonder how you ever did without it.

Enhancements in IGiS Version 2.0

- Advanced GIS / Image Processing
- Microwave SAR Analysis
- Meteorological Analysis
- COM Based Scalable Architecture
- New Ribbon Bar GUI
- Python Customization
- OGC Standards

Product Development Partner

इसरो isro

Government of India | Department of Space
Indian Space Research Organisation - (ISRO)

SGL © | Scanpoint Geomatics Ltd.
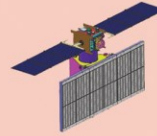
www.scanpointgeomatics.com

Scanpoint Geomatics Ltd.
Corporate Office : 12, Abhishree Corporate Park, Iskcon - Ambli Road, Ahmedabad - 380 058. Gujrat (India)
[P] +91 2717 297096-98 [F] +91 2717 297039 [E] info@scanpointgeomatics.com [W] www.scanpointgeomatics.com

INDIAN SPACE RESEARCH ORGANISATION
GOVERNMENT OF INDIA

nrsc

इसरो isro

Only Organization in the Country
to Acquire & Supply
Satellite Data to Users

*A Smart Destination
For
Geospatial
Solutions*

Aerial Acquisition for Specific
User Demands &
Disaster Management Support

Open Data & Value Added
Products Dissemination
Through Bhuvan

Region Specific Solutions

National Remote Sensing Centre
Hyderabad, India
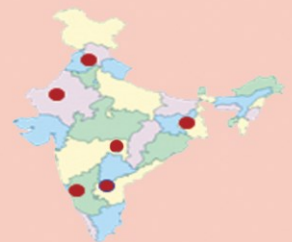www.nrsc.gov.in
www.bhuvan.nrsc.gov.in
data@nrsc.gov.in

Capacity Building in
Remote Sensing Applications